STABILITY ANALYSIS OF CELESTIAL OBJECTS AND COSMOS

By

Saadia Mumtaz

A THESIS
SUBMITTED IN PARTIAL FULFILLMENT OF THE
REQUIREMENTS FOR THE DEGREE OF
DOCTOR OF PHILOSOPHY
IN
MATHEMATICS

Supervised By

Prof. Dr. Muhammad Sharif

DEPARTMENT OF MATHEMATICS
UNIVERSITY OF THE PUNJAB
LAHORE-PAKISTAN
JULY, 2017

CERTIFICATE

I certify that the research work presented in this thesis is the original work of **Miss Saadia Mumtaz** D/O **Mumtaz Hussain Minhas** and is carried out under my supervision. I endorse its evaluation for the award of **Ph.D.** degree through the official procedure of **University of the Punjab**.

Prof. Dr. Muhammad Sharif
(**Supervisor**)

DECLARATION

I, **Miss Saadia Mumtaz** D/O **Mumtaz Hussain Minhas**, hereby declare that the matter printed in this thesis is my original work. This thesis does not contain any material that has been submitted for the award of any other degree in any university and to the best of my knowledge, neither does this thesis contain any material published or written previously by any other person, except due reference is made in the text of this thesis. Most of the contents have been appeared as my research papers.

_____

Saadia Mumtaz

DEDICATED

To

My Loving Parents, Brother Zia
and Sister Amna

Table of Contents

List of Figures

Acknowledgements

"In the Name of Allah, the Lord of Grace, the ever Merciful." If oceans turn to ink and all of the wood become pens, even then the praises and thanks to **Allah Almighty** cannot be expressed in words. He is Allah, the Creator, the Evolver, the Bestower of forms. To Him belong the most beautiful names: whatever is in the heavens and on earth, doth declare His praises and glory. He is the exalted in Might, the Wise. **He** blessed me with strength and ability to learn and observe in the way of achieving this goal. All esteem and respect to **The Holy Prophet Muhammad (SAW)**, Who is forever a source of complete guidance for all knowledge seekers.

A good teacher is like a candle, it consumes itself to light the way for others. I wish to record my heartiest gratitude and deep sense of obligation to my competent supervisor **Prof. Dr. Muhammad Sharif** for every bit of skillful guidance, expertise, enthusiasm and constructive suggestions during my research work. I could not have imagined having a better mentor and advisor for my educational career. I feel extremely privileged to have worked under his supervision.

I would also like to acknowledge *Department of Mathematics* for providing a conducive learning environment and excellent research facilities during *nine* years of my educational career. I take this opportunity to pay my sincere thanks to all faculty members and my worthy teachers especially **Prof. Dr. Khalid Latif Mir** and **Prof. Dr. Shahid S. Siddiqi** for their guidance and helpful nature. I would like to thank all members of *The Group of Gravitation and Cosmology* especially my seniors Dr. Shamaila, Dr. Sehrish and Dr. Rubab for their fruitful discussions and opinions. I also express my sense of gratitude to my friends and fellows Kanwal, Iqra and Ayesha for their cooperative attitude. I would like to thank my hostel fellows especially Miss Marina for their nice company.

I feel weak and deficit in vocabulary to express my heartiest feelings and depth of gratitude for my parents for their endless love, unconditional support and efforts in all aspects. They always wish to see me flying high up in the skies of success. My **father** has always been a source of encouragement and my **mother**'s hands always arise in prayers for me. I am really indebted to my caring siblings **Muhammad Zia Mumtaz** and **Iram** for their continuous support and boundless love for me. Surely, this acknowledgement would remain incomplete if I do not acknowledge my loving and caring younger sister **Dr. Amna** for providing carefree environment, assistance, cooperation and encouragement. May Allah bless them all with long, happy and peaceful lives! Finally, I would like to dedicate this thesis to unforgettable memories of my precious nine years of educational career at Punjab University.

Lahore **Saadia Mumtaz**
July, 2017

Abstract

In this thesis, we study various evolutionary aspects of relativistic collapsing systems, thin-shell wormholes as well as cosmos by incorporating the effects of different physical parameters. We consider both spherical and cylindrical stellar objects filled with electromagnetic fluids and discuss their dynamical instability under radial oscillations. The dynamical instability of homogeneous sphere as well as relativistic polytropes is discussed by taking different values of charge in Newtonian and post Newtonian regimes. Moreover, we evaluate the ranges of radii as well as adiabatic index for both charged and uncharged dissipative homogeneous cylinder. It is noted that dynamical instability occurs in the presence of charge if the gaseous mass contracts to the limiting radius.

We discuss stability of thin-shell wormholes coupled with nonlinear electrodynamics in the vicinity of different cosmological models for exotic matter. A general equation of state is considered in the form of linear perturbation which explores stability of the respective wormhole solutions. We assume linear, logarithmic and Chaplygin gas models to study exotic matter at thin-shell and evaluate maximum viable regions for stability with different values of the involved parameters. We also study stability of thin-shell wormholes in Einstein Hoffmann-Born-Infeld electrodynamics following the same dynamical approach. It is found that the Hoffmann-Born-Infeld parameter and electric charge enhance the stability regions.

Finally, we discuss dynamical stability of isotropic and homogenous universe model via phase space analysis by taking a noninteracting mixture of electromagnetic and viscous radiating fluids whose viscous pressure satisfies a nonlinear version of the

Israel-Stewart transport equation. We evaluate corresponding critical points for various choices of physical parameters. It is found that bulk viscosity as well as electromagnetic field enhances the stability of accelerated expansion of the isotropic and homogeneous cosmos. We also study phase space analysis of locally rotationally symmetric Bianchi type I universe model by taking different linear combinations for the interactions between scalar field models and dark matter. This indicates a matter dominated epoch ultimately followed by a late accelerated expansion phase. We conclude that all the critical points lead to accelerated expansion of the universe for tachyon coupled field.

Abbreviations

In this thesis, the signatures of the spacetimes will be $(-,+,+,+)$. Also, we shall use the following list of abbreviations.

GR:	General Relativity
BH:	Black Hole
RN:	Reissner Nordström
WH:	Wormhole
pN:	post-Newtonian
DE:	Dark Energy
DM:	Dark Matter
NLED:	Nonlinear Electrodynamics
EoS:	Equation of State
CG:	Chaplygin Gas
GCG:	Generalized Chaplygin Gas
MCG:	Modified Generalized Chaplygin Gas
HBI:	Hoffmann-Born-Infeld

Introduction

Stellar evolution refers to the progressive changes of interior composition that a star experiences from its birth to death. It radiates an extensive amount of energy in the form of photons or neutrinos. Gravitational collapse is highly dissipative mechanism which evolves enormous amount of binding energy of the order $10^{54}erg$. During collapse, relativistic celestial objects may go through several dynamical phases. It is well-known that any stellar system will be insignificant if it becomes unstable upon perturbations. The perturbation scheme plays a pivotal role in demonstrating the stability criteria for stellar configuration and characterizing possible consequences of its evolution. The stability phenomenon of oscillating gaseous configurations can be classified into two types, i.e., non-relativistic (Newtonian) and relativistic (pN) [1]. This provides a platform to evaluate ranges of deviation and level of consistency between GR and Newton gravity.

The dynamical instability of collapsing configurations can be studied through stiffness parameter also known as adiabatic index (Γ). Chandrasekhar [2] was the pioneer who discussed the concept of dynamical instability of gaseous sphere by taking perfect fluid in terms of Γ at Newtonian and pN limits. He followed Eulerian approach for linearized perturbed hydrodynamic equations. He also studied dynamical stability of spherical collapsing system by taking radial and non-radial fluctuations [3]. Herrera

et al. [4] extended the analysis of Chandrasekhar with new mathematical approach to examine dynamical instability of spherical system and concluded that instability range increases in Newtonian regime but decreases in pN regime. Chan et al. [5] found that the effect of shearing viscosity is to decrease instability of spherical star in both Newtonian and relativistic regimes.

The dynamical instability of astrophysical objects in the presence of electromagnetic field has a primal history starting with Rosseland [6]. A general consensus about stellar bodies exhibits that the system does not occupy charge in huge amount [7] but there are some phenomena which induce immense amount of electric charge. Stettner [8] discussed the role of surface charge in increasing stability of spherical system. Glazer [9] studied dynamical stability of charged gaseous sphere under radial pulsations. Zhang et al. [10] computed the Oppenhiemer-Volkoff equations and found that charge does not influence the critical mass. Ghezzi [11] found that neutron stars with a charge larger than the extreme value will blow up. Thirukkanesh and Maharaj [12] argued that charged spherical solutions may define realistic compact spheres. Pinheiro and Chan [13] studied dynamical aspects of charged dissipating sphere incorporating enormous amount of electric charge whose implosion yields RN BH.

It is well-known that galaxies can be categorized according to their shape like spiral, barred spiral, elliptic and irregular galaxies. The deviation of stellar structure from spherical to other symmetries is an incidental characteristic which reveals significant mathematical results about self-gravitating objects. The implementation of cylindrical configurations to study various astrophysical phenomena has attracted many astronomers. Thorne [14] defined energy for the systems that are invariant

under rotations and translations along a symmetry axis known as locally measurable "cylindrical energy" or "C-energy". He also found that magnetic field may halt gravitational collapse of cylinder to form a singularity [15]. Nakao and Morisawa [16] discussed cylindrical gravitational collapse in the context of perfect fluid.

There is a large body of literature on the study of cylindrical gravitational collapse with and without electromagnetic field [17]. Chandrasekhar and Fermi [18] investigated stability of cylinder filled with incompressible and homogenous fluid in the presence of magnetic field. Sharif and Azam [19] explored the stability conditions for charged dissipative collapsing cylinder and found that Γ has smaller value for the respective fluid as compared to the isotropic sphere. Sharif and Bhatti [20] examined dynamical instability of anisotropic collapsing cylinder by taking expansion-free model and concluded that electric charge controls stability of the model.

Polytropic models are the generalization of classical Lane-Emden equation obtained from the hydrostatic equilibrium equation. Tooper [21] studied internal structure of spherically symmetric spacetime by taking polytropic EoS and computed solution of Lane-Emden equation for Newtonian polytropes. Abramowicz [22] developed general form of the Lane-Emden equation for higher-dimensional spherical, cylindrical and planar geometries. The dynamics of polytropic compact stars is studied under the influence of electromagnetic field [23]. Herrera and Barreto [24] discussed physical characteristics for both Newtonian and relativistic polytropes in spherical background. Breysse et al. [25] investigated instability conditions for cylindrical polytropic models under radial and non-radial fluctuations.

Thin-shell WHs belong to one of the WH classes in which exotic matter is restricted at the shell. To ensure that an observer does not encounter the non-physical

zone of BH, a thin-shell strengthens the WH provided that it possesses an exotic matter for its maintenance against gravitational collapse. The physical viability of thin-shell WHs is a challenging issue due to unavoidable amount of exotic matter that is a necessary ingredient for the existence of WHs. The presence of this matter makes the system to violate null energy condition which needs to be minimized. Visser [26] suggested that this can be done by choosing some appropriate WH geometries. Visser et al. [27] illustrated an efficient technique of cut and paste to construct spherically symmetric thin-shell WHs which makes infinitesimally small usage of the exotic matter by restricting it at the edges of throat.

The stability of thin-shell WHs can be studied either by taking perturbations around a static solution or by assuming EoS identifying exotic matter at the WH throat. In this scenario, many surveys have been done to construct thin-shell WHs by applying Visser's cut and paste method and investigated their stability. Kim and Lee [28] found that electromagnetic field has significant impact on stability of thin-shell WHs. Eiroa and Romero [29] generalized this analysis for Reissner-Nordström thin-shell WHs whose stability increases by increasing electric charge. Lobo [30] studied this analysis for spherical WH configurations with the inclusion of cosmological constant (Λ). Sharif and Azam [31] explored both stable and unstable spherical thin-shell WH solutions.

The presence of singularity is one of the most peculiar problems in GR. A comprehensive insight of BH demands singularity-free solutions known as regular BHs. Bardeen [32] was the pioneer who proposed a regular BH with particular mass to charge ratio. Ayon-Beato and Garcia [33] proposed another regular BH termed as

ABG BH characterized by its mass and electric charge. Later, Bronnikov [34] presented similar kind of massive regular BH coupled with NLED known as ABGB BH which behaves as ordinary RN BH. Hayward [35] suggested a similar class of regular BH which can be converted to de Sitter and Schwarzschild spacetimes as $r \to 0$ and $r \to \infty$, respectively. The stability problem of thin-shell WHs from regular BH has aspired many researchers. Rahaman et al. [36] found stable thin-shell WHs from charged regular BH coupled with NLED. Sharif and Azam [37] studied stability of regular ABG thin-shell WHs and found stable solutions with and without Λ. Halilsoy et al. [38] examined stability conditions for regular Hayward thin-shell WHs in the vicinity of linear, logarithmic and CG models. Sharif and Javed [39] explored stable Bardeen thin-shell WHs by taking different cosmic models for specific values of EoS parameter.

Nonlinear electrodynamics is the generalization of Maxwell theory which is assumed to be the most appropriate theory to remove initial singularities. Born and Infeld [40] introduced the most distinguished constituent of viable NLED to overcome the singularity problem upto some extent. Hoffmann [41] defined gravitational field of a charged spherical solution by coupling GR with Born-Infeld electrodynamics which corresponds to a BH. In this context, Eiroa and Aguirre [42] investigated stability of spherical thin-shell WHs in Born-Infeld theory by taking GCG. Sharif and Azam [43] found that stability of WH configurations tends to increase by increasing values of Born-Infeld parameter in the vicinity of MGCG.

The concept of scalar field, with EoS parameter other than -1, has played a remarkable role in cosmic evolution due to its progressive implementation in various cosmological problems like cosmic acceleration and cosmic coincidence problem. The

scalar field models may also predict the early inflationary cosmic era. We can choose scalar field models (in particular, phantom and tachyon) as a dynamical DE candidate interacting with DM by interchanging their energy which may solve the coincidence problem. The universe model undergoes accelerated expansion as the tachyon field rolls down [44]. Gibbons [45] discussed cosmological influence of the tachyon rolling down to its ground phase. A tachyonic matter may yield inflation at early era and ultimately some new form of DM at late times [46]. The interaction of DE (phantom or tachyon) and DM describes energy flow such that no component remains conserved separately. The interaction between the components may alleviate the coincidence problem [47].

The stability of different universe models via phase space helps to comprehend various patterns of their evolution. Guo et al. [48] analyzed phase space analysis of interacting phantom energy with DM. Garcia-Salcedo [49] examined the stability of FRW universe with the influence of NLED. Yang and Gao [50] discussed phase space analysis for k-essence cosmology and found that stable critical points have intense contribution in demonstrating the cosmic evolution. Acquaviva and Beesham [51] discussed the role of nonlinear bulk viscosity on the stability of current cosmic expansion of FRW model. Shahalam et al. [52] studied dynamical analysis of coupled phantom and tachyon fields by taking linear combinations of the coupling for FRW universe model.

Bianchi universe models have widely been studied in literature to discuss expected primordial anisotropy and some large angle anomalies observed by CMBR which leads to the contravention of statistical isotropy of the universe [53]. Coley and Dunn [54] followed phase space approach to explore behavior of Bianchi type V model containing

a viscous fluid. Burd and Coley [55] investigated the effects of shear as well as bulk viscosity on the stability of Bianchi universe models. Goliath and Ellis [56] discussed dynamical evolution of Bianchi universe model via phase space by including Λ. Sharif and Waheed [57] studied phase space analysis of locally rotationally symmetric (LRS) BI universe for chameleon scalar field in Brans-Dicke gravity. Chaubey and Raushan [58] studied phase space analysis of LRS BI model in the presence of scalar field.

This thesis is devoted to study the dynamical stability of celestial objects as well as evolution of the universe models with the influence of various physical quantities. We investigate stability of thin-shell WH solutions against linear perturbation in the vicinity of different cosmological models. We also discuss phase space analysis of cosmic models coupled with NLED and scalar field models. The thesis is organized as follows.

- Chapter **One** provides some basic concepts and definitions related to this thesis.
- Chapter **Two** deals with dynamical instability of charged gaseous sphere by following Eulerian and Lagrangian perturbation approaches. We also discuss stability of charged dissipative cylinder under radial oscillations.
- Chapter **Three** investigates stability of regular thin-shell WHs coupled with NLED and stable WH solutions in Einstein HBI electrodynamics.
- In chapter **Four**, we analyze stability of of isotropic and homogenous universe model in NLED via phase space analysis. The stability of anistropic universe model is also discussed by taking phantom and tachyon coupled fields.
- Finally, we provide summary of all the obtained results and outline some future lines of action for research in chapter **Five** .

Chapter 1

Overview

In this chapter, we furnish some basic concepts and terminologies required to understand this thesis. The signatures of the spacetimes will be $(-,+,+,+)$ throughout the thesis.

1.1 Dynamical Instability of Oscillating Systems

The process which interconnects all the particles of any system through combined gravitational force is known as self-gravitation. It plays an important role in characterizing possible trends of cosmic expansion (decelerating or accelerating). Stars, stellar clusters and galaxies without self-gravitation may expand or finally disappear. The dynamical evolution of self-gravitating structures has remarkable significance in astrophysics which describes how the stellar bodies change with time. Initially, any stable system remains in state of hydrostatic equilibrium unless its own gravity overcomes the outward pointing forces which causes a continuous diminishing of star leading to gravitational collapse. The collapsing system contracts to a point under the influence of its own gravity leading to the overwhelm structures like white dwarfs (mass$< 1.44M_{\odot}$), neutron stars ($1.5M_{\odot} - 3.2M_{\odot}$) or BHs (mass$> 3.2M_{\odot}$), where

$M_\odot$ is the mass of the Sun. Gravitational collapse of massive objects having range $10^6 M_\odot - 10^8 M_\odot$ gives rise to the emergence of spacetime singularities in cosmos [59]. The mystery about the eventual outcome of gravitational collapse has remained unresolved. It has been suggested through various substantial attempts that the ultimate destiny of the gravitational collapse would be BH or naked singularity depending on the nature of initial data of collapse.

It has always been interesting to explore what happens when the phase of equilibrium of self-gravitating system is disturbed? Oscillations of stellar interiors as well as BHs are one of the primal issues in relativistic gravitational physics. These oscillations are produced on perturbing a stellar system from its equilibrium phase which reverts back to its original state under a restoration force. The oscillating system will be dynamically stable if these disturbances gradually vanish and the system reattains its initial position. For unstable case, the perturbation tends to increase such that the oscillating system departs from its original position and never comes back [60]. If the collapsing system accomplishes its hydrostatic equilibrium after perturbation, it becomes stable otherwise, it will be dynamically unstable.

There are different approaches for the stability analysis of general relativistic bodies. Numerical techniques can be used to comprehend the behavior of field equations when exact solutions cannot be found. However, these numerical results become ambiguous due to the presence of various parameters which could not describe the criteria of dynamical instability where particular ranges are required. In order to explore intriguing consequences, these systems are modeled through linearized perturbations which are more appropriate than numerical techniques. Chandrasekhar's pioneer

work indicates Eulerian and Lagrangian approaches for linearized perturbed hydrodynamic equations [2]. It was found that the stellar system would be dynamically stable or unstable according to some numerical value of adiabatic index. There have been many extensions of Chandrasekhar's approach with adiabatic and non-adiabatic fluids. An adiabatic index describes the fractional rate between pressure and energy density in matter distribution whose value estimates the instability criteria.

It is found that stability criterion of any system, initially in hydrostatic equilibrium, can be studied by linearizing field as well as conservation equations through radial perturbation. The dynamical variables are perturbed with time dependent small infinitesimal perturbation in such a way that the system starts oscillating with some frequency. According to linear stability criterion of the dynamical system, the perturbed equation of motion comprises eigenvalues corresponding to the oscillations frequency [60]. In such scenario, the stability of perturbed system depends upon the nature of frequency. The dynamical configuration will be stable (respectively, unstable) for real (respectively, imaginary) values of frequency of the model. The system with zero frequency becomes marginally stable (neither stable nor unstable), i.e., the configuration will expand or contract with analogous characteristics.

The dynamical study of massive stars can be carried out in weak as well as strong-field limits. The analysis becomes ambiguous in strong-field regimes due to nonlinearity, hence the weak-field approximations will be effective to find physically interesting results. Linearized gravity is an example of such approximation technique in which useful approximate consequences are achieved by neglecting nonlinearity from spacetime metric. This approximation yields linearized equations that lead to weak gravitational field. In this perspective, Newtonian and pN limits are other weak-field

approximations of gravitational theory where metric coefficients and field equations are approximated in inverse power of c (speed of light). The idea of weak-field approximation (Newtonian and pN) [1] has remarkable significance in relativistic hydrodynamics. This yields a platform to manifest orders of deviations from Newton's gravitational law.

Post-Newtonian approximations have become a fundamental paradigm to verify the predictions of different theories. They are expanded in small parameters which can be applied to evaluate an approximate solution of the field equations. The Newtonian and pN approximations demonstrate the ranges of small perturbation of any system with homogenous and isotropic background. It is worth mentioning here that the consequences of any relativistic theory must be well consistent with Newtonian theory in the non-relativistic limits.

1.2 Junction Conditions

Junction conditions give the matching of two spacetime regions (interior and exterior) partitioned by a hypersurface Σ and explain whether the unification of these two metrics form a viable solution to the field equations or not. They are often employed to analyze the boundary of collapsing system, dynamics of thin-shells as well as gravitational waves. These are of two types.

1.2.1 Darmois Junction Conditions

The smooth matching of two spacetime regions via junction conditions implies the continuity of the induced metric and the extrinsic curvature on both sides of the

hypersurface which yields Darmois junction conditions [64] given as follows.

1. The continuity of spacetimes over Σ gives

$$(ds^2)_\Sigma = (ds^2_-)_\Sigma = (ds^2_+)_\Sigma, \tag{1.2.1}$$

where $(ds^2)_\Sigma$ is the induced metric over Σ and $(ds^2_-)_\Sigma$, $(ds^2_+)_\Sigma$ indicate the interior and exterior line elements, respectively. This can also be termed as the continuity of the first fundamental form.

2. The continuity of the extrinsic curvature over Σ yields

$$[K_{ab}] = K^+_{ab} - K^-_{ab} = 0, \tag{1.2.2}$$

also called continuity of the second fundamental form. Here K_{ij} is the extrinsic curvature defined by

$$K^\pm_{ab} = -n^\pm_\alpha \left(\frac{\partial^2 x^\alpha_\pm}{\partial \xi^a \partial \xi^b} + \Gamma^\alpha_{\mu\nu} \frac{\partial x^\mu_\pm \partial x^\nu_\pm}{\partial \xi^a \partial \xi^b}) \right), \quad (a, b = 0, 2, 3), \tag{1.2.3}$$

where $n^\pm_\alpha$ are the unit normal vectors in the direction orthogonal to the hypersurface while ξ^a and $x^\mu_\pm$ represent the coordinates on Σ and the manifold $\mathcal{M}$, respectively. The unit normal vector to the hypersurface is given by

$$n_\alpha = \frac{\epsilon \phi_{,\alpha}}{|g^{\mu\nu}\phi_{,\mu}\phi_{,\nu}|^{\frac{1}{2}}}. \tag{1.2.4}$$

1.2.2 Israel Junction Conditions

The existence of matter at the boundary surface yields discontinuity in the extrinsic curvature directed along the normal, i.e., $[K_{ab}] = \kappa_{ab}$, hence the Darmois junction conditions fail. This phenomenon corresponds to Israel thin-shell formalism [65] which

requires continuity of the line elements while the second condition gives the extrinsic curvature discontinuity as follows

$$[K_{ab}] = K^{+}_{ab} - K^{-}_{ab} = \kappa_{ab}. \tag{1.2.5}$$

The Israel formalism requires the normal vectors directed from interior to exterior. The dynamical analysis of matter at hypersurface is carried out by employing the Lanczos equations at Σ given by

$$S_{ab} = \frac{1}{8\pi}\{g_{ab}K - [K_{ab}]\}. \tag{1.2.6}$$

This condition provides a correspondence between the surface energy-momentum tensor S_{ab} and the extrinsic curvature discontinuity.

1.3 Thin-Shell Wormholes

One of the most captivating attributes of GR is the manifestation of hypothetical geometries having topological structure. Misner and Wheeler [61] defined these intriguing characteristics as solutions of the Einstein field equations known as wormholes. A WH is a theoretical passage through spacetime which is supposed to connect remote regions of the universe by reducing traveling time as well as distance. Besides the lack of some observational evidences, a WH is interpreted as an eternal BH. The Einstein-Rosen bridge is the best fitted example [62], in which WH throat implodes leading to the presence of singularity. A particle passing through this WH will reach the singularity at $r = 0$ rather than the other end. The following aspects are suggested to be responsible in the composition of non-traversable WHs.

- The tidal gravitational forces present at the WH throat would drag off any observer trying to travel through it.

- This WH is not static as its throat expands from zero and then collapses reversely to its initial state rapidly. This rapid expansion or contraction of throat does not allow anything to pass through it.

- This WH possesses a BH (horizon) at one side and a white hole (antihorizon) at the other side. This antihorizon is unstable under small disturbances which changes to a horizon leading to the collapse of WH throat.

Physicists have been excited by the proposal of Morris and Thorne for traversable WH configuration comprising two asymptotically flat regions connected by a throat [63]. These WH solutions are characterized by an exotic matter with negative energy density that helps to keep its throat open, which in turn, produces repulsion against collapse. The most prominent feature of these WHs is the lack of event horizon which permits an observer to traverse freely through its flat faces. A BH solution can be converted into WH with the addition of exotic matter. A thin-shell is generated by this exotic matter in the stable WH configuration which identifies positive pressure and negative energy density. The positive surface pressure rules out the collapse of WH throat while the negative energy density assures the existence of horizon outside WH throat which enables a two way communication between two regions of the universe.

For the physical viability of thin-shell WHs, the presence of this matter plays an essential role to stabilize WH and makes it traversable. The quantity of exotic matter supporting the WH throat must be reduced for physical viability of WH configurations. Visser [26] proposed an elegant method which could make infinitesimally small contribution of the unavoidable amount of exotic matter such that a traveler encountering the WH does not observe any tidal force. Figure **1.1** shows a thin-shell

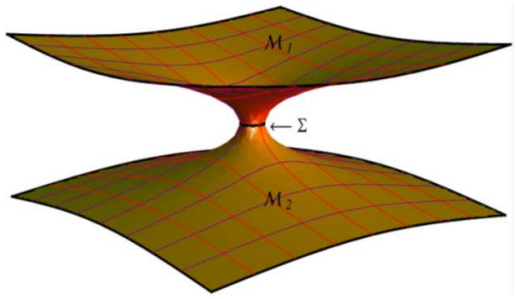

Figure 1.1: Thin-shell WH connecting two different regions.

WH constructed through cut and paste technique.

1.4 Some Mysterious Components of the Universe

Some mysterious exotic source of unusual anti-gravitational force is supposed to be responsible for the current cosmic expansion known as DE. It is an exotic energy constituent having large negative pressure (pushing galaxies apart from each other) which dominates over the matter content of cosmos. There are various alternative dynamical models like quintessence [66], phantom model [67] and tachyon field [68] which predict cosmic expansion. The generalization of simple barotropic EoS to more exotic forms like CG and its modification also correspond to DE candidates. The relevance of these models is an interesting subject in the dynamical investigation of thin-shell WHs as well as cosmos.

In the following, we discuss some of these interesting candidates briefly.

(i) Scalar Field Proposals

Scalar field is basically defined as a function that associates each point of the spacetime manifold with a scalar value (either a number or physical quantity). The physical background of scalar field models could be found through particle physics as well as string theory. This material with unusual characteristics can be speculated as the most appropriate candidate to develop a dynamical framework which is composed of kinetic and potential terms coupled to gravity. In cosmic history, various DE models have been developed on the basis of scalar field.

We briefly discuss some of the scalar field models such as quintessence, phantom and tachyon.

- **Quintessence**

  This is a hypothetical candidate of DE which can be acquired by including potential term in the Lagrangian of scalar field defined by

  $$\mathcal{L} = \frac{1}{2}\partial_\mu\phi\partial^\mu\phi - V(\phi), \tag{1.4.1}$$

  where ϕ is the scalar field and $V(\phi)$ corresponds to the scalar field potential. It is a dynamical model with varying EoS parameter whose evolution is only dominated by the nature of field potential. The energy density and pressure depending upon a time-varying scalar field are given by

  $$\sigma_Q = \frac{1}{2}\dot{\phi}^2 + V(\phi), \quad p_Q = \frac{1}{2}\dot{\phi}^2 - V(\phi). \tag{1.4.2}$$

  This model describes current cosmic expansion by generating negative pressure when potential dominates the kinetic term.

- **Phantom**

  Phantom model is the simplest description of DE that interprets the future

accelerated expansion of cosmos by the inclusion of negative sign for the kinetic energy term [67]. The corresponding Lagrangian is defined by

$$\mathcal{L} = -\frac{1}{2}\partial_\mu\phi\partial^\mu\phi - V(\phi). \tag{1.4.3}$$

A phantom field may arise from string theory [70] or due to bulk viscous stress in particle production [71]. It contains both kinetic and potential field terms with positive energy density and negative pressure

$$\sigma_P = -\frac{1}{2}\dot{\phi}^2 + V(\phi), \quad p_P = -\frac{1}{2}\dot{\phi}^2 - V(\phi), \tag{1.4.4}$$

which corresponds to the EoS parameter -1 and violates the energy conditions. The energy density increases and becomes infinite with the passage of time which causes gravitational repulsion between galaxies.

- **Tachyon Field**

  Tachyon fields are the scalar field candidates of DE that play a prominent role to explain initial as well as late cosmic scenarios [68]. The corresponding energy density and pressure are given by

$$\sigma_T = \frac{V(\phi)}{\sqrt{1-\dot{\phi}^2}}, \quad p_T = -V(\phi)\sqrt{1-\dot{\phi}^2}. \tag{1.4.5}$$

  In contrast to quintessence model (where we compare the squared scalar field term derivative with the field potential), this model can be compared with the unity. In this scenario, EoS parameter is smoothly interpolated between -1 and 0 for which $\dot{\phi}^2 < 1$ must be satisfied.

(ii) Chaplygin Gas Models

Chaplygin gas is a speculative substance to explore the DE ambiguity which satisfies an exotic EoS. The unification of dark sector of cosmos is a burning issue in cosmological framework. Chaplygin gas has the characteristic to behave as both DM and DE in a unified form [72]. It describes the early as well as late paradigms of cosmic expansion which is governed by the following EoS

$$p = -\frac{e}{\sigma}, \tag{1.4.6}$$

where e is a positive constant while $\sigma,\ p$ are the surface energy density and pressure, respectively. Chaplygin gas model behaves like a dust fluid in the initial phases but eventually acts like Λ. This candidate of DE does not require the presence of potential that let it free from all enigmas arising from the fine-tuning of free parameters. Several attempts have been done to propose various generalizations of CG with the inclusion of some new parameters.

- **Generalized Chaplygin Gas**

  The well-known extension of CG is GCG [73] defined by the EoS

  $$p = -\frac{e}{\sigma^{\gamma}}, \tag{1.4.7}$$

  where $0 < \gamma \leq 1$. Bento et al. [74] argued that GCG allows the unified description of DM and DE. This model coupled with dust at high energy density is consistent with recent observational data [75].

- **Modified Generalized Chaplygin Gas**

  Benaoum [76] extended GCG to MGCG defined by

  $$p = d\sigma - \frac{e}{\sigma^{\gamma}}, \tag{1.4.8}$$

where d is a positive constant. One can recover EoS for CG and GCG for different choices of parameters d, e and γ. The GCG possesses an interesting aspect to act as both DM as well as DE [77].

(iii) Viscous Force

The concept of viscous force comes from fluid dynamics where it is computed by the velocity gradient and can be categorized into bulk as well as shear viscosity. In cosmology, shear viscosity arises from the notion of spacetime anisotropy. The bulk viscosity refers to the measure of pressure required to restore an equilibrium state when cosmic expansion of any fluid occurs in an expanding universe scenario. It plays an important role to stabilize the density evolution and overcomes the rapid changes in cosmos. It promotes negative energy field in the fluid and hence can play the role of DE to describe the dynamics of cosmos. It is argued that a bulk viscous fluid is capable to cause an accelerated expansion of cosmos [78].

1.5 Phase Space Analysis

A phase space describes all possible states (position and momentum) associated with each point of the system. This provides dynamical behavior of a cosmological model by minimizing complexity of the equations. Phase portrait is basically a graphical demonstration of all solutions which incorporates the illustrative trajectories. This investigates the influence of initial data on stability of any system by checking whether the system remains stable for a long time [79].

The following algorithm has been adopted in literature to explore stability of

critical points for any set of field equations.

- Convert the dynamical system of equations to the autonomous system by using dimensionless variables.

- Evaluate critical points by solving the autonomous system of equations to study stability of cosmos.

- Calculate the eigenvalues of the Jacobi matrix which can characterize these critical points. The phase portraits of these critical point can be categorized according to the nature of eigenvalues of the linearly perturbed system.

- The fixed points can be classified into two types: hyperbolic points (eigenvalues having non-zero real parts) and non-hyperbolic points (the eigenvalues having only imaginary parts).

- The hyperbolic points can further be categorized into three types: source (oscillatory), sink (attractor) or saddle point. The fixed point is called a source (respectively, a sink) if both eigenvalues consist of positive (respectively negative) real parts. The real parts of the eigenvalues having opposite signs correspond to a saddle point of the system. For a given system, both oscillator and saddle points behave as unstable points while only attractors are stable points of that system. However, we cannot provide any information about the stability of the non-hyperbolic fixed points.

Chapter 2

Dynamical Instability of Charged Spherical and Cylindrical Gaseous Systems

This chapter explores the instability criteria for charged gaseous self-gravitating systems. In this context, we consider both spherically as well as cylindrically symmetric metrics filled with electromagnetic fluids and discuss their dynamical instability under radial oscillations. We follow the Eulerian and Lagrangian approaches to evaluate linearized perturbed equation of motion. The criteria for dynamical instability of homogeneous sphere as well as relativistic polytropes with different values of charge in Newtonian and pN regimes is evaluated. For cylindrical collapsing system, we compute the ranges of radii and adiabatic index for both charged as well as uncharged cases in Newtonian and pN limits with the effect of dissipation.

This chapter is divided into two sections. In section **2.1**, we provide a detailed description of charged spherically symmetric fluid models through dynamical equations. The results of this section have been published [80]. Section **2.2** investigates dynamical instability of charged dissipative gaseous cylinder whose results have been published [81].

2.1 Charged Spherical Gaseous Models

In this section, we study the role of electric charge on dynamical instability of gaseous sphere as well as relativistic polytropes under radial oscillations approaching the RN limit.

2.1.1 Field Equations and Matter Configuration

We consider a spherical system in the interior region defined by the line element

$$ds^2 = -e^{\nu}dt^2 + e^{\lambda}dr^2 + r^2(d\theta^2 + \sin^2\theta d\phi^2), \tag{2.1.1}$$

where $\nu = \nu(t, r)$ and $\lambda = \lambda(t, r)$ are the gravitational potentials. The corresponding field equations can be written as

$$-\frac{8\pi G}{c^4}T_0^0 = \frac{1}{r^2} - \frac{1}{r^2}\frac{\partial}{\partial r}(re^{-\lambda}), \tag{2.1.2}$$

$$-\frac{8\pi G}{c^4}T_1^1 = \frac{1}{r^2} - e^{-\lambda}(\frac{1}{r^2} + \frac{1}{r}\frac{\partial \nu}{\partial r}), \tag{2.1.3}$$

$$\frac{8\pi G}{c^4}T_0^1 = \dot{\lambda}\frac{e^{-\lambda}}{r}, \tag{2.1.4}$$

where dot denotes derivative with respect to time. We assume the energy-momentum tensor corresponding to charged perfect fluid in the form

$$T_j^i = (\sigma + p)u^i u_j + p\delta_j^i + \frac{1}{4\pi}[F_{jk}F^{ik} - \frac{1}{4}\delta_j^i F_{kl}F^{kl}], \tag{2.1.5}$$

where $u^i = \frac{dx^i}{ds}$ is the four velocity. The electromagnetic field tensor F_{ij} can be defined in terms of four potential, $F_{ij} = \Phi_{j;i} - \Phi_{i;j}$, which satisfies the Maxwell field equations

$$F^{ij}_{\ ;j} = 4\pi J^i, \quad F_{[ij,k]} = 0,$$

where J^i is the four current. The only non-vanishing radial component of electromagnetic field tensor ($F^{01}=-F^{10}$) implies that

$$\frac{d\left(r^2e^{(\lambda+\nu)/2}F^{01}\right)}{dr}=4\pi r^2e^{\lambda/2}\rho,$$

whose integration yields

$$F^{01}=\frac{e^{-(\lambda+\nu)/2}Q(t,r)}{r^2},$$

where $Q(t,r)=4\pi\int_0^r r^2\rho e^{\lambda/2}dr$ is the total amount of charge within the sphere.

The energy-momentum tensor follows the conservation identity, which governs hydrodynamics of the fluid and leads to the following relations

$$\frac{\partial T_0^0}{\partial t}+\frac{\partial T_1^0}{\partial r}+\frac{1}{2}\left(\frac{4}{r}+\frac{\partial}{\partial r}(\lambda+\nu)\right)T_0^1+\frac{1}{2}\left(T_0^0-T_1^1\right)\frac{\partial\lambda}{\partial t}=0, \tag{2.1.6}$$

$$\frac{\partial T_1^0}{\partial t}+\frac{\partial T_1^1}{\partial r}+\frac{1}{2}\left(T_1^1-T_0^0\right)\frac{\partial\nu}{\partial r}-\frac{2}{r}\left(p-T_1^1\right)+\frac{1}{2}T_1^0\frac{\partial}{\partial t}(\lambda+\nu)=0, \tag{2.1.7}$$

where $T_0^1=-e^{\nu-\lambda}T_1^0$. The non-zero components of energy-momentum tensor are

$$T_0^0=-\sigma-\frac{Q^2}{8\pi r^4},\quad T_1^1=p-\frac{Q^2}{8\pi r^4},\quad T_2^2=T_3^3=p+\frac{Q^2}{8\pi r^4}.$$

All the quantities governing the motion remain independent of time during the state of hydrostatic equilibrium. The surface stresses describing equilibrium state are denoted by zero subscript. In this context, Eqs.(2.1.2), (2.1.3) and (2.1.7) take the form

$$\frac{d}{dr}(re^{-\lambda_0}) = 1-\frac{8\pi Gr^2}{c^4}\sigma_0-\frac{GQ^2}{c^4r^2}, \tag{2.1.8}$$

$$\frac{1}{r}e^{-\lambda_0}\frac{d\nu_0}{dr} = \frac{1}{r^2}(1-e^{-\lambda_0})+\frac{8\pi Gp_0}{c^4}-\frac{GQ^2}{c^4r^4}, \tag{2.1.9}$$

$$\frac{dp_0}{dr} = \frac{1}{2}\frac{d\nu_0}{dr}(p_0+\sigma_0)+\frac{1}{8\pi}\frac{d}{dr}\left(\frac{Q^2}{r^4}\right)+\frac{Q^2}{4\pi r^5}. \tag{2.1.10}$$

Following Eqs.(2.1.2) and (2.1.3), we also have a useful relation

$$\frac{e^{-\lambda_0}}{r}\frac{d}{dr}(\lambda_0+\nu_0)=(p_0+\sigma_0)\frac{8\pi G}{c^4}. \tag{2.1.11}$$

We take RN spacetime in the exterior region as

$$\begin{aligned} ds^2 &= -\left(1-\frac{2GM}{rc^2}+\frac{GQ^2}{r^2c^4}\right)dt^2+\left(1-\frac{2GM}{rc^2}+\frac{GQ^2}{r^2c^4}\right)^{-1}dr^2 \\ &+ r^2(d\theta^2+\sin^2\theta d\phi^2), \end{aligned} \tag{2.1.12}$$

where M corresponds to the total mass of the sphere. The hydrostatic equilibrium describes the state of fluid in which pressure gradient force is balanced by the gravitational force. When one of these forces overcome the other, the stability of the system is disturbed leading to an unstable system. The equation describing hydrostatic equilibrium is obtained by eliminating ν_0 from Eqs.(2.1.9) and (2.1.10) as

$$\begin{aligned} &\left(1-\frac{2GM_r}{rc^2}+\frac{GQ^2}{r^2c^4}\right)\frac{dp_0}{dr}=-\frac{1}{c^2}\left(\frac{GM_r}{r^2}-\frac{GQ^2}{r^3c^2}+\frac{4\pi G}{c^2}pr\right) \\ &\times(p_0+\sigma_0)+\frac{1}{4\pi}\left(1-\frac{2GM_r}{rc^2}+\frac{GQ^2}{r^2c^4}\right)\left(\frac{Q^2}{r^5}+\frac{1}{2}\frac{d}{dr}\left(\frac{Q^2}{r^5}\right)\right), \end{aligned} \tag{2.1.13}$$

where the left and right hand sides correspond to pressure gradient and gravitational terms, respectively and

$$M_r=\frac{4\pi G}{c^4}\int_0^r\sigma_0 r^2dr+\frac{G}{2c^4}\int_0^r\frac{Q^2}{r^2}dr, \tag{2.1.14}$$

is the Misner-Sharp mass function.

2.1.2 Equations Governing Radial Oscillations

Here we discuss the motion of gaseous masses undergoing radial oscillations. The non-zero components of four velocity are given by

$$u^0=e^{-\frac{\nu_0}{2}},\quad u_0=-e^{\frac{\nu_0}{2}},\quad u^1=ve^{-\frac{\nu_0}{2}},\quad u_1=ve^{\frac{\lambda_0-\nu_0}{2}}, \tag{2.1.15}$$

where $v=\frac{dr}{dt}$ is the radial velocity component. The stability of any gaseous mass under perturbation ultimately gives rise to the dynamical evolution of gravitating

system. We assume that an equilibrium configuration is perturbed such that it does not affect the spherical symmetry. We consider only linear terms so that the respective values in the perturbed state become

$$\lambda=\lambda_0+\delta\lambda,\quad \nu=\nu_0+\delta\nu,\quad p=p_0+\delta p,\quad \sigma=\sigma_0+\delta\sigma,\quad Q=Q_0+\delta Q. \tag{2.1.16}$$

We follow the Eulerian approach [3] for perturbations such that the corresponding linearized forms (governing the radial perturbations) through Eqs.(2.1.8) and (2.1.9) are

$$\frac{\partial}{\partial r}(re^{-\lambda_0}\delta\lambda) = \frac{2G}{c^4}\left(4\pi r^2\delta\sigma-\frac{Q_0\delta Q}{r^2}\right), \tag{2.1.17}$$

$$\frac{e^{-\lambda_0}}{r}\left[\frac{\partial}{\partial r}\delta\nu-\delta\lambda\frac{d\nu_0}{dr}\right] = \frac{1}{r^2}e^{-\lambda_0}\delta\lambda+\frac{8\pi G}{c^4}\delta p-\frac{2GQ_0\delta Q}{c^4r^4}, \tag{2.1.18}$$

here $\delta\lambda$, $\delta\nu$, $\delta\sigma$, δp and δQ represent the Eulerian changes. Equations (2.1.4) and (2.1.7) can be written appropriately in linearized forms as

$$\frac{e^{-\lambda_0}}{r}\frac{\partial}{\partial t}\delta\lambda=-\frac{4\pi G}{c^4}\left(2(p_0+\sigma_0)v-\frac{Q_0\delta Q}{r^4}\right), \tag{2.1.19}$$

$$(p_0+\sigma_0)e^{\lambda_0-\nu_0}\frac{\partial v}{\partial t}+\frac{\partial}{\partial r}\delta p+\frac{1}{2}(p_0+\sigma_0)\frac{\partial}{\partial r}\delta\nu$$
$$+\frac{1}{2}(\delta p+\delta\sigma)\frac{d\nu_0}{dr}+\frac{1}{8\pi}\frac{Q_0\delta Q}{r^4}-\frac{1}{4\pi}\frac{\partial}{\partial r}\left[\frac{Q_0\delta Q}{r^4}\right]=0. \tag{2.1.20}$$

Let us introduce a Lagrangian displacement "η" such that $v=\frac{\partial\eta}{\partial t}$. Integration of Eq.(2.1.19) leads to

$$\frac{e^{-\lambda_0}}{r}\delta\lambda=-\frac{8\pi G}{c^4}(p_0+\sigma_0)\eta+\frac{4\pi GQ_0}{c^4r^4}\int\delta Q dt. \tag{2.1.21}$$

Using Eq.(2.1.11), this equation takes the form

$$\delta\lambda=-\frac{d}{dr}(\lambda_0+\nu_0)\eta+\frac{4\pi GQ_0e^{\lambda_0}}{c^4r^3}\int\delta Q dt. \tag{2.1.22}$$

Solving Eq.(2.1.17) and (2.1.32), it follows that

$$\delta\sigma = \frac{1}{r^2}\frac{\partial}{\partial r}\left[-r^2(\sigma_0+p_0)\eta + \frac{Q^2}{2r^4}\int \delta Q dt\right] + \frac{Q_0}{4\pi r^4}\delta Q, \tag{2.1.23}$$

which yields

$$\begin{aligned}\delta\sigma &= -\eta\frac{dp_0}{dr} - \eta\frac{d\sigma_0}{dr} - \frac{1}{r^2}(p_0+\sigma_0)\frac{\partial}{\partial r}(\eta r^2) + \frac{1}{r^2}\frac{\partial}{\partial r}\left[\frac{Q_0}{2r^4}\int \delta Q dt\right] \\ &+ \frac{Q_0}{4\pi r^4}\delta Q.\end{aligned} \tag{2.1.24}$$

Using Eq.(2.1.10), we have

$$\begin{aligned}\delta\sigma &= -\eta\frac{d\sigma_0}{dr} - \frac{e^{\nu_0/2}}{r^2}(p_0+\sigma_0)\frac{\partial}{\partial r}\left[\eta r^2 e^{-\nu_0/2}\right] - \frac{\eta}{8\pi}\frac{d}{dr}\left[\frac{Q^2}{r^4}\right] \\ &+ \frac{1}{r^2}\frac{\partial}{\partial r}\left[\frac{Q_0}{2r^4}\int \delta Q dt\right] + \frac{Q_0}{4\pi r^4}\delta Q.\end{aligned} \tag{2.1.25}$$

Substituting $\delta\lambda$ from Eq.(2.1.21) in (2.1.18), we obtain

$$\begin{aligned}\frac{e^{-\lambda_0}}{r}\frac{\partial}{\partial r}\delta\nu &= \left[(p_0+\sigma_0)\left(\frac{1}{r}+\frac{d\nu_0}{dr}\right)\eta + \delta p\right]\frac{8\pi G}{c^4} \\ &+ \frac{4\pi G Q_0}{c^4 r^4}\left[\frac{d\nu_0}{dr} - \frac{\eta}{r}\right]\int \delta Q dt - \frac{2GQ_0}{c^4 r^4}\delta Q,\end{aligned} \tag{2.1.26}$$

which in accordance of Eq.(2.1.11) leads to

$$\begin{aligned}(p_0+\sigma_0)\frac{\partial}{\partial r}\delta\nu &= \frac{d}{dr}(\lambda_0+\nu_0)\left\{\left[\delta p - (p_0+\sigma_0)\left(\frac{1}{r}+\frac{d\nu_0}{dr}\right)\eta\right]\right. \\ &+ \left.\frac{Q_0}{2r^4}\left[\frac{d\nu_0}{dr} - \frac{\eta}{r}\right]\int \delta Q dt - \frac{Q_0}{4\pi r^4}\delta Q\right\}.\end{aligned} \tag{2.1.27}$$

Now we assume perturbations have time dependence of the form $e^{i\varrho t}$, where ϱ is the characteristic frequency to be evaluated. The Lagrangian displacement η connects the fluid elements in equilibrium with corresponding one in the perturbed configuration. Since the equations have natural modes of oscillations, so they will depend on time.

Considering $\delta\lambda,\ \delta\nu,\ \delta p,\ \delta\sigma$ and δQ as time dependent amplitudes of the respective quantities, Eq.(2.1.20) with (2.1.27) can be rewritten as

$$\begin{aligned}\varrho^2 e^{\lambda_0-\nu_0}(p_0+\sigma_0)\eta &= \delta p\frac{d}{dr}\left(\nu_0+\frac{1}{2}\lambda_0\right)+\frac{d}{dr}\delta p+\frac{1}{2}\delta\sigma\frac{d\nu_0}{dr}-\frac{1}{2}(p_0+\sigma_0)\\ &\times \left(\frac{d\nu_0}{dr}+\frac{d\lambda_0}{dr}\right)\left(\frac{1}{r}+\frac{d\nu_0}{dr}\right)\eta+\frac{Q_0}{8\pi r^4}\frac{d}{dr}(\lambda_0+\nu_0)\\ &\times \left\{2\pi\left(\frac{d\nu_0}{dr}-\frac{\eta}{r}\right)\int\delta Q dt-\delta Q\right\}+\frac{1}{4\pi}\left\{\frac{Q_0\delta Q}{2r^4}\right.\\ &- \left.\frac{d}{dr}\left(\frac{Q_0\delta Q}{r^4}\right)\right\}. \qquad (2.1.28)\end{aligned}$$

2.1.3 The Conservation of Baryon Number

The study of perturbed pressure in terms of Lagrangian displacement requires an additional assumption through which one can discuss physical aspects of gaseous mass undergoing adiabatic radial oscillations. In this context, the required supplementary condition can be justified by conservation of baryon number in the framework of GR as $(\widetilde{N}u^j)_{;j}=0$, or

$$\frac{\partial}{\partial x^j}(\widetilde{N}u^j)+\widetilde{N}u^j\frac{\partial}{\partial x^j}\ln\sqrt{-g}=0, \qquad (2.1.29)$$

where $\widetilde{N}$ is the baryon number per unit volume. The conservation of baryon number plays a vital role in collecting different models of the universe. According to this law, the total number of particles will remain conserved during the fluid flow. This change occurs due to loss or gain of net fluxes. Here we consider a fluid obeying this identity. Equation (2.1.29) through (2.1.15) leads to

$$\begin{aligned}&\frac{\partial}{\partial t}(\widetilde{N}e^{-\nu_0/2})+\frac{\partial}{\partial r}(\widetilde{N}ve^{-\nu_0/2})+\widetilde{N}ve^{-\nu_0/2}\frac{\partial}{\partial r}\left(\frac{2}{r}+\frac{1}{2}[\nu+\lambda]\right)\\ &+\frac{\widetilde{N}}{2}e^{-\nu_0/2}\frac{\partial}{\partial t}(\nu+\lambda)=0. \qquad (2.1.30)\end{aligned}$$

We assume a perturbation of the form

$$\widetilde{N} = \widetilde{N}_0(r) + \delta\widetilde{N}(r,t). \tag{2.1.31}$$

Keeping only the linear terms in v, Eq.(2.1.30) becomes

$$\begin{aligned}&\frac{1}{r^2}\frac{\partial}{\partial r}(\widetilde{N}_0 r^2 v e^{-\nu_0/2}) + e^{-\nu_0/2}\frac{\partial}{\partial t}\delta\widetilde{N} + \frac{1}{2}\widetilde{N}_0 e^{-\nu_0/2}\frac{d}{dr}(\nu_0+\lambda_0)\\ &+\frac{1}{2}\widetilde{N}_0 e^{-\nu_0/2}\frac{\partial}{\partial t}\delta\lambda = 0,\end{aligned} \tag{2.1.32}$$

whose integration in terms of Lagrangian displacement leads to

$$\delta\widetilde{N} + \frac{\widetilde{N}_0}{2}\left[\eta\frac{d}{dr}(\nu_0+\lambda_0) + \delta\lambda\right] + \frac{1}{r^2}e^{\nu_0/2}\frac{\partial}{\partial r}\left(\widetilde{N}_0 r^2\eta e^{-\nu_0/2}\right) = 0. \tag{2.1.33}$$

Using Eq.(2.1.22), it follows that

$$\delta\widetilde{N} = -\eta\frac{d\widetilde{N}_0}{dr} - \frac{\widetilde{N}_0}{r^2}e^{\nu_0/2}\frac{\partial}{\partial r}\left(r^2\eta e^{-\nu_0/2}\right) + \frac{2\pi G\widetilde{N}_0 Q_0}{c^4 r^3}e^{\lambda_0}\int\delta Q dt. \tag{2.1.34}$$

We consider an EoS in the form

$$\widetilde{N} = \widetilde{N}(\sigma, p), \tag{2.1.35}$$

such that Eqs.(2.1.25) and (2.1.34) together give

$$\delta p = -\eta\frac{dp_0}{dr} - p_0\Gamma\frac{e^{\nu_0/2}}{r^2}\frac{\partial}{\partial r}\left(r^2\eta e^{-\nu_0/2}\right) + \frac{\alpha_1 Q_0}{r^3}\int\delta Q dt, \tag{2.1.36}$$

where

$$\alpha_1 = \frac{1}{\partial\widetilde{N}/\partial p}\left\{\frac{2\pi G\widetilde{N}_0}{c^4}e^{\lambda_0} - \frac{1}{2r}\frac{d\widetilde{N}}{d\sigma}\right\}, \tag{2.1.37}$$

and Γ is the adiabatic index (ratio of specific heats) defined by

$$\Gamma = \frac{1}{p\partial\widetilde{N}/\partial p}\left\{\widetilde{N} - (\sigma+p)\frac{\partial\widetilde{N}}{\partial\sigma}\right\}, \tag{2.1.38}$$

which estimates the fluid stiffness and describes the pressure and density fluctuations.

2.1.4 Pulsation Equation and Variational Principle

The linear pulsation corresponds to the oscillation frequencies and different modes of small perturbations applied to equilibrium spherical configuration. Inserting the values of $\delta\sigma$ and δp from Eqs.(2.1.23) and (2.1.36) in (2.1.28), it follows that

$$\varrho^2 e^{\lambda_0-\nu_0}(p_0+\sigma_0)\eta = -\eta\left(\frac{d\nu_0}{dr}+\frac{1}{2}\frac{d\lambda_0}{dr}\right)\frac{dp_0}{dr} - \frac{d}{dr}\left(\eta\frac{dp_0}{dr}\right) - \frac{1}{2}\left\{\frac{2}{r}\right.$$
$$\left.\times\,(p_0+\sigma_0)\eta + \frac{d}{dr}[(p_0+\sigma_0)\eta]\right\} - \frac{1}{2}\eta(p_0+\sigma_0)\left(\frac{d\nu_0}{dr}+\frac{d\lambda_0}{dr}\right)\left(\frac{1}{r}+\frac{d\nu_0}{dr}\right)$$
$$-e^{-(\nu_0+\frac{\lambda_0}{2})}\frac{d}{dr}\left\{e^{(\nu_0+\frac{\lambda_0}{2})}\Gamma p_0\frac{e^{\nu_0/2}}{r^2}\frac{d}{dr}(r^2\eta e^{-\nu_0/2})\right\} + e^{-\lambda_0/2}\frac{d}{dr}\left\{\frac{\alpha_1 Q_0}{r^3}\right.$$
$$\left.\times\, e^{\lambda_0/2}\int\delta Q dt\right\} + \frac{Q_0}{r^3}\frac{d\nu_0}{dr}\int\delta Q dt\left\{\alpha_1+\frac{1}{4r}+\frac{1}{4\pi r}\left(\frac{d\nu_0}{dr}-\frac{\eta}{r}\right)\right\}$$
$$+\frac{Q_0}{4\pi r^4}\frac{d\lambda_0}{dr}\left\{\frac{d\nu_0}{dr}-\frac{\eta}{r}\int\delta Q dt-\frac{\delta Q}{2}\right\} + \frac{Q_0}{8\pi r^4}\delta Q + \frac{e^{\nu_0/2}}{4\pi}\frac{d}{dr}\left\{\frac{Q_0 e^{\nu_0/2}\delta Q}{r^4}\right\}.$$

Substituting $\frac{dp_0}{dr}$ from Eq.(2.1.10) in the above equation, we have

$$\varrho^2 e^{\lambda_0-\nu_0}(p_0+\sigma_0)\eta = \frac{1}{2}(p_0+\sigma_0)\eta\left\{\frac{d^2\nu_0}{dr^2}-\frac{3}{r}\frac{d\nu_0}{dr}-\frac{1}{r}\frac{d\lambda_0}{dr}-\frac{1}{2}\frac{d\lambda_0}{dr}\frac{d\nu_0}{dr}\right\}$$
$$-\frac{5}{2\pi}\frac{Q^2}{r^6}-\frac{1}{8\pi r^4}\frac{d^2}{dr^2}(Q^2)+e^{-\lambda_0}\frac{d}{dr}\left\{\frac{\alpha_1 Q_0}{r^3}e^{-\lambda_0/2}\widetilde{Q}\right\}+\frac{Q_0\widetilde{Q}}{r^3}\frac{d\nu_0}{dr}\left\{\alpha_1+\frac{1}{4\pi}\right.$$
$$\left.+\frac{1}{4\pi r}\left(\frac{d\nu_0}{dr}-\frac{\eta}{r}\right)\right\}+\frac{Q_0}{4\pi r^4}\frac{d\lambda_0}{dr}\left\{\left(\frac{d\nu_0}{dr}-\frac{\eta}{r}\right)\widetilde{Q}-\frac{\delta Q}{2}\right\}+\frac{Q_0\delta Q}{8\pi r^4}$$
$$+\frac{e^{\nu_0/2}}{4\pi}\frac{d}{dr}\left\{\frac{Q_0 e^{-\nu_0/2}\delta Q}{r^4}\right\}, \qquad (2.1.39)$$

where $\int\delta Q dt=\widetilde{Q}$. Under the equilibrium condition, Eq.(2.1.4) yields

$$\left\{\frac{16\pi G p_0}{c^4}+\frac{2GQ_0^2}{c^4r^4}\right\}e^{\lambda_0}=\frac{d^2\nu_0}{dr^2}+\frac{1}{r}\frac{d}{dr}(\nu_0-\lambda_0)+\frac{1}{2}\left(\frac{d\nu_0}{dr}\right)^2-\frac{1}{2}\frac{d\lambda_0}{dr}\frac{d\nu_0}{dr}, \quad (2.1.40)$$

which, through Eq.(2.1.10), takes the form

$$\varrho^2 e^{\lambda_0-\nu_0}(p_0+\sigma_0)\eta=\frac{4}{r}\frac{dp_0}{dr}\eta-\frac{1}{p_0+\sigma_0}\left(\frac{dp_0}{dr}\right)^2\eta+\frac{8\pi G p_0}{c^4}e^{\lambda_0}$$

$$\times(p_0+\sigma_0)\eta+\frac{d}{dr}\left[e^{\lambda 0+3\nu_0/2}\frac{p_0\Gamma}{r^2}\frac{d}{dr}\left(r^2\eta e^{-\nu_0/2}\right)\right]e^{-(\nu_0+\lambda_0/2)}$$
$$+\frac{1}{p_0+\sigma_0}\frac{dp_0}{dr}\eta\left(\frac{1}{4\pi r^4}\frac{d(Q^2)}{dr}-\frac{Q^2}{\pi r^5}\right)+\frac{dQ^2}{dr}\frac{\eta}{2\pi r^5}\left[\frac{1}{p_0+\sigma_0}\frac{Q^2}{4\pi r^4}-1\right]$$
$$-\frac{\eta}{p_0+\sigma_0}\frac{1}{(2\pi r^4)^2}\left[\frac{Q^4}{r^2}+\frac{1}{16}\left(\frac{dQ^2}{dr}\right)^2\right]-\frac{5Q^2}{2\pi r^6}-\frac{1}{8\pi r^4}\frac{d^2}{dr^2}(Q^2)$$
$$+\frac{GQ_0^2}{c^4r^4}(p_0+\sigma_0)\eta e^{\lambda_0}+e^{-\lambda_0}\frac{d}{dr}\left(\frac{\alpha_1 Q_0\widetilde{Q}}{r^3}e^{\lambda_0/2}\right)+\frac{Q_0\widetilde{Q}}{r^3}\frac{d\nu_0}{dr}\left[\alpha_1+\frac{1}{4\pi}\right.$$
$$\left.+\frac{1}{4\pi r}\left(\frac{d\nu_0}{dr}-\frac{\eta}{r}\right)\right]+\frac{Q_0\delta Q}{8\pi r^4}\left(1-\frac{d\lambda_0}{dr}\right)+\frac{e^{\nu_0/2}}{4\pi}\frac{d}{dr}\left(\frac{Q_0\delta Q}{r^4}e^{-\nu_0/2}\right). \tag{2.1.41}$$

This is the required pulsation equation which satisfies the boundary conditions, i.e., $\eta=0$ at $r=0$ and $\delta p=0$ at $r=R$. This constitutes a characteristic value problem for ϱ^2 obtained by multiplying the equation with $\eta r^2 e^{(\lambda_0+\nu_0)/2}$ and integrating over values of r as

$$\varrho^2\int_0^R e^{(3\lambda-\nu)/2}r^2\eta^2(p+\sigma)dr=\int_0^R e^{(\lambda+3\nu)/2}\frac{p\Gamma}{r^2}\left[\frac{d}{dr}\left(r^2\eta e^{-\nu/2}\right)\right]^2dr$$
$$+\frac{8\pi G}{c^4}\int_0^R e^{(3\lambda+\nu)/2}pr^2\eta^2(p+\sigma)dr-\int_0^R\frac{r^2\eta^2}{p+\sigma}e^{(\lambda+\nu)/2}\left(\frac{dp}{dr}\right)^2dr$$
$$+4\int_0^R r\eta^2e^{(\lambda+\nu)/2}\frac{dp}{dr}dr+\int_0^R\frac{\eta^2}{p+\sigma}e^{(\lambda+\nu)/2}\frac{dp}{dr}\left(\frac{1}{4\pi}\frac{dQ^2}{dr}-\frac{Q^2}{\pi r^3}\right)dr$$
$$+\int_0^R\frac{\eta^2}{2\pi r^3}e^{(\lambda+\nu)/2}\frac{dQ^2}{dr}\left(\frac{1}{p+\sigma}\frac{Q^2}{4\pi r^4}-1\right)dr-\frac{5}{2\pi}\int_0^R\frac{\eta Q^2}{r^4}e^{(\lambda+\nu)/2}dr$$
$$-\int_0^R\frac{\eta^2}{p+\sigma}\frac{e^{(\lambda+\nu)/2}}{(2\pi r^3)^2}\left[\left(\frac{Q^2}{r}\right)^2+\frac{1}{16}\left(\frac{dQ^2}{dr}\right)^2\right]dr+\int_0^R\frac{GQ_0^2\eta^2}{c^4r^4}$$
$$\times(p+\sigma)e^{(3\lambda+\nu)/2}dr-\int_0^R\frac{\eta e^{(\lambda+\nu)}}{8\pi r^2}\frac{d^2}{dr^2}\left(Q^2\right)dr+\int_0^R r^2\eta e^{(\nu-\lambda)/2}$$
$$\times\frac{d}{dr}\left(\frac{\alpha_1Q_0\widetilde{Q}}{r^3}e^{\lambda_0/2}\right)dr+\int_0^R\frac{\eta Q_0\delta Q}{8\pi r^2}e^{(\nu+\lambda)/2}\left(1-\frac{d\lambda_0}{dr}\right)dr$$
$$+\int_0^R\frac{\eta Q_0\widetilde{Q}}{r}e^{(\nu+\lambda)/2}\frac{d\nu_0}{dr}\left[\alpha_1+\frac{1}{4\pi}+\frac{1}{4\pi r}\left(\frac{d\nu_0}{dr}-\frac{\eta}{r}\right)\right]dr$$

$$+\int_0^R \frac{\eta r^2}{4\pi} e^{(\nu+\lambda)/2} \frac{d}{dr}\left(\frac{Q_0 \delta Q}{r^4} e^{-\nu_0/2}\right) dr. \tag{2.1.42}$$

The corresponding orthogonality condition is defined as

$$\int_0^R e^{(3\lambda-\nu)/2} r^2 (p+\sigma)\eta^{(c_1)}\eta^{(c_2)} = 0, \quad (c_1 \neq c_2), \tag{2.1.43}$$

where $\eta^{(i)}$ and $\eta^{(j)}$ give proper solutions associated with different characteristic values of ϱ^2. To investigate dynamical instability of spherical star, the right-hand side of Eq.(2.1.42) should vanish by choosing a trial function ξ satisfying the given boundary conditions.

In the following, we discuss the conditions for dynamical instability by taking two special models.

The Homogeneous Model of Sphere

First we consider the homogeneous sphere with constant energy density and study the conditions for its dynamical instability. Equations (2.1.13) and (2.1.14) governing the hydrostatic equilibrium allow the integration [2] such that we can write

$$x^2 = 1 - \frac{r^2}{a_*^2} + \frac{b_*^2}{r^2}, \quad x_1^2 = 1 - \frac{R^2}{a_*^2} + \frac{b_*^2}{R^2}, \tag{2.1.44}$$

where $a_*^2 = \frac{3c^4}{8\pi G\sigma}$ and $b_*^2 = \frac{2GQ^2}{c^4}$. The solutions of the relevant physical quantities can be determined in terms of x and x_1 as

$$p = \sigma \frac{x - x_1}{3x_1 - x}, \quad e^{\nu} = \frac{1}{4}[3x_1 - x]^2, \quad e^{\lambda} = \frac{1}{x^2}. \tag{2.1.45}$$

The necessary condition for the positivity of pressure yields $3x_1 > 1$ which leads to

$$\frac{R^2}{a_*^2} - \frac{b_*^2}{R^2} < \frac{8}{9}.$$

Using the inertial mass, this takes the form

$$R > \frac{9}{8}\left(\frac{2GM}{c^2} - \frac{GQ^2}{Rc^4}\right) = \frac{9}{8}R_N, \tag{2.1.46}$$

where R_N is RN limiting radius. Inserting the physical quantities in Eq.(2.1.42), it follows that

$$\begin{aligned}
& 4a_*^2\varrho^2 x_1\int_0^{\xi_1}\frac{\xi^2\eta^2}{x^3(3x_1-x)^2}d\xi = x_1\int_0^{\xi_1}\frac{2x^2-9x_1^2-1}{x^3(3x_1-x)^2}\xi^2\eta^2 d\xi \\
+ \;& \frac{\Gamma}{8}\int_0^{\xi_1}(x-x_1)(3x_1-x)^2\frac{1}{x\xi}\left[\frac{d}{d\xi}(\eta\xi^2 e^{-\nu/2})\right]^2 d\xi + \frac{1}{16\pi a_*^3 x_1} \\
\times \;& \int_0^{\xi_1}\frac{\eta^2}{x\xi^2}\frac{dp}{d\xi}\left(\frac{dQ^2}{d\xi} - \frac{4Q^2}{\xi}\right)d\xi - \frac{5}{4\pi a_*^3}\int_0^{\xi_1}\frac{Q^2\eta}{\xi^4}\frac{3x_1-x}{x}d\xi \\
+ \;& \frac{1}{4\pi a_*^3}\int_0^{\xi_1}\frac{\eta^2(3x_1-x)}{x\xi^2}\left[\frac{Q^2(3x_1-x)}{8\pi a_*^4 x_1\xi^4} - 1\right]d\xi - \frac{1}{16\pi a_* x_1} \\
\times \;& \int_0^{\xi_1}\frac{\eta^2(3x_1-x)^2}{x(2\pi a_*^3\xi^3)^2}\left(\frac{dQ^2}{d\xi} - \frac{4Q^2}{\xi}\right)d\xi + \frac{Gx_1}{c^4}\int_0^{\xi_1}\frac{\eta^2 Q_0^2}{x^3\xi^2}d\xi \\
- \;& \frac{1}{32\pi a_*^3}\int_0^{\xi_1}\frac{\eta(3x_1-x)^2}{x^2\xi^2}\frac{d^2}{d\eta^2}(Q^2)d\xi + \frac{1}{2a_*}\int_0^{\xi_1}x(3x_1-x)\eta\xi^2 \\
\times \;& \frac{d}{d\xi}\left[\frac{\alpha_1 Q_0\widetilde{Q}}{\xi^3}e^{-\lambda/2}\right]d\xi + \frac{1}{2a_*^2}\int_0^{\xi_1}\frac{\eta Q_0\widetilde{Q}}{\xi}\frac{3x_1-x}{x}\frac{d\nu_0}{d\xi}\left[\alpha_1 + \frac{1}{4\pi\xi}\right. \\
\times \;& \left.\left(\frac{d\nu_0}{d\xi} - \frac{\eta}{\xi}\right)\right]d\xi + \frac{1}{16\pi a_*^2}\int_0^{\xi_1}\frac{\eta Q_0\delta Q}{\xi^2}\frac{3x_1-x}{x}\left(1 - \frac{1}{a_*}\frac{d\lambda_0}{d\xi}\right)d\xi \\
+ \;& \frac{1}{4\pi a_*^2}\int_0^{\xi_1}\frac{\eta\xi^2(3x_1-x)}{x}\frac{d}{d\xi}\left(\frac{Q_0\delta Q}{\xi^4(3x_1-x)}\right)d\xi,
\end{aligned} \tag{2.1.47}$$

where $\xi = \frac{r}{a_*}$, $\xi_1 = \frac{R}{a_*} - \frac{b_*}{R}$ and Γ is assumed to be constant.

We take the trial function as

$$\eta = \xi e^{\nu/2} = \frac{1}{2}\xi(x_1 - x), \tag{2.1.48}$$

for which Eq.(2.1.47) becomes

$$(a_*\varrho)^2 x_1\int_0^{\xi_1}\frac{\xi^4}{x^3}d\xi = \frac{1}{4}x_1\int_0^{\xi_1}(2x^2 - 1 - 9x_1^2)\frac{\xi^4}{x^3}d\xi + \frac{9}{8}\int_0^{\xi_1}(x - x_1)$$

$$\times \quad (3x_1-x)^2\frac{\xi^2}{x}d\xi+\frac{1}{4a_*^3xx_1}\int_0^{\xi_1}(3x_1-x)^4\left(-\frac{Q^2}{\pi\xi}\right)\frac{d}{d\xi}\left(\frac{x-x_1}{3x_1-x}\right)d\xi$$
$$- \quad \frac{1}{(4\pi a_*^3)^2x_1}\int_0^{\xi_1}\frac{(3x_1-x)^2}{x}\left(\frac{Q^2}{\xi}\right)^2d\xi+\frac{Gx_1}{4c^4}\int_0^{\xi_1}Q_0^2\frac{(3x_1-x)^2}{\xi x^3}d\xi$$
$$- \quad \frac{5}{8\pi a_*^3}\int_0^{\xi_1}\frac{Q^2(3x_1-x)^2}{x\xi^3}d\xi+\frac{1}{4a_*}\int_0^{\xi_1}x\xi^3(3x_1-x)\frac{d}{d\xi}\left(\frac{3Q_0\widetilde{Q}}{x\xi^3}\right)d\xi$$
$$+ \quad \frac{1}{32\pi a_*^2}\int_0^{\xi^1}\frac{Q_0\delta Q}{x\xi}(3x_1-x)^2d\xi+\frac{1}{8\pi a_*^2}\int_0^{\xi_1}\frac{\xi^3}{x}(3x_1-x)^2$$
$$\times \quad \frac{d}{d\xi}\left(\frac{Q_0\delta Q}{(3x_1-x)\xi^4}\right)d\xi. \tag{2.1.49}$$

Substituting $x=\cos\theta$ and $\xi=\sin\theta$ in the above equation, we obtain

$$(a_*\varrho)^2\cos\theta_1\int_0^{\theta_1}\frac{\sin^4\theta}{\cos^2\theta}d\theta=\frac{\cos\theta_1}{4}\int_0^{\theta_1}(2\cos^2\theta-1-9\cos^2\theta_1)\frac{\sin^4\theta}{\cos^2\theta}d\theta$$
$$+ \quad \frac{9}{8}\Gamma\int_0^{\theta_1}(\cos\theta-\cos\theta_1)(3\cos\theta_1-\cos\theta)^2\sin^2\theta d\theta-\frac{1}{4a_*^3\cos\theta_1}$$
$$\times \quad \int_0^{\theta_1}\frac{(3\cos\theta_1-\cos\theta)^3}{\cos\theta}\frac{Q^2}{\pi\sin\theta}\frac{d}{d\theta}\left(\frac{\cos\theta-\cos\theta_1}{3\cos\theta_1-\cos\theta}\right)d\theta-\frac{1}{a(4\pi a_*^3)^2\cos\theta_1}$$
$$\times \quad \int_0^{\theta_1}(3\cos\theta_1-\cos\theta)^2\left(\frac{Q^2}{\sin\theta}\right)^2d\theta+\frac{G\cos\theta_1}{4c^4}\int_0^{\theta_1}(3\cos\theta_1-\cos\theta)^2$$
$$\times \quad \frac{Q_0^2}{\sin\theta\cos^2\theta}d\theta-\frac{5Q^2}{8\pi a_*^3}\int_0^{\theta_1}\frac{(3\cos\theta_1-\cos\theta)^2}{\sin^3\theta}d\theta, \tag{2.1.50}$$

where $\theta_1=\sin^{-1}\left(\frac{R}{a_*}-\frac{b_*}{R}\right)$. Solving the integrals and setting $\varrho^2=0$, we obtain exact condition for marginal stability. The values of Γ_1 (corresponding to θ_1) are found such that Γ should be less than certain Γ_1 for the existence of dynamical instability. In Newtonian limit, Γ takes finite values for marginal stability, i.e., $\Gamma>\frac{4}{3}+\frac{8Q^2}{21}$. We calculate the radii of marginal stability and Γ for homogeneous model of gaseous sphere by taking different values of charge which show finite values of Γ. We observe that radius $\frac{R}{R_N}\to\infty$ for $\Gamma<0$ which leads to the expansion while $\frac{R}{R_N}$ remains positive for $\Gamma>0$ showing marginal stability of gaseous model. The corresponding results are given in Table **2.1**.

Table 2.1: Adiabatic Index and Radii for Dynamical Stability of Homogeneous Sphere

θ_1	R/R_N	Γ_1 for $Q=0.2$	Γ_1 for $Q=0.6$
0^o	∞	-0.0182	-0.1622
10^o	33.163	0.1127	0.1776
20^o	8.549	0.1275	0.2278
25^o	5.598	0.1319	0.3192
30^o	4.000	0.3766	1.2643
35^o	3.0396	3246.43	1970.41
40^o	2.4203	5918.49	2527.00
50^o	1.704	6594.94	4352.86
60^o	1.333	6822.02	5631.08

When $\varrho^2 < 0$, the perturbation diverges exponentially either by expansion or contraction which yields stellar dynamical instability. In the limit $\theta_1 \to 0$, the condition for dynamical instability is

$$\Gamma - \frac{4}{21}\left(4Q^2+7\right) < \frac{14}{43}\theta_1^2 = \frac{14}{43}\left[\frac{R^2}{a_*^2} - \frac{b_*^2}{R^2}\right]. \tag{2.1.51}$$

In terms of inertial mass, this takes the form

$$R < \frac{14}{43\left[\Gamma - \frac{4}{21}\left(4Q^2+7\right)\right]}\left[\frac{2GM}{c^2} - \frac{GQ^2}{Rc^4}\right], \tag{2.1.52}$$

which can be written as

$$\frac{R}{R_N} < \frac{K}{\left[\Gamma - \frac{4}{21}\left(4Q^2+7\right)\right]}, \tag{2.1.53}$$

where $K = \frac{14}{43}$ for the homogeneous sphere. This means that if Γ exceeds $\frac{4}{3} + \frac{8Q^2}{21}$ by a small amount, the dynamical instability can be prevented till the mass contracts to the RN radius. If the radius of gaseous mass is greater than R_N, it remains stable. The ranges for instability of homogeneous spherical system are shown in Figure **2.1**. Since the radius of stability is a factor of the RN radius, so the ratio $\frac{R}{R_N}$ should be greater than or equal to zero for physical results. We consider different values of

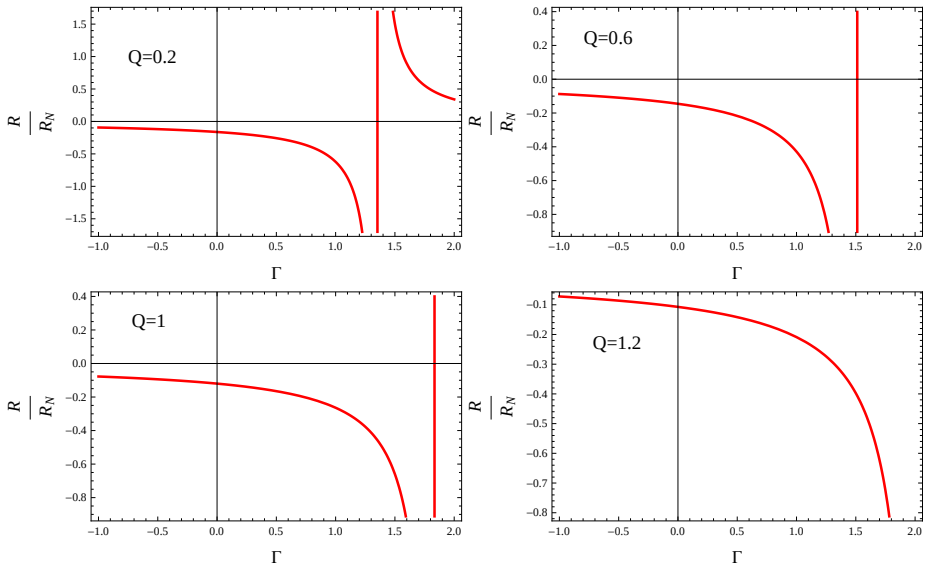

Figure 2.1: Plots of $\frac{R}{R_N}$ for dynamical stability/instability of homogeneous sphere corresponding to different values of Q.

charge and find that $0.1 < Q < 0.4$ and $\Gamma > 1.5$ provide valid radii ranges for the stability of sphere. For $\Gamma < 1.5$, we only have unstable radii along with non-physical region corresponding to $Q > 0.4$. Also, we observe that the gaseous sphere becomes unstable for larger values of charge, i.e., $Q > 1.2$. It is obvious from the graph that the radius of stability is greater than R_N for $\Gamma > \frac{4}{3} + \frac{8Q^2}{21}$.

Relativistic Polytropic Model

In relativistic polytropic models, pressure and energy density can be expressed in terms of a single function Θ_1 as [21]

$$p = p_c\Theta_1^{n+1}, \quad \sigma = \sigma_c\Theta_1^n, \tag{2.1.54}$$

where p_c and σ_c represent respective values at center and n denotes the polytropic index. The polytropic models are the generalized form of the classical Lane-Emden

equation which can be obtained from the equations of hydrostatic equilibrium. Let

$$\xi = \frac{r}{\bar{a}}, \tag{2.1.55}$$

where $\bar{a} = \left(\frac{s(n+1)c^4}{4\pi G\sigma_c}\right)^{\frac{1}{2}}$ and $s = \frac{p_c}{\sigma_c}$. We can reduce Eqs.(2.1.13) and (2.1.14) to the pair of equations which express Θ_1 as a function of ξ

$$\left(\frac{\xi^2}{1+s\Theta_1} - \frac{c^2Q^2s(n+1)}{32\pi G\sigma_c}\right)\left(1 - \frac{2Vs(n+1)}{\xi} + \frac{Q^2Vs(n+1)}{\xi M}\right)\frac{d\Theta_1}{d\xi}$$
$$+V - \frac{Q^2V}{M} + s\Theta_1\frac{dV}{d\xi} = 0, \tag{2.1.56}$$

$$\frac{dV}{d\xi} = \xi\Theta_1^n. \tag{2.1.57}$$

We assume pN approximation of the form

$$\Theta_1 = \tilde{\theta} + s\varphi, \tag{2.1.58}$$

where φ is an arbitrary function, $\tilde{\theta}$ represents classical Lane-Emden function and s is treated as a small constant. Using Eqs.(2.1.56) and (2.1.57), the classical Lane-Emden equation becomes

$$\frac{d^2\tilde{\theta}}{d\xi^2} + \frac{2}{\xi}\frac{d\tilde{\theta}}{d\xi} + \left(1 - \frac{Q^2}{M}\right)\tilde{\theta}^n = \frac{c^2Q^2}{32\pi G\sigma_c}. \tag{2.1.59}$$

Equation (2.1.42) in terms of Θ_1 and ξ takes the form

$$\frac{(\bar{a}\varrho)^2}{s}\int_0^{\xi_1}\Theta_1^n(1+s\Theta_1)\xi^2\eta^2e^{(3\lambda-\nu)/2}d\xi = 2(n+1)s\int_0^{\xi_1}\Theta_1^{(2n+1)}(1+s\Theta_1)$$
$$\times\xi^2\eta^2e^{(3\lambda+\nu)/2}d\xi + 4(n+1)\int_0^{\xi_1}\Theta_1^n\xi\eta^2e^{(\lambda+\nu)/2}\left(1 - \frac{s\xi(n+1)}{4(1+s\Theta_1)}\right)d\xi$$
$$+\Gamma\int_0^{\xi_1}\frac{\Theta_1^{n+1}}{\xi^2}e^{(\lambda+3\nu)/2}\left(\frac{d}{d\xi}\left[\eta\xi^2e^{-\nu/2}\right]\right)^2d\xi + \left(\frac{1}{2\pi\bar{a}^3}\right)^2\int_0^{\xi_1}\frac{e^{(\lambda+\nu)/2}}{\Theta_1^n(1+s\Theta_1)}$$
$$\times\left(\frac{\eta Q}{\xi^4}\right)^2\left[\frac{\xi}{2\bar{a}} - Q^2\right]d\xi - \frac{1}{2\pi\bar{a}^3}\int_0^{\xi_1}\frac{\eta^2}{\xi^3}e^{(\lambda+\nu)/2}\left[1 + \frac{s(n+1)Q^2}{1+s\Theta_1}\frac{d\Theta_1}{d\xi}\right.$$

$$-\frac{GQ_0^2}{\xi^4}\Bigg]\,d\xi+\frac{1}{4\pi}\int_0^{\xi_1}\frac{\eta^2}{1+s\Theta_1}e^{(\lambda+\nu)/2}\frac{dQ^2}{d\xi}\left[s\frac{d\Theta_1}{d\xi}-\frac{1}{\Theta_1^n\left(\bar{a}^3\xi^3\right)\frac{dQ^2}{d\xi}}\right]d\xi$$
$$-\frac{1}{8\pi\bar{a}^3}\int_0^{\xi_1}\frac{\eta}{\xi^2}e^{(\lambda+\nu)}\frac{d^2}{dr^2}\left(Q^2\right)d\xi+\int_0^{\xi_1}\xi^2\eta e^{(\nu-\lambda)/2}\frac{d}{d\xi}\left[\frac{\beta Q_0\widetilde{Q}e^{\lambda_0}}{\bar{a}\xi^3}\right]d\xi$$
$$+\frac{1}{4\pi\bar{a}^2}\int_0^{\xi_1}\xi^2\eta e^{(\nu+\lambda)/2}\frac{d}{d\xi}\left(\frac{Q_0\delta Q e^{-\nu/2}}{\xi^4}\right)d\xi. \tag{2.1.60}$$

The pN approximation treats the effects of GR as first order corrections. We can write

$$\Gamma_1-\frac{4}{21}(4Q^2+7)=Cs, \tag{2.1.61}$$
$$R_1=\frac{K}{\Gamma_1-\frac{4}{21}(4Q^2+7)}\left[\frac{2GM}{c^2}-\frac{GQ^2}{Rc^4}\right], \tag{2.1.62}$$

where C and K are constants depending on density distribution. The pN approximation yields

$$e^{-\lambda} = 1+2s(1+n)\xi\frac{d\tilde{\theta}}{d\xi}-\frac{GQ^2(1+n)s}{M}\frac{d\tilde{\theta}}{d\xi}, \tag{2.1.63}$$
$$e^{\nu} = 1-2s(1+n)[\tilde{\theta}+\xi_1|\tilde{\theta}_1|]+\frac{Q^2(1+n)s|\tilde{\theta}_1|}{M}, \tag{2.1.64}$$

where $|\tilde{\theta}_1|=-\left(d\tilde{\theta}/d\xi\right)_{\xi=\xi_1}$. Using the relations of p_c and σ_c for polytropes in terms of M, Q and R, it follows that

$$s=\frac{1}{2(n+1)\xi_1|\tilde{\theta}_1|}\left[\frac{2GM}{Rc^2}-\frac{GQ^2}{R^2c^4}\right]. \tag{2.1.65}$$

We calculate Γ for the emergence of dynamical instability corresponding to different values of Q. The numerical values of Γ for the polytropes of index 3 are given in Table **2.2**. Similarly, the constants C and K for polytropes are given by the relation

$$K=\frac{C}{2(n+1)\xi_1|\tilde{\theta}_1|}. \tag{2.1.66}$$

Table 2.2: Adiabatic Index with Different Values of Charge for Dynamical Instability of Polytropes with Index 3

s	Γ_1 for $Q=0.2$	Γ_1 for $Q=0.4$	Γ_1 for $Q=0.6$
0.015	1.3500	1.3593	1.4715
0.040	1.3527	1.3983	1.4744
0.1	1.3586	1.4043	1.4805
0.2	1.3686	1.4143	1.4905
0.5	1.3953	1.4440	1.5204

Table 2.3: Values of Constants C and K with Different Values of Charge for Polytropes of Index 0

C	K for $Q=0.2$	K for $Q=0.4$	K for $Q=0.6$
0.243	0.6458	0.6372	0.576
0.826	2.1953	2.1662	1.9608
1.205	3.2034	3.161	2.8612
1.8095	4.809	4.745	4.296

In order to determine the radii from Eq.(2.1.62), we need to calculate K whose value depends upon the polytropic index, Lane-Emden function and charge. Different polytropic indices lead to different stellar structures such that the configurations with $n<5$ are considered to be realistic stars [83]. For $n=0$, we solve the Lane-Emden equation analytically to find the values of $\tilde{\theta}$ corresponding to different values of Q but we solve this equation numerically for $n=2,3,4$ as shown in Figures **2.2-2.3**. The values of constants C and K for $n=0$ are given in Table **2.3**. We see that the values of K decrease gradually by increasing the value of charge.

Inserting the values of e^{ν} and $e^{-\lambda}$ in Eq.(2.1.60) and neglecting second as well as higher order terms in s, we obtain

$$\frac{(\bar{a}\varrho)^2}{s}\left\{\int_0^{\xi_1}\tilde{\theta}^n\xi^2\eta^2 d\xi+\int_0^{\xi_1}H(\xi)\tilde{\theta}^{n-1}\xi^2\eta^2 d\xi\right\}=\Gamma s(n+1)\int_0^{\xi_1}\frac{\tilde{\theta}^{n+1}}{\xi^2}$$

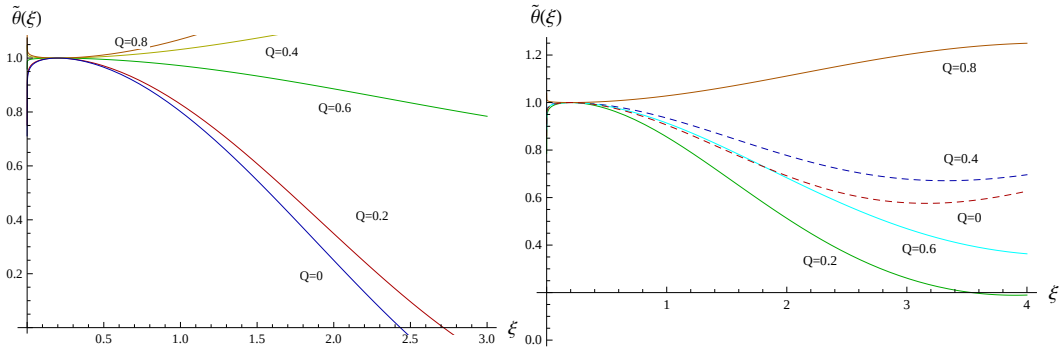

Figure 2.2: Plots of classical Lane-Emden function for polytropes of index $n = 1, 2$ corresponding to different values of charge.

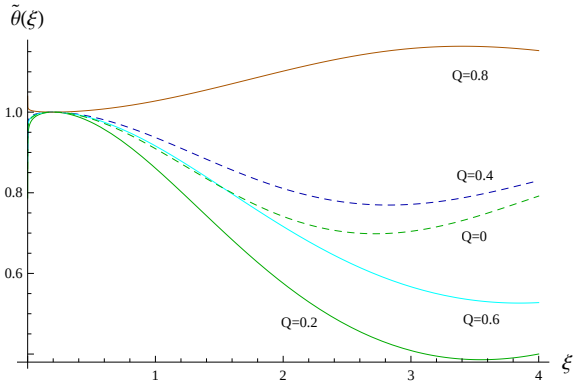

Figure 2.3: Plots of classical Lane-Emden function for $n = 3$ corresponding to different values of charge.

$$\times\left\{\left(\frac{GQ^2}{2M}-\xi\right)+3|\tilde{\theta}_1|\left(\frac{Q^2}{2M}-\xi_1\right)-3\tilde{\theta}\right\}\left[\frac{d}{d\xi}(\xi^2\eta)\right]^2 d\xi+\Gamma\int_0^{\xi_1}H(\xi)$$
$$\times\frac{\tilde{\theta}^{n+1}}{\xi^2}\left\{\frac{d}{d\xi}\left(\xi^2\eta\right)\right\}^2 d\xi+s(n+1)\int_0^{\xi_1}I(\xi)\tilde{\theta}^{n-1}\xi\eta^2 d\xi+s(n+1)\int_0^{\xi_1}\frac{d\tilde{\theta}}{d\xi}$$
$$\times\left[\left(\frac{GQ^2}{2M}-\xi\right)+|\tilde{\theta}_1|\left(\frac{Q^2}{2M}-\xi_1\right)-\tilde{\theta}\right]S(\xi)d\xi+s(n+1)\int_0^{\xi_1}\tilde{\theta}^{n+1}\xi^2\eta^2$$
$$\times U(\xi)d\xi+\frac{1}{(2\pi)^2}\int_0^{\xi_1}\frac{\eta^2Q^2}{(\bar{a}^3\xi^2)^3}\left[\frac{\xi}{2\bar{a}}-Q^2\right]d\xi-\frac{1}{8\pi}\int_0^{\xi_1}\frac{\eta}{\bar{a}^3\xi^2}\frac{d^2}{d\xi^2}(Q^2)d\xi$$
$$-\frac{1}{2\pi}\int_0^{\xi_1}\frac{GQ^2}{\bar{a}^3\xi^4}d\xi+\int_0^{\xi_1}\xi^2\eta\frac{d}{d\xi}\left(\frac{\alpha_1Q_0\widetilde{Q}}{\bar{a}\xi^3}\right)d\xi, \tag{2.1.67}$$

where

$$\begin{aligned}
H(\xi) &= 2\tilde{\theta}^2(n+2)+3(n+1)\left(\frac{GQ^2}{2M}-\xi\right)\frac{d\tilde{\theta}}{d\xi}+\left(2\xi_1-\frac{Q^2}{2M}\right)\\
&\times\ (n+1)|\tilde{\theta}_1|, &(2.1.68)\\
I(\xi) &= -4\theta(n+1)\frac{d\tilde{\theta}}{d\xi}\left[-\xi\frac{d\tilde{\theta}}{d\xi}-\tilde{\theta}-\xi|\tilde{\theta}_1|+\frac{Q^2}{2M}\left(G\frac{d\tilde{\theta}}{d\xi}+|\tilde{\theta}_1|\right)\right], &(2.1.69)\\
S(\xi) &= \frac{\eta^2Q^2}{2\pi^2(\bar{a}^3\xi^2)^2}\left(\frac{\xi}{2\bar{a}}-Q^2\right)-\frac{\eta^2}{2\pi\bar{a}^3\xi^3}+\frac{GQ_0^2}{2\pi\bar{a}^3\xi^4}-\frac{\eta}{4\pi\bar{a}^3\xi^2}\\
&\times\ \frac{d^2}{d\xi^2}(Q^2)+\xi^2\eta\frac{d}{d\xi}\left\{\frac{\alpha_1Q_0\widetilde{Q}}{\bar{a}\xi^3}+\eta\xi^2\frac{d}{d\xi}\left(\frac{Q_0\delta Q}{\xi^4}\right)\right\}, &(2.1.70)\\
U(\xi) &= 3\tilde{\theta}\left(\frac{Q^2}{2M}-\xi\right)\frac{d\tilde{\theta}}{d\xi}+\tilde{\theta}|\tilde{\theta}_1|\left(\frac{Q^2}{2M}-2\xi_1\right)-2\tilde{\theta}^2. &(2.1.71)
\end{aligned}$$

In pN approximation, we are interested to find the condition for marginal stability of polytropic configuration by taking $\eta=\xi$ and $\varrho^2=0$ so that Eq.(2.1.67) takes the form

$$9\left(\Gamma-\frac{4}{3}-\frac{8Q^2}{21}\right)\int_0^{\xi_1}\tilde{\theta}^{n+1}\xi^2d\xi+s(n+1)\left[3\int_0^{\xi_1}\tilde{\theta}^nS(\xi)\widetilde{S}(\xi)d\xi\right.$$
$$\left.+\int_0^{\xi_1}\tilde{\theta}^{n-1}I(\xi)\xi^3d\xi+\int_0^{\xi_1}\tilde{\theta}^{n+1}\xi^4U(\xi)d\xi\right]+\frac{1}{8\pi}\int_0^{\xi_1}\frac{\widetilde{U}(\xi)}{\bar{a}^3\xi^3}d\xi$$
$$+\int_0^{\xi_1}\xi^3\frac{d}{d\xi}\left(\frac{\alpha_1Q\widetilde{Q}}{\bar{a}\xi^3}\right)d\xi=0, \tag{2.1.72}$$

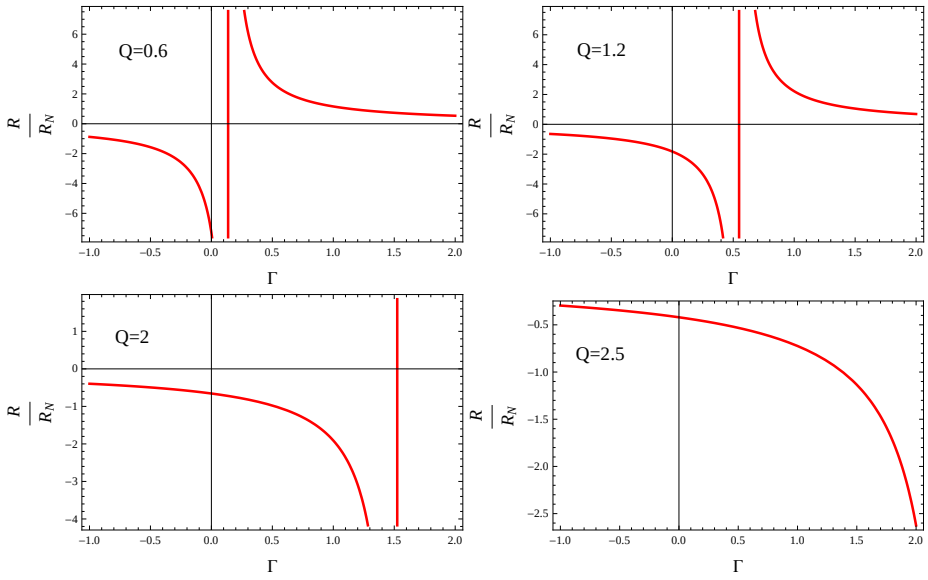

Figure 2.4: Plots for radii of stability/instability corresponding to $n = 1$ and different values of charge.

with

$$\widetilde{S}(\xi) = \left(3\Gamma\xi^2\tilde{\theta} + \tilde{\theta}^{-n}\right)\left\{\frac{d\tilde{\theta}}{d\xi}\left(\frac{GQ^2}{2M} - \xi\right) + 3|\tilde{\theta}_1|\left(\frac{Q^2}{2M} - \xi_1\right) - 3\tilde{\theta}\right\} \quad (2.1.73)$$

$$\widetilde{U}(\xi) = 4Q^2\left(G + \frac{\xi}{2M} - Q^2\right) - \xi^3\left(1 + \frac{d^2}{d\xi^2}(Q^2)\right). \quad (2.1.74)$$

In pN limit, the dynamical stability will require that $\Gamma > \Gamma_1 = \frac{4}{3} + \frac{8Q^2}{21} + \epsilon$, where ϵ is a small quantity depending on s. To check the conditions for marginal stability as well as dynamical instability, we calculate the values of K and plot different radii corresponding to polytropic indices $n = 1, 2, 3$ as shown in Figures **2.4-2.6**. It is found that K attains negative values for $n = 1, 2, 3$, so we take both positive and negative values of Γ to obtain physically viable values of radii. Figures **2.4** and **2.5** show viable radii for $\Gamma > \frac{4}{3} + \frac{8Q^2}{21}$ corresponding to $n = 1, 2$. For $n = 1$, we find that radii of stability along with non-physical region appear for $Q = 0.6$ and positive

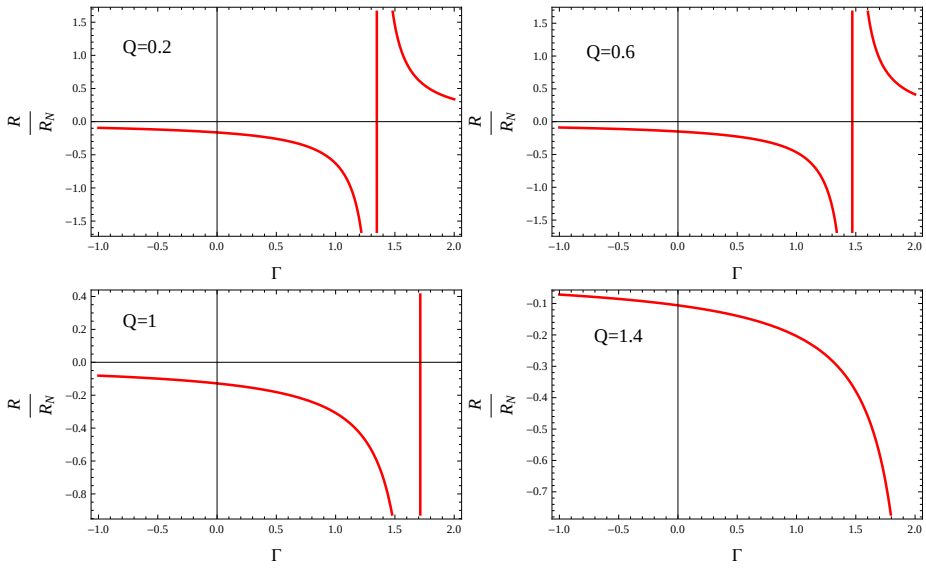

Figure 2.5: Plots for radii of stability/instability corresponding to $n = 2$ and different values of charge.

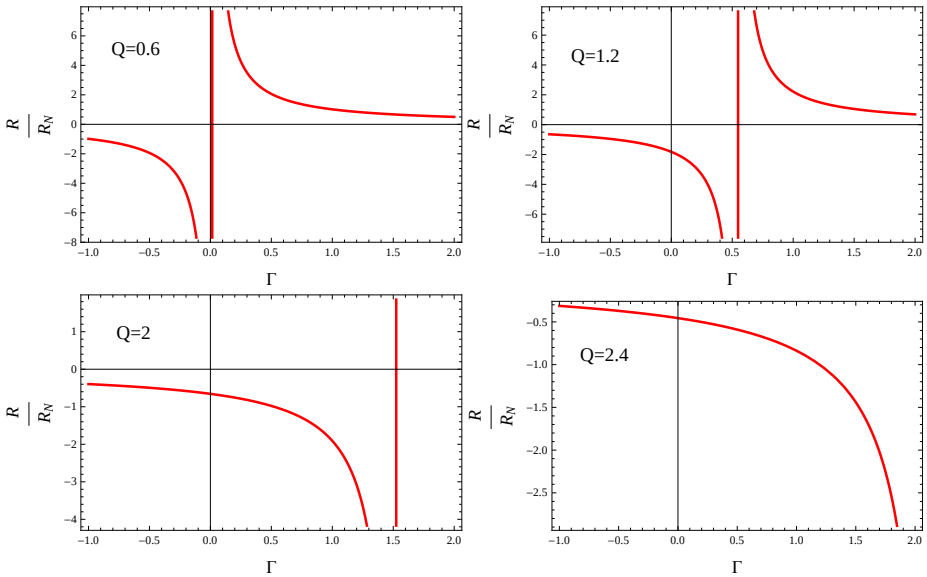

Figure 2.6: Plots for radii of stability/instability corresponding to $n = 3$ and different values of charge.

values of Γ while negative values of Γ show the emergence of instability. The region of instability gets larger by increasing Q for both positive as well as negative values of Γ and the radii of marginal stability vanishes for $Q = 2$. We observe that the corresponding polytropic model becomes unstable for $Q > 2.4$ (Figure **2.4**).

For $n = 2$, we analyze stable radii for $1.5 < \Gamma < 2$ and unstable radii for small values of Γ (both positive and negative) corresponding to $Q < 1$. The stability radius tends to decrease which leads to unstable region for $Q = 1$. We find that the non-physical region disappears and the polytropic model will remain unstable with $Q \geq 1.4$ (Figure **2.5**). For $n = 3$, we have viable ranges for radii with $0 < \Gamma < 2$, i.e., Γ can be less than $\frac{4}{3} + \frac{8Q^2}{21}$ for stable stellar structures (Figure **2.6**). We find both stable and unstable radii for polytropic model with $0.1 < Q < 2$ which changes to unstable radii for $Q \geq 2$. The dynamical instability occurs when gaseous mass contracts to R_N.

2.2 Charged Cylindrical Gaseous Models

Here we extend the analysis of dynamical instability for charged dissipative cylinder.

2.2.1 Cylindrical System and the Field Equations

We consider a cylindrically symmetric system in the interior region given by

$$ds^2 = -W^2(t,r)dt^2 + X^2(t,r)dr^2 + Y^2(t,r)d\theta^2 + dz^2, \tag{2.2.1}$$

where the following restrictions on coordinates are taken to preserve symmetry

$$-\infty < t < \infty, \quad 0 \leq r < \infty, \quad 0 \leq \theta \leq 2\pi, \quad -\infty < z < \infty.$$

The corresponding Einstein field equations are given by

$$\frac{8\pi G}{c^4}T_0^0 = \frac{1}{X^2}\left\{\frac{Y''}{Y}-\frac{X'Y'}{XY}\right\}-\frac{\dot{X}\dot{Y}}{W^2XY}, \tag{2.2.2}$$

$$\frac{8\pi G}{c^4}T_1^1 = \frac{1}{W^2}\left\{\frac{\dot{W}\dot{Y}}{WY}-\frac{\ddot{Y}}{Y}\right\}+\frac{W'Y'}{WX^2Y}, \tag{2.2.3}$$

$$\frac{8\pi G}{c^4}T_2^2 = \frac{1}{WX}\left\{\frac{W''}{X}-\frac{\ddot{X}}{W}+\frac{\dot{W}\dot{X}}{W^2}-\frac{W'X'}{X^2}\right\}, \tag{2.2.4}$$

$$\begin{aligned}\frac{8\pi G}{c^4}T_3^3 &= \frac{W''}{WX^2}-\frac{\ddot{X}}{W^2X}+\frac{\dot{W}\dot{X}}{W^3X}-\frac{W'X'}{WX^3}+\frac{\dot{W}\dot{Y}}{W^3Y}-\frac{\ddot{Y}}{W^2Y}\\ &- \frac{X'Y'}{X^3Y}+\frac{Y''}{X^2Y}+\frac{W'Y'}{WX^2Y}-\frac{\dot{X}\dot{Y}}{W^2XY},\end{aligned} \tag{2.2.5}$$

$$\frac{8\pi G}{c^4}T_0^1 = \frac{1}{X^2}\left\{\frac{W'\dot{Y}}{WY}+\frac{\dot{X}Y'}{XY}-\frac{\dot{Y}'}{Y}\right\}, \tag{2.2.6}$$

where prime denotes derivative with respect to r. The matter source is assumed to be locally charged dissipative perfect fluid defined by

$$T_j^i = (\sigma+p)u^iu_j+p\delta_j^i+q^iu_j+q_ju^i+\frac{1}{4\pi}[F_{jk}F^{ik}-\frac{1}{4}\delta_j^iF_{kl}F^{kl}], \tag{2.2.7}$$

where q^i represents radial heat flux satisfying $q_iu^i=0$.

The conservation equation for four current yields

$$Q(t,r) = 4\pi\int_0^r \rho XY dr,$$

which is the total amount of charge within cylinder. We define the electric field intensity as

$$\bar{E}(t,r) = \frac{Q(r)}{2\pi Y}. \tag{2.2.8}$$

The conservation of energy-momentum tensor leads to the following relations

$$\frac{\partial T_0^0}{\partial t}+\frac{\partial T_1^0}{\partial r}+\frac{\dot{X}}{X}\left(T_0^0-T_1^1\right)+T_0^1\left(\frac{X'}{X}+\frac{W'}{W}\right)=0, \tag{2.2.9}$$

$$\frac{\partial T_1^0}{\partial t}+\frac{\partial T_1^1}{\partial r}+\frac{W'}{W}\left(T_1^1-T_0^0\right)+\left(\frac{\dot{W}}{W}+\frac{\dot{X}}{X}\right)T_1^0=0, \tag{2.2.10}$$

where $T_0^1=-\frac{W^2}{X^2}T_1^0$. The components of energy-momentum tensor are

$$T_0^0=-\sigma+\frac{\pi}{2}\bar{E}^2, \quad T_1^1=p+\frac{\pi}{2}\bar{E}^2, \quad T_2^2=T_3^3=p-\frac{\pi}{2}\bar{E}^2.$$

In hydrostatic equilibrium, all the quantities governing motion remain time independent. In this context, Eqs.(2.2.2), (2.2.3) and (2.2.10) become

$$\frac{d}{dr}\left(\frac{Y_0'}{X_0}\right) = \frac{8\pi G}{c^4}X_0Y_0\left(-\sigma_0+\frac{\pi\bar{E}^2}{2}\right), \tag{2.2.11}$$

$$\frac{dW_0}{dr}\frac{dY_0}{dr} = \frac{8\pi G}{c^4}W_0X_0^2C_0\left(p_0+\frac{\pi\bar{E}^2}{2}\right), \tag{2.2.12}$$

$$(\sigma_0+p_0)\frac{dW_0}{dr} = -W_0\frac{d}{dr}\left(p_0+\frac{\pi\bar{E}^2}{2}\right). \tag{2.2.13}$$

We also have a useful relation through Eqs.(2.2.2) and (2.2.3) given by

$$\frac{8\pi G}{c^4}(p_0+\sigma_0)=\frac{1}{W_0Y_0}\left\{\frac{1}{X_0^2}\frac{dW_0}{dr}\frac{dY_0}{dr}\right\}-\frac{1}{X_0Y_0}\left\{\frac{d}{dr}\left(\frac{Y_0'}{X_0}\right)\right\}. \tag{2.2.14}$$

We take the exterior region for cylindrically symmetric spacetime in retarded time coordinate $\wp$ defined as

$$ds^2=-\left(-\frac{2GM}{Rc^2}+\frac{GQ^2}{R^2c^4}\right)d\wp^2-2d\wp dR+R^2(d\theta^2+h^2dz^2), \tag{2.2.15}$$

where h is an arbitrary constant. We choose the Schwarzschild coordinate as $Y=r$ [82]. Thorne [14] defined C-energy for cylindrically symmetric spacetime in the form of mass function given by

$$m(r)=\frac{1}{8}\left[1-\frac{1}{X_0^2}\right]+2\pi^2r\bar{E}^2. \tag{2.2.16}$$

Differentiating this equation and using Eq.(2.2.3), we have

$$\frac{dm}{dr}=\frac{2\pi rG}{c^4}\sigma_0-\frac{r\pi^2G\bar{E}^2}{c^4}+\frac{d}{dr}(2\pi^2r\bar{E}^2), \tag{2.2.17}$$

whose integration leads to

$$m(r)=\frac{2\pi G}{c^4}\int_0^r r\sigma_0 dr-\frac{G}{4c^4}\int_0^r\frac{Q^2}{r}dr+\frac{Q^2}{2r}. \tag{2.2.18}$$

The equation for hydrostatic equilibrium can be obtained as

$$\frac{dp_0}{dr}+\frac{G(8\pi r^2p_0+Q^2)}{rc^4(1-8m+4Q^2)}-\frac{rQQ'-Q^2}{4\pi r^3}=0. \tag{2.2.19}$$

2.2.2 Radial Oscillations and Dynamical Equations

In this section, we study dynamical characteristics of gaseous mass undergoing radial oscillations. The non-vanishing components of four velocity can be written as

$$u^0=\frac{1}{W_0},\quad u_0=-W_0,\quad u^1=\frac{v}{W_0},\quad u_1=\frac{X_0^2}{W_0}v. \tag{2.2.20}$$

We perturb an equilibrium configuration in such a way that its cylindrical symmetry does not change. The perturbed state with linear terms yields

$$\begin{aligned} W &= W_0+\delta W,\quad X=X_0+\delta X,\quad p=p_0+\delta p,\quad \sigma=\sigma_0+\delta\sigma,\\ Q &= Q_0+\delta Q,\quad q=q_0+\delta q. \end{aligned} \tag{2.2.21}$$

Using Eulerian approach for perturbations, Eqs.(2.2.11) and (2.2.12) turn out to be

$$\frac{1}{r}\frac{\partial}{\partial r}\left(\frac{\delta X}{X_0^3}\right)=\frac{8\pi G}{c^4}\left(\delta\sigma-\frac{Q_0\delta Q}{4\pi r^2}\right), \tag{2.2.22}$$

$$\frac{8\pi G}{c^4}\left(\delta p+\frac{Q_0\delta Q}{4\pi r^2}\right)=\frac{1}{rW_0X_0^2}\frac{\partial}{\partial r}\left(\frac{\partial}{\partial r}\delta W-\frac{2\delta X}{X_0}\frac{dW_0}{dr}\right), \tag{2.2.23}$$

where δW, δX, $\delta\sigma$, δp and δQ define the Eulerian changes. The linearized form of Eqs.(2.2.6) and (2.2.10) can be appropriately written as

$$\frac{1}{rX_0^3}\frac{\partial}{\partial t}\delta X=-\frac{8\pi G}{c^4}\left[(p_0+\sigma_0)v+\delta q\right], \tag{2.2.24}$$

$$(p_0+\sigma_0)\left(\frac{X_0}{W_0}\right)^2\frac{\partial v}{\partial t}+\frac{\partial}{\partial r}\delta p+\frac{1}{W_0}(p_0+\sigma_0)\frac{\partial}{\partial r}\delta W$$
$$+\frac{1}{W_0}(\delta p+\delta\sigma)\frac{dW_0}{dr}+\frac{1}{4\pi r^2}\frac{\partial}{\partial r}(Q_0\delta Q)-\frac{1}{2\pi r^3}Q_0\delta Q$$
$$+[(p_0+\sigma_0)v-q_0]\left(\frac{X_0}{W_0}\right)^2\left[\frac{1}{W_0}\frac{\partial}{\partial t}\delta W+\frac{1}{X_0}\frac{\partial}{\partial t}\delta X\right]=0. \qquad (2.2.25)$$

Integration of Eq.(2.2.24) through the Lagrangian displacement gives

$$\frac{1}{X_0^3 r}\delta X=-\frac{8\pi G}{c^4}(p_0+\sigma_0)\eta+\int\delta q dt, \qquad (2.2.26)$$

which leads to

$$-\frac{1}{X_0}\delta X=\frac{1}{W_0}\frac{dW_0}{dr}+\frac{1}{X_0}\frac{dX_0}{dr}. \qquad (2.2.27)$$

Solving Eqs.(2.2.22) and (2.2.26), we have

$$\delta\sigma=-\eta\frac{d\sigma_0}{dr}-\eta\frac{dp_0}{dr}-\frac{1}{r}(p_0+\sigma_0)\frac{\partial}{\partial r}(r\eta)+\frac{Q_0}{4\pi r^2}\delta Q, \qquad (2.2.28)$$

which, in accordance with Eq.(2.2.13), yields

$$\begin{aligned}\delta\sigma &= -\eta\frac{d\sigma_0}{dr}-\frac{W_0}{r}(p_0+\sigma_0)\frac{\partial}{\partial r}\left[\frac{r\eta}{W_0}\right]-\frac{\eta}{8\pi}\frac{d}{dr}\left[\frac{Q^2}{r^4}\right]\\ &+ \frac{Q_0}{4\pi r^2}\delta Q. \end{aligned} \qquad (2.2.29)$$

Substituting δX from Eq.(2.2.26) in (2.2.23), we obtain

$$\begin{aligned}\frac{1}{rW_0X_0^2}\frac{\partial}{\partial r}\delta W &= \frac{8\pi G}{c^4}\left[\delta p-\frac{2(p_0+\sigma_0)\eta}{W_0}\frac{dW_0}{dr}\right]+\frac{2GQ_0}{r^2c^4}\delta Q\\ &- \frac{16\pi G}{c^4W_0}\frac{dW_0}{dr}\int\delta q dt, \end{aligned} \qquad (2.2.30)$$

which, through Eq.(2.2.14), becomes

$$\begin{aligned}(p_0+\sigma_0)\frac{\partial}{\partial r}\delta W &= \frac{dW_0}{dr}+\frac{W_0}{X_0}\frac{dX_0}{dr}\left[\delta p-\frac{2}{W_0}\frac{dW_0}{dr}\left\{(p_0+\sigma_0)\eta\right.\right.\\ &+ \left.\left.\int\delta q dt\right\}+\frac{Q_0}{4\pi r^2}\delta Q\right]. \end{aligned} \qquad (2.2.31)$$

We can rewrite Eq.(2.2.25) by taking $\delta W,\ \delta X,\ \delta p,\ \delta\sigma,\ \delta q$ and δQ as time dependent amplitudes of the respective quantities as

$$\begin{aligned}
& \varrho^2\eta(p_0+\sigma_0)\left(\frac{X_0}{W_0}\right)^2 = \frac{d}{dr}\delta p+\delta p\left[\frac{2}{W_0}\frac{dW_0}{dr}+\frac{1}{X_0}\frac{dX_0}{dr}\right] \\
+ & \frac{1}{W_0}\delta\sigma\frac{dW_0}{dr}-\frac{2}{W_0}\left[(p_0+\sigma_0)\eta+\int qdt\right]\left[\frac{1}{W_0}\frac{dW_0}{dr}+\frac{1}{X_0}\frac{dX_0}{dr}\right] \\
+ & \frac{Q_0\delta Q}{4\pi r^2}\left[\frac{1}{W_0}\frac{dW_0}{dr}+\frac{1}{X_0}\frac{dX_0}{dr}-\frac{2}{r}\right]+[(\sigma_0+p_0)v-q_0] \\
\times & \left(\frac{X_0}{W_0}\right)^2\left[\frac{1}{W_0}\frac{\partial}{\partial t}\delta W+\frac{1}{X_0}\frac{\partial}{\partial t}\delta X\right]. \qquad (2.2.32)
\end{aligned}$$

2.2.3 The Conservation of Baryon Number

We consider conservation of baryon number such that Eq.(2.1.29) with (2.2.20) gives

$$\begin{aligned}
& \frac{\partial}{\partial t}\left(\frac{\widetilde{N}}{W_0}\right)+\frac{\partial}{\partial r}\left(\frac{\widetilde{N}v}{W_0}\right)+\frac{\widetilde{N}v}{W_0}\left[\frac{1}{W_0}\frac{\partial W}{\partial t}+\frac{1}{X_0}\frac{\partial X}{\partial t}\right] \\
& +\frac{\widetilde{N}v}{W_0}\left[\frac{1}{W_0}\frac{\partial W}{\partial r}+\frac{1}{X_0}\frac{\partial X}{\partial r}+\frac{1}{r}\right]=0. \qquad (2.2.33)
\end{aligned}$$

We take the perturbation (2.1.32) such that Eq.(2.2.33) with linear terms in v yields

$$\frac{1}{r^2}\frac{d}{dr}(\frac{\widetilde{N}_0r^2v}{W_0/2})+\frac{1}{W_0}\frac{\partial}{\partial t}\delta\widetilde{N}+\frac{\widetilde{N}_0}{W_0X_0}\frac{\partial}{\partial t}\delta X+\frac{\widetilde{N}_0v}{W_0X_0}\frac{dX_0}{dr}=0, \qquad (2.2.34)$$

whose integration leads to

$$\frac{1}{W_0}\delta\widetilde{N}+\frac{1}{r^2}\frac{d}{dr}\left(\frac{\widetilde{N}_0r^2\eta}{W_0}\right)+\frac{\widetilde{N}_0}{W_0X_0}\left[\delta X+\eta\frac{dX_0}{dr}\right]=0. \qquad (2.2.35)$$

Using Eq.(2.2.27), it follows that

$$\delta\widetilde{N}=\widetilde{N}_0\left[\frac{\eta}{W_0}\frac{dW_0}{dr}-rX_0^2\int\delta qdt\right]-\eta\frac{d\widetilde{N}_0}{dr}-\frac{\widetilde{N}_0W_0}{r^2}\frac{\partial}{\partial r}\left(\frac{r^2\eta}{W_0}\right)=0. \qquad (2.2.36)$$

In this case, we again consider an EoS (2.1.35) such that Eqs.(2.2.29) and (2.2.36) lead to

$$\delta p=-\eta\frac{dp_0}{dr}-p_0\Gamma\frac{W_0}{r}\frac{\partial}{\partial r}\left(\frac{r\eta}{W_0}\right)+\alpha_2, \qquad (2.2.37)$$

where $\int \delta q dt = \widetilde{q}$. Using Eqs.(2.2.6) and (2.2.13), we have

$$\begin{aligned}
&\varrho^2 X_0^2(p_0+\sigma_0)\eta = \frac{8\pi G}{c^4} p_0 X_0^2(p_0+\sigma_0)\\
&+\frac{\eta}{r}\left[\frac{dp_0}{dr}+\frac{1}{8\pi}\frac{d}{dr}\left(\frac{Q^2}{r^2}\right)\right]-\frac{\eta}{8\pi}\frac{d^2}{dr^2}\left(\frac{Q^2}{r^2}\right)\\
&+\frac{\eta}{8\pi}\frac{d}{dr}\left(\frac{Q^2}{r^2}\right)\left[\frac{2}{W_0}\frac{dW_0}{dr}+\frac{1}{X_0}\frac{dX_0}{dr}\right]\\
&-\frac{d}{dr}\left[p_0\Gamma\frac{W_0}{r}\frac{\partial}{\partial r}(\eta r W_0)+\alpha_2\right]-\frac{2}{W_0}\frac{dW_0}{dr}\tilde{q}\\
&\times\left[\frac{1}{W_0}\frac{dW_0}{dr}+\frac{1}{X_0}\frac{dX_0}{dr}\right]\\
&+\frac{Q_0\delta Q}{4\pi r^2}\left[\frac{1}{W_0}\frac{dW_0}{dr}+\frac{1}{X_0}\frac{dX_0}{dr}-\frac{2}{r}\right],
\end{aligned} \tag{2.2.40}$$

which is the required pulsation equation satisfying the boundary conditions

$$\eta = 0, \quad r = 0, \quad \delta p = 0, \quad r = R.$$

Taking the product of pulsation equation with $\eta r^2 W_0 X_0$ and integrating over values of r, it yields a characteristic value problem for ϱ^2 as

$$\begin{aligned}
&\varrho^2\int_0^R r^2\eta^2 W X^3(p+\sigma)dr = \frac{8\pi G}{c^4}\int_0^R p(p+\sigma)r^2\eta^2 W X^3 dr\\
&+\int_0^R r\eta^2 W X\left[\frac{dp}{dr}+\frac{1}{8\pi}\frac{d}{dr}\left(\frac{Q^2}{r^2}\right)\right]dr-\int_0^R r^2\eta^2\frac{dp}{dr}\\
&\times W X\left(p\Gamma\frac{W}{r}\frac{d}{dr}\left(\frac{\eta r}{W}\right)+\alpha_2\right)dr-\int_0^R r^2\eta^2 W X\left[p\Gamma\frac{W}{r}\right.\\
&\left.\times\frac{d}{dr}\left(\frac{\eta r}{W}\right)+\alpha_2\right]\left[\frac{1}{W}\frac{dW}{dr}+\frac{1}{X}\frac{dX}{dr}\right]dr-2\int_0^R r^2 X\eta\frac{dW}{dr}\\
&\times\tilde{q}\left[\frac{1}{W}\frac{dW}{dr}+\frac{1}{X}\frac{dX}{dr}\right]dr+\frac{1}{8\pi}\int_0^R Q_0 W X\eta\delta Q\left[\frac{1}{W}\frac{dW}{dr}\right.\\
&\left.+\frac{1}{X}\frac{dX}{dr}-\frac{2}{r}\right]dr.
\end{aligned} \tag{2.2.41}$$

We can define the orthogonality relation associated with this equation as

$$\int_0^R W X^3 r^2(p+\sigma)\eta^{(c_1)}\eta^{(c_2)} = 0, \quad (c_1 \neq c_2). \tag{2.2.42}$$

where

$$\begin{aligned}\alpha_2 &= \frac{1}{\partial\widetilde{N}/\partial p}\left[\frac{1}{4\pi}\frac{\partial\widetilde{N}}{\partial\sigma}\left\{\frac{\eta}{2}\frac{d}{dr}\left(\frac{Q^2}{r^4}-\frac{Q_0\delta Q}{r^2}\right)\right\}\right.\\ &+ \left.\widetilde{N}_0\left\{\frac{\eta}{W_0}\frac{dW_0}{dr}-rX_0^2\int\delta q dt\right\}\right].\end{aligned}$$

2.2.4 Pulsation Equation and Variational Principle

Inserting $\delta\sigma$ and δp in Eq.(2.2.32), we have

$$\begin{aligned}&\varrho^2X_0^2(p_0+\sigma_0)\eta=-\frac{d}{dr}\left(\eta\frac{dp_0}{dr}\right)-\eta\frac{dp_0}{dr}\left[\frac{2}{W_0}\frac{dW_0}{dr}\right.\\ &\left.+\frac{1}{X_0}\frac{dX_0}{dr}\right]-\frac{1}{W_0}\frac{dW_0}{dr}\left[2(p_0+\sigma_0)\eta\left\{\frac{1}{W_0}\frac{dW_0}{dr}\right.\right.\\ &\left.\left.+\frac{1}{X_0}\frac{dX_0}{dr}\right\}+\frac{1}{r}\frac{\partial}{\partial r}\{r(p_0+\sigma_0)\eta\}\right]\\ &-\frac{d}{dr}\left(p_0\Gamma\frac{W_0}{r}\frac{\partial}{\partial r}\left(\frac{\eta r}{W_0}\right)+\alpha_2\right)-\left[\frac{2}{W_0}\frac{dW_0}{dr}+\frac{1}{X_0}\frac{dX_0}{dr}\right]\\ &\times\left[p_0\Gamma\frac{W_0}{r}\frac{\partial}{\partial r}\left(\frac{\eta r}{W_0}\right)+\alpha_2\right]-\frac{2}{W_0}\frac{dW_0}{dr}\left[\frac{1}{W_0}\frac{dW_0}{dr}\right.\\ &\left.+\frac{1}{X_0}\frac{dX_0}{dr}\right]\int\delta q dt+\frac{Q_0\delta Q}{4\pi r^2}\left[\frac{1}{W_0}\frac{dW_0}{dr}+\frac{1}{X_0}\frac{dX_0}{dr}-\frac{2}{r}\right].\end{aligned}\tag{2.2.38}$$

Substituting $\frac{dp_0}{dr}$ from Eq.(2.2.13), this leads to

$$\begin{aligned}&\varrho^2X_0^2=\frac{1}{W_0}\left[\frac{d^2W_0}{dr^2}-\frac{1}{X_0}\frac{dX_0}{dr}+\frac{1}{r}\frac{dW_0}{dr}\right]\\ &-\frac{\eta}{8\pi}\frac{d^2}{dr^2}\left(\frac{Q^2}{r^2}\right)\left[\frac{2}{W_0}\frac{dW_0}{dr}+\frac{1}{X_0}\frac{dX_0}{dr}\right]+\frac{\eta}{8\pi}\frac{d}{dr}\left(\frac{Q^2}{r^2}\right)\\ &-\frac{d}{dr}\left[p_0\Gamma\frac{W_0}{r}\frac{\partial}{\partial r}\left(\frac{\eta r}{W_0}+\alpha_2\right)\right]-\left[p_0\Gamma\frac{W_0}{r}\frac{\partial}{\partial r}\left(\frac{\eta r}{W_0}+\alpha_2\right)\right]\\ &\times\left[\frac{2}{W_0}\frac{dW_0}{dr}+\frac{1}{X_0}\frac{dX_0}{dr}\right]-\frac{2}{W_0}\frac{dW_0}{dr}\tilde{q}\left[\frac{2}{W_0}\frac{dW_0}{dr}+\frac{1}{X_0}\frac{dX_0}{dr}\right]\\ &-\frac{Q_0\delta Q}{4\pi r^2}\left[\frac{1}{W_0}\frac{dW_0}{dr}+\frac{1}{X_0}\frac{dX_0}{dr}-\frac{2}{r}\right],\end{aligned}\tag{2.2.39}$$

In the following, we evaluate conditions for dynamical instability by taking a homogeneous cylindrical model.

The Homogeneous Model of Cylinder

We study the conditions for dynamical instability of a homogeneous cylinder with constant energy density. Equations (2.2.18) and (2.2.19) governing the hydrostatic equilibrium allow the integration such that we can write

$$y^2=-\frac{r}{\bar{a}_*^2}+\frac{\bar{b}_*^2}{r^2},\quad y_1^2=-\frac{R}{\bar{a}_*^2}+\frac{\bar{b}_*^2}{R^2}, \tag{2.2.43}$$

where $\bar{a}_*^2=\frac{c^4}{2\pi G\sigma}$ and $\bar{b}_*^2=\frac{GQ^2(1-2c^2)}{2c^4}$. We can determine solutions of the relevant physical quantities in terms of y and y_1 as

$$p=\sigma\frac{y-y_1}{3y_1-y},\quad W^2=\frac{1}{4}[3y_1-y]^2,\quad X^2=\frac{1}{y^2}. \tag{2.2.44}$$

For positivity of pressure, we have $3y_1>1$ which yields

$$\frac{R}{\bar{a}_*^2}-\frac{\bar{b}_*^2}{R^2}<\frac{1}{9}.$$

Using the inertial mass, this leads to

$$R>9\left(\frac{2GM}{c^2}-\frac{GQ^2}{Rc^4}\right)=9R_*, \tag{2.2.45}$$

where R_* is the limiting radius for charged cylinder. Inserting the above physical quantities in Eq.(2.2.41), it follows that

$$\begin{aligned}
&2\bar{a}_*\varrho^2y_1\int_0^{\xi_1}\frac{\xi^2\eta^2}{y^3}d\xi=6y_1\int_0^{\xi_1}\frac{y-y_1}{y^3(3y_1-y)^2}\xi^2\eta^2d\xi\\
&+\frac{3}{2\bar{a}_*}\int_0^{\xi_1}\frac{3y_1-y}{y}\xi\eta^2\frac{d}{d\xi}\left[\frac{y-y_1}{3y_1-y}+\frac{G}{3\bar{a}_*c^4}\frac{d}{d\xi}\left(\frac{Q^2}{\xi^2}\right)\right]d\xi\\
&-\frac{1}{2}\int_0^{\xi_1}\eta\xi^2\frac{3y_1-y}{y}\frac{d}{d\xi}\left[\frac{y-3y_1}{\bar{a}_*^3\xi}\Gamma\frac{\partial}{\partial\xi}\left(\frac{\eta\xi}{3y_1-y}\right)+\frac{3c^4\alpha_2}{8\pi G}\right]d\xi
\end{aligned}$$

$$
\begin{aligned}
&-\frac{\bar{a}_*^2}{2}\int_0^{\xi_1}\xi^2\eta\frac{3y_1-y}{y}\left[\frac{y-y_1}{\bar{a}_*\xi}\Gamma\frac{\partial}{\partial\xi}\left(\frac{\eta\xi}{3y_1-y}\right)+\frac{3c^4\alpha_2}{8\pi G}\right]\\
&\times\left[\frac{2}{3y_1-y}\frac{d}{d\xi}\left(3y_1-y\right)+y\frac{d}{d\xi}\left(\frac{1}{y}\right)\right]d\xi-\frac{3\bar{a}_*c^4}{8\pi G}\int_0^{\xi_1}\frac{\eta\xi^2}{y}\tilde{q}\\
&\times\frac{d}{d\xi}(3y_1-y)\left[\frac{1}{3y_1-y}\frac{d}{d\xi}(3y_1-y)+y\frac{d}{d\xi}\frac{1}{y}\right]d\xi\\
&+\frac{3c^4}{(8\pi)^2G}\int_0^{\xi_1}Q_0\xi\delta Q\frac{3y_1-y}{2y}\left[\frac{2}{3y_1-y}\frac{d}{d\xi}(3y_1-y)+y\frac{d}{d\xi}\frac{1}{y}\right]d\xi, \quad (2.2.46)
\end{aligned}
$$

where $\xi=\frac{r}{\bar{a}_*}$, $\xi_1=\frac{R}{\bar{a}_*}-\frac{\bar{b}_*}{R}$ and Γ is taken to be constant.

We consider a trial function

$$
\eta=\xi W=\frac{1}{2}\xi(y_1-y), \quad (2.2.47)
$$

such that Eq.(2.2.46) becomes

$$
\begin{aligned}
&\frac{\bar{a}_*\varrho^2y_1}{2}\int_0^{\xi_1}\frac{\xi^4(3y_1-y)^2}{y^3}d\xi=\frac{3y_1}{2\bar{a}_*}\\
&\times\int_0^{\xi_1}\frac{\xi^4(y-y_1)(3y_1-y)}{4y^3}d\xi+\frac{3}{2\bar{a}_*}\int_0^{\xi_1}\frac{\xi^3(3y_1-y)^3}{2y}\\
&\times\frac{d}{d\xi}\left[\frac{y-y_1}{3y_1-y}+\frac{G}{3\bar{a}_*c^4}\frac{d}{d\xi}\left(\frac{Q^2}{\xi^2}\right)\right]d\xi-\frac{1}{4}\int_0^{\xi_1}\frac{\xi^3(3y_1-y)^2}{y}\\
&\times\frac{d}{d\xi}\left[\frac{y-3y_1}{\bar{a}_*^3\xi}\Gamma\frac{\partial}{\partial\xi}\left(\frac{\xi^2}{2}\right)+\frac{3c^4\alpha_2}{8\pi G}\right]d\xi-\frac{\bar{a}_*^2}{4}\int_0^{\xi_1}\xi^3\\
&\times\frac{(3y_1-y)^2}{y}\left[\frac{y-y_1}{\bar{a}_*\xi}\Gamma\frac{\partial}{\partial\xi}\left(\frac{\xi^2}{2}\right)+\frac{3c^4\alpha_2}{8\pi G}\right]\\
&\times\left[\frac{2}{3y_1-y}\frac{d}{d\xi}\left(3y_1-y\right)+y\frac{d}{d\xi}\left(\frac{1}{y}\right)\right]d\xi\\
&-\frac{3\bar{a}_*c^4}{16\pi G}\int_0^{\xi_1}\frac{\xi^3(3y_1-y)}{y}\tilde{q}\frac{d}{d\xi}(3y_1-y)\\
&\times\left[\frac{1}{3y_1-y}\frac{d}{d\xi}(3y_1-y)+y\frac{d}{d\xi}\frac{1}{y}\right]d\xi\\
&+\frac{3c^4}{(16\pi)^2G}\int_0^{\xi_1}Q_0\xi\delta Q\frac{(3y_1-y)^2}{y}\\
&\times\left[\frac{2}{3y_1-y}\frac{d}{d\xi}(3y_1-y)+y\frac{d}{d\xi}\frac{1}{y}\right]d\xi. \quad (2.2.48)
\end{aligned}
$$

Inserting $y=\cos\theta$ and $\xi=\sin\theta$ in the above equation, we have

$$\frac{(\bar{a}_*\varrho)^2\cos\theta_1}{2}\int_0^{\theta_1}\frac{\sin^4\theta}{\cos^2\theta}(3\cos^2\theta_1-\cos\theta)^2d\theta=\frac{3\cos\theta_1}{2}$$
$$\times\int_0^{\theta_1}\frac{\sin^4\theta}{\cos^2\theta}[4\cos\theta\cos\theta_1-3\cos^2\theta_1\cos^2\theta]d\theta$$
$$+\frac{3}{4}\int_0^{\theta_1}(3\cos\theta_1-\cos\theta)^3\frac{\sin^3\theta}{\cos\theta}\frac{d}{d\theta}\left[\frac{\cos\theta-\cos\theta_1}{3\cos\theta_1-\cos\theta}\right.$$
$$\left.-\frac{2GQ^2}{3\bar{a}_*c}\frac{1}{\sin^3\theta}\right]d\theta-\frac{\bar{a}_*}{4}\int_0^{\theta_1}(3\cos\theta_1-\cos\theta)^2\frac{\sin^3\theta}{\cos\theta}$$
$$\times\frac{d}{d\theta}\left[\frac{\cos\theta_1-\cos\theta}{\bar{a}_*^3\sin^4\theta}\Gamma+\frac{3c^4\alpha_2}{8\pi G}\right]d\theta$$
$$-\frac{\bar{a}_*^3}{4}\int_0^{\theta_1}(3\cos\theta_1-\cos\theta)^2\sin^3\theta\left[\frac{\cos\theta-\cos\theta_1}{\bar{a}_*}\Gamma\right.$$
$$\left.+\frac{3c^4\beta}{8\pi G}\right]\left[\frac{2\sin\theta}{\cos\theta(3\cos\theta_1-\cos\theta)}+\tan\theta\sec\theta\right]d\theta$$
$$-\frac{3\bar{a}_*c^4}{16\pi G}\int_0^{\theta_1}\frac{\sin^3\theta}{\cos\theta}(3\cos\theta_1-\cos\theta)\tilde{q}\frac{d}{d\theta}(3\cos\theta_1-\cos\theta)$$
$$\times\left[\frac{\sin\theta}{\cos\theta(3\cos\theta_1-\cos\theta)}+\tan\theta\sec\theta\right]d\theta+\frac{3c^4\alpha_2}{(16\pi)^2G}$$
$$\times\int_0^{\theta_1}Q_0\delta Q\sin\theta(3\cos\theta_1-\cos\theta)^2$$
$$\times\left[\frac{2\sin\theta}{\cos\theta(3\cos\theta_1-\cos\theta)}+\tan\theta\sec\theta\right]d\theta, \tag{2.2.49}$$

where $\theta_1=\sin^{-1}\left(\frac{R}{\bar{a}_*}-\frac{\bar{b}_*}{R}\right)$. By taking $\varrho^2=0$ and solving the integrals, we find exact condition for marginal stability. We evaluate the values of Γ_1 such that $\Gamma\leq\Gamma_1$ for the existence of dynamical instability. We also consider Newtonian limit which implies that the resulting criteria for marginal stability is $\Gamma>-\frac{9}{8}-\frac{81Q^2}{4}$. We compute Γ and radii of marginal stability for homogeneous gaseous cylinder corresponding to $Q=0.4$ and $q=0.5$ which exhibit finite values of Γ in Newtonian and pN limits. We note that $\frac{R}{R_*}$ remains positive for $\Gamma>0$ showing marginal stability of gaseous cylindrical model in pN limit. The respective results are given in Table **2.4**.

Table 2.4: Adiabatic Index and Radii for Homogeneous Cylinder

θ_1	R/R_*	Γ_1 for $Q = 0.4$
0^o	10.364	-4.365
10^o	33.163	2.894×10^7
20^o	8.549	3×10^7
30^o	4.000	23647.19
40^o	2.4203	131557
50^o	1.704	87550
60^o	1.333	118265.5

Since the radius of stability is a factor of R_*, so physically interesting results can be obtained if $\frac{R}{R_*} \geq 0$. We obtain the following condition for dynamical instability of relativistic gaseous masses including charge as $\theta_1 \to 0$

$$\Gamma + \frac{3}{4}\left(\frac{3}{2} + 27Q^2\right) < \frac{57}{42}\theta_1^2 = \frac{57}{42}\left[\frac{R}{\bar{a}_*^2} - \frac{\bar{b}_*^2}{R^2}\right]. \tag{2.2.50}$$

We can write

$$R < \frac{57}{42\left[\Gamma + \frac{3}{4}\left(\frac{3}{2} + 27Q^2\right)\right]}\left[\frac{2GM}{c^2} - \frac{GQ^2}{Rc^4}\right], \tag{2.2.51}$$

which leads to

$$\frac{R}{R_*} < \frac{K}{\left[\Gamma + \frac{3}{4}\left(\frac{3}{2} + 27Q^2\right)\right]}, \tag{2.2.52}$$

where $K = \frac{57}{42}$ for the homogeneous cylinder. This means that if Γ exceeds $-\frac{3}{4}\left(\frac{3}{2} + 27Q^2\right)$ by a small amount, the dynamical instability can be prevented till the mass contracts to radius R_*. The gaseous cylinder remains stable if its radius is larger than R_*. The ranges of instability for charged homogeneous cylindrical system are shown in Figure **2.7**. It can be seen that the radius of stability is greater than R_* for $\Gamma > -1$ in pN limit. We also discuss the criteria and ranges of instability for uncharged cylinder (Figure **2.8**). It is found that $\frac{R}{R_*} \geq 0$ when Γ exceeds $-\frac{9}{8}$ by a small amount showing stable cylindrical configuration. It is observed that $\Gamma < -1.125$ leads to un-physical results as $\frac{R}{R_*} < 0$.

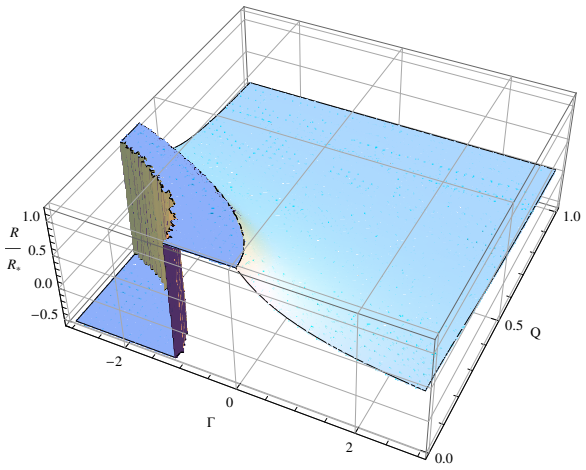

Figure 2.7: Plot of $\frac{R}{R_*}$ for dynamical stability/instability of charged homogeneous cylinder.

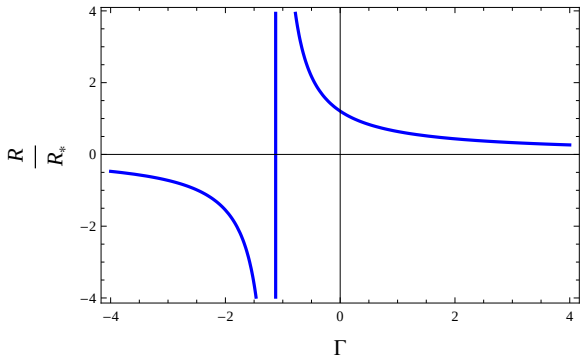

Figure 2.8: Plot of $\frac{R}{R_*}$ for dynamical stability/instability of homogeneous uncharged cylinder.

Chapter 3

Stability of Thin-Shell Wormholes

In this chapter, we investigate stability of thin-shell WHs coupled with NLED and Einstein HBI electrodynamics by employing Israel thin-shell approach. The surface stresses are formulated by using Lanczos equations. We explore stability conditions for the existence of traversable thin-shell WHs with arbitrarily small amount of cosmic fluids for exotic matter and analyze maximum viable regions for stability of the respective thin-shell WHs. The chapter is designed in the following format. In the next section, we provide dynamical investigation of regular ABGB thin-shell WHs whose results have been published [84]. In section **3.2**, we apply general formalism to study stability of thin-shell WHs in HBI electrodynamics. A research paper based on the corresponding results has been published [85].

3.1 Regular ABGB Thin-Shell Wormholes

Here we study the formation of thin-shell WHs from regular ABGB BHs through cut and paste method and analyze their stability under linear perturbations.

3.1.1 Basic Formalism

It is well-known that electrovacuum asymptotically flat spacetimes are not sufficient for the existence of regular BH solutions. To derive the nonlinear electromagnetic field for regular BH, one needs to enlarge the class of electrodynamics to nonlinear ones [33]. These regular BHs behave as ordinary RN BH solutions. This motivates us to discuss stability of viable thin-shell WH in the framework of NLED. The system of gravity coupled with NLED in the presence of Λ is described by the action

$$S=\frac{1}{16\pi}\int\sqrt{-g}\left[(R-2\Lambda)-\mathcal{L}(F)\right]d^4x, \tag{3.1.1}$$

where R is the scalar curvature and $\mathcal{L}(F)$ is the Lagrangian for NLED given by

$$\mathcal{L}(F)=F\left[1-\tanh^2\left(\frac{Q}{2M}\left(\frac{FQ^2}{2}\right)^{\frac{1}{4}}\right)\right], \tag{3.1.2}$$

which depends on a single invariant $F=F^{ij}F_{ij}$. The static spherically symmetric nonsingular ABGB BH is given by [86]

$$ds^2=-N(r)dt^2+N^{-1}(r)dr^2+r^2(d\theta^2+\sin^2\theta d\phi^2), \tag{3.1.3}$$

where

$$N(r)=1-\frac{2M}{r}\left[1-\tanh\left(\frac{Q^2}{2Mr}\right)\right]-\frac{\Lambda r^2}{3}, \tag{3.1.4}$$

Q is the charge. It is noted that the presence of Λ does not destroy the regularity of the solution describing a regular ABGB-de Sitter BH with $\Lambda>0$ which reduces to ABGB BH for $\Lambda=0$ [34]. This metric is regular at the center $r=0$ while the metric function for small Q and $r\to\infty$ can be expanded as

$$N(r)=1-\frac{2M}{r}+\frac{Q^2}{r^2}-\frac{\Lambda r^2}{3}-\frac{Q^6}{12M^2r^4}+...,$$

which behaves as RN-de Sitter BH. Its event and cosmological horizons can be determined by the real roots of the metric function $N(r) = 0$.

To construct thin-shell WHs, we employ standard procedure by cutting the interior region of regular ABGB BH with $r < \tilde{a}$. The resulting 4D geometries are joined at the hypersurface $\Sigma^{\pm} = \Sigma = \{r = \tilde{a}\}$. A 3D induced spacetime is considered at the shell as

$$ds^2 = -d\tau^2 + \tilde{a}^2(\tau)(d\theta^2 + \sin^2\theta d\phi^2), \tag{3.1.5}$$

where τ is the proper time on the shell. For dynamical evolution of thin-shell, we follow Israel formalism which enables the joining of two regions of spacetime partitioned by Σ. The surface stresses at the shell are determined by Lanczos equations (1.2.6) given by

$$\sigma = -\frac{1}{2\pi\tilde{a}}\sqrt{N(\tilde{a}) + \dot{\tilde{a}}^2}, \tag{3.1.6}$$

$$p = \frac{1}{4\pi}\left[\frac{\sqrt{N(\tilde{a}) + \dot{\tilde{a}}^2}}{\tilde{a}} + \frac{2\ddot{\tilde{a}} + N'(\tilde{a})}{2\sqrt{N(\tilde{a}) + \dot{\tilde{a}}^2}}\right]. \tag{3.1.7}$$

These equations give rise to the violation of null and weak energy conditions at the shell and hence indicate the presence of exotic matter which should be reduced for viable thin-shell WHs. It would be interesting to explore attractive and repulsive characteristics of the regular ABGB thin-shell WHs for which observer's four-acceleration is defined as

$$a^{\mu} = u^{\mu}_{;\nu}u^{\nu},$$

where $u^{\mu} = \frac{dx^{\mu}}{d\tau} = (\frac{1}{\sqrt{N(r)}}, 0, 0, 0)$ is the observer four velocity. The non-zero four acceleration component is computed as

$$a^r = \Gamma^r_{tt}\left(\frac{dt}{d\tau}\right)^2 = \frac{M}{r^2}\left\{1 - \tanh\left(\frac{Q^2}{2Mr}\right)\right\} - \frac{1}{2}\frac{Q^2}{r^3}\cosh^{-2}\left(\frac{Q^2}{2Mr}\right) - \frac{\Lambda r}{3}. \tag{3.1.8}$$

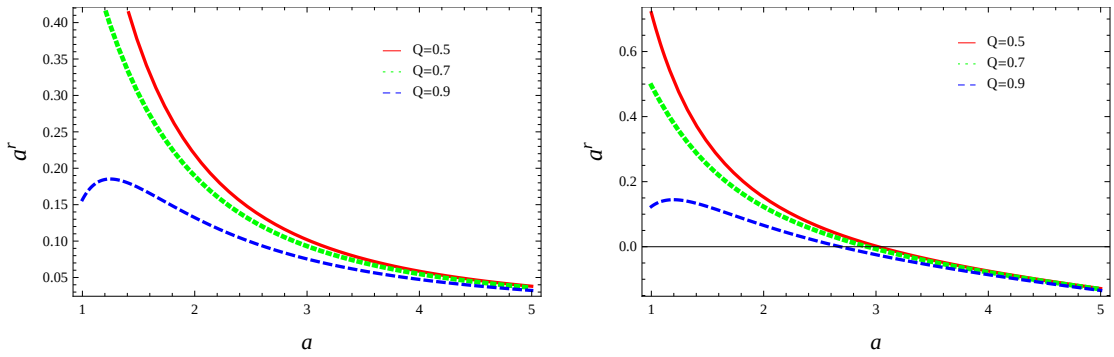

Figure 3.1: Plots of a^r without Λ (left hand side) and with $\Lambda = 0.1$ (right hand side) corresponding to $\frac{Q}{M} = 0.5,\ 0.77,\ 0.99$.

An important condition for traveling through WH implies that an observer should not be pushed away by enormous tidal forces which requires the observer's acceleration less than that of Earth's acceleration. It is observed that a WH exhibits attractive behavior if its radial acceleration is positive, i.e., $a^r > 0$ while it will have repulsive characteristics for $a^r < 0$. Figure **3.1** shows the respective plots for attractive and repulsive characteristics of regular ABGB thin-shell WHs with and without Λ. We observe that regular ABGB thin-shell WH will remain attractive for different values of Q which supports the fact that an observer must maintain an outward-directed radial acceleration to avoid gravitational pull by the WH. In de Sitter case, we find that the WH is attractive for small throat radii while it shows repulsive behavior for larger throat radii. An observer must have an inward directed radial acceleration to keep away from being pushed by the WH.

3.1.2 General Approach for Stability

Here, we discuss a particular approach for the stability of ABGB thin-shell WHs through linear perturbations. The surface energy density and surface pressure for static WH configuration ($\tilde{a} = a_0$) yield

$$\sigma_0 = -\frac{\sqrt{N(a_0)}}{2\pi a_0}, \quad p_0 = \frac{1}{4\pi}\left[\frac{\sqrt{N(a_0)+}}{a_0} + \frac{N'(a_0)}{2\sqrt{N(a_0)}}\right]. \tag{3.1.9}$$

The surface stresses satisfy the conservation equation, $S^{ij}_{;j} = 0$, which leads to

$$\frac{d}{d\tau}(\sigma\varsigma) + p\frac{d\varsigma}{d\tau} = 0, \tag{3.1.10}$$

where $\varsigma = 4\pi\tilde{a}^2$ corresponds to WH throat area. We can formulate thin-shell equation of motion by rearranging Eq.(3.1.6) as $\dot{\tilde{a}}^2 + \Delta(\tilde{a}) = 0$, which provides WH dynamics while the potential function $\Delta(\tilde{a})$ is given by

$$\Delta = N(\tilde{a}) - [2\pi\tilde{a}\sigma]^2, \tag{3.1.11}$$

here σ represents the perturbed energy density. To discuss WH stability, we assume a linear perturbation in the form of barotropic EoS

$$p = \Upsilon(\sigma), \tag{3.1.12}$$

such that $\Upsilon(\sigma)$ is taken arbitrarily for the shell which governs the polytropic EoS $p \approx \sigma^{1+\frac{1}{n}}$ as $0 \leq n < \infty$.

The basic condition for stability of WH static solution yields $\Delta'(a_0) = 0 = \Delta(a_0)$ and $\Delta''(a_0) > 0$. For this purpose, we use Eq.(3.1.12) and $\sigma' = \frac{\dot{\sigma}}{\dot{\tilde{a}}}$ in conservation equation as

$$\sigma' = -\frac{2}{\tilde{a}}(\sigma + \Upsilon), \tag{3.1.13}$$

which takes the form

$$\sigma'' = \frac{2}{\tilde{a}^2}(\sigma + \Upsilon)(3 - \tilde{a}\Upsilon'). \tag{3.1.14}$$

The first derivative of Eq.(3.1.11) through (3.1.13) turns out to be

$$\Delta'(a_0) = N'(a_0) + 8\pi^2 a_0 \sigma_0[\sigma_0 + 2p(\sigma_0)], \tag{3.1.15}$$

leading to the second derivative of potential function as

$$\Delta''(a_0) = N''(a_0) - 8\pi^2 \left\{[\sigma_0 + 2p_0]^2 + 2\sigma_0[\sigma_0 + p_0][1 + 2\Upsilon'(\sigma_0)]\right\}, \tag{3.1.16}$$

where $\Upsilon_0 = p_0$.

3.1.3 Some Models for Exotic Matter

This section deals with stability of thin-shell WHs from regular charged BH in the vicinity of different models for exotic matter. In a recent work, Halilsoy *et al.* [38] examined the dynamics of Hayward thin-shell WHs for linear, logarithmic and CG models. Here we consider these fluids to explore the stable behavior of regular ABGB and ABGB-de Sitter thin-shell WHs. This would help us to investigate the role of charge and Λ on the stability of WH configurations. In the following, we study the stability formalism by taking these candidates for exotic matter at the shell.

(i) Linear Gas

We choose a linear gas fluid [87] to support the exotic matter at the shell. The EoS for linear gas is defined as

$$\Upsilon = p_0 + \mu(\sigma - \sigma_0), \tag{3.1.17}$$

where μ is a constant parameter. Differentiating this equation with respect to σ, we obtain $\Upsilon'(\sigma_0) = \mu$. We find that $\Delta(\tilde{a})$ and $\Delta'(\tilde{a})$ disappear by inserting the values of $\sigma(a_0)$ and $p(a_0)$. We are interested to explore the possibility of stable WH solutions and check the role of increasing charge in stability regions. We choose parameter $\frac{Q}{M} = 0,\ 0.707,\ 0.999,\ 1.1$ and explore stable zones for ABGB thin-shell WHs in de Sitter background. Figure **3.2** displays stable regions (red curves) for regular ABGB thin-shell WHs corresponding to linear gas EoS with $\frac{Q}{M} = 0,\ 0.5,\ 0.77,\ 0.99$. Here $\frac{Q}{M} = 0$ corresponds to the Schwarzschild case. The metric function $N(r)$ is also plotted to estimate the location of event horizon and WH throat. We assume $a_0 > r_h$ for the viability of thin-shell WHs without event horizons. For $a_0 \leq r_h$, no static solution exists leading to non-physical region. It is found that increasing value of $\frac{Q}{M}$ decreases stability areas for regular ABGB thin-shell WHs.

We also plot stability regions for regular ABGB thin-shell WHs coupled with Λ in de Sitter background. The WH throat must have the range $r_h < a_0 < r_c$ for the existence of viable static WH solutions, where r_c is the cosmological horizon. The respective results show that stability region for WH configurations decreases by increasing charge $\frac{Q}{M}$ (Figure **3.3**). It is found that more stable WH solutions are possible for de Sitter case as compared to $\Lambda = 0$.

(ii) Chaplygin Gas

Here we consider CG model for which EoS is given by

$$\Upsilon(\sigma) = p_0 + \mu\left(\frac{1}{\sigma} - \frac{1}{\sigma_0}\right), \tag{3.1.18}$$

where $\Upsilon'(\sigma_0) = -\frac{\mu}{\sigma_0^2}$. Figures **3.4** and **3.5** show the results corresponding to regular ABGB and ABGB-de Sitter thin-shell WHs by taking CG model and different values

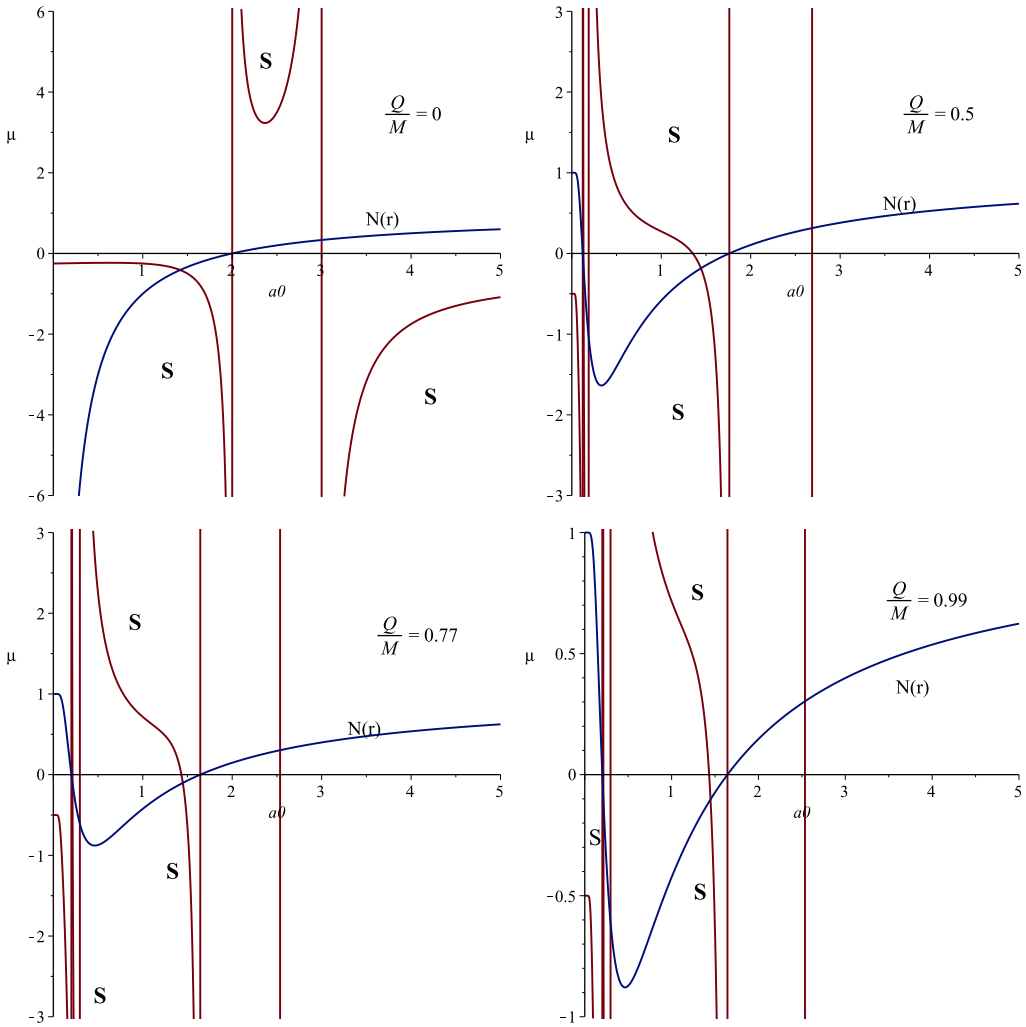

Figure 3.2: Plots for regular ABGB thin-shell WHs corresponding to linear gas EoS with $\frac{Q}{M} = 0,\ 0.5,\ 0.77,\ 0.99$. The stable regions and the metric function are represented by red and blue curves, respectively.

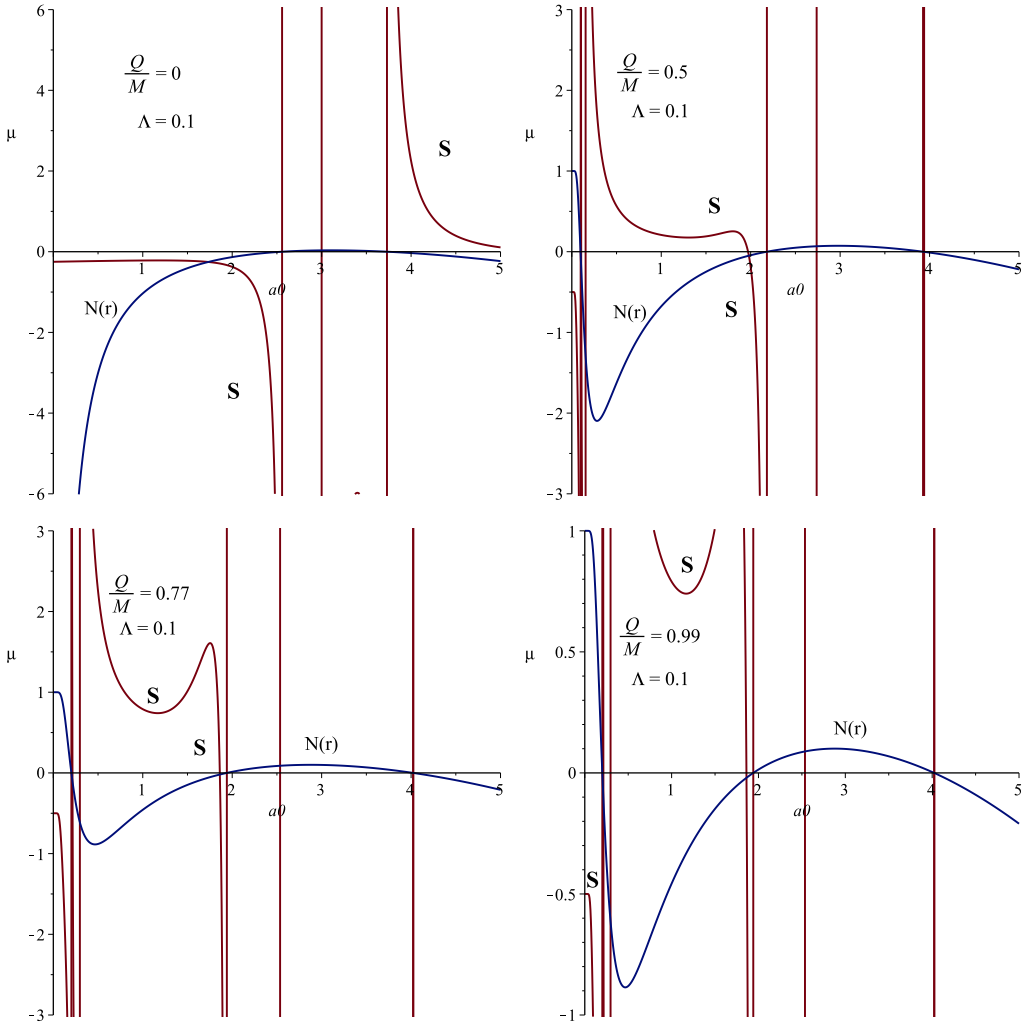

Figure 3.3: Plots for regular ABGB thin-shell WHs corresponding to linear gas EoS in de Sitter background.

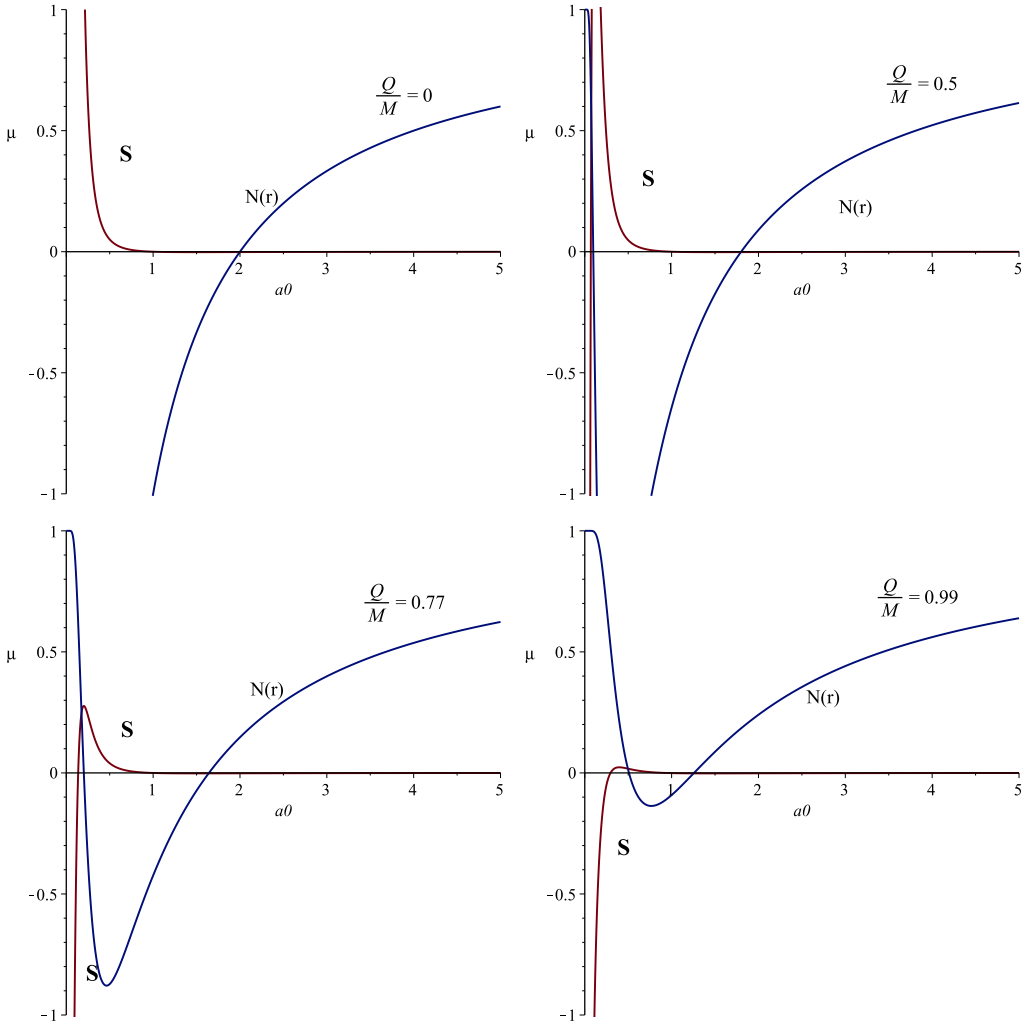

Figure 3.4: Plots for regular ABGB thin-shell WHs by taking CG EoS and $\frac{Q}{M} = 0,\ 0.5,\ 0.77,\ 0.99$.

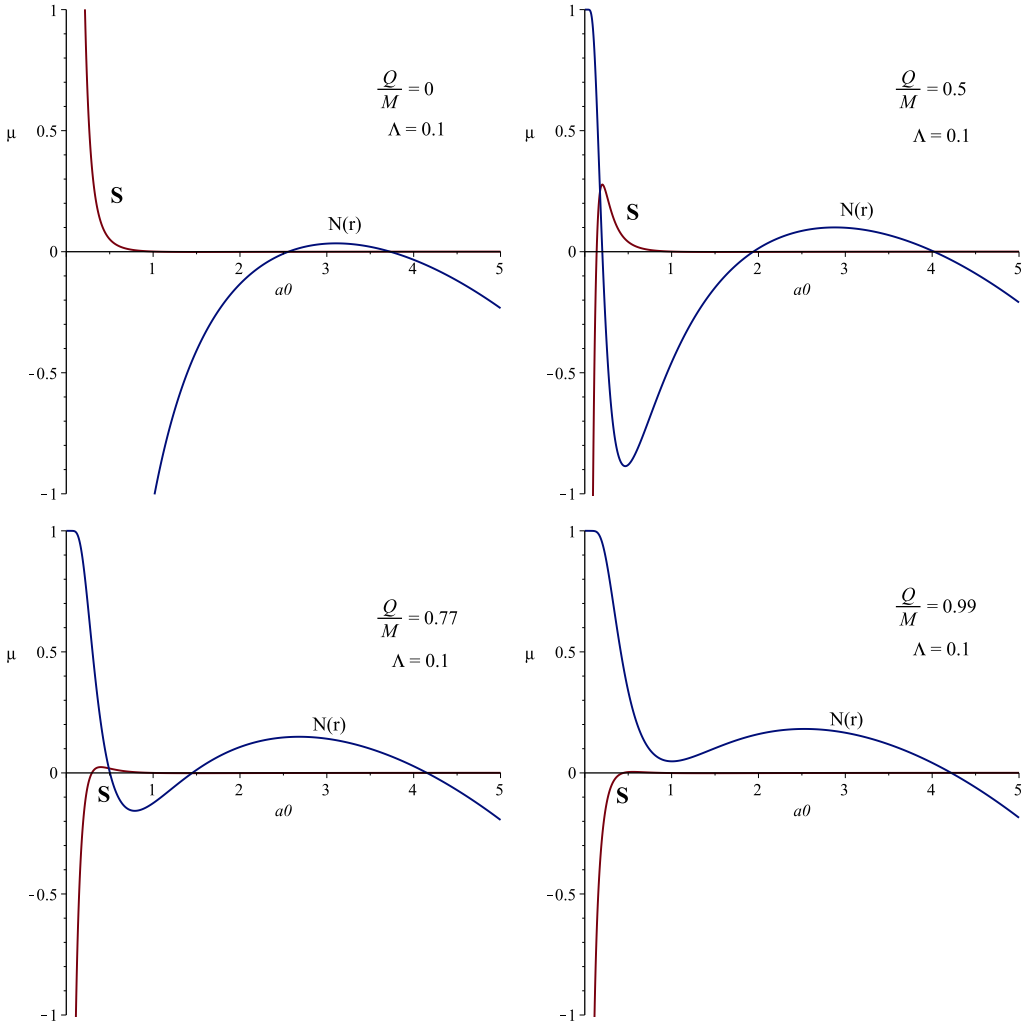

Figure 3.5: Plots for regular ABGB thin-shell WHs for CG EoS in de-Sitter background.

of charge. In both cases, only one stability region is obtained with $\frac{Q}{M} = 0, 0.5$. We examine two stability regions for positive and negative values of μ with $\frac{Q}{M} = 0.77$ while one stable region for negative values of μ and $\frac{Q}{M} = 0.99$. It is observed that CG provides least stable regions for regular ABGB thin-shell WHs which supports the fact that CG does not appear significant for stability regions.

(iii) Generalized Chaplygin Gas

Now we consider GCG fluid for exotic matter governed by an EoS

$$\Upsilon(\sigma) = p_0 + \mu\left(\frac{1}{\sigma^\gamma} - \frac{1}{\sigma_0^\gamma}\right). \tag{3.1.19}$$

We explore its role in increasing the stability regions of regular ABGB and ABGB-de Sitter thin-shell WHs. In this context, we set $\mu = p_0\sigma^\gamma$ such that the above EoS becomes

$$\Upsilon(\sigma) = p_0\left(\frac{\sigma_0}{\sigma}\right)^\gamma, \tag{3.1.20}$$

which yields $\Upsilon'(\sigma_0) = -\frac{p_0}{\sigma_0}\gamma$. We plot the respective stability regions numerically as shown in Figures **3.6** and **3.7**. Here, we find three stability regions for regular ABGB thin-shell WHs with $\frac{Q}{M} = 0, 0.5, 0.77$. It is noted that these regions decrease gradually by increasing $\frac{Q}{M}$ and reduce to only two stable regions for $\frac{Q}{M} = 0.99$. For regular ABGB-de Sitter configurations ($\Lambda = 0.1$), the stability regions are enlarged but have similar behavior as in the above case. We find that non-physical regions appear with small throat radii.

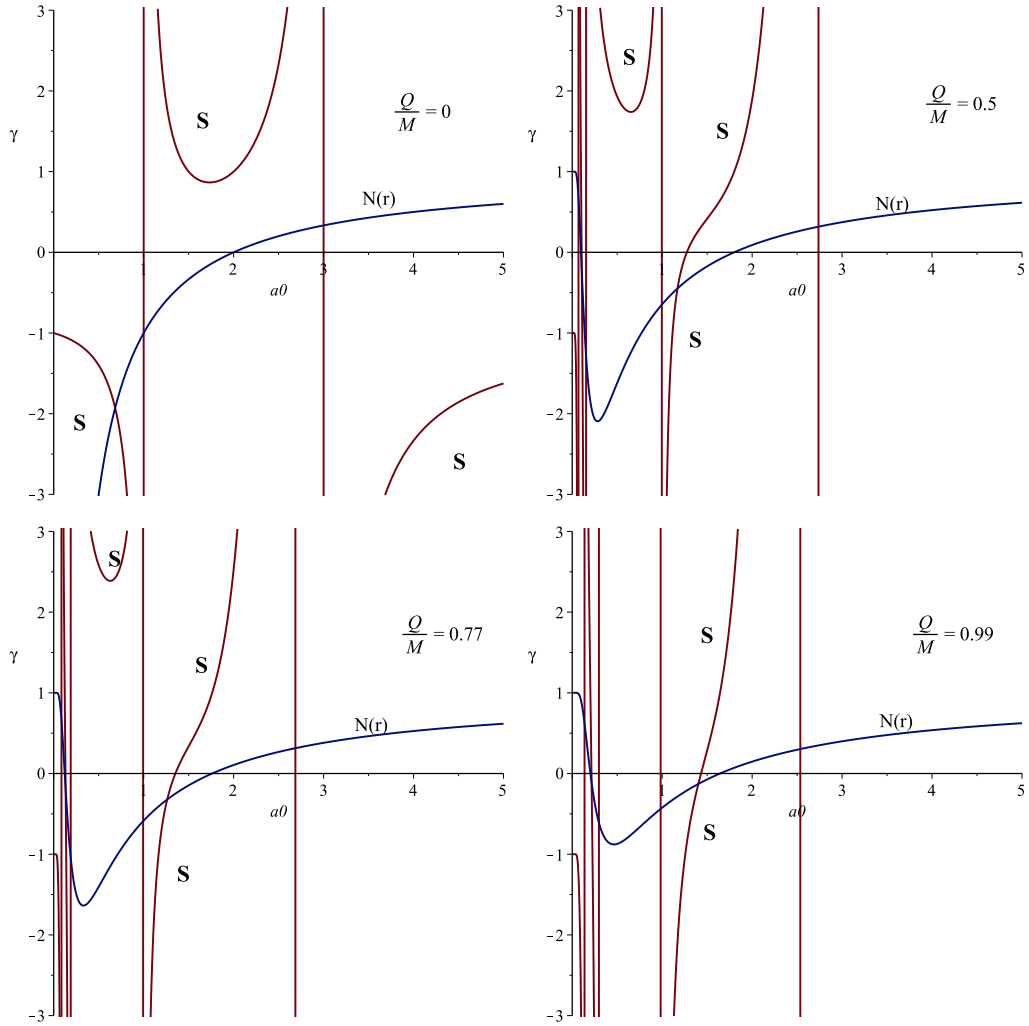

Figure 3.6: Plots for stability of regular ABGB thin-shell WHs in terms of γ by taking GCG and $\frac{Q}{M} = 0,\ 0.5,\ 0.77,\ 0.99$.

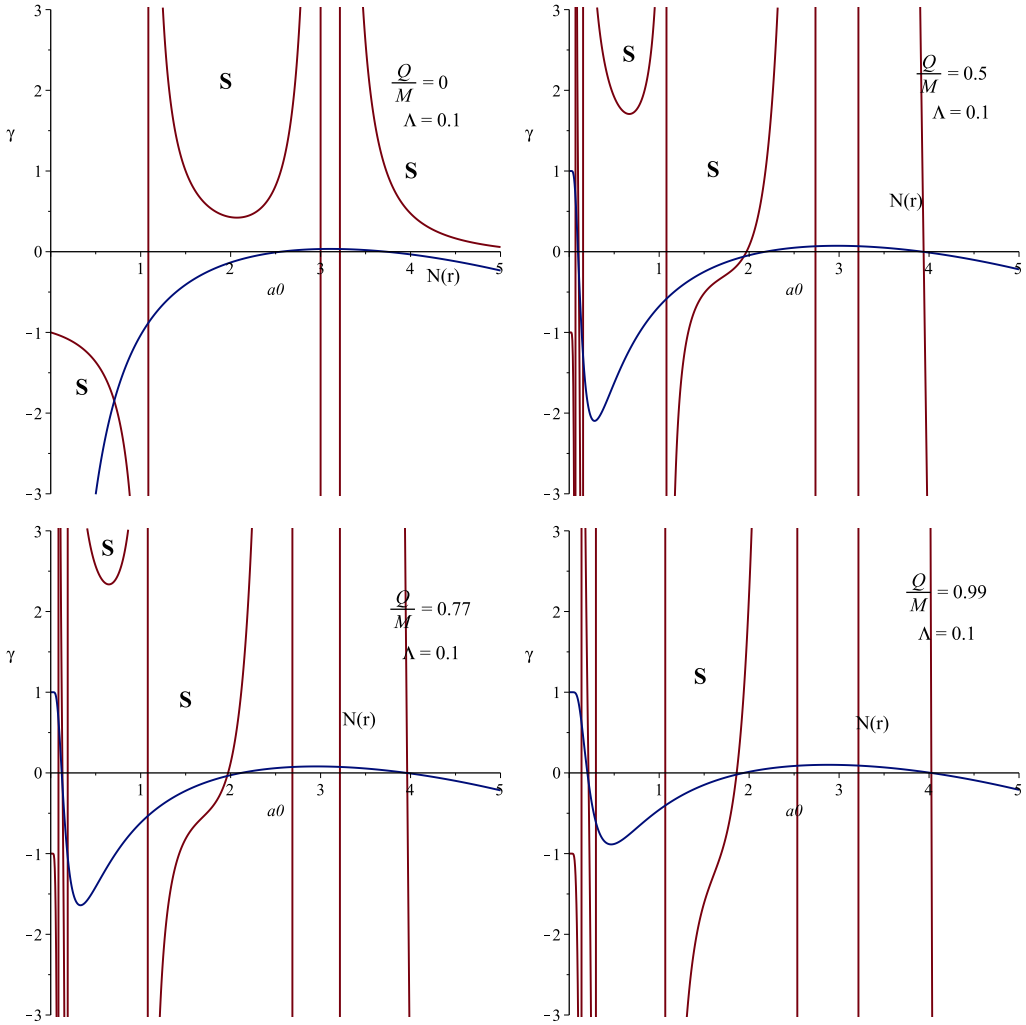

Figure 3.7: Plots for the stability of regular ABGB thin-shell WHs in terms of γ by taking GCG gas and $\Lambda = 0.1$.

(iv) Modified Generalized Chaplygin Gas

The EoS for MGCG is defined by

$$\Upsilon(\sigma) = p_0 + \xi_0(\sigma - \sigma_0) - w\left(\frac{1}{\sigma^\gamma} - \frac{1}{\sigma_0^\gamma}\right), \tag{3.1.21}$$

where ξ_0 and w are free parameters. Its differentiation yields

$$\Upsilon'(\sigma_0) = \xi_0 + \frac{w\gamma}{\sigma_0^{\gamma+1}}.$$

Figure **3.8** shows the corresponding graphs for $\xi_0 = \gamma = 1$ and different values of charge. For MGCG, we find that the possibility of stability regions increases by increasing the value of $\frac{Q}{M}$. For $\Lambda = 0.1$, it is observed that the increasing value of $\frac{Q}{M}$ provides more stable WH solutions corresponding to both positive and negative values of the parameter w (Figure **3.9**). It is worth mentioning that the effect of MGCG is to increase the stability regions for regular ABGB thin-shell WHs by increasing $\frac{Q}{M}$ as depicted in our numerical plots.

(v) Logarithmic Gas

Finally, we take logarithmic gas defined by the EoS

$$\Upsilon(\sigma) = p_0 + w\ln\left|\frac{\sigma}{\sigma_0}\right|, \tag{3.1.22}$$

where $\Upsilon'(\sigma_0) = \frac{w}{\sigma_0}$. We plot the corresponding stable ABGB thin-shell WHs for different values of charge without Λ as shown in Figure **3.10**. It is found that two stability regions exist for $\frac{Q}{M} = 0,\ 0.5,\ 0.77$ and $\xi_0 = \gamma = 1,\ \Lambda = 0.1, -0.5$ which reduce to only one stability region for maximum value of charge, i.e., $\frac{Q}{M} = 1.1$. In case of ABGB-de Sitter configurations, the number of stability region increases by increasing $\frac{Q}{M}$ and reduces to only one region for $\frac{Q}{M} = 1.1$ (Figure **3.11**). We analyze maximum number of stable regions for $\frac{Q}{M} = 0.5$ in de Sitter background.

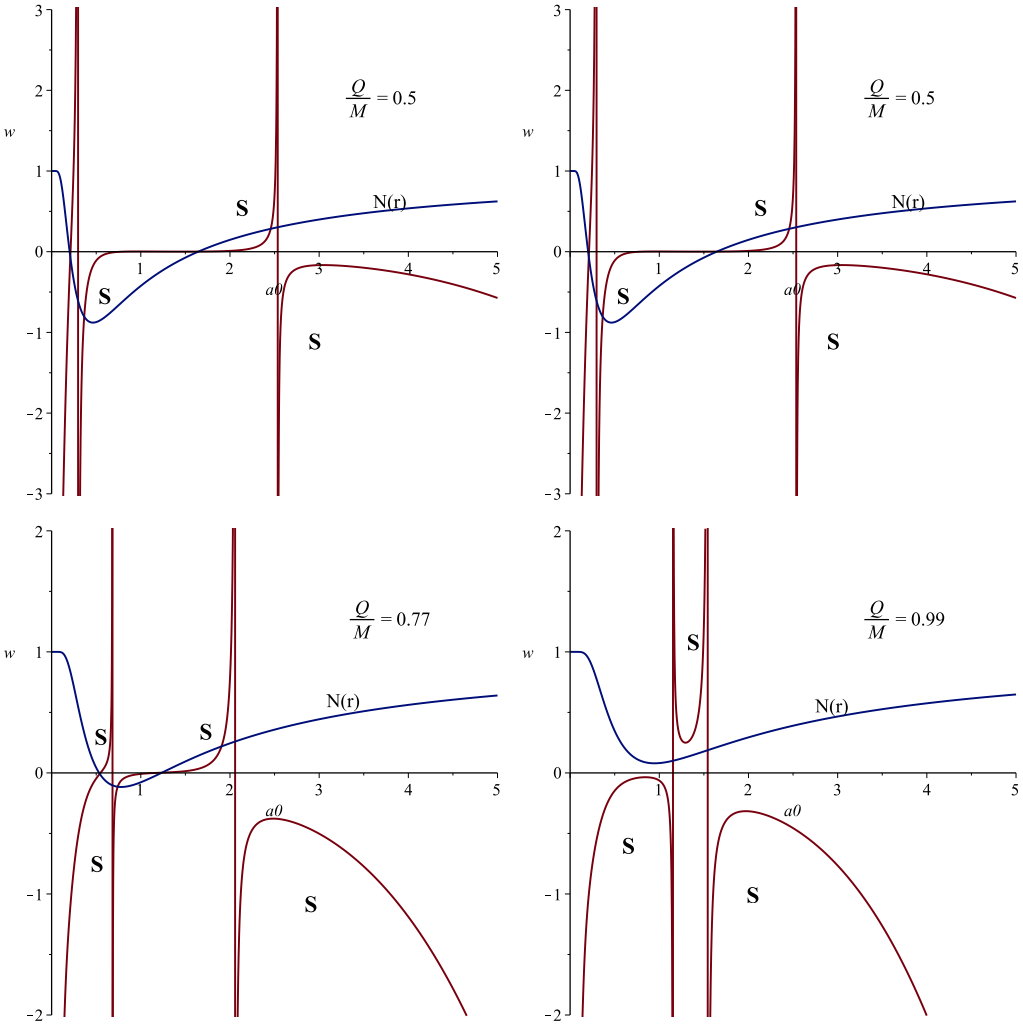

Figure 3.8: Plots for stable regular ABGB thin-shell WHs in the context of MGCG gas with $\xi_0 = \gamma = 1$ and different values of charge.

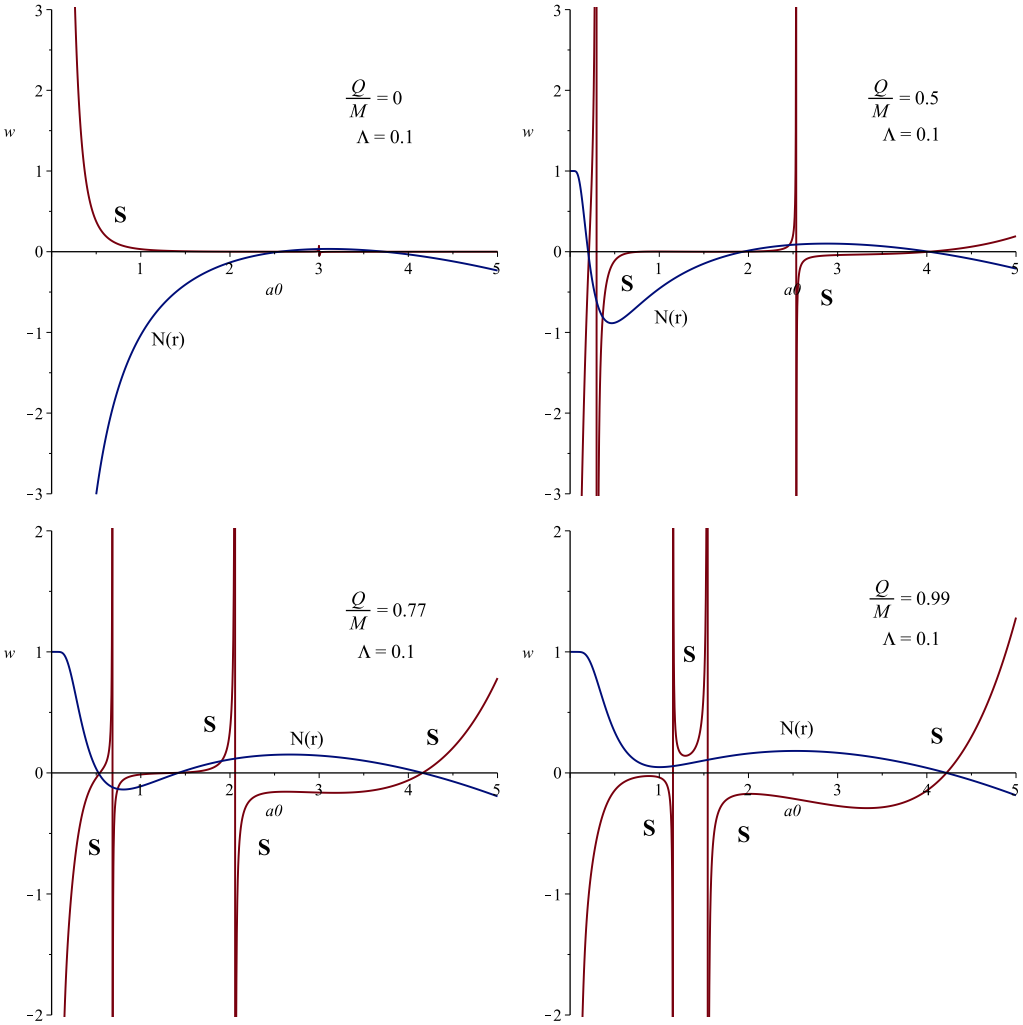

Figure 3.9: Plots for stability regions of regular ABGB thin-shell WHs by taking MGCG gas with $\xi_0 = \gamma = 1$ and different values of charge in de Sitter background.

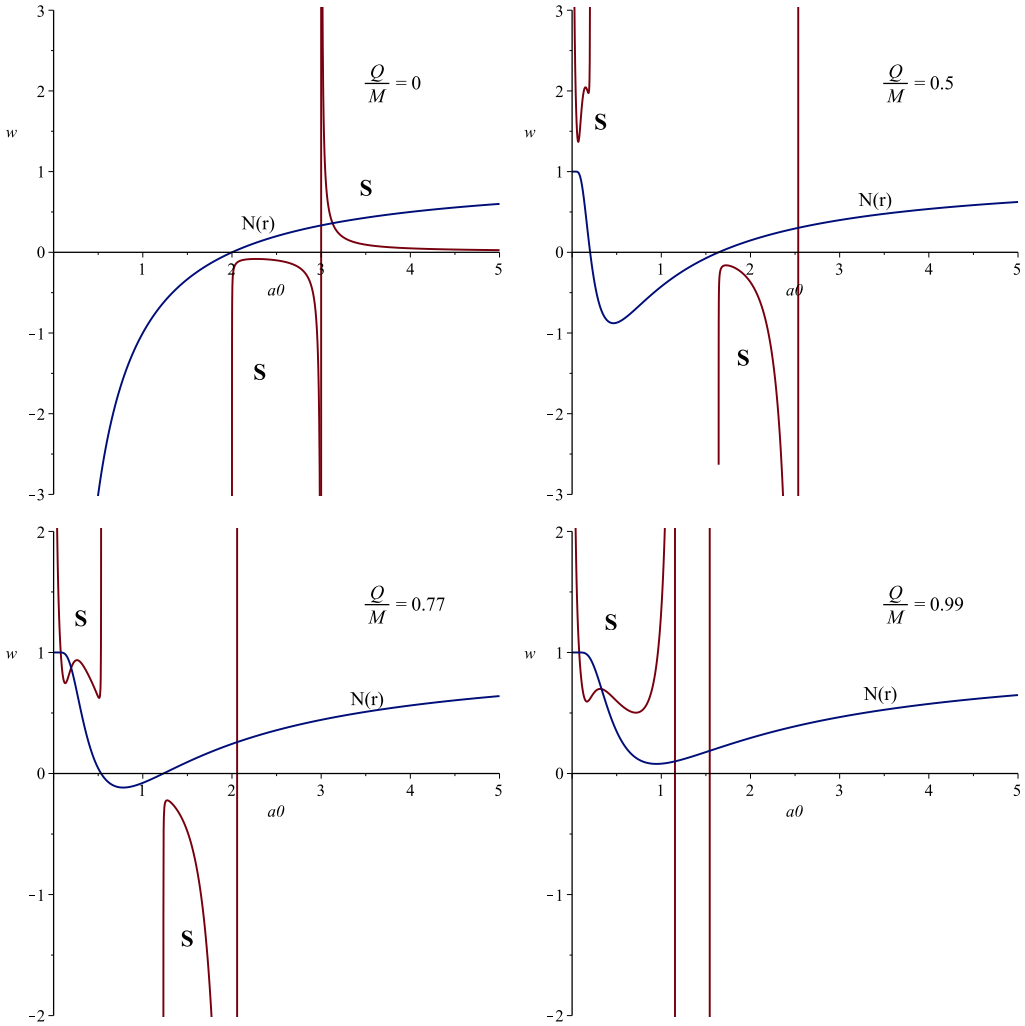

Figure 3.10: Plots for regular ABGB thin-shell WHs by taking logarithmic gas EoS for $\frac{Q}{M} = 0,\ 0.5,\ 0.77,\ 0.99$.

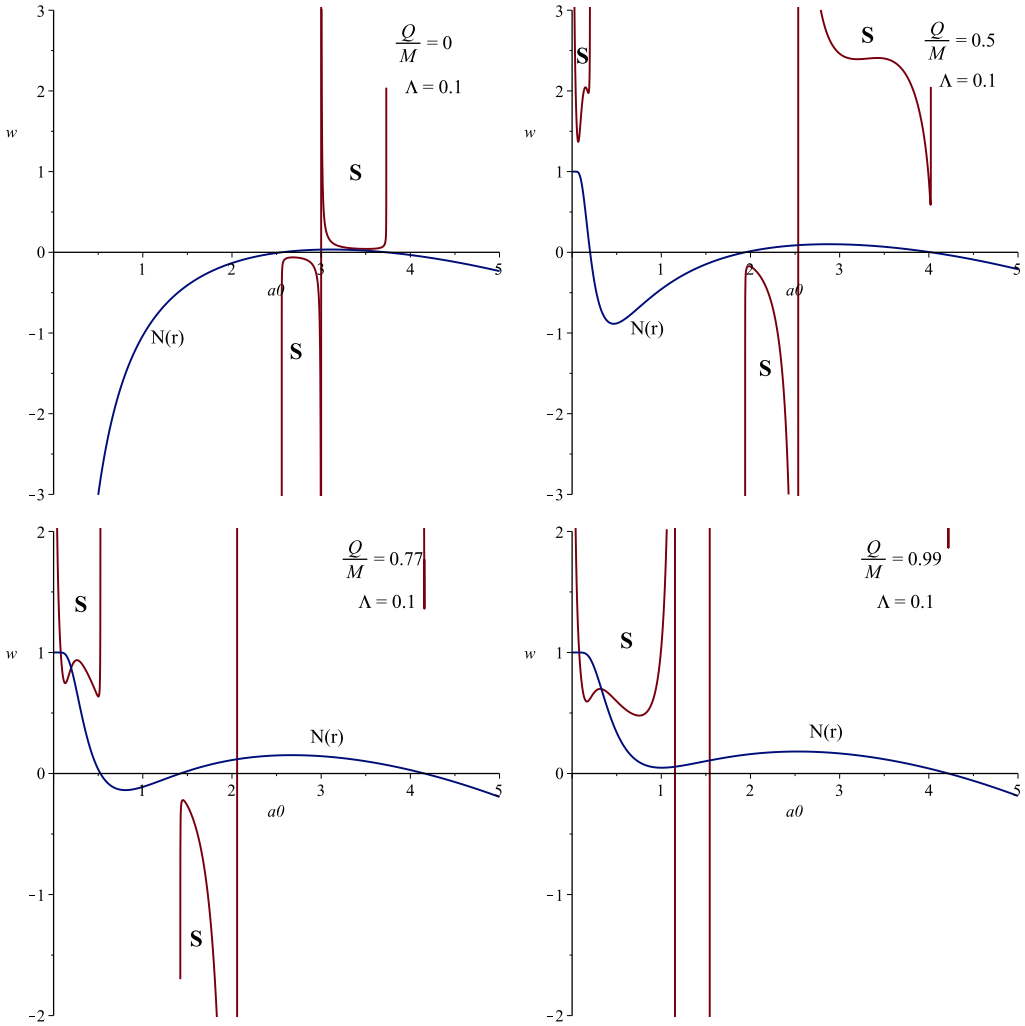

Figure 3.11: Plots for regular ABGB thin-shell WHs by taking logarithmic gas EoS with $\frac{Q}{M} = 0,\ 0.5,\ 0.77,\ 0.99$ and $\Lambda = 0.1$.

3.1.4 Stability Analysis against Velocity Perturbations

Here we investigate the effect of velocity perturbations on stability of regular ABGB thin-shell WHs. We confine ourselves to small velocity perturbations about static configuration $\tilde{a} = a_0$ such that after any perturbation, an approximately static fluid can be taken for exotic matter. For this purpose, we compute the following EoS through Eq.(3.1.9) as

$$p = -\frac{1}{2}\left(1 + \frac{\tilde{a}N'(\tilde{a})}{2N(\tilde{a})}\right)\sigma. \tag{3.1.23}$$

Substituting σ and p from Eqs.(3.1.6) and (3.1.7), it takes the form

$$\ddot{\tilde{a}} - \frac{N'(\tilde{a})}{2N(\tilde{a})}\dot{\tilde{a}}^2 = 0, \tag{3.1.24}$$

which represents one-dimensional motion of the WH throat. Integration of this equation leads to

$$\dot{\tilde{a}} = \dot{a_0}\frac{\sqrt{N(\tilde{a})}}{\sqrt{N(a_0)}}, \tag{3.1.25}$$

whose second integration gives

$$\frac{\dot{a_0}}{\sqrt{N(a_0)}}(\tau - \tau_0) = \int_{a_0}^{\tilde{a}} \frac{d\tilde{a}}{\sqrt{N(\tilde{a})}}. \tag{3.1.26}$$

Here $\dot{a}_0$ is considered to be non-zero initial small velocity of throat after perturbation. For regular ABGB spacetime, Eq.(3.1.26) upto second order of small values of Q yields

$$\begin{aligned}\frac{\dot{a_0}}{\sqrt{N(a_0)}}(\tau - \tau_0) &= \frac{\tilde{a}(\tilde{a} - 2M) + Q^2}{\tilde{a}\sqrt{N(\tilde{a})}} - \frac{a_0(a_0 - 2M) + Q^2}{a_0\sqrt{N(a_0)}} \\ &+ M\ln\left(\frac{\tilde{a} - M + \tilde{a}\sqrt{N(\tilde{a})}}{a_0 - M + a_0\sqrt{N(a_0)}}\right),\end{aligned} \tag{3.1.27}$$

which indicates that this motion is clearly not oscillatory. Consequently, the ABGB WH throat remains unstable against velocity perturbations. Equation (3.1.24) also shows that acceleration of the WH throat $\ddot{\tilde{a}} = \frac{N'(\tilde{a})}{2N(\tilde{a})}\dot{\tilde{a}}^2$ is positive leading to unstable ABGB thin-shell WHs.

3.2 Einstein Hoffman-Born-Infeld Electrodynamics and Thin-Shell Wormholes

In this section, we discuss general formalism for the construction of thin-shell WHs in Einstein HBI electrodynamics and investigate the role of various physical parameters on stability of the respective thin-shell WHs.

3.2.1 General Equations

Nonlinear electrodynamics with various compositions has restorative effects on the divergent results that appear naturally in linear Maxwell theory. In this context, Born and Infeld [40] proposed the most prominent constituent of viable NLED theories to resolve this problem upto some extent. However, this theory has some drawbacks that are not completely eliminated. To overcome this specific issue, Hoffman and Infeld [41] proposed a Lagrangian having a logarithmic term with significant consequences which removed the singularity arising in the Cartesian components of the electric field E. Mazharimousavi et al. [88] rediscovered the global logarithmic term of Lagrangian in Einstein NLED theory. They used HBI Lagrangian in both GR as well as Gauss-Bonnet gravity to construct BHs and thin-shell WHs. Motivated by this proposal, we examine the role of HBI electrodynamics on the stability of thin-shell WHs. We consider Einstein HBI Lagrangian

$$\mathcal{L}(F)=\begin{cases}\mathcal{L}_{+}=-\frac{2}{\tilde{b}^{2}}(k+\beta_{1}\xi_{+}-\ln\xi_{+}), & r\geq\sqrt{Q\tilde{b}},\\ \mathcal{L}_{-}=-\frac{2}{\tilde{b}^{2}}(k+\beta_{1}\xi_{-}-\ln|\xi_{-}|), & r\leq\sqrt{Q\tilde{b}},\end{cases} \tag{3.2.1}$$

in which $\beta_1 = 1$, $k = \ln 2 - 2$ and $\xi_\pm = 1 \pm \sqrt{1 + 2\tilde{b}^2 F}$, where $\tilde{b}$ is the constant HBI parameter, F is the trace of electromagnetic field tensor. This Lagrangian imposes $\mathcal{L}_+ = \mathcal{L}_-$ at $r^4 = Q^2\tilde{b}^2$. The coupling of GR with HBI electrodynamics leads to intriguing features that make it worthy to apply on strong electromagnetic and gravitational fields. The coupling of Einstein gravity with 4D HBI electrodynamics is defined by the action

$$S = \frac{1}{2}\int \sqrt{-g}[R + \mathcal{L}(F)]d^4x. \tag{3.2.2}$$

The metric coefficient for static electrically charged spherically symmetric BH in HBI theory is given by

$$\begin{aligned} N(r) &= 1 - \frac{2M}{r} + \frac{r^2}{3\tilde{b}^2}\ln\left(\frac{r^4}{r^4 + Q^2\tilde{b}^2}\right) - \frac{Q^2\sqrt{2}}{3r\sqrt{Q\tilde{b}}}\left[\tan^{-1}\left(\frac{r\sqrt{2}}{\sqrt{Q\tilde{b}}} + 1\right)\right. \\ &+ \left.\tan^{-1}\left(\frac{r\sqrt{2}}{\sqrt{Q\tilde{b}}} - 1\right)\right] - \frac{Q^2\sqrt{2}}{6r\sqrt{Q\tilde{b}}}\ln\left(\frac{r^2 + Q\tilde{b} - r\sqrt{2q\tilde{b}}}{r^2 + Q\tilde{b} + r\sqrt{2Q\tilde{b}}}\right) \\ &+ \frac{Q^2\pi\sqrt{2}}{3r\sqrt{Q\tilde{b}}}. \end{aligned} \tag{3.2.3}$$

The horizons of the spacetime can be found numerically by taking $N(r) = 0$. Here one can easily find that the given line element reduces to RN and Schwarzschild spacetimes in the limits $\tilde{b} \to 0$ and $\tilde{b} \to \infty$, respectively.

The mathematical construction of thin-shell WHs follows the usual steps of cut and paste technique. For this purpose, we take two copies of HBI spacetimes such that we cut the interior region with $r \leq \tilde{a}$ from each geometry given by $\mathcal{M}^{1,2} = \left\{x^\mu_{1,2} :\ r_{1,2} \leq \tilde{a} | \tilde{a} > \sqrt{Q\tilde{b}}\right\}$, where we assume $\tilde{a} > r_h$ to avoid the presence of singularities. These copies are pasted at the hypersurface such that we obtain a new

geodesically complete manifold $\mathcal{M}=\mathcal{M}^1\cup\mathcal{M}^2$. We adopt a timelike induced metric (3.1.5) with coordinates $\xi^i=(\tau,\theta,\phi)$ at thin-shell.

In order to explore attractive or repulsive behavior of HBI thin-shell WHs, we compute the non-zero radial component of four-acceleration as

$$\begin{aligned}
a^r &= \frac{M}{r^2}+\frac{r}{3\tilde{b}^2}\ln\left(\frac{r^4}{r^4+Q^2\tilde{b}^2}\right)+\frac{2(r^4+Q^2\tilde{b}^2)}{3r^2\tilde{b}^2}\left(\frac{r^3}{r^4}-\frac{r^7}{(r^4+Q^2\tilde{b}^2)^2}\right)\\
&+ \frac{Q^2}{3r^2\sqrt{2Q\tilde{b}}}\left[\tan^{-1}\left(\frac{r\sqrt{2}}{\sqrt{Q\tilde{b}}}+1\right)+\tan^{-1}\left(\frac{r\sqrt{2}}{\sqrt{Q\tilde{b}}}-1\right)\right]\\
&+ \frac{Q}{3r\tilde{b}}\left[\frac{1+\tan\left(\frac{r\sqrt{2}}{\sqrt{Q\tilde{b}}}+1\right)^2}{\tan\left(\frac{r\sqrt{2}}{\sqrt{Q\tilde{b}}}+1\right)^2}+\frac{1+\tan\left(\frac{r\sqrt{2}}{\sqrt{Q\tilde{b}}}-1\right)^2}{\tan\left(\frac{r\sqrt{2}}{\sqrt{Q\tilde{b}}}-1\right)^2}\right]\\
&+ \frac{Q^2}{6r^2\sqrt{2Q\tilde{b}}}\ln\left(\frac{r^2+Q\tilde{b}-r\sqrt{2Q\tilde{b}}}{r^2+Q\tilde{b}+r\sqrt{2Q\tilde{b}}}\right)-\frac{Q^2(r^2+Q\tilde{b}+r\sqrt{2Q\tilde{b}})}{6r\sqrt{2Q\tilde{b}}(r^2+Q\tilde{b}-r\sqrt{2Q\tilde{b}})}\\
&\times \left(\frac{2r-\sqrt{2Q\tilde{b}}}{r^2+Q\tilde{b}+r\sqrt{2Q\tilde{b}}}-\frac{(2r+\sqrt{2Q\tilde{b}})(r^2+Q\tilde{b}-r\sqrt{2Q\tilde{b}})}{(r^2+Q\tilde{b}+r\sqrt{2Q\tilde{b}})^2}\right)-\frac{Q^2\pi}{3r^2\sqrt{2Q\tilde{b}}}.
\end{aligned}\tag{3.2.4}$$

The respective results for thin-shell WHs coupled with HBI electrodynamics are shown in Figure **3.12**. It is noted that a WH has attractive or repulsive features if $a^r>0$ or $a^r<0$, respectively. We find that the constructed WH configurations have repulsive behavior for smaller throat radius which will become attractive on increasing throat radius.

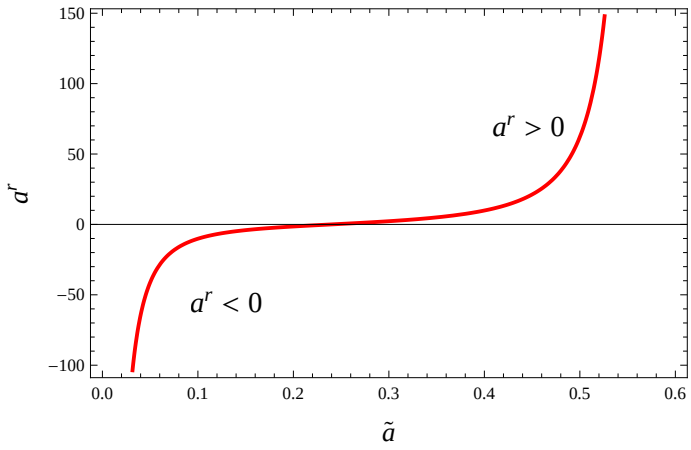

Figure 3.12: Plot of a^r for $\frac{Q}{M} = 1.1$ and $\tilde{b} = 0.6$.

3.2.2 Stability Analysis

We are interested to explore WH stability by taking barotropic EoS (3.1.12) as a linear perturbation. We follow the same stability approach as given for ABGB thin-shell WHs. We consider three different candidates (CG, linear and logarithmic gas models) to explore stability of HBI thin-shell WHs as follows.

(i) Chaplygin Gas

We consider CG model (3.1.18) for the dynamical investigation of HBI thin-shell WHs. We explore the role of increasing values of charge as well as HBI parameter in the WH stability. The corresponding results for the WH stability are shown in Figures **3.13** and **3.14**. For $\frac{Q}{M} = 0.5,\ 0.7$ and $\tilde{b} = 0.6$, we find one stable region (red curve) for both positive as well as negative values of parameter μ while the metric function $N(r)$ cuts the radial axis once showing an event horizon. It is mentioned here that $\frac{Q}{M} = 1.1$ provides only one stable region for negative values of parameter

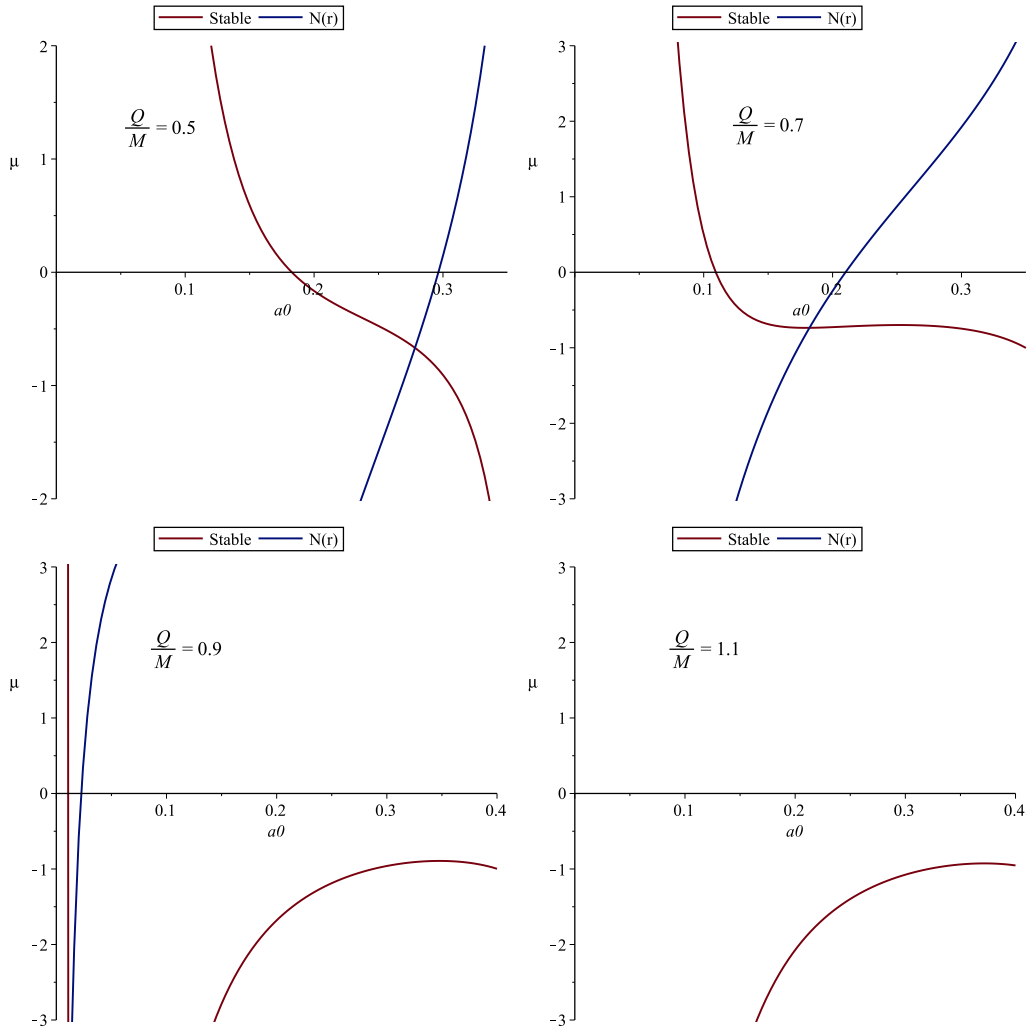

Figure 3.13: Plots for stable regions of thin-shell WHs taking CG EoS and HBI parameter $\tilde{b} = 0.6$ with different values of charge.

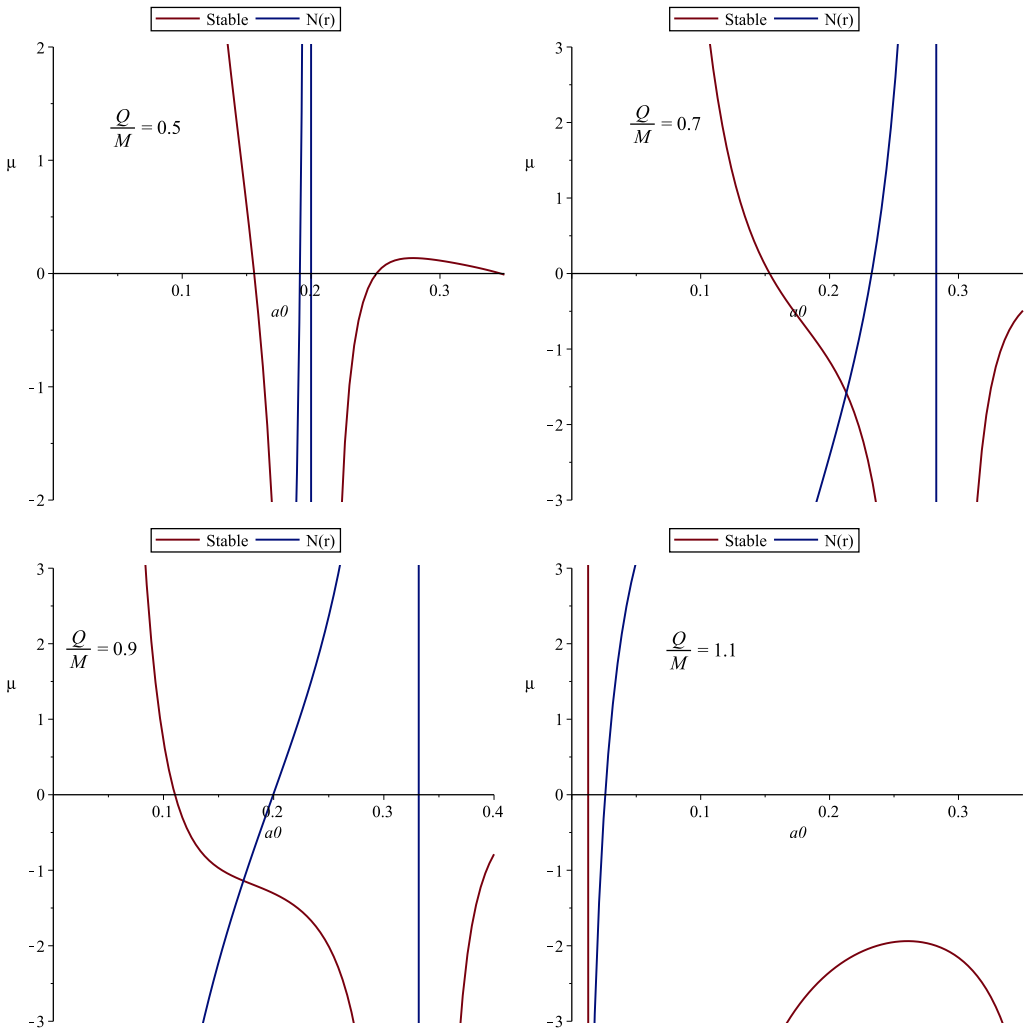

Figure 3.14: Plots for stable WHs with CG EoS, $\tilde{b} = 1$ and different values of charge.

μ in the absence of event horizon (Figure **3.13**). For $\tilde{b} = 1$, we analyze enlargement in the stability areas (two regions) for both positive as well as negative values of μ corresponding to $\frac{Q}{M} = 0.5,\ 0.7,\ 0.9$. In this case, we observe that the event horizon does not vanish for $\frac{Q}{M} = 1.1$ but reduces to one (**3.14**). The HBI parameter is effective to increase the WH stability for CG model while the increasing values of $\frac{Q}{M}$ tend to diminish the presence of event horizon.

(ii) Linear Gas

Here we plot stable solutions for linear gas (3.1.17) by taking $\tilde{b} = 0.6$ as shown in Figure **3.15**. The event horizon gets smaller by enlarging the values of charge and finally vanishes for the maximum value of $\frac{Q}{M}$. The possibility of stable regions increases by increasing HBI parameter such that we find maximum stability regions for $b = 1$. We investigate stable regions for both positive as well as negative values of μ with $\frac{Q}{M} = 0.5,\ 0.7$ while stable regions exist only for negative values of μ corresponding to large values of charge. The event horizon does not vanish for maximum value of charge (Figure **3.16**).

(iii) Logarithmic Gas

For logarithmic gas, the respective stable HBI thin-shell WHs with $\frac{Q}{M} = 0.5,\ 0.7,\ 0.9,$ 1.1 and $\tilde{b} = 0.6$ are shown in Figure **3.17**. Here we find least stable solutions for smaller values of charge as compared to the previous case which tend to increase on increasing charge. We also analyze more stable solutions by increasing $\tilde{b}$ for larger values of $\frac{Q}{M}$ while the event horizon does not disappear in this case (Figure **3.18**).

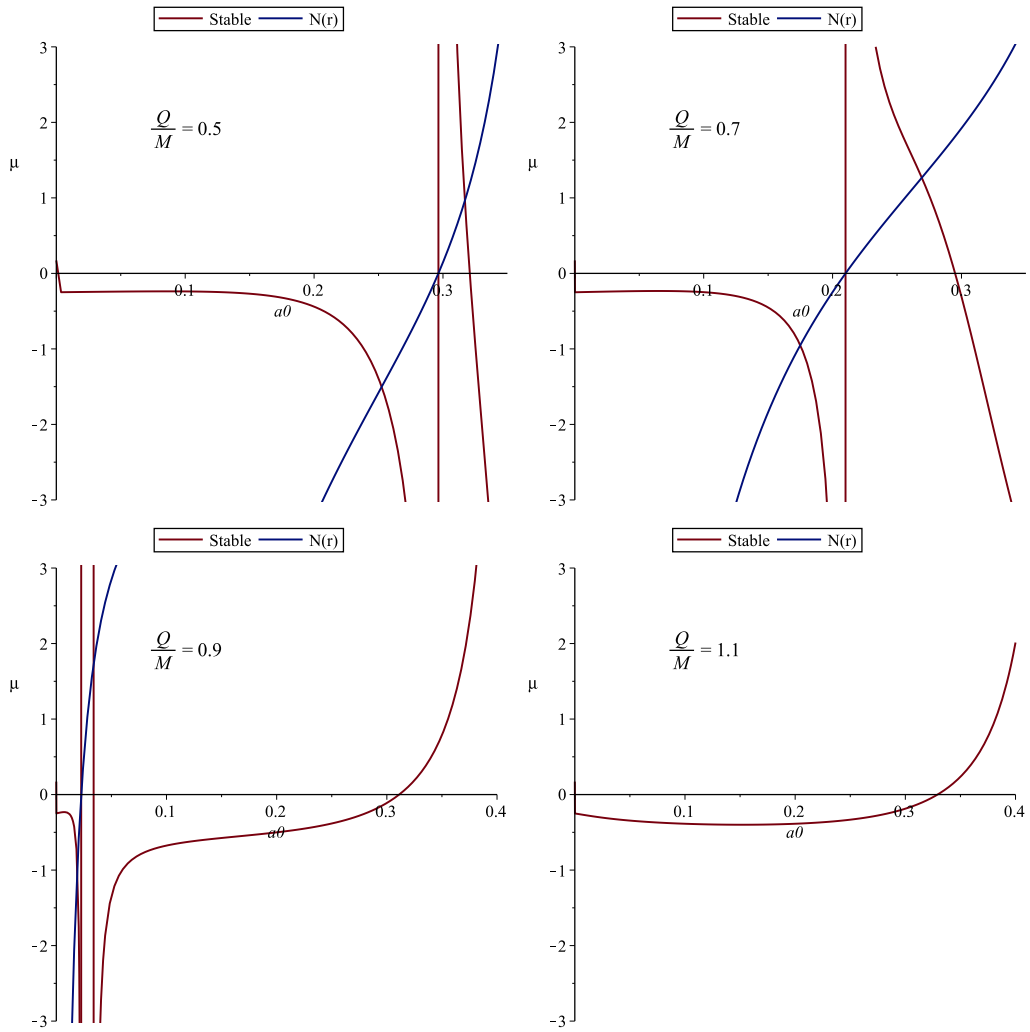

Figure 3.15: Plots for stability of thin-shell WHs with linear gas and HBI parameter $\tilde{b} = 0.6$.

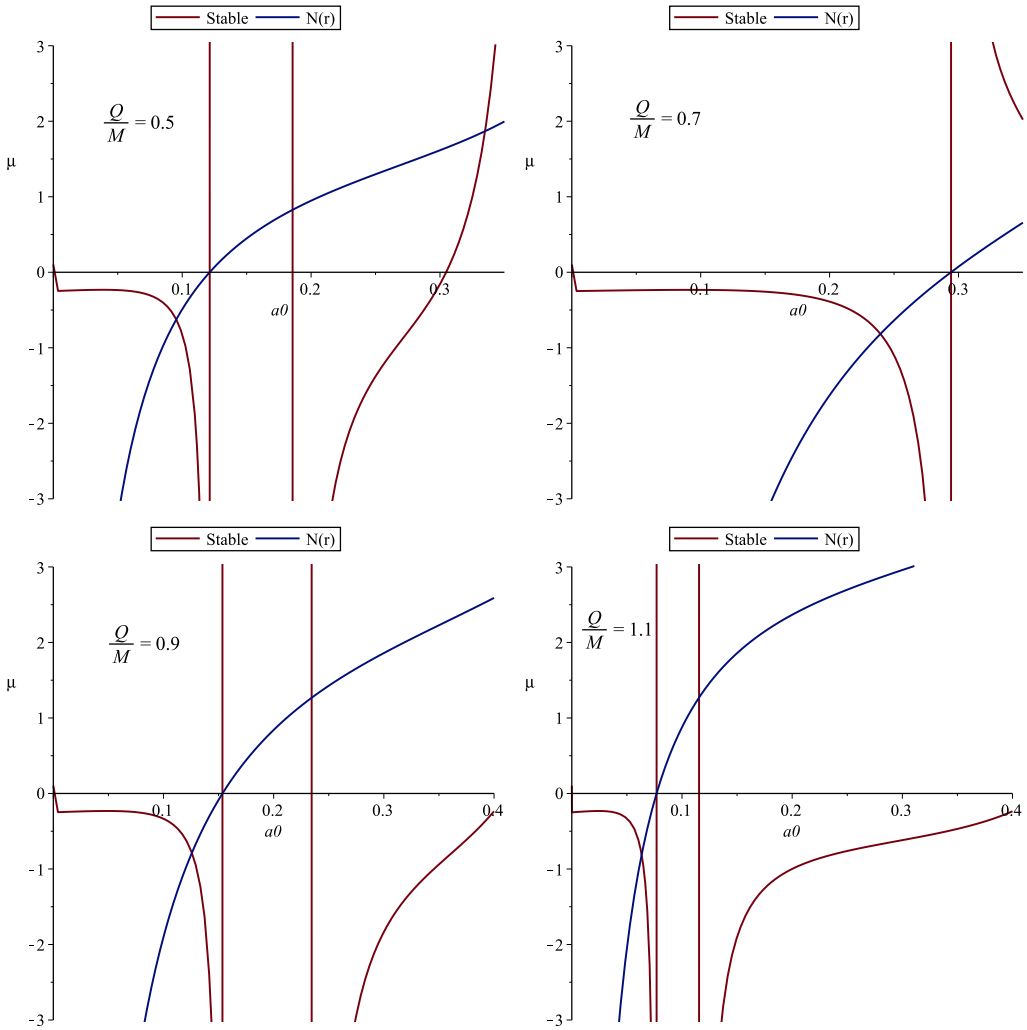

Figure 3.16: Plots for stability regions of WH configuration with linear gas corresponding to $\tilde{b} = 1$.

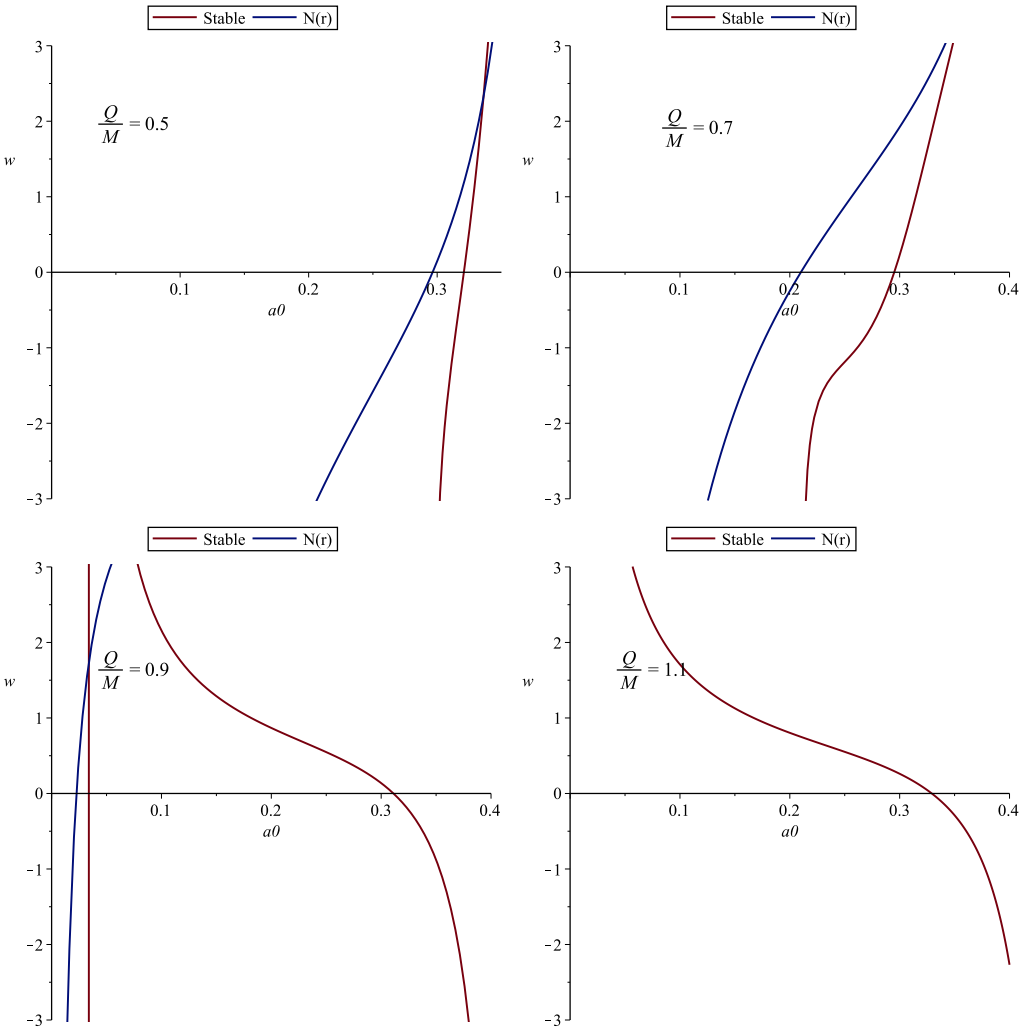

Figure 3.17: Plots for logarithmic gas and HBI parameter $\tilde{b} = 0.6$ with different values of charge.

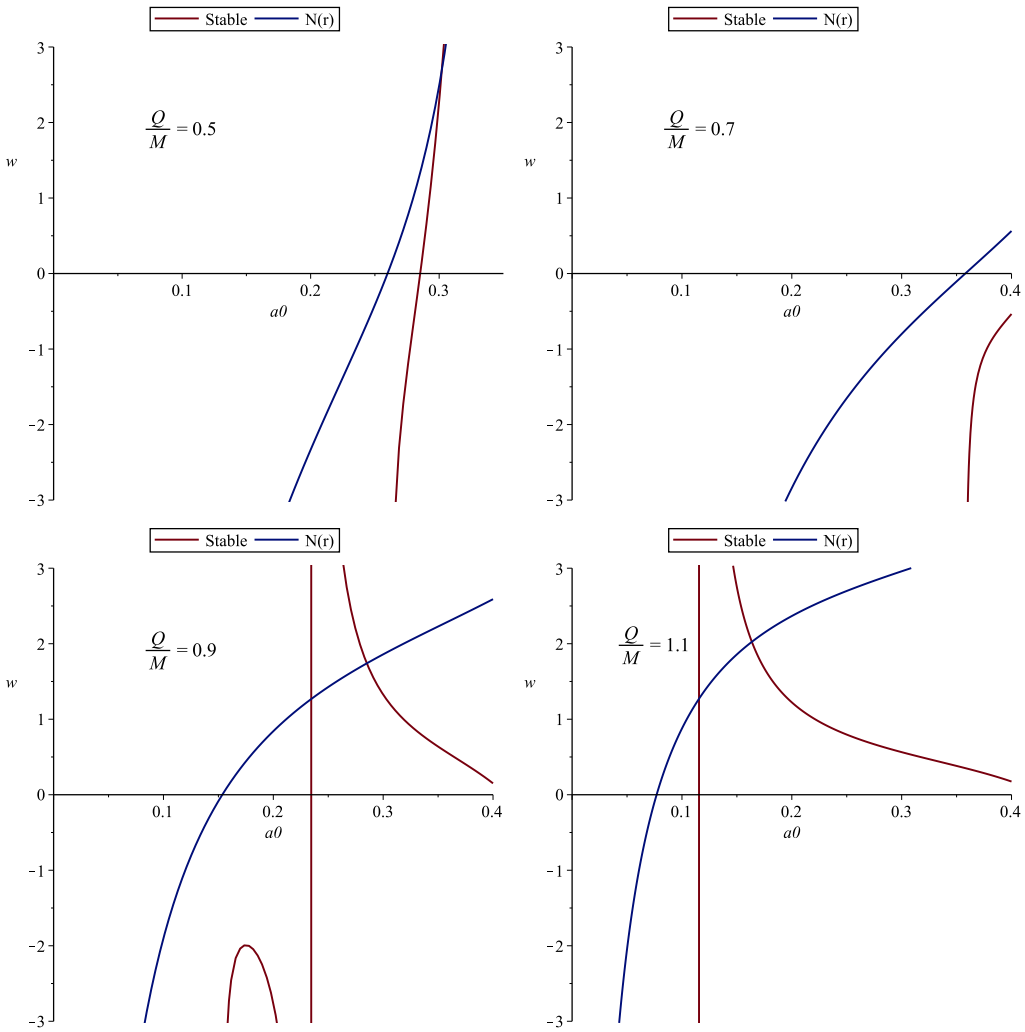

Figure 3.18: Plots for logarithmic gas with $\tilde{b} = 1$ and different values of charge.

Chapter 4

Phase Space Analysis of Isotropic and Anisotropic Universe Models

This chapter is devoted to study stability of accelerated expansion in FRW and LRS BI universe models via phase space analysis. We establish an autonomous system of equations by introducing normalized dimensionless variables. In order to analyze stability of the system, we find corresponding critical points for different values of the parameters. We also evaluate power-law scale factor whose behavior indicates different phases of the universe model. The chapter is classified in two sections. In the next section, we discuss stability of viscous isotropic cosmos in the framework of NLED whose results have been published [89]. Subsequently, we study phase space analysis of LRS BI universe model by taking different linear combinations for the interactions between scalar field models and DM in section **4.2**. A research paper based on the respective results has been submitted for publication [90].

4.1 Nonlinear Electrodynamics and Stability of FRW Universe

Nonlinear electrodynamics is the generalization of Maxwell theory which is assumed to be the most appropriate theory to abolish the initial singularities. Vollick [91] studied physical aspects of FRW universe model in NLED and found that the respective model undergoes accelerated expansion for $E^2 < 3B^2$. Kruglov [92] showed that NLED model tends to accelerate the universe in magnetic background at the early epoch. Ovgun [93] developed analytical nonsingular extension of FRW model by introducing a new theoretical model in nonlinear magnetic monopole fields. For situations where strong electromagnetic field occurs, it makes sense to couple gravitation with NLED. The coupling of Einstein gravity with NLED is defined by the action

$$S = \frac{1}{16\pi}\int \sqrt{-g}[R - \mathcal{L}(F, F^*)]d^4x. \tag{4.1.1}$$

We consider nonlinear extension of Maxwell Lagrangian density upto second order terms in the field invariants $F = F_{ij}F^{ij}$ and $F^* = F^*_{ij}F^{ij}$ given by [91]

$$\mathcal{L} = \mathcal{L}(F, F^*) = -\frac{1}{4\mu_0}F + \varepsilon_1 F^2 + \varepsilon_2 F^{*2}, \tag{4.1.2}$$

where μ_0 denotes magnetic permeability, $\varepsilon_1,\ \varepsilon_2 > 0$ are arbitrary constants which yield linear density for $\varepsilon_1,\ \varepsilon_2 \to 0$ and F^*_{ij} is the dual of electromagnetic field tensor. We do not consider the term FF^* involving F^* in order to preserve the parity [94]. The linear term of this Lagrangian dominates during radiation dominated era while the quadratic terms dominate in the early universe that corresponds to the bouncing behavior of the universe to avoid initial singularity. The energy-momentum tensor

associated with this Lagrangian has the following form

$$T_{ij(EM)} = -4\partial_F \mathcal{L} F_i^k F_{kj} + (\partial_{F^*} \mathcal{L} F^* - \mathcal{L}) g_{ij}. \tag{4.1.3}$$

The energy-momentum tensor of the electromagnetic field associated with $\mathcal{L}(F, F^*)$ can be written as that of a perfect fluid

$$T_{ij} = (\sigma + p) u_i u_j + p g_{ij}, \tag{4.1.4}$$

such that

$$\sigma_{EM} = -\mathcal{L} - 4E^2 \partial_F \mathcal{L}, \tag{4.1.5}$$

$$p_{EM} = \mathcal{L} - \frac{4}{3}(2B^2 - E^2)\partial_F \mathcal{L}, \tag{4.1.6}$$

where ∂_F represents partial derivative with respect to $F = F_{ij}F^{ij} = 2(B^2 - E^2)$, E and B denote the averaged electric and magnetic fields, respectively.

We consider FRW universe model given by

$$ds^2 = -dt^2 + a^2(t)(dr^2 + r^2 d\theta^2 + r^2 \sin^2\theta d\phi^2), \tag{4.1.7}$$

where $a(t)$ is the scale factor. We assume the universe model to be filled with two cosmic fluids, i.e., a noninteracting electromagnetic fluid with energy density σ_{EM} as well as pressure p_{EM} and a viscous fluid having energy density σ_v as well as pressure $p = p_v(\sigma_v) + \Psi$. Here p_v represents the equilibrium part of viscous pressure whereas Ψ is the non-equilibrium part, i.e., bulk viscous pressure satisfying an evolution equation. The main contribution of bulk viscosity to the effective pressure is its dissipative effect. We obtain Raychaudhuri and constraint equations from the field equations given by

$$\dot{\Theta} = -\frac{1}{3}\Theta^2 - \frac{1}{2}\left[\sigma_{EM} + \sigma_v + 3(p_{EM} + p_v + \Psi)\right], \tag{4.1.8}$$

$$0 = \sigma_{EM} + \sigma_v - \frac{1}{3}\Theta^2, \tag{4.1.9}$$

where $\Theta = 3H$ is the expansion scalar. The conservation of energy-momentum tensor yields the following evolution equations for viscous and electromagnetic field components

$$\dot{\sigma}_v = -[\sigma_v + p_v + \Psi]\Theta, \tag{4.1.10}$$

$$\dot{\sigma}_{EM} = -[\sigma_{EM} + p_{EM}]\Theta. \tag{4.1.11}$$

We consider a barotropic EoS for viscous fluid defined by

$$p_v = (\gamma - 1)\sigma_v, \tag{4.1.12}$$

where $1 \leq \gamma \leq 2$. Using Eqs.(4.1.8) and (4.1.9), Raychaudhuri and conservation equations for viscous fluid turn out to be

$$\dot{\Theta} = -\frac{1}{2}\Theta^2 - \frac{3}{2}[p_{EM} + (\gamma - 1)\sigma_v + \Psi], \tag{4.1.13}$$

$$\dot{\sigma}_v = -[\gamma\sigma_v + \Psi]\Theta. \tag{4.1.14}$$

We characterize viscous pressure variable by the following evolution equation [95]

$$\tau_1\dot{\Psi} = -\zeta\Theta - \Psi\left(1 + \frac{\tau_*}{\zeta}\Psi\right)^{-1} - \frac{1}{2}\tau_1\Psi\left[\Theta + \frac{\dot{\tau_1}}{\tau_1} - \frac{\dot{\zeta}}{\zeta} - \frac{\dot{T}}{T}\right], \tag{4.1.15}$$

where ζ, T, τ_1 and τ_* denote bulk viscosity, local equilibrium temperature, linear relaxation time and characteristic time in nonlinear background, respectively. This equation is derived by using a nonlinear model describing a relationship between thermodynamic flux "Ψ" and thermodynamic force "χ" in the form

$$\Psi = -\frac{\zeta\chi}{1 + \tau_*\chi}. \tag{4.1.16}$$

This is a nonlinear extension of Israel-Stewart equation which reduces to its linear form as $\tau_* \to 0$. The nonlinear term in Eq.(4.1.15) must be positive for thermodynamic consistency and positivity of entropy production rate. The parameters involved in Eq.(4.1.15) can be defined by the relations $\zeta = \zeta_0\Theta$ ($\zeta > 0$), $\tau_1 = \frac{\zeta}{\gamma\nu_*^2\sigma_v}$, $\tau_* = k^2\tau_1$ and $T = T_0\sigma^{(\gamma-1)/\gamma}$. Here k is a constant such that $k = 0$ gives linear (Israel-Steward) case while T_0 represents constant temperature. Also, ν_* corresponds to the dissipative effect of the speed of sound V_1 such that $V_1^2 = c_s^2 + \nu_*^2$, where c_s^2 is its adiabatic contribution. By causality, $V_1 \leq 1$ and $c_s^2 = \gamma - 1$ which yields

$$\nu_*^2 \leq 2 - \gamma, \quad 1 \leq \gamma \leq 2. \tag{4.1.17}$$

The explicit form of evolution equation by using the above relations yields

$$\dot{\Psi} = -\gamma\nu_*^2\sigma_v\Theta - \frac{\gamma\nu_*^2\Psi\sigma_v}{\zeta_0\Theta}\left(1 + \frac{k^2\Psi}{\gamma\nu_*^2\sigma_v}\right)^{-1} - \frac{1}{2}\Psi\left[\Theta - \left(\frac{2\gamma-1}{\gamma}\right)\frac{\dot{\sigma_v}}{\sigma_v}\right]. \tag{4.1.18}$$

4.1.1 Phase Space Analysis

In this section, we discuss phase space analysis of isotropic and homogeneous universe model for radiation case. Due to many arbitrary parameters, it seems difficult to find analytical solution of the evolution equation. In this context, we define normalized dimensionless variables $\Omega = \frac{3\sigma_v}{\Theta^2}$ and $\tilde{\Psi} = \frac{3\Psi}{\Theta^2}$ such that the corresponding dynamical system can be reduced to autonomous one. We also define a new variable $\tilde{\tau}$ for time through which the corresponding derivative is represented by prime such that $\frac{dt}{d\tilde{\tau}} = \frac{3}{\Theta}$. Here each term is associated with some physical explicit background since the chosen dimensionless variables Ω and $\tilde{\Psi}$ occur due to physical impact of viscous energy density and pressure, respectively. The system of Eqs.(4.1.13) and (4.1.14) in

terms of these normalized variables takes the form

$$\frac{\Theta'}{\Theta} = -\frac{3}{2}\left[1+p_{EM}+(\gamma-1)\Omega+\tilde{\Psi}\right], \tag{4.1.19}$$

$$\frac{3\rho_v'}{\Theta^2} = -3[\gamma\Omega+\tilde{\Psi}]. \tag{4.1.20}$$

Differentiation of the dimensionless variable for energy density gives

$$\Omega' = \frac{3\sigma_v'}{\Theta^2} - 2\Omega\frac{\Theta'}{\Theta}. \tag{4.1.21}$$

Using Eqs.(4.1.19) and (4.1.20), this equation turns out to be

$$\Omega' = 3(\Omega-1)[\Omega(\gamma-1)+\tilde{\Psi}+3p_{EM}]. \tag{4.1.22}$$

Now we introduce the concept of a new evolution equation for $\tilde{\Psi}$. The first derivative of $\tilde{\Psi}$ with respect to $\tilde{\tau}$ through Eq.(4.1.19) leads to an evolution equation of the form

$$\begin{aligned}\tilde{\Psi}' &= -3\gamma\nu_*^2\Omega\left[1+\frac{\tilde{\Psi}}{3\zeta_0}\left(1+\frac{k^2\tilde{\Psi}}{\gamma\nu_*^2\Omega}\right)^{-1}\right] \\ &+ 3\tilde{\Psi}\left[1+3p_{EM}\left(1-\frac{3}{\Omega}\frac{2\gamma-1}{2\gamma}\right)\right]-3(\gamma-1)\tilde{\Psi}(1-\Omega).\end{aligned} \tag{4.1.23}$$

It is mentioned here that Eqs.(4.1.22) and (4.1.23) play a remarkable role to describe the respective dynamical system for phase space analysis.

In order to find the critical points $\{\Omega_c, \tilde{\Psi}_c\}$, we need to solve the dynamical system by imposing the condition $\Omega' = \tilde{\Psi}' = 0$. The stability of FRW universe model can be analyzed according to the nature of critical points. Here we restrict the phase space region to a condition which is necessary for the positivity of entropy production rate given by

$$\tilde{\Psi} > -\frac{\gamma\nu_*^2\Omega}{k^2}. \tag{4.1.24}$$

This condition tends the possible negative values of $\tilde{\Psi}$ towards zero for $k^2 \gg \nu_*^2$. Contrarily, the bulk pressure will be less restrictive if $k^2 \ll \nu_*^2$. It is noted that finite values of k allow only positive values of bulk pressure in the limit $\nu_* \to 0$. It would be more convenient to consider $k^2 \leq \nu_*^2$ along with $\nu_*^2 \leq 2-\gamma$ and $\tau_* = k^2\tau_1$ which leads to the fact that the characteristic time for nonlinear effects τ_* does not exceed the characteristic time in linear background τ_1. We characterize the critical points by deceleration parameter $\bar{q} = -1 - \frac{\Theta'}{\Theta}$ and effective EoS parameter $\gamma_{eff} = -\frac{2\Theta'}{3\Theta}$ which yield

$$\bar{q} = \frac{1}{2}\left[1 + 9p_{EM} + 3(\gamma-1)\Omega + 3\tilde{\Psi}\right], \tag{4.1.25}$$

$$\gamma_{eff} = 1 + 3p_{EM} + (\gamma-1)\Omega + \tilde{\Psi}. \tag{4.1.26}$$

To examine a region of phase space undergoing accelerated expansion, we impose $\bar{q} < 0$ in Eq.(4.1.25) which gives

$$\tilde{\Psi} < -\frac{1}{3} - 3p_{EM} - (\gamma-1)\Omega. \tag{4.1.27}$$

The possibility of accelerated expansion in the physical phase space is determined by comparing Eqs.(4.1.24) and (4.1.25) through $q < 0$ given by

$$\frac{\nu_*^2}{k^2} > \frac{1 + 9p_{EM} + 3(\gamma-1)\Omega}{3\gamma\Omega}. \tag{4.1.28}$$

Substituting $\Omega' = 0$ in Eq.(4.1.22), we find the following conditions

$$\Omega_c = 1, \tag{4.1.29}$$

$$(\gamma-1)\Omega_c + \tilde{\Psi}_c + 3p_{EM} = 0. \tag{4.1.30}$$

We insert these conditions in $\tilde{\Psi}'$ to find the location of critical points. This analysis is carried out by characterizing the viscous fluid through the choice of its EoS parameter

γ (radiation). We consider $0 < k^2 = \nu_*^2 \leq 2 - \gamma$ for which the case of stiff matter ($\gamma = 2$) is excluded from the analysis as it yields $\nu_*^2 = 0$.

4.1.2 Radiation Case ($\gamma = \frac{4}{3}$)

We consider the radiation case for phase space analysis by taking $\gamma = \frac{4}{3}$. Imposing the condition (4.1.29) and $\tilde{\Psi}' = 0$ in Eq.(4.1.23), we have

$$\frac{3\nu_*^2}{4\zeta_0}\tilde{\Psi}^3 - \frac{\nu_*^2}{\zeta_0}\tilde{\Psi}^2 - 3\tilde{\Psi}\left(1 - \frac{4\nu_*^2}{9\zeta_0} - \frac{21p_{EM}}{8}\right) + 4\nu_*^2 = 0. \tag{4.1.31}$$

This cubic equation yields three roots among which we retain only those roots that lie in the physical phase space. The general form of the dynamical system is given by

$$\Omega' = f(\Omega, \tilde{\Psi}), \quad \tilde{\Psi}' = g(\Omega, \tilde{\Psi}). \tag{4.1.32}$$

The eigenvalues of the system can be determined by the Jacobian matrix

$$\bar{Z} = \begin{pmatrix} \frac{\partial f}{\partial \Omega} & \frac{\partial f}{\partial \tilde{\Psi}} \\ \frac{\partial g}{\partial \Omega} & \frac{\partial g}{\partial \tilde{\Psi}} \end{pmatrix}_{|P_i^{\pm}}. \tag{4.1.33}$$

We find the eigenvalues corresponding to the points $P_r^{\pm}$ as

$$\eta_1 = 1 + 3\tilde{\Psi} + 9p_{EM}, \tag{4.1.34}$$

$$\eta_2 = -\frac{16\nu_*^2}{3\zeta_0}\left[\frac{1}{4+\tilde{\Psi}} - \frac{\tilde{\Psi}}{(4+\tilde{\Psi})^2}\right] - \frac{63p_{EM}}{8} + 6\tilde{\Psi} + 3. \tag{4.1.35}$$

In case of viscous radiating fluid, we can explore source and sink according to the sign of eigenvalues as well as direction of the trajectories. We investigate two critical points $P_r^+ = \{1, \tilde{\Psi}_c^+\}$ and $P_r^- = \{1, \tilde{\Psi}_c^-\}$ corresponding to positive ($\tilde{\Psi}_c^+$) and negative ($\tilde{\Psi}_c^-$) roots, respectively. By taking $\Omega_c = 0$ and the second condition (4.1.30) with $\tilde{\Psi}_c = -\frac{\Omega_c}{3} - 3p_{EM}$, we obtain $P_r^0 = \{0, -3p_{EM}\}$.

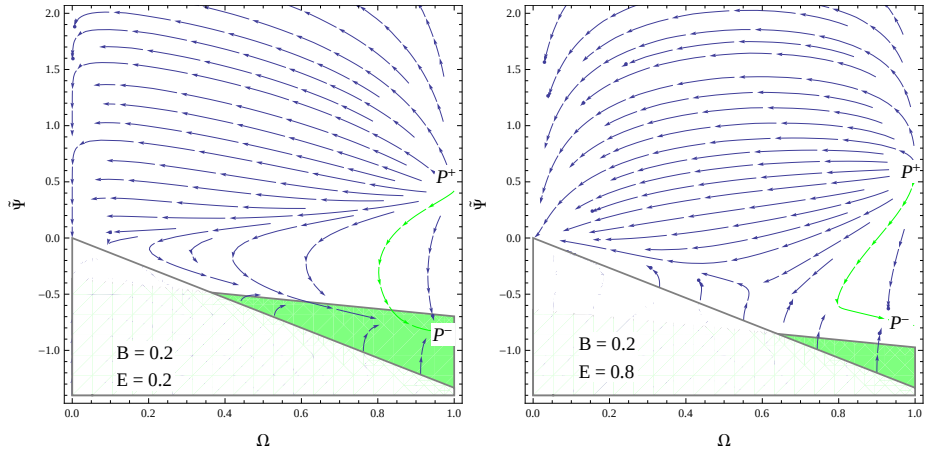

Figure 4.1: Plots for the phase plane evolution of viscous radiating fluid with $\gamma = 4/3$, $\nu_* = k = \sqrt{1/5}$, $\zeta_0 = 0.2$, $\alpha = 0.01$ and different values of B and E.

Case I $(E,\ B \neq 0)$

We are interested to analyze the impact of electromagnetic field on the stability of critical points in the presence of nonlinear bulk viscosity. The energy density (4.1.5) and pressure (4.1.6) are given by

$$\sigma_{EM} = \frac{1}{2\mu_0}(B^2+E^2) - 4\alpha(B^2-E^2)(B^2+3E^2), \tag{4.1.36}$$

$$p_{EM} = \frac{1}{6\mu_0}(B^2+E^2) - \frac{4\alpha}{3}(B^2-E^2)(5B^2-E^2). \tag{4.1.37}$$

The dynamical behavior of critical points for different values of electric and magnetic fields as well as other parameters is shown in Figures **4.1** and **4.2**. The green trajectory depicts a flow from the point P_d^+ towards P_d^-. The white region corresponds to the negative entropy production rate that diverges on its boundary whereas the green region shows accelerated expansion of the universe. Here the point P_d^0 shows varying behavior, i.e., either it is a saddle point or a sink depending on the values of different parameters.

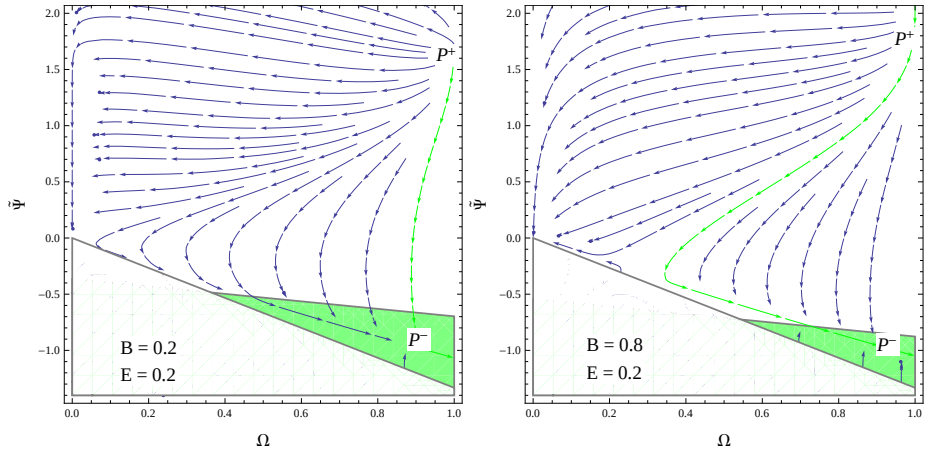

Figure 4.2: Plots for the phase plane evolution of viscous radiating fluid with $\gamma = 4/3$, $\nu_* = k = 1$, $\zeta_0 = 1$, $\alpha = 0.01$ and different values of B and E.

In these plots, we have taken $\zeta_0 = 0.2, 1$ by varying ν_*, k, B and E. For $\nu_* = k = \sqrt{1/5}$ and $\zeta_0 = 0.2$, it is found that the global attractor P_d^- lies in green region showing accelerated expansion for the same values of B and E. This region tends to decrease by increasing E such that the point P_d^- lies in the deceleration region. By increasing ζ_0, we find accelerated expansion with different values of B, E and larger values of the parameters ν_* and k. For $\nu_* = k = 1$ and $\zeta_0 = 1$, we find accelerated expansion of the universe model for all choices of electric and magnetic fields. The point P_d^0 behaves as a sink for $\zeta_0 = 0.2$ which becomes a saddle point for larger values of ζ_0. We observe that the increasing value of bulk viscosity increases the region for accelerated expansion in the presence of NLED. In the following, we discuss two different cases for electric as well as magnetic universe.

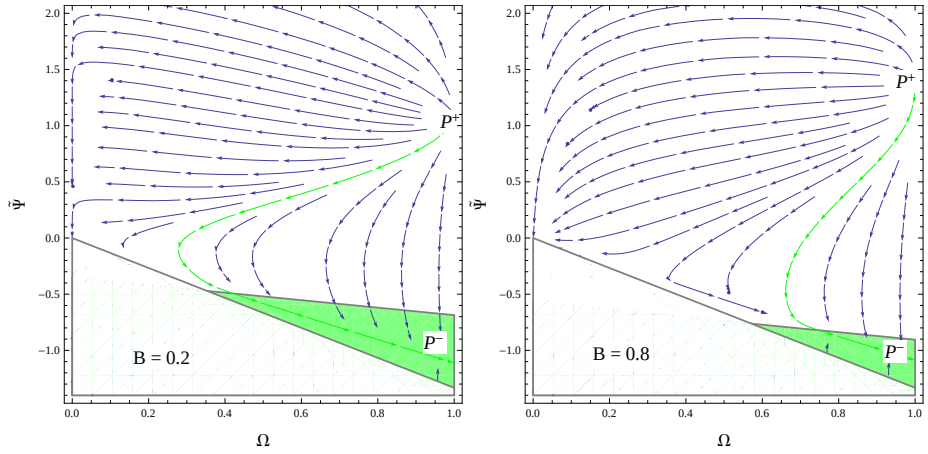

Figure 4.3: Plots for the phase plane evolution of viscous radiating fluid with $\gamma = 4/3$, $\nu_* = k = \sqrt{2/3}$, $\zeta_0 = 1$, $\alpha = 0.01$ and $B = 0.2, 0.8$.

Case II $(E = 0)$

Some recent results indicate that a magnetic universe is appropriate to avoid the initial singularity and ultimately shows late time accelerated expansion [96]. Here we assume the squared electric field $< E^2 >$ to be zero such that the magnetic field $(F = 2B^2)$ rules over the universe known as magnetized universe. Thus the energy density (4.1.5) and pressure (4.1.6) take the form

$$\sigma_B = \frac{B^2}{2\mu_0}(1 - 8\mu_0\alpha B^2), \tag{4.1.38}$$

$$p_B = \frac{B^2}{6\mu_0}(1 - 40\mu_0\alpha B^2). \tag{4.1.39}$$

The respective evolution plots are given in Figure **4.3**. For $\nu_* = k = \sqrt{2/3}$ and $\zeta_0 = 1$, we find that sink lies in green region showing the stability of accelerated expansion for the magnetized universe. This region tends to decrease by increasing the value of magnetic field B. The point P_d^0 behaves as saddle for small values of magnetic field. It is mentioned here that increasing values of the bulk viscosity and

the parameters ν_* as well as k with different values of B give rise to stability of accelerated expansion of the universe for different choices of B. We also find that a smaller value of bulk viscosity shows decelerated expansion with increasing values of B.

Case III ($B = 0$)

Here, we deal with the electric universe by setting $< B^2 >= 0$. The corresponding energy density and pressure are given by

$$\sigma_E = \frac{E^2}{2\mu_0}(1 + 24\mu_0\alpha E^2), \tag{4.1.40}$$

$$p_E = \frac{E^2}{6\mu_0}(1 - 8\mu_0\alpha E^2). \tag{4.1.41}$$

The plots corresponding to different choices of electric field E are shown in Figure **4.4**. For $\nu_* = k = \sqrt{2/3}$ and $\zeta_0 = 1$, we analyze sink P_d^- in the green region showing accelerated expansion of the universe for different values of E. The point P_d^0 behaves as a saddle for small values of magnetic field. We find that the region for accelerated expansion tend to decrease by increasing electric field E. It is observed that accelerated expanding region exists for increasing values of bulk viscosity and parameters ν_* as well as k with all choices of E. It supports the fact that the role of bulk viscosity and electric field is to increase the stability of accelerated expansion of the universe model. The summary of results for the universe filled with viscous radiating fluid is given in Table **4.1**.

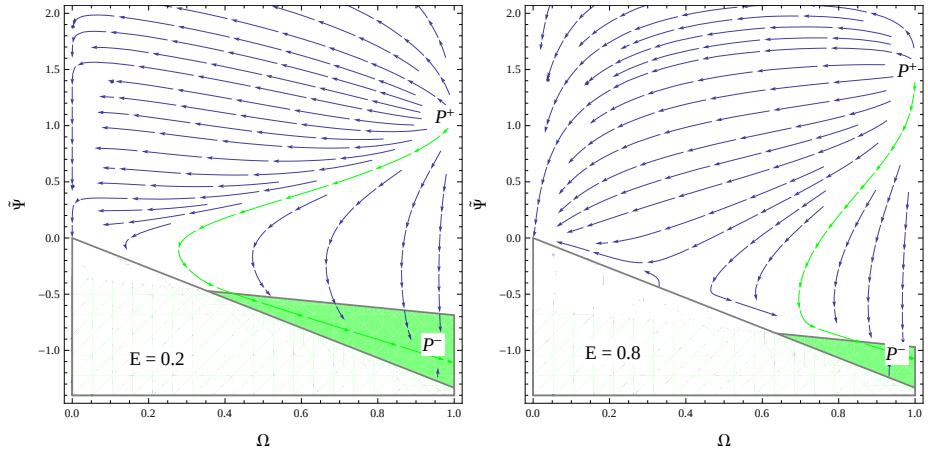

Figure 4.4: Plots for the phase plane evolution of viscous radiating fluid with $\gamma = 4/3$, $\nu_* = k = \sqrt{2/3}$, $\zeta_0 = 1$, $\alpha = 0.01$ and $E = 0.2, 0.8$.

Table 4.1: Stability Analysis of Critical Points for Radiation Dominated Fluid

Critical Point	Behavior	Stability
P_r^+	Source	Unstable
P_r^-	Sink	Stable
P_r^0	Saddle/Sink	Unstable/Stable

4.1.3 Power-Law Scale Factor

In this section, we discuss power-law behavior of the scale factor corresponding to the critical points. For this purpose, we integrate Eq.(4.1.19) which leads to

$$\dot{\Theta} = -\frac{1}{2}\left[1 + 3p_{EM} + (\gamma - 1)\Omega + \tilde{\Psi}\right]\Theta^2. \tag{4.1.42}$$

For $\Theta \neq 0$, we formulate power-law scale factor whenever $1+3p_{EM}+(\gamma-1)\Omega+\tilde{\Psi} \neq 0$. Solving $\Theta = \frac{3\dot{a}}{a}$ for $a(t)$, we obtain the generic critical point as

$$a = a_0(t - t_0)^{\frac{2}{3[1+3p_{EM}+(\gamma-1)\Omega_c+\tilde{\Psi}_c]}}. \tag{4.1.43}$$

The following condition must hold for exponentially expanding models (identified by the condition $1+3p_{EM}+(\gamma-1)\Omega+\tilde{\Psi}=0$) to be present in the physical phase space region (bounded by Eq.(4.1.24))

$$(1-\gamma)\Omega_c - 3p_{EM} - 1 > -\frac{\gamma\nu_*^2}{k^2}\Omega. \tag{4.1.44}$$

This condition is not satisfied in the physical phase space for $\nu_*^2 = k^2$. The above inequality must be satisfied in the following physical phase space region

$$(1+3p_{EM})\left[1-\gamma\left(1-\frac{\nu_*^2}{k^2}\right)\right]^{-1} < \Omega \leq 1. \tag{4.1.45}$$

It is mentioned here that sign of the term $1+3p_{EM}+(\gamma-1)\Omega+\tilde{\Psi}$ is quite important to evaluate different cosmological stages. If $1+3p_{EM}+(\gamma-1)\Omega+\tilde{\Psi}=0$, it corresponds to the exponential expansion of the universe model. Also, $1+3p_{EM}+(\gamma-1)\Omega+\tilde{\Psi} \gtrless 0$ yields accelerated expansion or contraction of the cosmological model, respectively. If $\nu_*^2 < k^2$, the possibility of having accelerated expansion will narrow down. Figure **4.5** shows the physical phase space region (excluding the white region with negative entropy production rate) whereas yellow and dark gray regions correspond to accelerated and exponential expansion of the universe model for $v^2 > k^2$, respectively. Table **4.2** provides the polynomial behavior of power-law scale factor for different critical points with $1+3p_{EM}+(\gamma-1)\Omega+\tilde{\Psi} \neq 0$.

Table 4.2: Power-law Scale Factors for Different Critical Points

Critical Point	**Scale factor for $\gamma = 4/3$**
P_r^0	$a_0(t-t_0)^{-\frac{2}{9p_{EM}}}$
P_r^+	$a_0(t-t_0)^{\frac{2}{3(3p_{EM}+\tilde{\Psi}_c^+ +\frac{4}{3})}}$
P_r^-	$a_0(t-t_0)^{\frac{2}{3(3p_{EM}+\tilde{\Psi}_c^- +\frac{4}{3})}}$

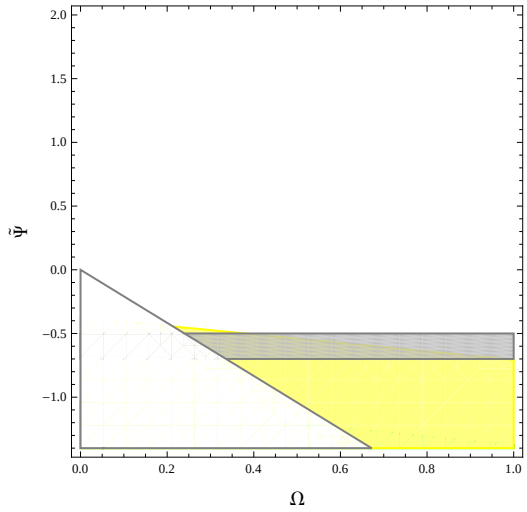

Figure 4.5: Plot of qualitative phase space analysis for power-law scale factor with $\nu_*^2 > k^2$. Yellow and dark gray regions indicate the accelerated and exponential expansion of the universe model, respectively.

4.2 Stability of Anisotropic Universe Model

This section deals with dynamical investigation of LRS BI cosmos by taking two interacting scalar field models as cosmic fluids.

4.2.1 LRS BI Universe Model and Dynamical Equations

We consider LRS BI model with anisotropic effects defined by the line element

$$ds^2 = -dt^2 + a^2(t)dx^2 + b^2(t)(dy^2 + dz^2), \tag{4.2.1}$$

where $a(t)$ and $b(t)$ represent the cosmic expansion radii. We can define the mean Hubble parameter as

$$H = \frac{1}{3}[H_1 + H_2] = \frac{1}{3}\left[\frac{\dot{a}}{a} + \frac{2\dot{b}}{b}\right], \tag{4.2.2}$$

where $H_1 = \frac{\dot{a}}{a}$, $H_2 = \frac{\dot{b}}{b}$ are directional Hubble parameters. For a spatially homogeneous spacetime, the normal congruence to homogeneous expansion leads to a constant ratio, i.e., the expansion and shear scalars are proportional to each other. We assume a power-law relation $a = b^m$, $m \neq 0, 1$, where m is a constant anisotropic parameter which differentiates the expansion along x and y directions and represents the deviation of anisotropic universe model from isotropic. We define the average Hubble expansion by a relationship between mean and directional Hubble parameters as

$$H_1 = mH_2 = \left(\frac{3m}{m+2}\right) H. \tag{4.2.3}$$

Collins [97] studied physical consequences of this assumption by taking perfect fluid and barotropic EoS in a general way.

The cosmic fluid is considered by coupling phantom field and matter. We consider that these two components interact through the interaction term Q_* such that the conservation of energy yield

$$\dot{\sigma}_m + 3(\sigma_m + p_m)H = Q_*, \tag{4.2.4}$$

$$\dot{\sigma}_\phi + 3(\sigma_\phi + p_\phi)H = -Q_*, \tag{4.2.5}$$

$$\dot{\sigma} + 3(\sigma + p)H = 0, \tag{4.2.6}$$

where $\sigma = \sigma_m + \sigma_\phi$, $p = p_m + p_\phi$, σ_m, σ_ϕ, p_m and p_ϕ correspond to energy densities and pressures of matter and phantom energy, respectively. It is noted that the sign of interaction term denotes the transfer of energy between two components. For $Q_* > 0$, the energy flows from phantom to matter while $Q_* < 0$ corresponds to vice versa. The interaction term gives an additional degree of freedom which can be restricted by the constant energy density ratio at late times. It has always been interesting to study cosmological consequences of these interactions by considering their several forms

[98]. It is clear from the above conservation equations that $Q_* = Q_*(H, \sigma_m, \sigma_\phi)$. The constraint and Raychaudhuri equations obtained from the field equations are given by

$$H^2 = \frac{(m+2)^2}{9(2m+1)}(\sigma_m + \sigma_\phi), \tag{4.2.7}$$

$$0 = \left(\frac{6}{m+2}\right)\dot{H} + \frac{27}{(m+2)^2}H^2 + p_\phi, \tag{4.2.8}$$

where $\sigma_\phi = -\frac{1}{2}\dot{\phi}^2 + V(\phi)$, $p_\phi = -\frac{1}{2}\dot{\phi}^2 - V(\phi)$.

In order to solve the evolution equations, we define the following normalized dimensionless quantities

$$\mu_1 = \frac{(m+2)\dot{\phi}}{\sqrt{6}(2m+1)H}, \quad \nu_1 = \frac{(m+2)\sqrt{V}}{\sqrt{3}(2m+1)H}, \quad \lambda_1 = -\frac{V'}{V}, \tag{4.2.9}$$

that direct the evolution equations into an autonomous system. Differentiating μ_1 and ν_1 with respect to $N_1 = \frac{m+2}{3m}\ln a$, we have

$$\mu_1' = \frac{(m+2)}{3m}\mu_1\left[\frac{\ddot{\phi}}{H\dot{\phi}} - \frac{\dot{H}}{H^2}\right], \tag{4.2.10}$$

$$\nu_1' = -\frac{(m+2)}{3m}\nu_1\left[\sqrt{6}\mu_1\lambda_1 + \frac{\dot{H}}{H^2}\right]. \tag{4.2.11}$$

For an exponential potential, Raychaudhuri and conservation equations in terms of these dimensionless quantities become

$$\frac{\dot{H}}{H^2} = -\frac{1}{2(m+2)}\left[9 + (2m+1)^2\{\mu_1^2 - \nu_1^2\}\right], \tag{4.2.12}$$

$$\frac{\ddot{\phi}}{H\dot{\phi}} = 3 - \sqrt{\frac{3}{2}}\frac{2m+1}{m+2}\frac{\lambda_1\nu_1^2}{\mu_1} + \frac{Q_*}{H\dot{\phi}^2}, \tag{4.2.13}$$

where λ_1 is taken as a constant. We can write from the constraint equation

$$\Omega_\phi = \frac{(m+2)^2}{9(2m+1)}\frac{\sigma_\phi}{H^2} = \frac{2m+1}{3}[-\mu_1^2 + \nu_1^2]. \tag{4.2.14}$$

The effective EoS for the cosmic fluid and phantom field are given by

$$\gamma_{eff} = -1 - \frac{2\dot{H}}{3H^2}, \quad \gamma_{\phi} = \frac{\gamma_{eff}}{\Omega_{\phi}}. \tag{4.2.15}$$

4.2.2 Dynamics of Interacting Phantom Energy

This section deals with stability of LRS BI model through phase space analysis by taking interaction between phantom energy and matter. We consider scalar field models for dynamical analysis to study whether we can alleviate the ambiguities like fine-tuning as well as cosmic coincidence arising from the consistency of Λ_1 with the recent cosmic observations. In order to find critical points $\{\mu_1, \nu_1\}$, we need to solve the dynamical system of Eqs.(4.2.10) and (4.2.11) by imposing the condition $\mu_1' = \nu_1' = 0$. The stability of LRS BI universe model will be discussed according to the nature of critical points and the corresponding eigenvalues. In the following, we consider three different forms of interactions between phantom field and matter.

(i) Coupling $Q_* = \alpha\dot{\sigma}_m$

Firstly, we take a model of interaction $Q_* = \alpha\dot{\sigma}_m$ for cosmos where both phantom field as well as DM are present [52]. Different forms of coupling have been discussed in literature which are proportional to the time derivative of their energy densities [48]. Equation (4.2.13), in terms of this coupling, turns out to be

$$\frac{\ddot{\phi}}{H\dot{\phi}} = 3 - \sqrt{\frac{3}{2}}\frac{2m+1}{m+2}\frac{\lambda_1\nu_1^2}{\mu_1} - \frac{3\alpha\Omega_m}{2(1-\alpha)\mu_1}, \tag{4.2.16}$$

where $\Omega_m = 1 - \Omega_{\phi}$. The corresponding autonomous system of equations reduces to

$$\mu_1' = \frac{(m+2)}{3m}\mu_1\left[3 - \sqrt{\frac{3}{2}}\frac{2m+1}{m+2}\frac{\lambda_1\nu_1^2}{\mu_1} - \frac{3\alpha\Omega_m}{2(1-\alpha)\mu_1^2} + \frac{1}{2(m+2)}\right.$$

$$\times \quad \{9+(2m+1)^2(\mu_1^2-\nu_1^2)\}\big], \tag{4.2.17}$$

$$\nu_1' = -\frac{(m+2)}{3m}\nu_1\left[\sqrt{6}\mu_1\lambda_1-\frac{1}{2(m+2)}\{9+(2m+1)^2(\mu_1^2-\nu_1^2)\}\right]. \tag{4.2.18}$$

For $P_1=\left(-\frac{1}{\sqrt{6}\lambda_1}\left\{\frac{6-\alpha(2m+7)}{2(1-\alpha)}\right\},0\right)$, the eigenvalues of Jacobian matrix are given by

$$\eta_1 = \frac{(m+2)}{3m}\left[3-\frac{3\alpha}{2(1-\alpha)}\left\{\frac{24(1-\alpha)^2\lambda_1^2}{[6-\alpha(2m+1)]^2}-\frac{2m+1}{3}\right\}\right.$$
$$+ \quad \left.\frac{1}{2(m+2)}\left\{9+\frac{(2m+1)^2[6-\alpha(2m+7)]^2}{8(1-\alpha)^2\lambda_1^2}\right\}\right], \tag{4.2.19}$$

$$\eta_2 = -\frac{(m+2)}{3m}\left[\frac{\alpha(2m+7)-6}{2(1-\alpha)}-\frac{1}{2(m+2)}\{9\right.$$
$$+ \quad \left.\frac{(2m+1)^2[6-\alpha(2m+7)]^2}{24(1-\alpha)^2\lambda_1^2}\right\}\right]. \tag{4.2.20}$$

We study the impact of parameters m and α on the stability of critical points in the presence of scalar field model. We plot the dynamical behavior of critical points for $Q_*=\alpha\dot{\sigma}_m$ by taking different values of α and m as shown in Figure **4.6**. In these numerical plots, we observe that the eigenvalues are positive indicating the point P_1 as an unstable past attractor for $m>0$ in the physical phase space except for $\alpha=1, m=-2$ at which the system becomes undetermined. For $m<0$, this point becomes stable future attractor. The dynamical analysis shows a matter dominated era ultimately followed by a late accelerated expansion phase of the universe. For $P_2=\left(\frac{\sqrt{6}\lambda_1\pm\sqrt{6\lambda_1^2-\left(\frac{3(2m+1)}{m+2}\right)^2}}{\frac{(2m+1)^2}{m+2}},0\right)$, the corresponding eigenvalues are

$$\eta_1 = \frac{(m+2)}{3m}\left[3-\frac{3\alpha}{2(1-\alpha)}\left\{\frac{(2m+1)^4}{(m+2)^2\left[\sqrt{6}\lambda_1\pm\sqrt{6\lambda_1^2-\left(\frac{3(2m+1)}{m+2}\right)^2}\right]^2}\right.\right.$$

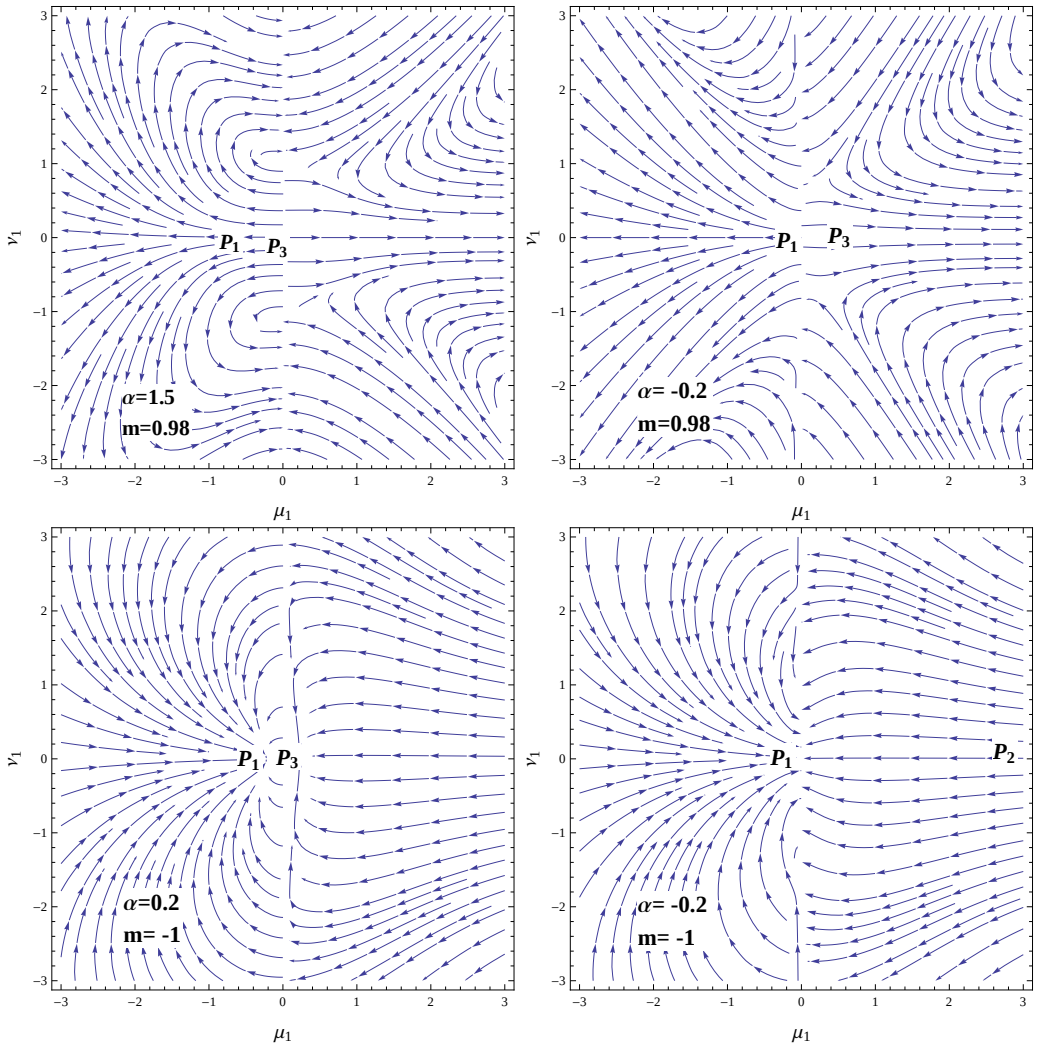

Figure 4.6: Plots for the phase plane evolution of phantom coupled universe model with $Q_* = \alpha\dot{\sigma}_m$ and $\lambda_1 = 2$.

$$- \quad \frac{2m+1}{3}\Bigg\} + \frac{1}{2(m+2)}\Bigg\{9+(2m+1)^2\Bigg[\frac{(2m+1)^4}{(m+2)^2}$$

$$\times \quad \frac{1}{\left[\sqrt{6}\lambda_1 \pm \sqrt{6\lambda_1^2 - \left(\frac{3(2m+1)}{m+2}\right)^2}\right]}\Bigg]\Bigg\}\Bigg], \tag{4.2.21}$$

$$\eta_2 = -\frac{(m+2)}{3m}\Bigg[\sqrt{6}(m+2)\lambda_1\Bigg\{\frac{\sqrt{6}\lambda_1 \pm \sqrt{6\lambda_1^2 - \left(\frac{3(2m+1)}{m+2}\right)^2}}{(2m+1)^2}\Bigg\} - \frac{1}{2(m+2)}$$

$$\times \quad \Bigg\{9+(2m+1)^2(m+2)^2\left[\frac{\sqrt{6}\lambda_1 \pm \sqrt{6\lambda_1^2 - \left(\frac{3(2m+1)}{m+2}\right)^2}}{2m+1}\right]^2\Bigg\}\Bigg]. \tag{4.2.22}$$

This point corresponds to unstable past attractor without accelerated expansion for $m > 0$. By taking negative values of parameter m, this point becomes stable future attractor or a saddle point depending on values of α. It is noted that the stable point undergoes accelerated expansion as $\bar{q} < 0$.

For $P_3 = \left(\frac{\sqrt{3(2m+7)+\alpha(2m^2-m-19)+\sqrt{[3(2m+7)+\alpha(2m^2-m-19)]^2-\alpha(\alpha-1)(m+2)(2m+1)}}}{2(\alpha-1)(2m+1)}, 0\right)$, we have

$$\eta_1 = \frac{(m+2)}{3m}\Bigg[3 - \frac{3\alpha}{2(1-\alpha)}\Bigg\{\frac{2(\alpha-1)(2m+1)}{3(2m+7)+\alpha(2m^2-m-19)+\xi_1}$$

$$- \quad \frac{2m+1}{3}\Bigg\} + \frac{1}{2(m+2)}\Bigg\{9+\frac{3(2m+1)^2}{2(\alpha-1)(2m+1)}\left[3(2m+7)\right.$$

$$+ \quad \left.\alpha(2m^2-m-19)+\xi_1\right]\Bigg\}\Bigg], \tag{4.2.23}$$

$$\eta_2 = -\frac{(m+2)}{3m}\Bigg[\frac{\sqrt{3}\lambda_1\sqrt{3(2m+7)+\alpha(2m^2-m-19)+\xi_1}}{(\alpha-1)(2m+1)}$$

$$- \quad \frac{1}{2(m+2)}\Bigg\{9+\frac{(2m+1)^2}{2(\alpha-1)(2m+1)}[3(2m+7)\alpha(2m^2-m-19)$$

$$+ \quad \xi_1]\Bigg\}\Bigg], \tag{4.2.24}$$

where $\xi_1 = \sqrt{[3(2m+7)+\alpha(2m^2-m-19)]^2-\alpha(\alpha-1)(m+2)(2m+1)}$. We find the same behavior of this point for positive values of m. This point is also a stable future attractor for $m < 0$ showing accelerated expanding universe model. The effective potential for the cosmic fluid is given by

$$\gamma_{eff} = -1 + \frac{1}{m+2}[9 + (2m+1)(\mu_1^2 - \nu_1^2)]. \tag{4.2.25}$$

The effective EoS parameter and deceleration parameter are given by

$$\gamma_\phi = \frac{1}{\mu_1^2+\nu_1^2}\left[-1 + \frac{1}{m+2}\{9 + (2m+1)(\mu_1^2-\nu_1^2)\}\right], \tag{4.2.26}$$

$$\bar{q} = -1 + \frac{1}{m+2}[9 + (2m+1)(\mu_1^2 - \nu_1^2)]. \tag{4.2.27}$$

It is mentioned here that points P_1 and P_2 undergo decelerated expansion while the point P_3 is a stable future attractor that lies in accelerated expanding phase as $\bar{q} < 0$ and $\gamma_\phi < -1$. The summary of the results for evolution as well as stability of LRS BI model coupled with phantom energy and matter is given in Table **4.3**.

(ii) Coupling $Q_* = \beta\dot{\sigma}_\phi$

For this coupling, Eq.(4.2.13) takes the form

$$\frac{\ddot{\phi}}{H\dot{\phi}} = 3 - \sqrt{\frac{3}{2}}\frac{2m+1}{m+2}\frac{\lambda_1\nu_1^2}{\mu_1} - \frac{3\beta}{1+\beta}. \tag{4.2.28}$$

The autonomous system of equations becomes

$$\mu_1' = \frac{(m+2)}{3m}\mu_1\left[3 - \sqrt{\frac{3}{2}}\frac{2m+1}{m+2}\frac{\lambda_1\nu_1^2}{\mu_1} - \frac{3\beta}{1-\beta} + \frac{1}{2(m+2)}\right.$$
$$\times \left.\{9 + (2m+1)^2(\mu_1^2-\nu_1^2)\}\right], \tag{4.2.29}$$

$$\nu_1' = -\frac{(m+2)}{3m}\nu_1\left[\sqrt{6}\mu_1\lambda_1 - \frac{1}{2(m+2)}\{9 + (2m+1)^2(\mu_1^2-\nu_1^2)\}\right]. \tag{4.2.30}$$

Table 4.3: Stability Analysis for the Phantom Coupled System with $Q_* = \alpha\dot{\sigma}_m$.

Ranges of α and m for Critical Points	**Stability**	**Acceleration**
P_1		
$\alpha > 0,\ m > 0\ (\alpha \neq 1)$	Unstable	No
$\alpha < 0,\ m > 0$	Unstable	No
$\alpha < 0,\ m < 0\ (m \neq -2)$	Stable	No
$\alpha > 0,\ m < 0$	Stable	No
P_2		
$\alpha > 0,\ m > 0\ (\alpha \neq 1)$	Unstable	No
$\alpha < 0,\ m > 0$	Unstable/Saddle	No
$\alpha < 0,\ m < 0\ (m \neq -0.5, -2)$	Stable/Saddle	Yes
$\alpha > 0,\ m < 0$	Stable/Saddle	Yes
P_3		
$\alpha > 0,\ m > 0\ (\alpha \neq 1)$	Unstable/Saddle	No
$\alpha < 0,\ m > 0$	Saddle	No
$\alpha < 0,\ m < 0\ (m \neq -0.5, -2)$	Stable	Yes
$\alpha > 0,\ m < 0$	Stable	No

For $P_1 = (0, 0)$, we have

$$\eta_1 = \frac{3}{2m} + \frac{m+2}{m(1+\beta)}, \quad \eta_2 = \frac{3}{2m}. \tag{4.2.31}$$

This point shows a varying behavior for different values of parameters β and m. For $\alpha = 0.8, -0.2$, we find that point P_1 is unstable/saddle node by taking only positive values of m and $\lambda_1 = 2$ (Figure **4.7**). For $\beta = -1$, the eigenvalues become undetermined, hence we neglect it. We observe that negative values of m show a stable future attractor. It is mentioned here that point P_1 undergoes decelerated cosmic expansion since $\bar{q} > 0$ for all choices of parameters.

For $P_2 = \left(\frac{1}{2m+1}\sqrt{\frac{3[3\beta-(2m+1)]}{1+\beta}}, 0\right)$, the eigenvalues are given by

$$\eta_1 = \frac{m+2}{m(1+\beta)} + \frac{3[1+4\beta-2(m+1)]}{2m(1+\beta)}, \tag{4.2.32}$$

$$\eta_2 = -\frac{\sqrt{2}(m+2)\lambda_1}{m(2m+1)}\sqrt{\frac{3\beta-(2m+1)}{1+\beta}} + \frac{3+6\beta-2(m+1)}{2m(1+\beta)}. \tag{4.2.33}$$

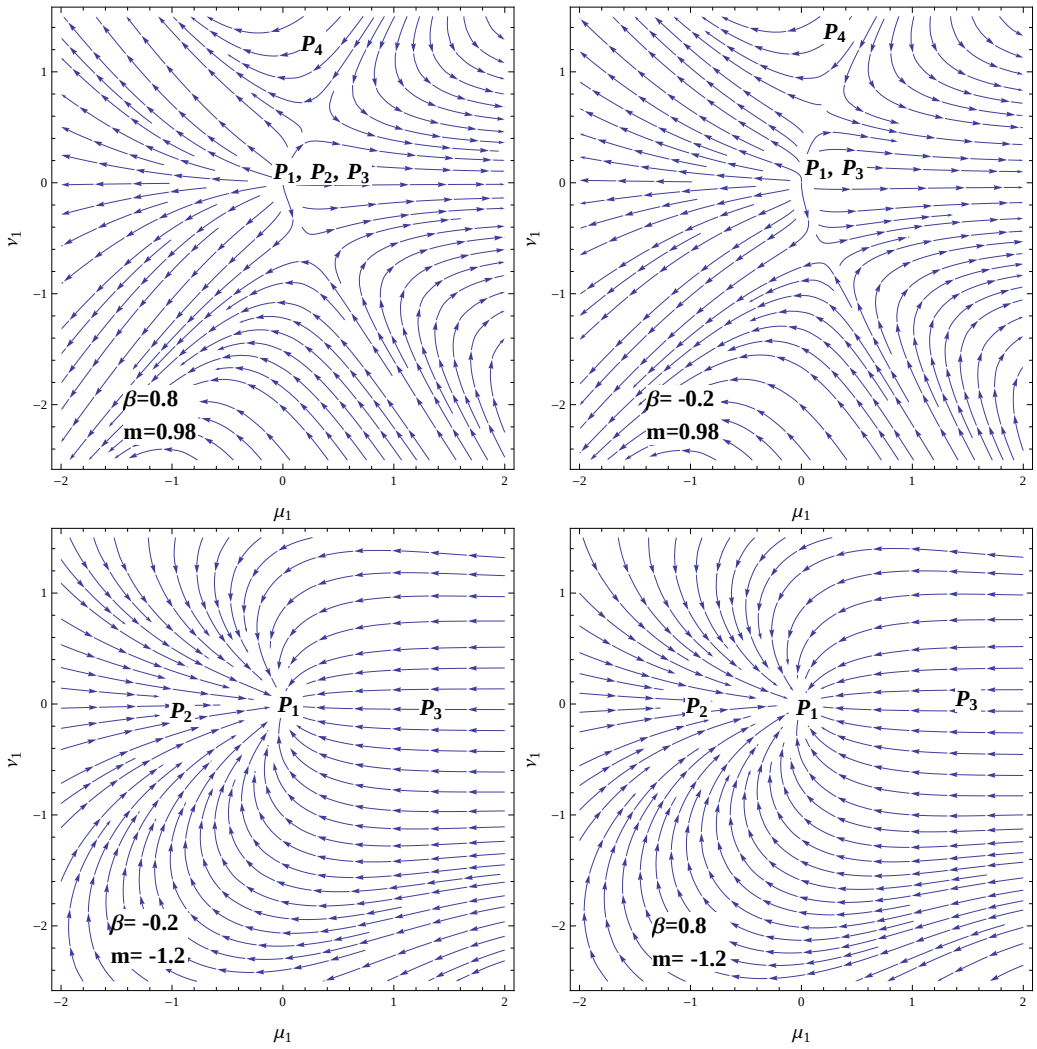

Figure 4.7: Plots for the phase plane evolution of phantom coupled universe model with $Q_* = \beta\dot{\sigma}_\phi$ and $\lambda_1 = 2$.

This point shows opposite behavior as compared to the previous point. Here all choices of m and α give stable nodes except $m>0$ and $\alpha>0$ that correspond to unstable node. In this case, the universe is in decelerated expanding phase for all values of m. For $P_3=\left(-\frac{1}{2m+1}\sqrt{\frac{3[3\beta-(2m+1)]}{1+\beta}},0\right)$, the corresponding eigenvalues yield

$$\eta_1 = \frac{m+2}{m(1+\beta)}+\frac{3[1+4\beta-2(m+1)]}{2m(1+\beta)}, \tag{4.2.34}$$

$$\eta_2 = \sqrt{\frac{2}{3}}\frac{(m+2)\lambda_1}{m(2m+1)}\sqrt{\frac{3[3\beta-(2m+1)]}{1+\beta}}+\frac{3+6\beta-2(m+1)}{2m(1+\beta)}. \tag{4.2.35}$$

We find that point P_3 is an unstable past attractor for all values of α and m except for $-0.9<\beta<-0.1$ at which it behaves as a stable node. For $P_4=\left(0,\pm\frac{3}{2m+1}\right)$, the eigenvalues are

$$\eta_1=\frac{m+2}{m(1+\beta)}, \quad \eta_2=\frac{m+2}{m(1+\beta)}. \tag{4.2.36}$$

This point is also an unstable past attractor for positive values of m. It is noted that for $Q_*=\beta\dot{\sigma}_\phi$, all points lie in a region of decelerated expansion. A general dynamical analysis is given in Table **4.4**.

(iii) Coupling $Q_*=\rho(\dot{\sigma}_m+\dot{\sigma}_\phi)$

Here we consider the coupling as a linear combination of $\dot{\sigma}_m$ and $\dot{\sigma}_\phi$ for which Eq.(4.2.13) becomes

$$\frac{\ddot{\phi}}{H\dot{\phi}}=3-\sqrt{\frac{3}{2}}\frac{2m+1}{m+2}\frac{\lambda_1\nu_1^2}{\mu_1}-\frac{3\rho\Omega_m}{2(1-\rho)\mu_1^2}-\frac{3\rho}{1+\rho}. \tag{4.2.37}$$

The evolution and conservation equations yield

$$\mu_1' = \frac{(m+2)}{3m}\mu_1\left[3-\sqrt{\frac{3}{2}}\frac{2m+1}{m+2}\frac{\lambda_1\nu_1^2}{\mu_1}-\frac{3\rho\Omega_m}{2(1-\rho)\mu_1^2}-\frac{3\rho}{1+\rho}+\frac{1}{2(m+2)}\right.$$

Table 4.4: Stability Analysis for the Phantom Coupled System with $Q_* = \beta\dot{\sigma}_\phi$.

Ranges of β and m for Critical Points	**Stability**	**Acceleration**
P_1		
$\beta > 0,\ m > 0$	Unstable	No
$\beta < 0,\ m > 0,\ \beta \neq -1$	Unstable/Saddle	No
$\beta < 0,\ m < 0$	Stable	No
$\beta > 0,\ m < 0$	Stable	No
P_2		
$\beta > 0,\ m > 0$	Unstable	No
$\beta < 0,\ m > 0,\ \beta \neq -1$	Stable	No
$\beta < 0,\ m < 0,\ m \neq -0.5$	Stable	No
$\beta > 0,\ m < 0$	Stable	No
P_3		
$\beta > 0,\ m > 0$	Unstable	No
$\beta < 0,\ m > 0,\ \beta \neq -1$	Stable/Unstable	No
$\beta < 0,\ m < 0,\ m \neq -0.5$	Unstable	No
$\beta > 0,\ m < 0$	Stable for $-0.9 < \beta < -0.1$	No
P_4		
$\beta > 0,\ m > 0$	Unstable	No
$\beta < 0,\ m > 0,\ \beta \neq -1$	Unstable	No
$\beta < 0,\ m < 0$	Stable	No
$\beta > 0,\ m < 0$	Stable	No

$$\times \quad \{9 + (2m+1)^2(\mu_1^2 - \nu_1^2)\}\Big], \tag{4.2.38}$$

$$\nu_1' = -\frac{(m+2)}{3m}\nu_1\left[\sqrt{6}\mu_1\lambda_1 - \frac{1}{2(m+2)}\{9 + (2m+1)^2(\mu_1^2 - \nu_1^2)\}\right]. \tag{4.2.39}$$

For $P_1 = \left(\frac{\sqrt{6}\lambda_1 + \sqrt{6\lambda_1^2 - \left(\frac{3(2m+1)}{m+2}\right)^2}}{(2m+1)^2/2(m+2)}, 0\right)$, the corresponding eigenvalues are

$$\eta_1 = \frac{(m+2)}{3m}\left[3 - \left\{\frac{(2m+1)^4}{4(m+2)^2\left\{\sqrt{6}\lambda_1 + \sqrt{6\lambda_1^2 - \left(\frac{3(2m+1)}{m+2}\right)^2}\right\}}\right.\right.$$
$$\left.\left. - \frac{2m+1}{3}\right\}\frac{3\rho}{2(1-\rho)} - \frac{3\rho}{1+\rho} + \frac{1}{2(m+2)}\left\{9 + 12(m+2)^2\right.\right.$$

$$- \left[\frac{\sqrt{6}\lambda_1 + \sqrt{6\lambda_1^2\left(\frac{3(2m+1)}{m+2}\right)^2}}{2m+1}\right]^2\Bigg\}\Bigg], \tag{4.2.40}$$

$$\eta_2 = -\frac{(m+2)}{3m}\left[2\sqrt{6}(m+2)\lambda_1\left\{\frac{6\lambda_1 + \sqrt{6\lambda_1^2 - \left(\frac{3(2m+1)}{m+2}\right)^2}}{(2m+1)^2}\right\}\right.$$
$$\left. - \frac{1}{2m+1}\left\{9 + 4(m+2)^2\left[\frac{6\lambda_1 + \sqrt{6\lambda_1^2 - \left(\frac{3(2m+1)}{m+2}\right)^2}}{(2m+1)}\right]^2\right\}\right]. \tag{4.2.41}$$

In this case, the nature of eigenvalues indicates unstable nodes for $m > 0$ with all choices of ρ except for $\rho = 1, -1$ (Figure **4.8**). We find both eigenvalues negative for $m = -0.2$ showing stable attractors. All the choices of parameters m and ρ show decelerated expanding universe as $\bar{q} > 0$. The summary of respective results is shown in Table **4.5**.

For $P_2 = \left(\frac{\sqrt{6}\lambda_1 - \sqrt{6\lambda_1^2 - \left(\frac{3(2m+1)}{m+2}\right)^2}}{(2m+1)^2/2(m+2)}, 0\right)$, the eigenvalues are given as

$$\eta_1 = \frac{(m+2)}{3m}\left[3 - \left\{\frac{(2m+1)^4}{4(m+2)^2\left\{\sqrt{6}\lambda_1 - \sqrt{6\lambda_1^2 - \left(\frac{3(2m+1)}{m+2}\right)^2}\right\}}\right.\right.$$
$$\left. - \frac{2m+1}{3}\right\}\frac{3\rho}{2(1-\rho)} - \frac{3\rho}{1+\rho} + \frac{1}{2(m+2)}\left\{9 + 12(m+2)^2\right.$$
$$\left.\left. - \left[\frac{\sqrt{6}\lambda_1 - \sqrt{6\lambda_1^2 - \left(\frac{3(2m+1)}{m+2}\right)^2}}{2m+1}\right]^2\right\}\right], \tag{4.2.42}$$

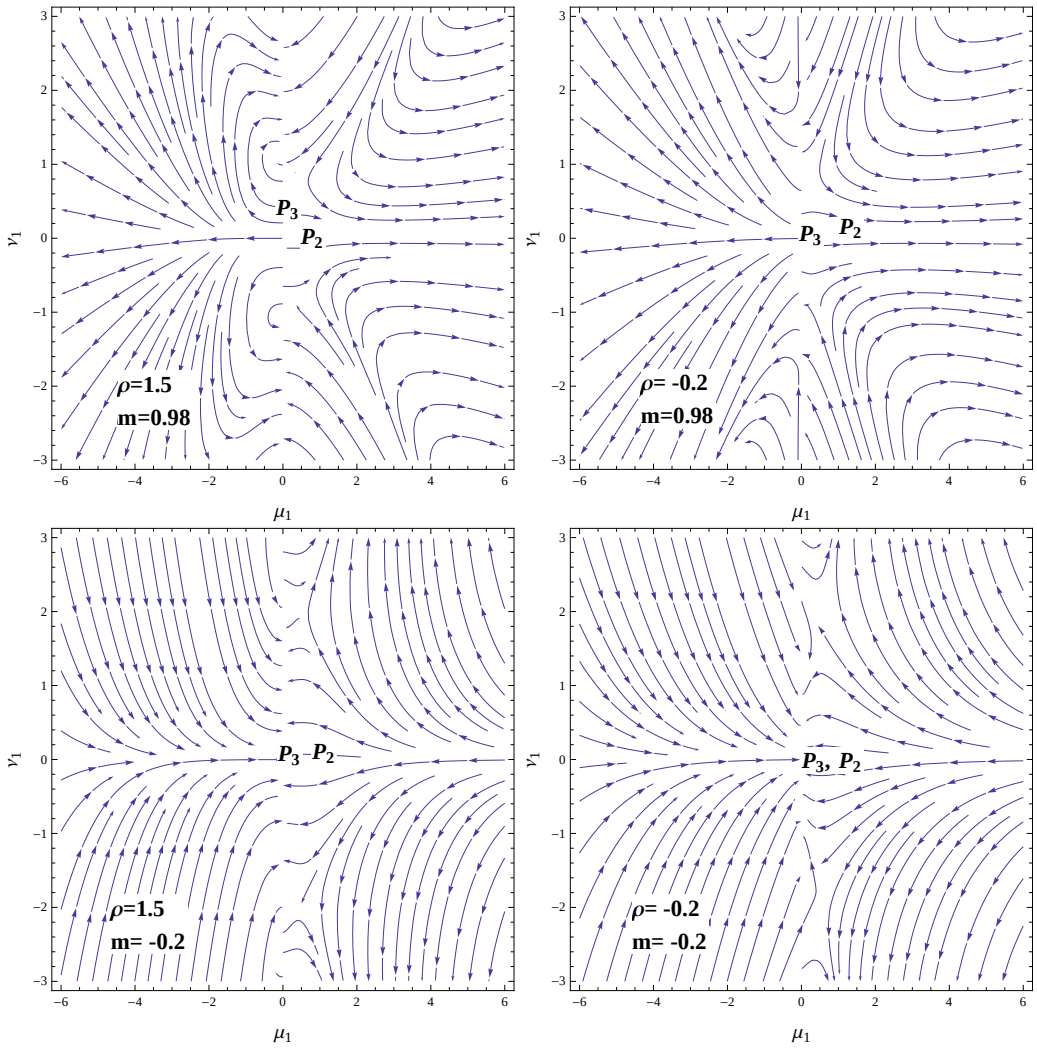

Figure 4.8: Plots for the phase plane evolution of phantom coupled universe model with $Q_* = \rho(\dot{\sigma}_m + \dot{\sigma}_\phi)$ and $\lambda_1 = 2$.

Table 4.5: Stability Analysis for the Phantom Coupled System with $Q_* = \rho(\dot{\sigma}_m + \dot{\sigma}_\phi)$.

Ranges of ρ and m for Critical Points	**Stability**	**Acceleration**
$\mathbf{P}_1$		
$\rho > 0,\ m > 0,\ \rho \neq 1$	Unstable	No
$\rho < 0,\ m > 0,\ \rho \neq -1$	Unstable	No
$\rho < 0,\ m < 0,\ m \neq -0.5, -2$	Stable for $m = -0.2$	No
$\rho > 0,\ m < 0$	Stable for $m = -0.2$	No
$\mathbf{P}_2$		
$\rho > 0,\ m > 0,\ \rho \neq 1$	Unstable	No
$\rho < 0,\ m > 0,\ \rho \neq -1$	Unstable/Saddle	No
$\rho < 0,\ m < 0,\ m \neq -0.5, -2$	Saddle	No
$\rho > 0,\ m < 0$	Saddle	No
$\mathbf{P}_3$		
$\rho > 0,\ m > 0,\ \rho \neq 1$	Unstable/Saddle	No
$\rho < 0,\ m > 0,\ \rho \neq -1$	Unstable/Saddle	No
$\rho < 0,\ m < 0,\ m \neq -2$	Stable	Yes
$\rho > 0,\ m < 0$	Stable	Yes

$$\begin{aligned}\eta_2 &= -\frac{(m+2)}{3m}\left[2\sqrt{6}(m+2)\lambda_1\left\{\frac{6\lambda_1 - \sqrt{6\lambda_1^2 - \left(\frac{3(2m+1)}{m+2}\right)^2}}{(2m+1)^2}\right\}\right. \\ &- \left.\frac{1}{2m+1}\left\{9 + 4(m+2)^2\left[\frac{6\lambda_1 - \sqrt{6\lambda_1^2 - \left(\frac{3(2m+1)}{m+2}\right)^2}}{(2m+1)}\right]^2\right\}\right],\end{aligned} \tag{4.2.43}$$

which corresponds to either unstable or saddle node that lies in matter dominated era for all choices of different parameters. For $P_3 = \left(\frac{\tilde{\xi_1}}{\sqrt{2}}, 0\right)$, the eigenvalues are

$$\begin{aligned}\eta_1 &= \frac{(m+2)}{3m}\left[3 - \frac{3\rho}{2(1-\rho)}\left\{\frac{2}{\tilde{\xi_1}^2} - \frac{2m+1}{3}\right\} - \frac{3\rho}{1+\rho}\right. \\ &+ \left.\frac{1}{2(m+2)}\left\{9 + \frac{3(2m+1)^2\tilde{\xi_1}^2}{2}\right\}\right],\end{aligned} \tag{4.2.44}$$

$$\eta_2 = -\frac{(m+2)}{3m}\left[\sqrt{3}\lambda_1\tilde{\xi_1} - \frac{1}{2(m+2)}\left(9+\frac{(2m+1)\tilde{\xi_1}^2}{2}\right)\right], \quad (4.2.45)$$

where

$$\tilde{\xi_1} = \sqrt{\frac{3(2m+3)+\rho(2m^2-m-10)+\rho^2(2m^2-5m-25)}{(2m+1)^2(\rho^2-1)}}+\tilde{\xi}_2,$$
$$\tilde{\xi_2} = \sqrt{(-12\rho(\rho+1)(\rho^2-1)(m+2)(2m+1)^2+39-5\rho(5\rho+2)+\tilde{\xi}_3)^2},$$
$$\tilde{\xi_3} = 2m^2\rho(\rho+1)+m(5\rho^2-\rho+6)^2.$$

The nature of eigenvalues as well as trajectories show that point P_3 is unstable past attractor in deceleration region for $m > 0$ with $\rho \neq 1, -1$. This point becomes a stable global attractor for negative values of m except for $m = -0.5, -2$ that give undetermined eigenvalues. In this case, $\bar{q} < 0$ and $\gamma_\phi < -1$ showing accelerated expansion of the universe.

4.2.3 Coupled Tachyon Dynamics

Now we discuss phase space analysis of the universe model by taking a tachyon coupled cosmic component. The conservation equations are

$$\dot{\sigma}_m + 3(\sigma_m + p_m)H = Q_*, \quad (4.2.46)$$
$$\dot{\sigma}_\phi + 3(\sigma_\phi + p_\phi)H = -Q_*, \quad (4.2.47)$$

where $\sigma_\phi = \frac{V(\phi)}{\sqrt{1-\dot{\phi}^2}}$ and $p_\phi = -V(\phi)\sqrt{1-\dot{\phi}^2}$. The evolution equations yield

$$H^2 = \frac{(m+2)^2}{9(2m+1)}\left[\frac{V(\phi)}{\sqrt{1-\dot{\phi}^2}}+\sigma_m\right], \quad (4.2.48)$$
$$\frac{\ddot{\phi}}{1-\dot{\phi}^2} = -\left[3H\dot{\phi}+\frac{V'(\phi)}{V(\phi)}+\frac{Q_*\sqrt{1-\dot{\phi}^2}}{V(\phi)\dot{\phi}}\right]. \quad (4.2.49)$$

We introduce the following dimensionless parameters

$$\mu_1 = \frac{(m+2)\dot{\phi}}{2m+1}, \quad \nu_1 = \frac{(m+2)\sqrt{V}}{\sqrt{3}(2m+1)H}, \quad \lambda_1 = -\frac{V'}{V\sqrt{V}}, \tag{4.2.50}$$

such that the autonomous system of equations takes the form

$$\mu_1' = \frac{(m+2)^2}{3m(2m+1)}\frac{\ddot{\phi}\mu_1}{H\dot{\phi}}, \tag{4.2.51}$$

$$\nu_1' = -\frac{(2m+1)\lambda_1\mu_1\nu_1^2}{2\sqrt{3}m(m+2)} - \frac{(m+2)\nu_1}{3m}\frac{\dot{H}}{H^2}. \tag{4.2.52}$$

In this case, we consider the only coupling $Q_* = \beta\dot{\sigma}_\phi$ for which Eqs.(4.2.48) and (4.2.49) give

$$\frac{\dot{H}}{H^2} = \frac{(2m+1)^2}{2(m+2)}\nu_1^2\sqrt{1-\left(\frac{2m+1}{m+2}\right)^2\mu_1^2} - \frac{9}{2(m+2)}, \tag{4.2.53}$$

$$\frac{\ddot{\phi}}{\dot{\phi}H} = \left[1-\left(\frac{2m+1}{m+2}\right)^2\mu_1^2\right]\left[\frac{\sqrt{3}\nu_1\lambda_1}{\mu_1} + \frac{3\beta}{1+\beta} - 3\right]. \tag{4.2.54}$$

The effective EoS and deceleration parameters are given by

$$\gamma_{eff} = -1 - \frac{1}{3(m+2)}\left[(2m+1)^2\nu_1^2\sqrt{1-\left(\frac{2m+1}{m+2}\right)^2\mu_1^2} - 9\right], \tag{4.2.55}$$

$$\bar{q} = -1 - \frac{1}{2(m+2)}\left[(2m+1)^2\nu_1^2\sqrt{1-\left(\frac{2m+1}{m+2}\right)^2\mu_1^2} - 9\right]. \tag{4.2.56}$$

The critical points and their corresponding eigenvalues for tachyon coupled field are given as follows. For $P_1 = (0,0)$, we have

$$\eta_1 = -\frac{(m+2)^2}{m(2m+1)(1+\beta)}, \quad \eta_2 = \frac{3}{2m}. \tag{4.2.57}$$

We investigate stability of critical points corresponding to different values of m and other parameters. We find that point P_1 is saddle/unstable node for positive values of m (Figure **4.9**). This point becomes global stable node for $m < 0$ ($m \neq -0.5, \beta \neq -1$)

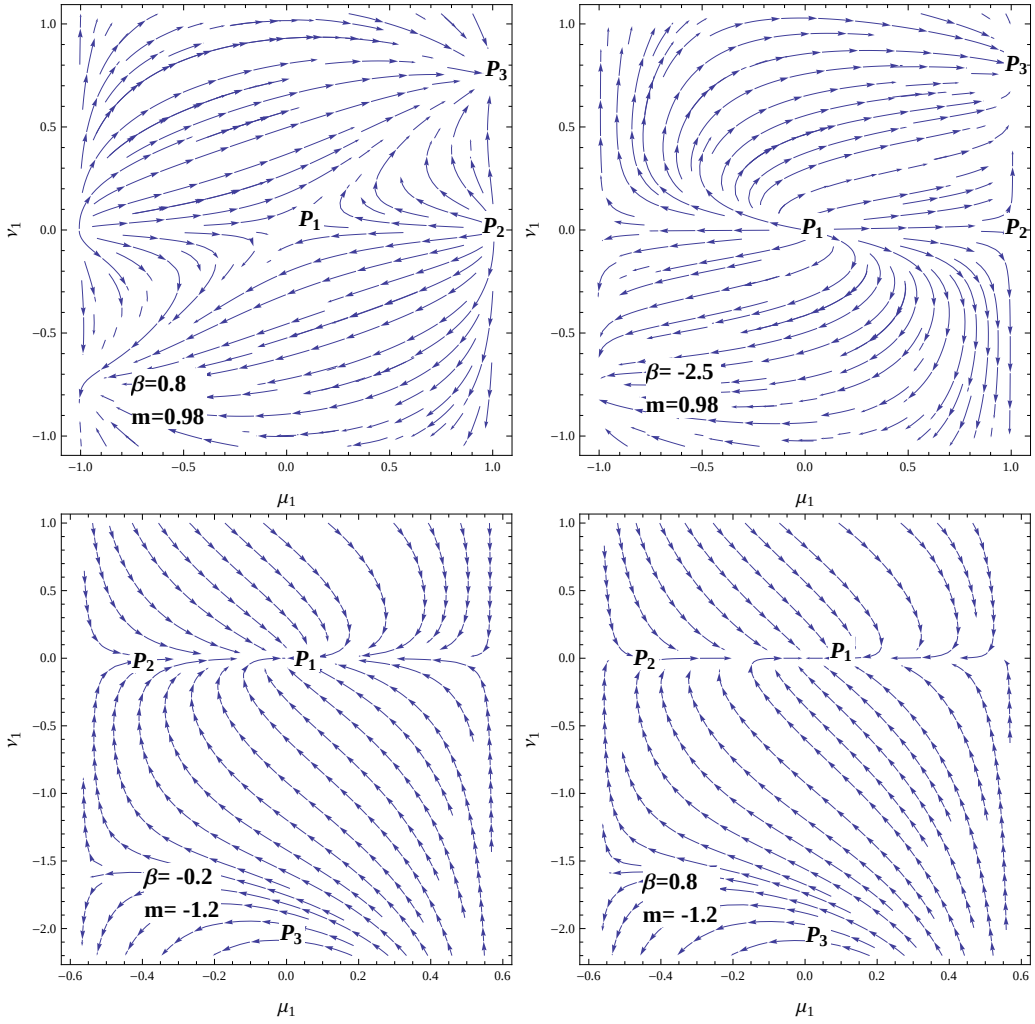

Figure 4.9: Plots for the phase plane evolution of tachyon coupled universe model with $Q_* = \beta\dot{\sigma}_\phi$ and $\lambda_1 = 2$.

Table 4.6: Stability Analysis for the Tachyon Coupled System with $Q_* = \beta\dot{\sigma}_\phi$.

Ranges of β and m for Critical Points	**Stability**	**Acceleration**
$\mathbf{P}_1$		
$\beta > 0,\ m > 0,\ \beta \neq -1$	Saddle	Yes
$\beta < 0,\ m > 0$	Unstable	Yes
$\beta < 0,\ m < 0,\ m \neq -0.5$	Stable	Yes
$\beta > 0,\ m < 0$	Stable	Yes
$\mathbf{P}_2$		
$\beta > 0,\ m > 0$	Unstable	Yes
$\beta < 0,\ m > 0,\ \beta \neq -1$	Unstable	Yes
$\beta < 0,\ m < 0,\ m \neq -0.5$	Saddle	Yes
$\beta > 0,\ m < 0$	Saddle	Yes
$\mathbf{P}_3$		
$\beta > 0,\ m > 0$	Stable	Yes
$\beta < 0,\ m > 0,\ \beta \neq -1$	Stable	Yes
$\beta < 0,\ m < 0,\ m \neq -0.5$	Saddle/Unstable	Yes
$\beta > 0,\ m < 0$	Saddle/Unstable	Yes

showing accelerated expansion of the universe model as $\bar{q} < 0$. The summary of the obtained results is given in Table **4.6**.

For $P_2 = \left(\pm\frac{m+2}{2m+1}, 0\right)$, the eigenvalues become

$$\eta_1 = \frac{2(m+2)^2}{m(2m+1)(1+\beta)}, \quad \eta_2 = \frac{3}{2m}, \tag{4.2.58}$$

which correspond to unstable nodes for positive values of parameter m lying in accelerated expanding phase of cosmos. For $m < 0$, we have stable global attractors undergoing accelerated expansion of the universe. When $P_3 = \left(0, \pm\frac{3}{2m+1}\right)$, the eigenvalues are given by

$$\eta_1 = -\frac{(m+2)^2}{m(2m+1)(1+\beta)}, \quad \eta_2 = -\frac{3}{m}. \tag{4.2.59}$$

In this case, the nature of eigenvalues indicate stable future attractor for $\beta > 0$ and $m > 0$ which undergoes accelerated expansion of the universe as $\bar{q} < 0$. For $\beta < 0$ and

$m > 0$, the point P_3 is stable except for $\beta = -1$. In this case, $\bar{q} = -1$ and $\gamma_{eff} = -1$ which indicate de Sitter phase of the universe. For $\beta > 0$, $m < 0$, it also shows saddle/unstable point which corresponds to de Sitter ($\bar{q} = -1$, $\gamma_{eff} = -1$) phase.

4.2.4 Power-Law Scale Factor

In this section, we discuss power-law behavior of the scale factor corresponding to both phantom as well as tachyon coupled fields by applying some assumptions. In this context, we integrate Eq.(4.2.12) which leads to

$$\dot{\Theta} = -\frac{1}{6(m+2)}[9 + (2m+1)^2(\mu_1^2 - \nu_1^2)]\Theta^2. \tag{4.2.60}$$

For $\Theta \neq 0$, we determine power-law scale factor whenever $9+(2m+1)^2(\mu_1^2-\nu_1^2) \neq 0$. We find the corresponding generic critical point by solving $\Theta = \frac{\dot{a}}{a} + \frac{2\dot{b}}{b}$ for $a(t)$ and $b(t)$ as

$$b^{(m+2)} = b_0^{(m+2)}(t - t_0)^{\frac{6(m+2)}{9+(2m+1)^2(\mu_1^2-\nu_1^2)}}. \tag{4.2.61}$$

If $9+(2m+1)^2(\mu_1^2-\nu_1^2) = 0$, it gives exponential expansion of the cosmological model while $9+(2m+1)^2(\mu_1^2-\nu_1^2) \gtrless 0$ corresponds to accelerated expansion or contraction of the universe, respectively. Figure **4.10** shows different cosmological phases for power-law scale factor, where blue and gray regions correspond to contraction and accelerated expansion of the universe model, respectively. For $m < 0$, there exists gray region only which shows that the universe model undergoes accelerated expansion.

In case of tachyon coupled fluid, Eq.(4.2.53) yields

$$\dot{\Theta} = -\frac{1}{6(m+2)}\left[(2m+1)^2\nu_1^2\sqrt{1-\left(\frac{2m+1}{m+2}\right)^2\mu_1^2} - \frac{9}{2(m+2)}\right]\Theta^2. \tag{4.2.62}$$

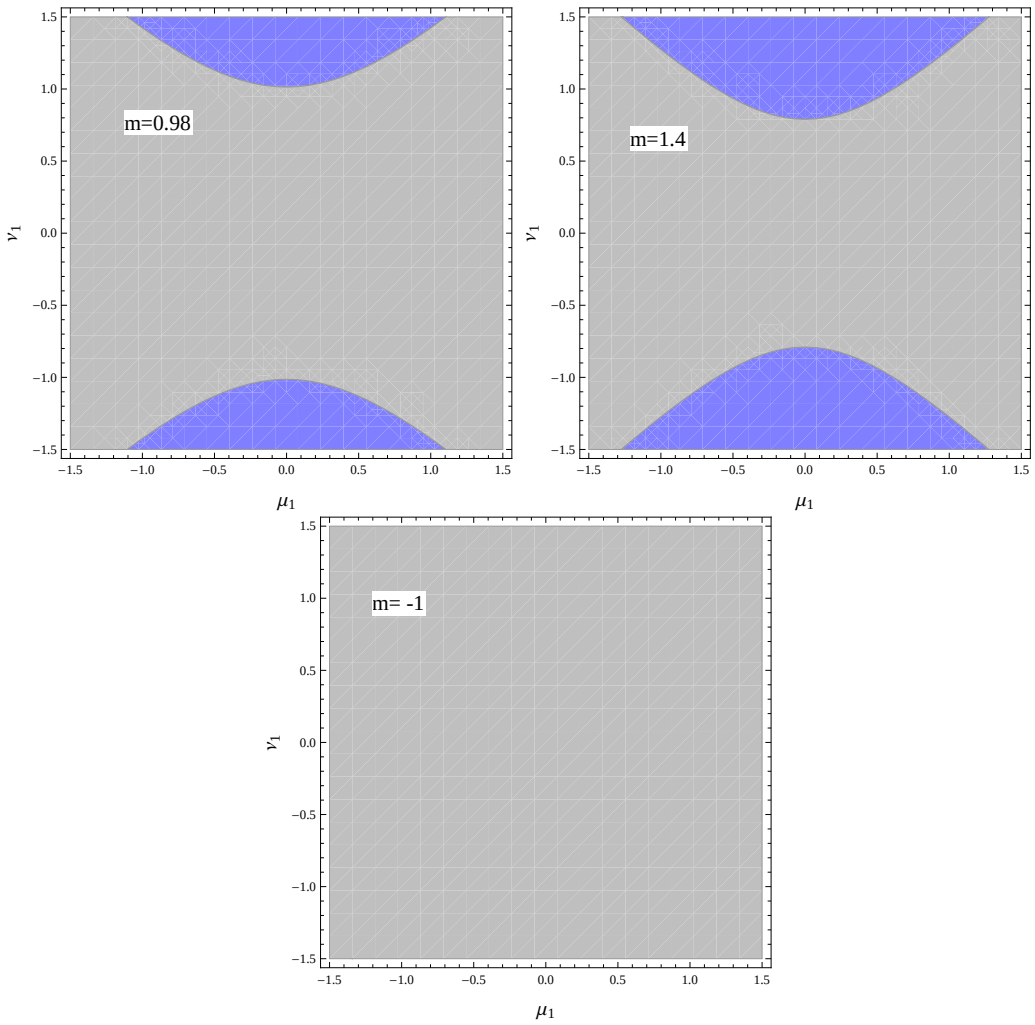

Figure 4.10: Plots of qualitative phase space analysis for power-law scale factor with phantom coupled matter. Blue and gray regions indicate contraction and accelerated expansion of the universe model, respectively.

For $\Theta \neq 0$, we again evaluate power-law scale factor if $(2m+1)^2\nu_1^2\sqrt{1-\left(\frac{2m+1}{m+2}\right)^2\mu_1^2}-\frac{9}{2(m+2)} \neq 0$. The generic critical point is found as

$$b^{(m+2)} = b_0^{(m+2)}(t-t_0)^{\frac{6(m+2)}{(2m+1)^2\nu_1^2\sqrt{1-\left(\frac{2m+1}{m+2}\right)^2\mu_1^2}-\frac{9}{2(m+2)}}}. \tag{4.2.63}$$

We explore different cosmological phases according to $(2m+1)^2\nu_1^2\sqrt{1-\left(\frac{2m+1}{m+2}\right)^2\mu_1^2}-\frac{9}{2(m+2)} \gtrless 0$. In contrast to the phantom coupled matter, we find different results for tachyon coupled field. We observe that the region for decelerated expansion decreases by increasing m while $m < 0$ shows contraction region only which means that the universe model undergoes decelerated expansion for negative values of m (Figure **4.11**).

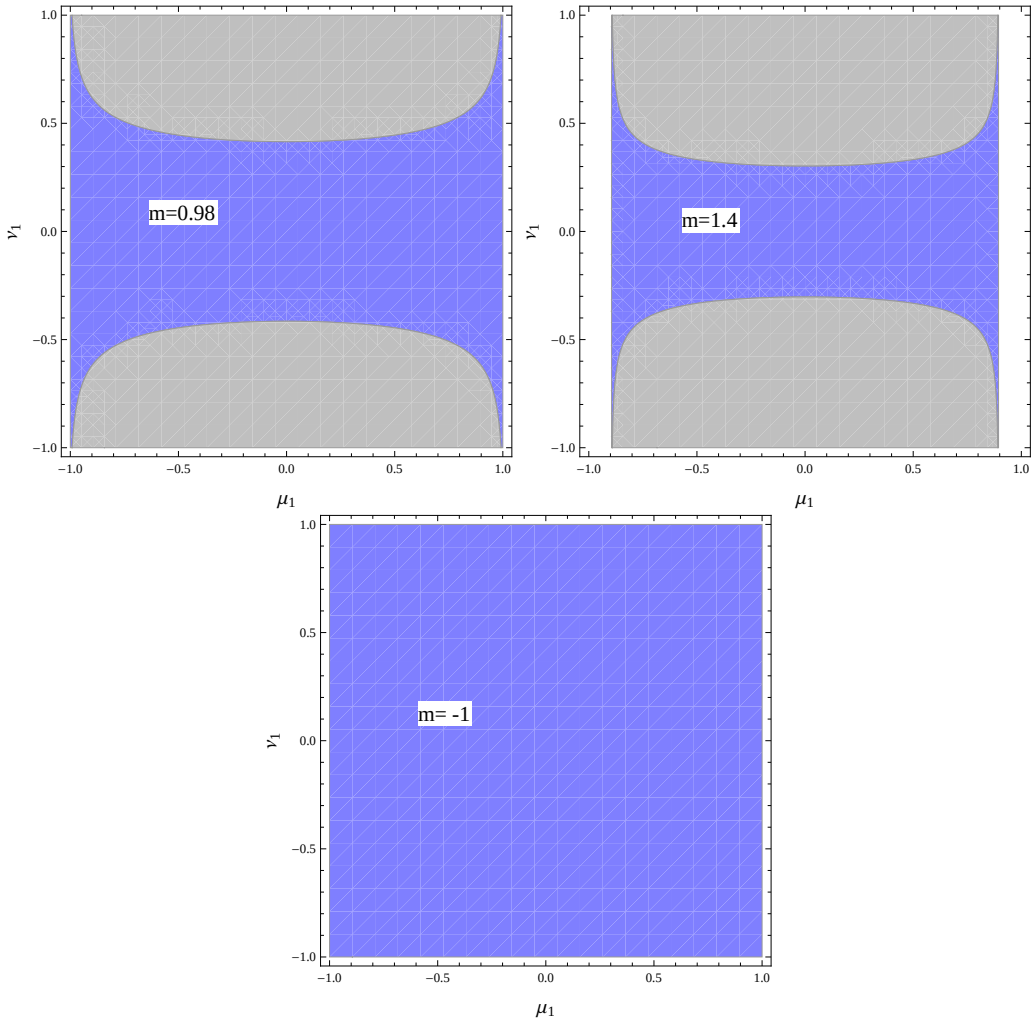

Figure 4.11: Plots of qualitative phase space analysis for power-law scale factor with tachyon coupled matter.

Chapter 5

Concluding Remarks

In this chapter, we briefly discuss the results of this thesis and conclude the discussion. The main results of this thesis are summarized as follows.

Chapter **Two** is devoted to study the effect of electric charge on dynamical instability of gaseous sphere and cylinder. For spherical collapsing system, we have found the values of adiabatic index Γ as well as radii for marginal stability of homogeneous sphere (Table **2.1**). It turns out that Γ takes finite positive values less or greater than $\frac{4}{3}+\frac{8Q^2}{21}$ corresponding to different values of charge at Newtonian limit. The radius $\frac{R}{R_N}$ approaches to infinity for $\Gamma < 0$ which leads to expansion rather than collapse. In pN limit, the dynamical instability occurs if Γ exceeds $\frac{4}{3}+\frac{8Q^2}{21}$ by a small quantity and the gaseous mass is contracted to RN limiting radius. We have found that $0.1 < Q < 0.4$ and $\Gamma > 1.5$ provide valid radii ranges for stability of sphere. It turns out that only unstable radii exist corresponding to $Q > 1.2$.

We have also discussed the stability/instability conditions for relativistic polytropic models of indices $0, 1, 2$ and 3. We have evaluated radii of instability and different values of Γ for dynamical instability of polytropes and found that $\Gamma > \frac{4}{3}+\frac{8Q^2}{21}$. The dynamical instability occurs when the mass of polytropic configuration approaches to

the RN radius limit. We find that the presence of charge has substantial role in the emergence of instability of gaseous sphere as compared to [3]. For charged homogeneous sphere, the system becomes stable for both negative as well a as positive values of adiabatic index, while it remains stable for $\Gamma > \frac{4}{3}$ without charged system [3].

For charged dissipative cylinder, it is found that Γ takes finite values greater than or equal to $-\frac{3}{4}\left(\frac{3}{2}+27Q^2\right)$ for $Q = 0.4$ and $q = 0.5$ in Newtonian limit. In pN limit, $\frac{R}{R_*}$ remains positive for $\Gamma > 0$ showing marginal stability of gaseous cylindrical model. The gaseous cylinder remains stable as long as its radius is larger than R_* but becomes unstable as its radius contracts to the radius R_*. In pN limit, the gaseous cylinder undergoes dynamical instability if Γ exceeds $-\frac{3}{4}\left(\frac{3}{2}+27Q^2\right)$ by a small amount. It is found that $\Gamma > -1$ and $Q > 0.3$ provide valid ranges of radii for the stability of cylinder whereas only unstable radii exist corresponding to $\Gamma < -1$ and $Q < 0.3$ (Figure **2.7**). There is no effect of dissipation on stability of collapsing system in this case. It is worth mentioning here that the gaseous cylinder becomes unstable for smaller values of charge. For uncharged cylinder, we have found that Γ exceeds $-\frac{9}{8}$ by a small amount showing stable cylindrical configuration (Figure **2.8**). It is observed that $\frac{R}{R_*} < 0$ for $\Gamma < -1.125$ leading to un-physical results. We conclude that inclusion of charge in the gaseous cylinder enhances its stability.

In chapter **Three**, we have constructed regular ABGB thin-shell WHs with and without Λ by incorporating the effects of NLED. It is found that thin-shell WH remains attractive for $\Lambda = 0$ while it shows both attractive and repulsive characteristics for different throat radii in de Sitter background (**Figure 3.1**). There exist three stability regions for regular ABGB thin-shell WHs with GCG gas which decrease gradually by increasing $\frac{Q}{M}$ and reduce to only two stable regions for $\frac{Q}{M} = 0.99$. We

have investigated non-physical regions for small throat radii while stability regions become enlarged for de Sitter configurations but have similar behavior as in the above case. For MGCG, the possibility of stability regions increases by increasing the value of $\frac{Q}{M}$ in both cases with and without Λ. It is worth mentioning here that MGCG has remarkable significance as it provides maximum stable regions for WH configurations which are more viable as compared to that of GCG. We have found that the effect of logarithmic gas is to increase the stability regions for regular ABGB-de Sitter thin-shell WHs by increasing $\frac{Q}{M}$. We observe that there exist more stability regions for de Sitter case as compared to the general case without Λ. We have also studied small velocity dependent perturbations and found that ABGB WH configurations remain no more stable under these perturbations.

We have studied the effects of HBI parameter as well as electric charge on the stability of WH configurations. It is found that there exists only one stable region as well as event horizon for CG with smaller value of HBI parameter such that the event horizon diminishes for $\frac{Q}{M} = 1.1$. For linear gas, it provides more stable regions as compared to that of CG. The event horizon decreases by increasing the values of electric charge and finally vanishes. The logarithmic gas provides least stable solutions as compared to other cases for smaller values of charge. We conclude that linear gas is more effective for WH configurations in HBI electrodynamics which provides maximum stable regions as compared to other models while CG gives the least stable regions.

Chapter **4** deals with the phase space analysis of isotropic and homogeneous universe model by taking noninteracting mixture of electromagnetic and viscous radiating fluids. Firstly, we have discussed stability of critical points through their eigenvalues

corresponding to different values of E and B for viscous radiation dominated universe model. The point P_d^- is a global attractor in the physical phase space region which leads to an expanding universe model dominated by viscous matter for various choices of cosmological parameters. In the presence of both electric and magnetic fields, we find that bulk viscosity increases the region for accelerated expansion while the increasing values of E shows deceleration region for smaller values of bulk viscosity. It is worth mentioning here that the role of bulk viscosity is to increase the accelerated expansion with different choices of E and B for both electric as well as magnetic universe models. It is found that the power-law scale factor indicates various phases of evolution (accelerated or exponential expansion) of the respective universe model.

This chapter also discusses phase space analysis of LRS BI universe model by taking a coupling between scalar field models and DM. We have investigated the impact of m on stability of cosmic model in the presence of phantom and tachyon fields. For the coupling constant $Q_* = \alpha\dot{\sigma}_m$, we have found an unstable matter dominated state undergoing decelerated expansion for all points with $m > 0$ and various choices of α. The dynamical analysis shows a matter dominated era ultimately followed by a late accelerated expansion phase of the universe. For $m < 0$, all the points become stable future attractor undergoing accelerated expansion as $\bar{q} < 0$ except the point P_1 which lies in decelerated expanding region. In this case, the results for points P_2 and P_3 do not solve the coincidence problem which is well consistent with the results for FRW universe model [52, 99]. For the other couplings, all the eigenvalues and trajectories show unstable non-accelerating nodes for $m > 0$ which become stable for $m < 0$.

Secondly, we have studied stability of the universe model by taking interaction

between tachyon field and DM. For $Q_* = \beta\dot{\sigma}_\phi$ only. The cosmic portrait shows a matter dominated epoch ultimately followed by a late accelerated expansion phase (Figure **4.9**). For $m > 0$, we have found unstable/saddle node for points P_1 and P_2 while point P_3 gives stable future attractor which undergoes an accelerated expansion. For $m < 0$, the point P_1 corresponds to stable node showing accelerated expansion of the universe while the remaining points give saddle/unstable node that corresponds to de Sitter phase of the universe. We note that all the points show accelerated expansion of the universe for tachyon coupled field. Finally, we have studied the behavior of power-law scale factor corresponding to different values of m as shown in Figures **4.10** and **4.11**. For phantom coupled matter, the region for decelerated expansion gets larger by increasing m while $m < 0$ corresponds to accelerated expansion of cosmos. In case of tachyon coupled field, the contraction region decreases by increasing m while the gray region becomes larger. Also, $m < 0$ shows only blue region which corresponds to the decelerated expanding universe model. We conclude that negative values of m enhance stability of the universe model as compared to its positive values.

It would be interesting to extend this work in the following directions.

- To discuss the dynamical instability of self-gravitating system as well as relativistic polytropes by taking anisotropic matter distributions with electromagnetic effects following the Eulerian and Lagrangian approaches.

- To analyze physical characteristics as well as stability criteria for thin-shell WHs coupled with scalar field.

- To explore stability of thin-shell WHs containing quintessence parameter and magnetic field.

- To study counter-rotational effects on stability of charged thin-shell WHs.
- To investigate the influence of NLED on dynamical stability of bulk viscous isotropic and anisotropic cosmologies by taking bulk viscosity as a function of Hubble parameter, temperature as well as energy density.

Appendix A

List of Publications

The contents of this thesis are based on the following published/submitted research papers. These papers are also attached herewith.

1. Sharif, M. and **Mumtaz, S.**: *Dynamical Instability of Gaseous Sphere in the Reissner-Nordström Limit,*
   Gen. Relativ. Gravit. **48**(2016)92.

2. Sharif, M. and **Mumtaz, S.**: *Dynamical Instability of Charged Gaseous Cylinder,*
   Mon. Not. R. Astron. Soc. **471**(2017)1215.

3. Sharif, M. and **Mumtaz, S.**: *Influence of Nonlinear Electrodynamics on Stability of Thin-shell Wormholes,*
   Astrophys. Space Sci. **361**(2016)218.

4. Sharif, M. and **Mumtaz, S.**: *Dynamics of Thin-shell Wormholes with Different Cosmological Models,*
   Int. J. Mod. Phys. D **26**(2017)1741007.

5. Sharif, M. and **Mumtaz, S.**: *Stability of Accelerated Expansion in Nonlinear Electrodynamics,*
   Eur. Phys. J. C **77**(2017)136.

6. Sharif, M. and **Mumtaz, S.**: *Stability of Universe Model Coupled with Phantom and Tachyon Fields,*
   Submitted for Publication.

Also, the following papers related to this thesis have been published/submitted for publication.

1. Sharif, M. and **Mumtaz, S.**: *Stability of the Regular Hayward Thin-Shell Wormholes,*
   Adv. High Energy Phys. **2016**(2016)2868750.

2. Sharif, M. and **Mumtaz, S.**: *Stability of Thin-Shell Wormholes from Regular ABG Black Hole,*
   Eur. Phys. J. Plus **132**(2017)26.

3. Sharif, M. and **Mumtaz, S.**: *Stability Analysis of Bulk Viscous Anisotropic Universe Model,*
   Astrophys. Space Sci. **362**(2016)205.

4. Sharif, M. and **Mumtaz, S.**: *Stability Analysis of Oscillating Cylinder,*
   Eur. Phys. J. Plus **132**(2017)436.

5. Sharif, M. and **Mumtaz, S.**: *Stability Analysis of Bulk Viscous Cosmology,*
   Eur. Phys. J. Web of Conferences **168**(2018)08006.

6. Sharif, M. and **Mumtaz, S.**: *Phase Space Analysis for Anisotropic Universe with Nonlinear Bulk Viscosity,*
   Submitted for Publication.

7. Sharif, M. and **Mumtaz, S.**: *Rotating Thin-Shell Wormholes with Scalar Field,*
   Submitted for Publication.

8. Sharif, M., **Mumtaz, S.** and Javed, F.: *Dynamics of Thin-Shell Wormholes with Rotational Effects,*
   Submitted for Publication.

Bibliography

[1] Ayal, S. et al.: *Post-Newtonian Smoothed Particle Hydrodynamics*, Astrophys. J. **550**(2001)846; Marek, A. et al.: *Exploring the Relativistic Regime with Newtonian Hydrodynamics*, Astron. Astrophys. **445**(2006)273.

[2] Chandrasekhar, S.: *Dynamical Instability of Gaseous Masses Approaching the Schwarzschild Limit in General Relativity*, Astrophys. J. **140**(1964)417.

[3] Chandrasekhar, S.: *The Stability of Gaseous Masses for Radial and Non-Radial Oscillations in the Post-Newtonian Approximation of General Relativity*, Astrophys. J. **142**(1965)1519.

[4] Herrera, L., Le Denmat, G. and Santos, N.O.: *Dynamical Instability for Non-adiabatic Spherical Collapse*, Mon. Not. R. Astron. Soc. **237**(1989)257.

[5] Chan, R., Herrera, L. and Santos, N.O.: *Dynamical Instability for Shearing Viscous Collapse*, Mon. Not. R. Astron. Soc. **267**(1994)637.

[6] Rosseland, S.: *Electrical State of a Star*, Mon. Not. R. Astron. Soc. **84**(1924)720.

[7] Eddington, A.: *The Internal Constitution of the Stars* (Cambridge University Press, 1988).

[8] Stettner, R.: *On the Stability of Homogeneous, Spherically Symmetric, Charged Fluids in Relativity*, Ann. Phys. **80**(1973)212.

[9] Glazer, I.: *General Relativistic Pulsation Equation for Charged Fluids*, Ann. Phys. **101**(1976)594.

[10] Zhang, J.L., Chau, W.Y. and Deng, T.Y.: *The Influence of a Net Charge on the Critical Mass of a Neutron Star*, Astrophys. Space Sci. **88**(1982)81.

[11] Ghezzi, C.R.: *Relativistic Structure, Stability, and Gravitational Collapse of Charged Neutron Stars*, Phys. Rev. D **72**(2005)104017.

[12] Thirukkanesh, S. and Maharaj, S.D.: *Charged Anisotropic Matter with a Linear Equation of State*, Class. Quantum Gravit. **25**(2008)235001.

[13] Pinheiro, G. and Chan, R.: *Radiating Shear-Free Gravitational Collapse with Charge*, Gen. Relativ. Gravit. **45**(2013)243.

[14] Thorne, K.S.: *Energy of Infinitely Long, Cylindrically Symmetric Systems in General Relativity*, Phys. Rev. **138**(1965)B251.

[15] Thorne, K.S.: *Absolute Stability of Melvin's Magnetic Universe*, Phys. Rev. **139**(1965)B244.

[16] Nakao, K. and Morisawa, Y.: *High-Speed Cylindrical Collapse of Perfect Fluid*, Prog. Theor. Phys. **113**(2005)73.

[17] Sharif M. and Ahmad, Z.: *High-Speed Cylindrical Collapse of two Perfect Fluids*, Gen. Relativ. Gravit. **39**(2007)1331; Di Prisco, A. et al.: *Shearfree Cylindrical Gravitational Collapse*, Phys. Rev. D **80**(2009)064031; Sharif, M. and Abbas,

G.: *Charged Perfect Fluid Cylindrical Gravitational Collapse*, J. Phys. Soc. Jpn. **80**(2011)104002.

[18] Chandrasekhar, S. and Fermi, E.: *Problems of Gravitational Stability in the Presence of a Magnetic Field*, Astrophys. J. **118**(1953)116.

[19] Sharif, M. and Azam, M.: *Effects of Electromagnetic Field on the Dynamical Instability of Cylindrical Collapse*, J. Cosmol. Astropart. Phys. **02**(2012)043.

[20] Sharif, M. and Bhatti, M.Z.: *Stability of the Expansion-Free Charged Cylinder*, J. Cosmol. Astropart. Phys. **10**(2013)056.

[21] Tooper. R.F.: *General Relativistic Polytropic Fluid Spheres*, Astrophys. J. **140**(1966)434.

[22] Abramowicz, M.A.: *Polytropes in N-dimensional Spaces*, Acta Astron. **33**(1983)313.

[23] Ray, S. et al.: *Charged Polytropic Compact Stars*, Braz. J. Phys. **34**(2004)310; Fronsdal, C.: *Reissner-Nordström and Charged Gas Spheres*, Lett. Mathem. Phys. **82**(2007)255.

[24] Herrera, L. and Barreto, W.: *General Relativistic Polytropes for Anisotropic Matter: The General Formalism and Applications*, Phys. Rev. D **88**(2013)084022.

[25] Breysse, P.C., Kamionkowski, M. and Benson, A.: *Oscillations and Stability of Polytropic Filaments*, Mon. Not. R. Astron. Soc. **437**(2014)2675.

[26] Visser, M.: *Traversable Wormholes: Some Simple Examples*, Phys. Rev. D **39**(1989)3182.

[27] Visser, M., Kar, S. and Dadhich, N.: *Traversable Wormholes with Arbitrarily Small Energy Condition Violations*, Phys. Rev. Lett. **90**(2003)201102.

[28] Kim, S.W. and Lee, H.: *Exact Solutions of a Charged Wormhole*, Phys. Rev. D **63**(2001)064014.

[29] Eiroa, E.F. and Romero, G.E.: *Linearized Stability of Charged Thin-Shell Wormholes*, Gen. Relativ. Gravit. **36**(2004)651.

[30] Lobo, F.S.N.: *Surface Stresses on a Thin-Shell Surrounding a Traversable Wormhole*, Class. Quantum Grav. **21**(2004)4811.

[31] Sharif, M. and Azam, M.: *Spherical Thin-Shell Wormholes and Modified Chaplygin Gas*, J. Cosmol. Astropart. Phys. **05**(2013)025.

[32] Bardeen, J.M.: *Non-Singular General Relativistic Gravitational Collpase*, Int. Conf. GR 5 (Tbilisi, USA, 1968).

[33] Ayon-Beato, E. and Garcia, A.: *Regular Black Hole in General Relativity Coupled to Nonlinear Electrodynamics*, Phys. Rev. Lett. **80**(1998)5056.

[34] Bronnikov, K.A.: *Regular Magnetic Black Holes and Monopoles from Nonlinear Electrodynamics*, Phys. Rev. D **63**(2001)044005.

[35] Hayward, S.A.: *Formation and Evaporation of Nonsingular Black Holes*, Phys. Rev. Lett. **96**(2006)031103.

[36] Rahaman, F. et al.: *Thin-Shell Wormholes from Regular Charged Black Holes*, Int. J. Theor. Phys. **49**(2010)2364.

[37] Sharif, M. and Azam, M.: *Stability of Thin-Shell Wormholes in Nonlinear Electrodynamics*, J. Phys. Soc. Jpn. **81**(2012)124006.

[38] Halilsoy, M., Ovgun, A. and Mazharimousavi, S.H.: *Thin-Shell Wormholes from the Regular Hayward Black Hole*, Eur. Phys. J. C **74**(2014)2796.

[39] Sharif, M. and Javed, F.: *On the Stability of Bardeen Thin-Shell Wormholes*, Gen. Relativ. Gravit. **48**(2016)158.

[40] Born, M. and Infeld, L.: *Foundations of the New Field Theory*, Proc. R. Soc. A **144**(1934)425.

[41] Hoffmann, B.: *Gravitational and Electromagnetic Mass in the Born-Infeld Electrodynamics*, Phys. Rev. **47**(1935)877.

[42] Eiroa, E.F. and Aguirre, F.G.: *Thin-Shell Wormholes with a Generalized Chaplygin Gas in Einstein-Born-Infeld Theory*, Eur. Phys. J. C **72**(2012)2240.

[43] Sharif, M. and Azam, M.: *Thin-Shell Wormholes in Born-Infeld Electrodynamics with Modified Chaplygin Gas*, Phys. Lett. A **378**(2014)2737.

[44] Sami, M.: *Implementing Power-Law Inflation with Tachyon Rolling on the Brane*, Mod. Phys. Lett. A **18**(2003)691.

[45] Gibbons, G.W.: *Cosmological Evolution of the Rolling Tachyon*, Phys. Lett. B **537**(2002)1.

[46] Sami, M., Chingangbam, P. and Qureshi, T.: *Aspects of Tachyonic Inflation with an Exponential Potential*, Phys. Rev. D **66**(2002)043530.

[47] Chimento, L.P. et al.: *Interacting Quintessence Solution to the Coincidence Problem*, Phys. Rev. D **67**(2003)083513; Chimento, L.P. and Pavon, D.: *Dual Interacting Cosmologies and Late Accelerated Expansion*, Phys. Rev. D **73**(2006)063511.

[48] Guo, Z.K., Cai, R.G. and Zhang, Y.Z.: *Cosmological Evolution of Interacting Phantom Energy with Dark Matter*, J. Cosmol. Astropart. Phys. **05**(2005)002.

[49] Garcia-Salcedo, R. and Bretonn, N.: *Singularity-Free Bianchi Spaces with Nonlinear Electrodynamics*, Class. Quantum Grav. **22**(2005)4783.

[50] Yang, R.J. and Gao, X.T.: *Phase-Space Analysis of a Class of K-Essence Cosmology*, Class. Quantum Grav. **28**(2011)065012.

[51] Acquaviva, G. and Beesham, A.: *Nonlinear Bulk Viscosity and the Stability of Accelerated Expansion in FRW Spacetime*, Phys. Rev. D **90**(2014)023503.

[52] Shahalam, M. et al.: *Dynamics of Coupled Phantom and Tachyon Fields*, arXiv:1702.04720v2.

[53] Eriksen, H.K. et al.: *Inflation and Primordial Power Spectra at Anisotropic Spacetime Inspired by Planck's Constraints on Isotropy of CMB*, Astrophys. J. **605**(2004)14.

[54] Coley, A.A. and Dunn, K.A.: *Qualitative Analysis of a Class of Bianchi V Imperfect Fluid Cosmologies*, J. Math. Phys. **33**(1992)1772.

[55] Burd, A. and Coley, A.: *Viscous Fluid Cosmology*, Class. Quantum Grav. **11**(1994)83.

[56] Goliath, M. and Ellis, G.F.R.: *Homogeneous Cosmologies with a Cosmological Constant*, Phys. Rev. D **60**(1999)023502.

[57] Sharif, M. and Waheed, S.: *Magnetized Chameleonic Brans-Dicke Cosmology and Phase Space Analysis*, Astrophys. Space Sci. **351**(2014)329.

[58] Chaubey, R. and Raushan, R.: *Dynamical Analysis of Anisotropic Cosmological Model with Quintessence*, Astrophys. Space Sci. **361**(2016)215.

[59] Hawking, S.W. and Ellis, G.F.R.: *The Large Scale Structure of Spacetime* (Cambeidge University Press, 1979).

[60] Cox, J.P.: *Theory of Stellar Pulsation*, (Princeton Univ. Press, 1980); Kippenhahn, R. and Weigert, A.: *Stellar Structure and Evolution* (Springer, 1990).

[61] Misner, C.W. and Wheeler, J.A.: *Classical Physics as Geometry*, Ann. Phys. **2**(1957)525.

[62] Einstein, A. and Rosen, N.: *The Particle Problem in the General Theory of Relativity*, Phys. Rev. **48**(1935)73.

[63] Morris, M.S. and Thorne, K.S.: *Wormholes in Spacetime and their Use for Interstellar Travel: A Tool for Teaching General Relativity*, Am. J. Phys. **56**(1988)395.

[64] Israel, W.: *Singular Hypersurfaces and Thin-Shells in General Relativity*, Nuovo Cim. B **44**(1966)1.

[65] Darmois, G.: *Memorial des Sciences Mathematics* (Gautheir-Villars, 1927) Fasc. 25.

[66] Caldwell, R.R., Dave, R. and Steinhardt, P.J.: *Cosmological Imprint of an Energy Component with General Equation of State*, Phys. Rev. Lett. **80**(1998)1582.

[67] Carroll, S.M., Hoffman, M. and Trodden, M.: *Can the Dark Energy Equation of State Parameter w be less than −1?*, Phys. Rev. D **68**(2003)023509.

[68] Gorini, V. et al.: *Tachyons, Scalar Fields and Cosmology*, Phys. Rev. D **69**(2004)123512.

[69] DeBenedictis, A., Das, A. and Kloster, S.: *The Gravitating Perfect Fluid Scalar Field Equations: Quintessence and Tachyonic Matter*, Gen. Relativ. Gravit. **36**(2004)2481;

[70] Frampton, P.H.: *How to Test Stringy Dark Energy?*, Phys. Lett. B **555**(2003)139.

[71] Barrow, J.D.: *String-Driven Inflationary and Deflationary Cosmological Models*, Nucl. Phys. B **310**(1988)743.

[72] Bilic, N., Tupper, G.B. and Violler, R.: *Unification of Dark Matter and Dark Energy: The Inhomogeneous Chaplygin Gas*, Phys. Lett. B **535**(2002)17.

[73] Barreiro, T. and Sen, A.A.: *Generalized Chaplygin Gas in a Modified Gravity Approach*, Phys. Rev. D **70**(2004)124013.

[74] Bento, M.C., Bertolami, O. and Sen, A.A.: *Generalized Chaplygin Gas and Cosmic Microwave Background Radiation Constraints*, Phys. Rev. D **67**(2003)063003.

[75] Panotopoulos, G.: *Comparison between Different Cosmological Models*, Phys. Rev. D **77**(2008)107303.

[76] Benaoum, H.B.: arXiv hep-th/0205140.

[77] Xu, L., Wang, Y. and Noh, H.: *Modified Chaplygin Gas as a Unified Dark Matter and Dark Energy Model and Cosmic Constraints*, Eur. Phys. J. C **72**(2012)1931.

[78] Zimdahl, W.: *Bulk Viscous Cosmology*, Phys. Rev. D **53**(1996)5483.

[79] Bogoyavlensky, O.I.: *Qualitative Theory of Dynamical System in Astrophysics and Gas Dynamics* (Springer, 1985).

[80] Sharif, M. and Mumtaz, S.: *Dynamical Instability of Gaseous Sphere in the Reissner-Nordström Limit*, Gen. Relativ. Gravit. **48**(2016)92.

[81] Sharif, M. and Mumtaz, S.: *Dynamical Instability of Charged Gaseous Cylinder*, Mon. Not. R. Astron. Soc. **471**(2017)1215.

[82] Azam, M. et al.: *Study of Polytropes with Generalized Polytropic Equation of State*, Eur. Phys. J. C **76**(2016)510.

[83] Horedt, G.P.: *Polytropes: Applications in Astrophysics and Related Fields* (Kluwer Academic, 2004).

[84] Sharif, M. and Mumtaz, S.: *Influence of Nonlinear Electrodynamics on Stability of Thin-Shell Wormholes*, Astrophys. Space Sci. **361**(2016)218.

[85] Sharif, M. and Mumtaz, S.: *Dynamics of Thin-Shell Wormholes with Different Cosmological Models*, Int. J. Mod. Phys. D **26**(2017)1741007.

[86] Matyjasek, J., Tryniecki, D. and Klimek, M.: *Regular Black Holes in an Asymptotically de Sitter Universe*, Mod. Phys. Lett. A **23**, 3377(2008).

[87] Richarte, M.G. and Simeone, C.: *Wormholes in Einstein-Born-Infeld Theory*, Phys. Rev. D **80**(2009)104033.

[88] Mazharimousavi, S.H., Halilsoy, M. and Amirabi, Z.: *Black Hole and Thin-Shell Wormhole Solutions in Einstein-Hoffman-Born-Infeld Theory*, arXiv: 0908.3967; *Thin-Shell Wormhole Solutions in Einstein-Hoffmann-Born-Infeld Theory*, Phys. Lett. A **375**(2011)3649.

[89] Sharif, M. and Mumtaz, S.: *Stability of Accelerated Expansion in Nonlinear Electrodynamics*, Eur. Phys. J. C **77**(2017)136.

[90] Sharif, M. and Mumtaz, S.: *Stability of Universe Model Coupled with Phantom and Tachyon Fields*, (submitted for publication, 2017).

[91] Vollick, D.N.: *Homogeneous and Isotropic Cosmologies with Nonlinear Electromagnetic Radiation*, Phys. Rev. D **78**(2008)063524.

[92] Kruglov, S.I.: *Acceleration of Universe by Nonlinear Electromagnetic Fields*, Int. J. Mod. Phys. D **25**(2016)1640002.

[93] Ovgun, A.: *Acceleration of Universe by Nonlinear Magnetic Monopole Fields*, arXiv: 1604.01837.

[94] De Lorenci, V.A. et al.: *Nonlinear Electrodynamics and FRW Cosmology*, Phys. Rev. D **65**(2002)063501;

[95] Maartens, R. and Méndez, V.: *Nonlinear Bulk Viscosity and Inflation*, Phys. Rev. D **55**(1997)1937.

[96] Novello, M., Bergliaffa, S.E.P. and Salim, J.: *Nonlinear Electrodynamics and the Acceleration of the Universe*, Phys. Rev. D **69**(2004)127301; Novello, M. et al.: *Cosmological Effects of Nonlinear Electrodynamics*, Class. Quantum Grav. **24**(2007)3021.

[97] Collins, C.B.: *Special Exact Solutions of Einstein's Equations - A Theorem and Some Observations*, Phys. Lett. A **60**(1977)397.

[98] Wang, B., Gong, Y.G. and Abdalla, E.: *Transition of the Dark Energy Equation of State in an Interacting Holographic Dark Energy Model*, Phys. Lett. B **624**(2005)141; Gumjudpai, B. et al.: *Coupled Dark Energy: Towards a General Description of the Dynamics*, J. Cosmol. Astropart. Phys. **007**(2005)0506; Campo, S.D., Herrera, R. and Pavon, D.: *H(z) Diagnostics on the Nature of Dark Energy*, Int. J. Mod. Phys. D **20**(2011)561; Wei, H. and Cai, R.G.: *K-Chameleon and the Coincidence Problem*, Phys. Rev. D **71**(2005)043504.

[99] Chen, X., Gong, Y. and Saridakis, E.N.: *Phase-Space Analysis of Interacting Phantom Cosmology*, J. Cosmol. Astropart. Phys. **04**(2009)001.

Gen Relativ Gravit (2016) 48:92
DOI 10.1007/s10714-016-2090-x

RESEARCH ARTICLE

Dynamical instability of gaseous sphere in the Reissner–Nordström limit

M. Sharif[1] · **Saadia Mumtaz**[1]

Received: 1 January 2016 / Accepted: 24 May 2016 / Published online: 15 June 2016

Abstract In this paper, we study the dynamical instability of gaseous sphere under radial oscillations approaching the Reissner–Nordström limit. For this purpose, we derive linearized perturbed equation of motion following the Eulerian and Lagrangian approaches. We formulate perturbed pressure in terms of adiabatic index by employing the conservation of baryon numbers. A variational principle is established to evaluate characteristic frequencies of oscillations which lead to the criteria for dynamical stability. The dynamical instability of homogeneous sphere as well as relativistic polytropes with different values of charge in Newtonian and post-Newtonian regimes is explored. We also find their radii of instability in terms of the Reissner–Nordstörm radius. We conclude that dynamical instability occurs if the gaseous sphere contracts to the Reissner–Nordstörm radius for different values of charge.

Keywords Gravitational collapse · Instability · Electromagnetic field · Relativistic fluids

1 Introduction

It is a well-known fact that any relativistic model will be physically interesting if it is stable under fluctuations. The stability/instability of celestial objects has significant importance in general relativity (GR). This study is closely related to the evolution

✉ M. Sharif
msharif.math@pu.edu.pk

Saadia Mumtaz
sadiamumtaz17@gmail.com

[1] Department of Mathematics, University of the Punjab, Quaid-e-Azam Campus, Lahore 54590, Pakistan

and structure formation of self-gravitating objects. Initially, any stable gaseous mass remains in state of hydrostatic equilibrium for which the gravitational force is counter balanced by the internal pressure of the body acting in the opposite direction. The effect of gravity over the internal pressure causes the matter to collapse and the star contracts to a point under its own gravitational force forming compact stars.

The dynamics of massive stars can be discussed in weak as well as strong-field regimes. The idea of weak-field approximation [Newtonian and post-Newtonian approximations (pN)] [1], [2] has remarkable importance in the context of relativistic hydrodynamics. The analysis of dynamical instability in strong-field regimes becomes complicated due to non-linear terms, so the weak-field approximation schemes are used as an effective tool. Chandrasekhar [3] was the pioneer who studied the dynamical instability of Newtonian perfect fluid sphere approaching the Schwarzschild limit in terms of adiabatic index. He used Eulerian approach for hydrodynamic equations and developed a variational principle to find characteristic frequencies applicable to the radial oscillations at Newtonian and pN limits. He concluded that the system would be dynamically stable or unstable according to the numerical value of adiabatic index, i.e., $\Gamma > \frac{4}{3}$ or $\Gamma < \frac{4}{3}$, respectively. The same author [4] also investigated the stability of gaseous sphere under radial and non-radial oscillations at pN limit.

The dynamical instability of self-gravitating spherical objects has been studied by using various techniques. Herrera et al. [5] explored dynamical instability of spherical collapsing system for non-adiabatic fluid using perturbation scheme. They showed that heat conduction increases the instability range in Newtonian limit but decreases in pN limit. Later, many researchers [6], [7], [8] discussed the role of various physical factors on the dynamical instability of spherical systems using perturbation scheme and found interesting results.

The stability of self-gravitating objects in the presence of electromagnetic field has a primordial history starting with Rosseland [9]. There is a general consensus that astrophysical objects do not have charge in large amount [10] but there are some mechanisms which induce large amount of electric charge in collapsing stars. Stettner [11] showed that presence of net surface charge enhances the stability of sphere with uniform density. Glazer [12] investigated the dynamical stability of perfect fluid sphere pulsating radially with electric charge. Ghezzi [13] studied stability of neutron stars and found that the stars having a charge greater than the extreme value would explode. Sharif and collaborators [14], [15] discussed the role of electric charge in dynamical instability at Newtonian and pN regimes.

Polytropes are useful self-gravitating objects as they provide simplified models for internal structures of stellar objects. The polytropic equation of state deals with various fundamental astrophysical issues [16]. Tooper [17] studied the internal structure of gaseous sphere obeying polytropic equation of state and obtained Newtonian polytropes using numerical solution of the Lane-Emden equation. The effect of electromagnetic field on the dynamics of polytropic compact stars has also been studied [18], [19]. Herrera and Barreto [20] analyzed both Newtonian as well as relativistic polytropes in spherical symmetry. Recently, Breysse et al. [21] have discussed the dynamical instability of cylindrical polytropic fluid systems under radial and non-radial modes of oscillations.

In this paper, we study the dynamical instability of spherically symmetric gaseous systems following Chandrasekhar's approach [3] in the vicinity of electromagnetic field. The paper is organized as follows. The next section deals with matter distribution and the Einstein–Maxwell field equations. In Sect. 3, we discuss motion of the system under radial oscillations following the Eulerian approach. Section 4 provides the formulation of perturbed pressure and adiabatic index in terms of Lagrangian displacement using conservation of baryon number. In Sect. 5, we develop conditions for dynamical instability of homogeneous sphere and relativistic polytropes. Finally, we conclude our results in the last section.

2 Field equations and matter configuration

We consider a spherically symmetric system in the interior region given by

$$ds^2 = -e^{\nu}dt^2 + e^{\lambda}dr^2 + r^2(d\theta^2 + \sin^2\theta d\phi^2), \tag{1}$$

where $\nu = \nu(t, r)$ and $\lambda = \lambda(t, r)$ are the gravitational potentials. The corresponding Einstein field equations can be written as

$$-\frac{8\pi G}{c^4}T_0^0 = \frac{1}{r^2} - \frac{1}{r^2}\frac{\partial}{\partial r}(re^{-\lambda}), \tag{2}$$

$$-\frac{8\pi G}{c^4}T_1^1 = \frac{1}{r^2} - e^{-\lambda}(\frac{1}{r^2} + \frac{1}{r}\frac{\partial \nu}{\partial r}), \tag{3}$$

$$\frac{8\pi G}{c^4}T_0^1 = \dot{\lambda}\frac{e^{-\lambda}}{r}, \tag{4}$$

where dot denotes derivative w.r.t t. We assume the energy–momentum tensor corresponding to charged perfect fluid in the form

$$T_j^i = (\sigma + p)u^i u_j + p\delta_j^i + \frac{1}{4\pi}\left[F_{jk}F^{ik} - \frac{1}{4}\delta_j^i F_{kl}F^{kl}\right], \tag{5}$$

where $u^i = \frac{dx^i}{ds}$ is the four-velocity, p is the pressure and σ is the energy density. The electromagnetic field tensor F_{ij} can be defined in terms of four potential, $F_{ij} = \Phi_{j;i} - \Phi_{i;j}$, which satisfies the Maxwell field equations as

$$F^{ij}_{\ ;j} = 4\pi J^i, \quad F_{[ij,k]} = 0,$$

where $J^i = \rho u^i$ is the four current. The only non-vanishing radial component of electromagnetic field tensor ($F^{01} = -F^{10}$) implies that

$$\frac{d\left(r^2 e^{(\lambda+\nu)/2}F^{01}\right)}{dr} = 4\pi r^2 e^{\lambda/2}\rho,$$

whose integration yields

$$F^{01}=\frac{e^{-(\lambda+\nu)/2}Q(t,r)}{r^2},$$

where $Q(t,r)=4\pi\int_0^r r^2\rho e^{\lambda/2}dr$ is the total amount of charge within the sphere.

The energy-momentum tensor follows the conservation identity $T^{ij}_{;j}=0$, which governs hydrodynamics of the fluid and leads to the following relations

$$\frac{\partial T_0^0}{\partial t}+\frac{\partial T_1^0}{\partial r}+\frac{1}{2}\left(\frac{4}{r}+\frac{\partial}{\partial r}(\lambda+\nu)\right)T_0^1+\frac{1}{2}\left(T_0^0-T_1^1\right)\frac{\partial\lambda}{\partial t}=0, \tag{6}$$

$$\frac{\partial T_1^0}{\partial t}+\frac{\partial T_1^1}{\partial r}+\frac{1}{2}\left(T_1^1-T_0^0\right)\frac{\partial\nu}{\partial r}-\frac{2}{r}\left(p-T_1^1\right)+\frac{1}{2}T_1^0\frac{\partial}{\partial t}(\lambda+\nu)=0, \tag{7}$$

where $T_0^1=-e^{\nu-\lambda}T_1^0$. The non-zero components of energy–momentum tensor are

$$T_0^0=-\sigma-\frac{Q^2}{8\pi r^4},\quad T_1^1=p-\frac{Q^2}{8\pi r^4},\quad T_2^2=T_3^3=p+\frac{Q^2}{8\pi r^4}.$$

All the quantities governing the motion remain independent of time during the state of hydrostatic equilibrium. The surface stresses describing equilibrium state are denoted by zero subscript. In this context, Eqs. (2), (3) and (7) take the form

$$\frac{d}{dr}(re^{-\lambda_0})=1-\frac{8\pi Gr^2}{c^4}\sigma_0-\frac{GQ^2}{c^4r^2}, \tag{8}$$

$$\frac{1}{r}e^{-\lambda_0}\frac{d\nu_0}{dr}=\frac{1}{r^2}(1-e^{-\lambda_0})+\frac{8\pi Gp_0}{c^4}-\frac{GQ^2}{c^4r^4}, \tag{9}$$

$$\frac{dp_0}{dr}=\frac{1}{2}\frac{d\nu_0}{dr}(p_0+\sigma_0)+\frac{1}{8\pi}\frac{d}{dr}\left(\frac{Q^2}{r^4}\right)+\frac{Q^2}{4\pi r^5}. \tag{10}$$

Following Eqs. (2) and (3), we also have a useful relation

$$\frac{e^{-\lambda_0}}{r}\frac{d}{dr}(\lambda_0+\nu_0)=(p_0+\sigma_0)\frac{8\pi G}{c^4}. \tag{11}$$

We take the Reissner–Nordström (RN) spacetime in the exterior region as

$$ds^2=-\left(1-\frac{2GM}{rc^2}+\frac{GQ^2}{r^2c^4}\right)dt^2+\left(1-\frac{2GM}{rc^2}+\frac{GQ^2}{r^2c^4}\right)^{-1}dr^2 +r^2(d\theta^2+\sin^2\theta d\phi^2), \tag{12}$$

where M corresponds to the total mass of the sphere. The hydrostatic equilibrium describes the state of fluid in which pressure gradient force is balanced by the gravitational force. When one of these forces overcome the other, the stability of the system

is disturbed leading to an unstable system. The equation describing hydrostatic equilibrium is obtained by eliminating ν_0 from Eqs.(9) and (10) as

$$\left(1-\frac{2GM_r}{rc^2}+\frac{GQ^2}{r^2c^4}\right)\frac{dp_0}{dr}=-\frac{1}{c^2}\left(\frac{GM_r}{r^2}-\frac{GQ^2}{r^3c^2}+\frac{4\pi G}{c^2}pr\right)$$
$$\times(p_0+\sigma_0)+\frac{1}{4\pi}\left(1-\frac{2GM_r}{rc^2}+\frac{GQ^2}{r^2c^4}\right)\left(\frac{Q^2}{r^5}+\frac{1}{2}\frac{d}{dr}\left(\frac{Q^2}{r^5}\right)\right), \quad (13)$$

where the left and right hand sides correspond to pressure gradient and gravitational terms, respectively and

$$M_r=\frac{4\pi G}{c^4}\int_0^r\sigma_0r^2dr+\frac{G}{2c^4}\int_0^r\frac{Q^2}{r^2}dr, \quad (14)$$

is the Misner–Sharp mass function.

3 Equations governing radial oscillations

Here we discuss the motion of gaseous masses undergoing radial oscillations. The non-zero components of four-velocity are given by

$$u^0=e^{-\frac{\nu_0}{2}},\quad u_0=-e^{\frac{\nu_0}{2}},\quad u^1=ve^{-\frac{\nu_0}{2}},\quad u_1=ve^{\frac{\lambda_0-\nu_0}{2}}, \quad (15)$$

where $v=\frac{dr}{dt}$ is the radial velocity component. These components can be calculated with respect to spacetime coordinates by $u^i=\frac{dx^i}{ds}$. The stability of any gaseous mass under perturbation ultimately gives rise to the dynamical evolution of gravitating system. We assume that an equilibrium configuration is perturbed such that it does not affect the spherical symmetry. We consider only linear terms so that the respective values in the perturbed state become

$$\lambda=\lambda_0+\delta\lambda,\quad \nu=\nu_0+\delta\nu,\quad p=p_0+\delta p,\quad \sigma=\sigma_0+\delta\sigma,\quad Q=Q_0+\delta Q. \quad (16)$$

We follow the Eulerian approach [4] for perturbations such that the corresponding linearized forms (governing the radial perturbations) through Eqs. (8) and (9) are

$$\frac{\partial}{\partial r}(re^{-\lambda_0}\delta\lambda)=\frac{2G}{c^4}\left(4\pi r^2\delta\sigma-\frac{Q_0\delta Q}{r^2}\right), \quad (17)$$

$$\frac{e^{-\lambda_0}}{r}\left[\frac{\partial}{\partial r}\delta\nu-\delta\lambda\frac{d\nu_0}{dr}\right]=\frac{1}{r^2}e^{-\lambda_0}\delta\lambda+\frac{8\pi G}{c^4}\delta p-\frac{2GQ_0\delta Q}{c^4r^4}, \quad (18)$$

here $\delta\lambda$, $\delta\nu$, $\delta\sigma$, δp and δQ represent the Eulerian changes. Equations (4) and (7) can be written appropriately in linearized forms as

$$\frac{e^{-\lambda_0}}{r}\frac{\partial}{\partial t}\delta\lambda=-\frac{4\pi G}{c^4}\left(2(p_0+\sigma_0)v-\frac{Q_0\delta Q}{r^4}\right), \tag{19}$$

$$(p_0+\sigma_0)e^{\lambda_0-\nu_0}\frac{\partial v}{\partial t}+\frac{\partial}{\partial r}\delta p+\frac{1}{2}(p_0+\sigma_0)\frac{\partial}{\partial r}\delta\nu +\frac{1}{2}(\delta p+\delta\sigma)\frac{d\nu_0}{dr}+\frac{1}{8\pi}\frac{Q_0\delta Q}{r^4}-\frac{1}{4\pi}\frac{\partial}{\partial r}\left[\frac{Q_0\delta Q}{r^4}\right]=0. \tag{20}$$

Let us introduce a Lagrangian displacement "η" such that $v=\frac{\partial\eta}{\partial t}$. Integration of Eq. (19) leads to

$$\frac{e^{-\lambda_0}}{r}\delta\lambda=-\frac{8\pi G}{c^4}(p_0+\sigma_0)\eta+\frac{4\pi GQ_0}{c^4r^4}\int\delta Q dt. \tag{21}$$

Using Eq. (11), this equation takes the form

$$\delta\lambda=-\frac{d}{dr}(\lambda_0+\nu_0)\eta+\frac{4\pi GQ_0e^{\lambda_0}}{c^4r^3}\int\delta Q dt. \tag{22}$$

Solving Eq. (17) and (21), it follows that

$$\delta\sigma=\frac{1}{r^2}\frac{\partial}{\partial r}\left[-r^2(\sigma_0+p_0)\eta+\frac{Q^2}{2r^4}\int\delta Q dt\right]+\frac{Q_0}{4\pi r^4}\delta Q, \tag{23}$$

which yields

$$\delta\sigma=-\eta\frac{dp_0}{dr}-\eta\frac{d\sigma_0}{dr}-\frac{1}{r^2}(p_0+\sigma_0)\frac{\partial}{\partial r}(\eta r^2)+\frac{1}{r^2}\frac{\partial}{\partial r}\left[\frac{Q_0}{2r^4}\int\delta Q dt\right] +\frac{Q_0}{4\pi r^4}\delta Q. \tag{24}$$

Using Eq. (10), it follows that

$$\delta\sigma=-\eta\frac{d\sigma_0}{dr}-\frac{e^{\nu_0/2}}{r^2}(p_0+\sigma_0)\frac{\partial}{\partial r}\left[\eta r^2e^{-\nu_0/2}\right]-\frac{\eta}{8\pi}\frac{d}{dr}\left[\frac{Q^2}{r^4}\right] +\frac{1}{r^2}\frac{\partial}{\partial r}\left[\frac{Q_0}{2r^4}\int\delta Q dt\right]+\frac{Q_0}{4\pi r^4}\delta Q. \tag{25}$$

Substituting $\delta\lambda$ from Eq. (21) in (18), we obtain

$$\frac{e^{-\lambda_0}}{r}\frac{\partial}{\partial r}\delta\nu=\left[(p_0+\sigma_0)\left(\frac{1}{r}+\frac{d\nu_0}{dr}\right)\eta+\delta p\right]\frac{8\pi G}{c^4} +\frac{4\pi GQ_0}{c^4r^4}\left[\frac{d\nu_0}{dr}-\frac{\eta}{r}\right]\int\delta Q dt-\frac{2GQ_0}{c^4r^4}\delta Q, \tag{26}$$

which in accordance of Eq. (11) leads to

$$(p_0+\sigma_0)\frac{\partial}{\partial r}\delta\nu = \frac{d}{dr}(\lambda_0+\nu_0)\left\{\left[\delta p-(p_0+\sigma_0)\left(\frac{1}{r}+\frac{d\nu_0}{dr}\right)\eta\right]\right.$$
$$\left.+\frac{Q_0}{2r^4}\left[\frac{d\nu_0}{dr}-\frac{\eta}{r}\right]\int\delta Q dt-\frac{Q_0}{4\pi r^4}\delta Q\right\}. \tag{27}$$

Now we assume time dependent perturbations in the form of Lagrangian displacement, i.e., $\eta e^{i\omega t}$, where ω is the characteristic frequency to be evaluated. The Lagrangian displacement η connects the fluids elements in equilibrium with corresponding one in the perturbed configuration. Since the equations have natural modes of oscillations, so they will depend on time. Considering $\delta\lambda$, $\delta\nu$, δp, $\delta\sigma$ and δQ as time dependent amplitudes of the respective quantities, Eq. (20) with (27) can be rewritten as

$$\omega^2 e^{\lambda_0-\nu_0}(p_0+\sigma_0)\eta = \delta p\frac{d}{dr}\left(\nu_0+\frac{1}{2}\lambda_0\right)+\frac{d}{dr}\delta p+\frac{1}{2}\delta\sigma\frac{d\nu_0}{dr}-\frac{1}{2}(p_0+\sigma_0)$$
$$\times\left(\frac{d\nu_0}{dr}+\frac{d\lambda_0}{dr}\right)\left(\frac{1}{r}+\frac{d\nu_0}{dr}\right)\eta+\frac{Q_0}{8\pi r^4}\frac{d}{dr}(\lambda_0+\nu_0)$$
$$\times\left\{2\pi\left(\frac{d\nu_0}{dr}-\frac{\eta}{r}\right)\int\delta Q dt-\delta Q\right\}+\frac{1}{4\pi}\left\{\frac{Q_0\delta Q}{2r^4}\right.$$
$$\left.-\frac{d}{dr}\left(\frac{Q_0\delta Q}{r^4}\right)\right\}. \tag{28}$$

4 The conservation of Baryon number

In order to discuss the perturbed state of pressure in terms of Lagrangian displacement η, an additional assumption is required which can relate physical aspects of relativistic theory with the gaseous mass undergoing adiabatic radial oscillations. In this context, the required supplementary condition can be satisfied by conservation of baryon number in the framework of GR as $(Nu^j)_{;j}=0$, or

$$\frac{\partial}{\partial x^j}(Nu^j)+Nu^j\frac{\partial}{\partial x^j}\ln\sqrt{-g}=0, \tag{29}$$

where N is the baryon number per unit volume. The conservation of baryon number plays a vital role in collecting different models of the universe. According to this law, the number of particles may vary but their total number will remain conserved during the fluid flow. This change occurs due to loss or gain of net fluxes. Here we consider fluid obeying this identity. Equation (29) through (15) leads to

$$\frac{\partial}{\partial t}(Ne^{-\nu_0/2})+\frac{\partial}{\partial r}(Nve^{-\nu_0/2})+Nve^{-\nu_0/2}\frac{\partial}{\partial r}\left(\frac{2}{r}+\frac{1}{2}[\nu+\lambda]\right)$$
$$+\frac{N}{2}e^{-\nu_0/2}\frac{\partial}{\partial t}(\nu+\lambda)=0. \tag{30}$$

We assume the perturbation

$$N = N_0(r) + \delta N(r, t), \tag{31}$$

keeping only the linear terms in v, Eq. (30) takes the form

$$\frac{1}{r^2}\frac{\partial}{\partial r}(N_0 r^2 v e^{-\nu_0/2}) + e^{-\nu_0/2}\frac{\partial}{\partial t}\delta N + \frac{1}{2}N_0 e^{-\nu_0/2}\frac{d}{dr}(\nu_0 + \lambda_0) + \frac{1}{2}N_0 e^{-\nu_0/2}\frac{\partial}{\partial t}\delta\lambda = 0, \tag{32}$$

whose integration in terms of Lagrangian displacement η leads to

$$\delta N + \frac{N_0}{2}\left[\eta\frac{d}{dr}(\nu_0 + \lambda_0) + \delta\lambda\right] + \frac{1}{r^2}e^{\nu_0/2}\frac{\partial}{\partial r}\left(N_0 r^2 \eta e^{-\nu_0/2}\right) = 0. \tag{33}$$

Using Eq. (22), it follows that

$$\delta N = -\eta\frac{dN_0}{dr} - \frac{N_0}{r^2}e^{\nu_0/2}\frac{\partial}{\partial r}\left(r^2\eta e^{-\nu_0/2}\right) + \frac{2\pi G N_0 Q_0}{c^4 r^3}e^{\lambda_0}\int \delta Q dt. \tag{34}$$

We consider an equation of state in the form

$$N = N(\sigma, p), \tag{35}$$

so that Eqs.(25) and (34) together give

$$\delta p = -\eta\frac{dp_0}{dr} - p_0\Gamma\frac{e^{\nu_0/2}}{r^2}\frac{\partial}{\partial r}\left(r^2\eta e^{-\nu_0/2}\right) + \frac{\alpha Q_0}{r^3}\int \delta Q dt, \tag{36}$$

where

$$\alpha = \frac{1}{\partial N/\partial p}\left\{\frac{2\pi G N_0}{c^4}e^{\lambda_0} - \frac{1}{2r}\frac{dN}{d\sigma}\right\}, \tag{37}$$

and Γ is the adiabatic index (ratio of specific heats) defined by

$$\Gamma = \frac{1}{p\partial N/\partial p}\left\{N - (\sigma + p)\frac{\partial N}{\partial \sigma}\right\}. \tag{38}$$

This relates the pressure and density fluctuations and measures the stiffness of the fluid.

5 Pulsation equation and variational principle

The linear pulsation corresponds to the oscillation frequencies and different modes of small perturbations applied to equilibrium spherical configuration. Inserting the values of $\delta\sigma$ and δp from Eqs. (23) and (36) in (28), it follows that

$$\omega^2 e^{\lambda_0-\nu_0}(p_0+\sigma_0)\eta = -\eta\left(\frac{d\nu_0}{dr}+\frac{1}{2}\frac{d\lambda_0}{dr}\right)\frac{dp_0}{dr} - \frac{d}{dr}\left(\eta\frac{dp_0}{dr}\right) - \frac{1}{2}\left\{\frac{2}{r}\right.$$
$$\times\left.(p_0+\sigma_0)\eta + \frac{d}{dr}[(p_0+\sigma_0)\eta]\right\} - \frac{1}{2}\eta(p_0+\sigma_0)\left(\frac{d\nu_0}{dr}+\frac{d\lambda_0}{dr}\right)\left(\frac{1}{r}+\frac{d\nu_0}{dr}\right)$$
$$-e^{-(\nu_0+\frac{\lambda_0}{2})}\frac{d}{dr}\left\{e^{(\nu_0+\frac{\lambda_0}{2})}\Gamma p_0\frac{e^{\nu_0/2}}{r^2}\frac{d}{dr}(r^2\eta e^{-\nu_0/2})\right\} + e^{-\lambda_0/2}\frac{d}{dr}\left\{\frac{\beta Q_0}{r^3}\right.$$
$$\times\left. e^{\lambda_0/2}\int\delta Q dt\right\} + \frac{Q_0}{r^3}\frac{d\nu_0}{dr}\int\delta Q dt\left\{\beta+\frac{1}{4r}+\frac{1}{4\pi r}\left(\frac{d\nu_0}{dr}-\frac{\eta}{r}\right)\right\}$$
$$+\frac{Q_0}{4\pi r^4}\frac{d\lambda_0}{dr}\left\{\frac{d\nu_0}{dr}-\frac{\eta}{r}\int\delta Q dt-\frac{\delta Q}{2}\right\}+\frac{Q_0}{8\pi r^4}\delta Q+\frac{e^{\nu_0/2}}{4\pi}\frac{d}{dr}\left\{\frac{Q_0 e^{\nu_0/2}\delta Q}{r^4}\right\}. \tag{39}$$

Substituting $\frac{dp_0}{dr}$ from Eq. (10) in the above equation, we have

$$\omega^2 e^{\lambda_0-\nu_0}(p_0+\sigma_0)\eta = \frac{1}{2}(p_0+\sigma_0)\eta\left\{\frac{d^2\nu_0}{dr^2}-\frac{3}{r}\frac{d\nu_0}{dr}-\frac{1}{r}\frac{d\lambda_0}{dr}-\frac{1}{2}\frac{d\lambda_0}{dr}\frac{d\nu_0}{dr}\right\}$$
$$-\frac{5}{2\pi}\frac{Q^2}{r^6}-\frac{1}{8\pi r^4}\frac{d^2}{dr^2}(Q^2)+e^{-\lambda_0}\frac{d}{dr}\left\{\frac{\beta Q_0}{r^3}e^{-\lambda_0/2}\widetilde{Q}\right\}+\frac{Q_0\widetilde{Q}}{r^3}\frac{d\nu_0}{dr}\left\{\beta+\frac{1}{4\pi}\right.$$
$$\left.+\frac{1}{4\pi r}\left(\frac{d\nu_0}{dr}-\frac{\eta}{r}\right)\right\}+\frac{Q_0}{4\pi r^4}\frac{d\lambda_0}{dr}\left\{\left(\frac{d\nu_0}{dr}-\frac{\eta}{r}\right)\widetilde{Q}-\frac{\delta Q}{2}\right\}+\frac{Q_0\delta Q}{8\pi r^4}$$
$$+\frac{e^{\nu_0/2}}{4\pi}\frac{d}{dr}\left\{\frac{Q_0 e^{-\nu_0/2}\delta Q}{r^4}\right\}, \tag{40}$$

where $\int\delta Q dt = \widetilde{Q}$. Under the equilibrium condition, Eq. (4) yields

$$\left\{\frac{16\pi G p_0}{c^4}+\frac{2GQ_0^2}{c^4 r^4}\right\}e^{\lambda_0} = \frac{d^2\nu_0}{dr^2}+\frac{1}{r}\frac{d}{dr}(\nu_0-\lambda_0)+\frac{1}{2}\left(\frac{d\nu_0}{dr}\right)^2-\frac{1}{2}\frac{d\lambda_0}{dr}\frac{d\nu_0}{dr}. \tag{41}$$

Using this expression and Eq. (10), Eq. (40) takes the form

$$\omega^2 e^{\lambda_0-\nu_0}(p_0+\sigma_0)\eta = \frac{4}{r}\frac{dp_0}{dr}\eta-\frac{1}{p_0+\sigma_0}\left(\frac{dp_0}{dr}\right)^2\eta+\frac{8\pi G p_0}{c^4}e^{\lambda_0}$$
$$\times(p_0+\sigma_0)\eta+\frac{d}{dr}\left[e^{\lambda 0+3\nu_0/2}\frac{p_0\Gamma}{r^2}\frac{d}{dr}\left(r^2\eta e^{-\nu_0/2}\right)\right]e^{-(\nu_0+\lambda_0/2)}$$
$$+\frac{1}{p_0+\sigma_0}\frac{dp_0}{dr}\eta\left(\frac{1}{4\pi r^4}\frac{d(Q^2)}{dr}-\frac{Q^2}{\pi r^5}\right)+\frac{dQ^2}{dr}\frac{\eta}{2\pi r^5}\left[\frac{1}{p_0+\sigma_0}\frac{Q^2}{4\pi r^4}-1\right]$$
$$-\frac{\eta}{p_0+\sigma_0}\frac{1}{(2\pi r^4)^2}\left[\frac{Q^4}{r^2}+\frac{1}{16}\left(\frac{dQ^2}{dr}\right)^2\right]-\frac{5Q^2}{2\pi r^6}-\frac{1}{8\pi r^4}\frac{d^2}{dr^2}(Q^2)$$

$$+\frac{GQ_0^2}{c^4r^4}(p_0+\sigma_0)\eta e^{\lambda_0}+e^{-\lambda_0}\frac{d}{dr}\left(\frac{\beta Q_0\widetilde{Q}}{r^3}e^{\lambda_0/2}\right)+\frac{Q_0\widetilde{Q}}{r^3}\frac{d\nu_0}{dr}\left[\beta+\frac{1}{4\pi}\right.$$
$$\left.+\frac{1}{4\pi r}\left(\frac{d\nu_0}{dr}-\frac{\eta}{r}\right)\right]+\frac{Q_0\delta Q}{8\pi r^4}\left(1-\frac{d\lambda_0}{dr}\right)+\frac{e^{\nu_0/2}}{4\pi}\frac{d}{dr}\left(\frac{Q_0\delta Q}{r^4}e^{-\nu_0/2}\right). \tag{42}$$

This is the required pulsation equation which satisfies the boundary conditions, i.e., $\eta=0$ at $r=0$ and $\delta p=0$ at $r=R$. This constitutes a characteristic value problem for ω^2 obtained by multiplying the equation with $\eta r^2 e^{(\lambda_0+\nu_0)/2}$ and integrating over values of r as

$$\omega^2\int_0^R e^{(3\lambda-\nu)/2}r^2\eta^2(p+\sigma)dr=\int_0^R e^{(\lambda+3\nu)/2}\frac{p\Gamma}{r^2}\left[\frac{d}{dr}\left(r^2\eta e^{-\nu/2}\right)\right]^2dr$$
$$+\frac{8\pi G}{c^4}\int_0^R e^{(3\lambda+\nu)/2}pr^2\eta^2(p+\sigma)dr-\int_0^R\frac{r^2\eta^2}{p+\sigma}e^{(\lambda+\nu)/2}\left(\frac{dp}{dr}\right)^2dr$$
$$+4\int_0^R r\eta^2e^{(\lambda+\nu)/2}\frac{dp}{dr}dr+\int_0^R\frac{\eta^2}{p+\sigma}e^{(\lambda+\nu)/2}\frac{dp}{dr}\left(\frac{1}{4\pi}\frac{dQ^2}{dr}-\frac{Q^2}{\pi r^3}\right)dr$$
$$+\int_0^R\frac{\eta^2}{2\pi r^3}e^{(\lambda+\nu)/2}\frac{dQ^2}{dr}\left(\frac{1}{p+\sigma}\frac{Q^2}{4\pi r^4}-1\right)dr-\frac{5}{2\pi}\int_0^R\frac{\eta Q^2}{r^4}e^{(\lambda+\nu)/2}dr$$
$$-\int_0^R\frac{\eta^2}{p+\sigma}\frac{e^{(\lambda+\nu)/2}}{\left(2\pi r^3\right)^2}\left[\left(\frac{Q^2}{r}\right)^2+\frac{1}{16}\left(\frac{dQ^2}{dr}\right)^2\right]dr+\int_0^R\frac{GQ_0^2\eta^2}{c^4r^4}$$
$$\times(p+\sigma)e^{(3\lambda+\nu)/2}dr-\int_0^R\frac{\eta e^{(\lambda+\nu)}}{8\pi r^2}\frac{d^2}{dr^2}\left(Q^2\right)dr+\int_0^R r^2\eta e^{(\nu-\lambda)/2}$$
$$\times\frac{d}{dr}\left(\frac{\beta Q_0\widetilde{Q}}{r^3}e^{\lambda_0/2}\right)dr+\int_0^R\frac{\eta Q_0\delta Q}{8\pi r^2}e^{(\nu+\lambda)/2}\left(1-\frac{d\lambda_0}{dr}\right)dr$$
$$+\int_0^R\frac{\eta Q_0\widetilde{Q}}{r}e^{(\nu+\lambda)/2}\frac{d\nu_0}{dr}\left[\beta+\frac{1}{4\pi}+\frac{1}{4\pi r}\left(\frac{d\nu_0}{dr}-\frac{\eta}{r}\right)\right]dr$$
$$+\int_0^R\frac{\eta r^2}{4\pi}e^{(\nu+\lambda)/2}\frac{d}{dr}\left(\frac{Q_0\delta Q}{r^4}e^{-\nu_0/2}\right)dr. \tag{43}$$

The corresponding orthogonality condition is defined as

$$\int_0^R e^{(3\lambda-\nu)/2}r^2(p+\sigma)\eta^{(i)}\eta^{(j)}=0,\quad(i\neq j), \tag{44}$$

where $\eta^{(i)}$ and $\eta^{(j)}$ give proper solutions associated with different characteristic values of ω^2. To investigate dynamical instability of spherical star, the right-hand side of Eq. (43) should vanish by choosing a trial function ξ satisfying the given boundary conditions. In the following, we discuss the conditions for dynamical instability by taking two special models.

5.1 The homogeneous model of sphere

First we consider the homogeneous sphere with constant energy density σ and study the conditions for its dynamical instability. Equations (13) and (14) governing the hydrostatic equilibrium allow the integration [3] such that we can write

$$x^2 = 1 - \frac{r^2}{a^2} + \frac{b^2}{r^2}, \quad x_1^2 = 1 - \frac{R^2}{a^2} + \frac{b^2}{R^2}, \tag{45}$$

where $a^2 = \frac{3c^4}{8\pi G\sigma}$ and $b^2 = \frac{2GQ^2}{c^4}$. The solutions of the relevant physical quantities can be determined in terms of x and x_1 as

$$p = \sigma\frac{x - x_1}{3x_1 - x}, \quad e^{\nu} = \frac{1}{4}[3x_1 - x]^2, \quad e^{\lambda} = \frac{1}{x^2}. \tag{46}$$

The necessary condition for the positivity of pressure yields $3x_1 > 1$ which leads to

$$\frac{R^2}{a^2} - \frac{b^2}{R^2} < \frac{8}{9}.$$

Using the inertial mass, this takes the form

$$R > \frac{9}{8}\left(\frac{2GM}{c^2} - \frac{GQ^2}{Rc^4}\right) = \frac{9}{8}R_N, \tag{47}$$

where R_N is RN radius. Inserting the physical quantities in Eq. (43), it follows that

$$\begin{aligned}
&4a^2\omega^2 x_1\int_0^{\xi_1}\frac{\xi^2\eta^2}{x^3(3x_1-x)^2}d\xi = x_1\int_0^{\xi_1}\frac{2x^2-9x_1^2-1}{x^3(3x_1-x)^2}\xi^2\eta^2 d\xi\\
&+\frac{\Gamma}{8}\int_0^{\xi_1}(x-x_1)(3x_1-x)^2\frac{1}{x\xi}\left[\frac{d}{d\xi}(\eta\xi^2 e^{-\nu/2})\right]^2 d\xi + \frac{1}{16\pi a^3 x_1}\\
&\times\int_0^{\xi_1}\frac{\eta^2}{x\xi^2}\frac{dp}{d\xi}\left(\frac{dQ^2}{d\xi} - \frac{4Q^2}{\xi}\right)d\xi - \frac{5}{4\pi a^3}\int_0^{\xi_1}\frac{Q^2\eta}{\xi^4}\frac{3x_1-x}{x}d\xi\\
&+\frac{1}{4\pi a^3}\int_0^{\xi_1}\frac{\eta^2(3x_1-x)}{x\xi^2}\left[\frac{Q^2(3x_1-x)}{8\pi a^4 x_1\xi^4} - 1\right]d\xi - \frac{1}{16\pi a x_1}\\
&\times\int_0^{\xi_1}\frac{\eta^2(3x_1-x)^2}{x(2\pi a^3\xi^3)^2}\left(\frac{dQ^2}{d\xi} - \frac{4Q^2}{\xi}\right)d\xi + \frac{Gx_1}{c^4}\int_0^{\xi_1}\frac{\eta^2 Q_0^2}{x^3\xi^2}d\xi\\
&-\frac{1}{32\pi a^3}\int_0^{\xi_1}\frac{\eta(3x_1-x)^2}{x^2\xi^2}\frac{d^2}{d\eta^2}(Q^2)d\xi + \frac{1}{2a}\int_0^{\xi_1}x(3x_1-x)\eta\xi^2\\
&\times\frac{d}{d\xi}\left[\frac{\beta Q_0\widetilde{Q}}{\xi^3}e^{-\lambda/2}\right]d\xi + \frac{1}{2a^2}\int_0^{\xi_1}\frac{\eta Q_0\widetilde{Q}}{\xi}\frac{3x_1-x}{x}\frac{d\nu_0}{d\xi}\left[\beta + \frac{1}{4\pi\xi}\right.
\end{aligned}$$

$$\times\left(\frac{d\nu_0}{d\xi}-\frac{\eta}{\xi}\right)\Bigg]d\xi+\frac{1}{16\pi a^2}\int_0^{\xi_1}\frac{\eta Q_0\delta Q}{\xi^2}\frac{3x_1-x}{x}\left(1-\frac{1}{a}\frac{d\lambda_0}{d\xi}\right)d\xi$$
$$+\frac{1}{4\pi a^2}\int_0^{\xi_1}\frac{\eta\xi^2(3x_1-x)}{x}\frac{d}{d\xi}\left(\frac{Q_0\delta Q}{\xi^4(3x_1-x)}\right)d\xi, \tag{48}$$

where $\xi=\frac{r}{a}$, $\xi_1=\frac{R}{a}-\frac{b}{R}$ and Γ is assumed to be constant.

We take the trial function as

$$\eta=\xi e^{\nu/2}=\frac{1}{2}\xi(x_1-x), \tag{49}$$

for which Eq. (48) becomes

$$(a\omega)^2x_1\int_0^{\xi_1}\frac{\xi^4}{x^3}d\xi=\frac{1}{4}x_1\int_0^{\xi_1}(2x^2-1-9x_1^2)\frac{\xi^4}{x^3}d\xi+\frac{9}{8}\int_0^{\xi_1}(x-x_1)$$
$$\times(3x_1-x)^2\frac{\xi^2}{x}d\xi+\frac{1}{4a^3xx_1}\int_0^{\xi_1}(3x_1-x)^4\left(-\frac{Q^2}{\pi\xi}\right)\frac{d}{d\xi}\left(\frac{x-x_1}{3x_1-x}\right)d\xi$$
$$-\frac{1}{(4\pi a^3)^2x_1}\int_0^{\xi_1}\frac{(3x_1-x)^2}{x}\left(\frac{Q^2}{\xi}\right)^2d\xi+\frac{Gx_1}{4c^4}\int_0^{\xi_1}Q_0^2\frac{(3x_1-x)^2}{\xi x^3}d\xi$$
$$-\frac{5}{8\pi a^3}\int_0^{\xi_1}\frac{Q^2(3x_1-x)^2}{x\xi^3}d\xi+\frac{1}{4a}\int_0^{\xi_1}x\xi^3(3x_1-x)\frac{d}{d\xi}\left(\frac{3Q_0\widetilde{Q}}{x\xi^3}\right)d\xi$$
$$+\frac{1}{32\pi a^2}\int_0^{\xi^1}\frac{Q_0\delta Q}{x\xi}(3x_1-x)^2d\xi+\frac{1}{8\pi a^2}\int_0^{\xi_1}\frac{\xi^3}{x}(3x_1-x)^2$$
$$\times\frac{d}{d\xi}\left(\frac{Q_0\delta Q}{(3x_1-x)\xi^4}\right)d\xi. \tag{50}$$

Substituting $x=\cos\theta$ and $\xi=\sin\theta$ in the above equation, we obtain

$$(a\omega)^2\cos\theta_1\int_0^{\theta_1}\frac{\sin^4\theta}{\cos^2\theta}d\theta=\frac{\cos\theta_1}{4}\int_0^{\theta_1}(2\cos^2\theta-1-9\cos^2\theta_1)\frac{\sin^4\theta}{\cos^2\theta}d\theta$$
$$+\frac{9}{8}\Gamma\int_0^{\theta_1}(\cos\theta-\cos\theta_1)(3\cos\theta_1-\cos\theta)^2\sin^2\theta d\theta-\frac{1}{4a^3\cos\theta_1}$$
$$\times\int_0^{\theta_1}\frac{(3\cos\theta_1-\cos\theta)^3}{\cos\theta}\frac{Q^2}{\pi\sin\theta}\frac{d}{d\theta}\left(\frac{\cos\theta-\cos\theta_1}{3\cos\theta_1-\cos\theta}\right)d\theta-\frac{1}{a(4\pi a^3)^2\cos\theta_1}$$
$$\times\int_0^{\theta_1}(3\cos\theta_1-\cos\theta)^2\left(\frac{Q^2}{\sin\theta}\right)^2d\theta+\frac{G\cos\theta_1}{4c^4}\int_0^{\theta_1}(3\cos\theta_1-\cos\theta)^2$$
$$\times\frac{Q_0^2}{\sin\theta\cos^2\theta}d\theta-\frac{5Q^2}{8\pi a^3}\int_0^{\theta_1}\frac{(3\cos\theta_1-\cos\theta)^2}{\sin^3\theta}d\theta, \tag{51}$$

where $\theta_1=\sin^{-1}\left(\frac{R}{a}-\frac{b}{R}\right)$. Solving the integrals and setting $\omega^2=0$, we obtain exact condition for marginal stability. The values of Γ_c for any assigned value of θ are found

Table 1 Adiabatic index and radii for dynamical stability of homogeneous sphere

θ_1	R/R_N	Γ_c for $Q = 0.2$	Γ_c for $Q = 0.6$
0^o	∞	-0.0182	-0.1622
10^o	33.163	0.1127	0.1776
20^o	8.549	0.1275	0.2278
25^o	5.598	0.1319	0.3192
30^o	4.000	0.3766	1.2643
35^o	3.0396	3246.43	1970.41
40^o	2.4203	5918.49	2527.00
50^o	1.704	6594.94	4352.86
60^o	1.333	6822.02	5631.08

such that γ should be less than certain Γ_c for the existence of dynamical instability. In Newtonian limit, Γ takes finite values for marginal stability, i.e., $\Gamma > \frac{4}{3} + \frac{8Q^2}{21}$. We calculate the radii of marginal stability and Γ for homogeneous model of gaseous sphere by taking different values of charge which show finite values of Γ. We observe that radius $\frac{R}{R_N} \to \infty$ for $\Gamma < 0$ which leads to the expansion while $\frac{R}{R_N}$ remains positive for $\Gamma > 0$ showing marginal stability of gaseous model. The corresponding results are given in Table 1.

When $\omega^2 < 0$, the perturbation diverges exponentially either by expansion or contraction which yields stellar dynamical instability. In the limit $\theta_1 \to 0$, the condition for dynamical instability is

$$\Gamma - \frac{4}{21}\left(4Q^2 + 7\right) < \frac{14}{43}\theta_1^2 = \frac{14}{43}\left[\frac{R^2}{a^2} - \frac{b^2}{R^2}\right]. \tag{52}$$

In terms of inertial mass, this takes the form

$$R < \frac{14}{43\left[\Gamma - \frac{4}{21}\left(4Q^2 + 7\right)\right]}\left[\frac{2GM}{c^2} - \frac{GQ^2}{Rc^4}\right], \tag{53}$$

which can be written as

$$\frac{R}{R_N} < \frac{K}{\left[\Gamma - \frac{4}{21}\left(4Q^2 + 7\right)\right]}, \tag{54}$$

where $K = \frac{14}{43}$ for the homogeneous sphere. This means that if Γ exceeds $\frac{4}{3} + \frac{8Q^2}{21}$ by a small amount, the dynamical instability can be prevented till the mass contracts to the RN radius. If the radius of gaseous mass is greater than R_N, it remains stable. The ranges for instability of homogeneous spherical system are shown in Fig. 1. Since the radius of stability is a factor of the RN radius, so the ratio $\frac{R}{R_N}$ should be greater than or equal to zero for physical results. We consider different values of charge and find that $0.1 < Q < 0.4$ and $\Gamma > 1.5$ provide valid radii ranges for the stability of sphere. For $\Gamma < 1.5$, we only have unstable radii along with un-physical region corresponding to $Q > 0.4$. Also, we observe that the gaseous sphere becomes unstable forever with

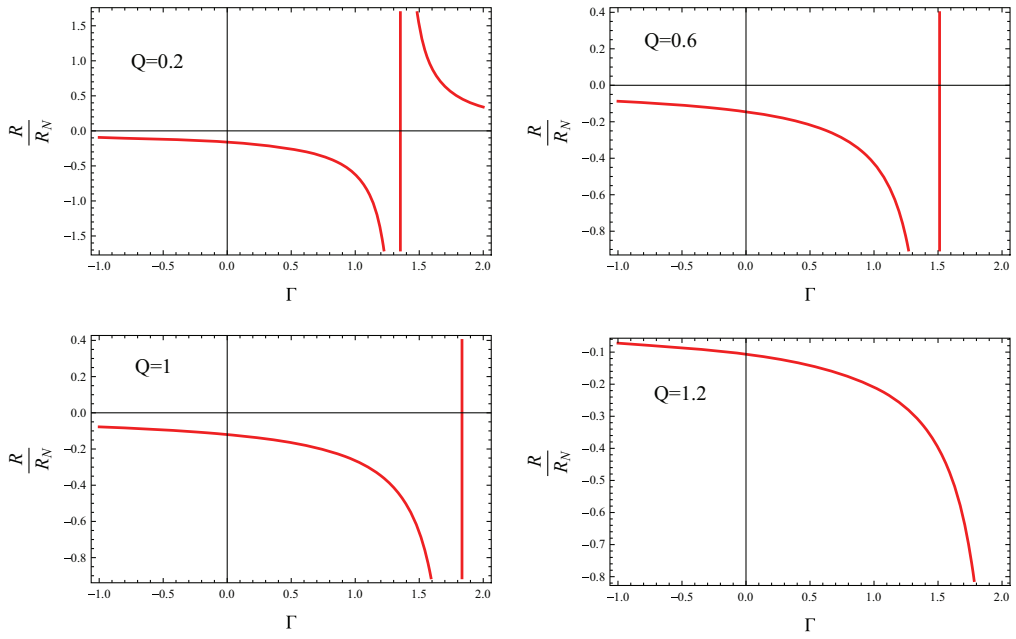

Fig. 1 Plots of $\frac{R}{R_N}$ for dynamical stability/instability of homogeneous sphere corresponding to different values of Q

larger values of charge, i.e., $Q > 1.2$. It is obvious from the graph that the radius of stability is greater than R_N for $\Gamma > \frac{4}{3} + \frac{8Q^2}{21}$.

5.2 Relativistic polytropic model

In relativistic polytropic models, pressure and energy density can be expressed in terms of a single function Θ as [17]

$$p = p_0\Theta^{n+1}, \quad \sigma = \sigma_0\Theta^n, \tag{55}$$

where p_0 and σ_0 represent respective values at center and n denotes the polytropic index. The polytropic models are the generalized form of the classical Lane-Emden equation which can be obtained from the equations of hydrostatic equilibrium. Let

$$\xi = \frac{r}{a}, \tag{56}$$

where $a = \left(\frac{q(n+1)c^4}{4\pi G\sigma_0}\right)^{\frac{1}{2}}$ and $q = \frac{p_0}{\sigma_0}$. We can reduce Eqs.(13) and (14) to the pair of equations which express Θ as a function of ξ

$$\left(\frac{\xi^2}{1+q\Theta} - \frac{c^2Q^2q(n+1)}{32\pi G\sigma_c}\right)\left(1 - \frac{2Vq(n+1)}{\xi} + \frac{Q^2Vq(n+1)}{\xi M}\right)\frac{d\Theta}{d\xi}$$
$$+V - \frac{Q^2V}{M} + q\Theta\frac{dV}{d\xi} = 0, \tag{57}$$

$$\frac{dV}{d\xi} = \xi\Theta^n. \tag{58}$$

We assume pN approximation of the form

$$\Theta = \theta + q\Phi, \tag{59}$$

where Φ is an arbitrary function, θ represents classical Lane–Emden function and q is treated as a small constant. Using Eqs.(57) and (58), the classical Lane-Emden equation becomes

$$\frac{d^2\theta}{d\xi^2} + \frac{2}{\xi}\frac{d\theta}{d\xi} + \left(1 - \frac{Q^2}{M}\right)\theta^n = \frac{c^2Q^2}{32\pi G\sigma_c}. \tag{60}$$

Equation (43) in terms of Θ and ξ takes the form

$$\begin{aligned}
&\frac{(a\omega)^2}{q}\int_0^{\xi_1}\Theta^n(1+q\Theta)\xi^2\eta^2e^{(3\lambda-\nu)/2}d\xi = 2(n+1)q\int_0^{\xi_1}\Theta^{(2n+1)}(1+q\Theta)\\
&\times\xi^2\eta^2e^{(3\lambda+\nu)/2}d\xi + 4(n+1)\int_0^{\xi_1}\Theta^n\xi\eta^2e^{(\lambda+\nu)/2}\left(1-\frac{q\xi(n+1)}{4(1+q\Theta)}\right)d\xi\\
&+\Gamma\int_0^{\xi_1}\frac{\Theta^{n+1}}{\xi^2}e^{(\lambda+3\nu)/2}\left(\frac{d}{d\xi}\left[\eta\xi^2e^{-\nu/2}\right]\right)^2d\xi + \left(\frac{1}{2\pi a^3}\right)^2\int_0^{\xi_1}\frac{e^{(\lambda+\nu)/2}}{\Theta^n(1+q\Theta)}\\
&\times\left(\frac{\eta Q}{\xi^4}\right)^2\left[\frac{\xi}{2a}-Q^2\right]d\xi - \frac{1}{2\pi a^3}\int_0^{\xi_1}\frac{\eta^2}{\xi^3}e^{(\lambda+\nu)/2}\left[1+\frac{q(n+1)Q^2}{1+q\Theta}\frac{d\Theta}{d\xi}\right.\\
&\left.-\frac{GQ_0^2}{\xi^4}\right]d\xi + \frac{1}{4\pi}\int_0^{\xi_1}\frac{\eta^2}{1+q\Theta}e^{(\lambda+\nu)/2}\frac{dQ^2}{d\xi}\left[q\frac{d\Theta}{d\xi} - \frac{1}{\Theta^n\left(a^3\xi^3\right)\frac{dQ^2}{d\xi}}\right]d\xi\\
&-\frac{1}{8\pi a^3}\int_0^{\xi_1}\frac{\eta}{\xi^2}e^{(\lambda+\nu)}\frac{d^2}{dr^2}\left(Q^2\right)d\xi + \int_0^{\xi_1}\xi^2\eta e^{(\nu-\lambda)/2}\frac{d}{d\xi}\left[\frac{\beta Q_0\widetilde{Q}e^{\lambda_0}}{a\xi^3}\right]d\xi\\
&+\frac{1}{4\pi a^2}\int_0^{\xi_1}\xi^2\eta e^{(\nu+\lambda)/2}\frac{d}{d\xi}\left(\frac{Q_0\delta Qe^{-\nu/2}}{\xi^4}\right)d\xi.
\end{aligned} \tag{61}$$

The pN approximation treats the effects of GR as first order corrections. We can write

$$\Gamma_c - \frac{4}{21}(4Q^2+7) = Cq, \tag{62}$$

$$R_c = \frac{K}{\Gamma_c - \frac{4}{21}(4Q^2+7)}\left[\frac{2GM}{c^2} - \frac{GQ^2}{Rc^4}\right], \tag{63}$$

where C and K are constants depending on density distribution. The pN approximation yields

Table 2 Adiabatic index with different values of charge for dynamical instability of polytropes with index 3

q	Γ_c for $Q=0.2$	Γ_c for $Q=0.4$	Γ_c for $Q=0.6$
0.015	1.3500	1.3593	1.4715
0.040	1.3527	1.3983	1.4744
0.1	1.3586	1.4043	1.4805
0.2	1.3686	1.4143	1.4905
0.5	1.3953	1.4440	1.5204

$$e^{-\lambda}=1+2q(1+n)\xi\frac{d\theta}{d\xi}-\frac{GQ^2(1+n)q}{M}\frac{d\theta}{d\xi}, \tag{64}$$

$$e^{\nu}=1-2q(1+n)[\theta+\xi_1|\tilde{\theta}_1|]+\frac{Q^2(1+n)q|\tilde{\theta}_1|}{M}, \tag{65}$$

where $|\tilde{\theta}_1|=-(d\theta/d\xi)_{\xi=\xi_1}$. Using the relations of p_c and σ_c for polytropes in terms of M, Q and R, it follows that

$$q=\frac{1}{2(n+1)\xi_1|\tilde{\theta}_1|}\left[\frac{2GM}{Rc^2}-\frac{GQ^2}{R^2c^4}\right]. \tag{66}$$

We calculate Γ with different values of Q for the emergence of dynamical instability. The numerical values of Γ for the polytropes of index 3 are given in Table 2. Similarly, the constants C and K for polytropes are given by the relation

$$K=\frac{C}{2(n+1)\xi_1|\tilde{\theta}_1|}. \tag{67}$$

In order to determine the radii from Eq. (63), we need to calculate K whose value depends upon the polytropic index, Lane-Emden function and charge. Different polytropic indices lead to different stellar structures such that the configurations with $n<5$ are considered to be realistic stars [22]. For $n=0$, we solve the Lane-Emden equation analytically corresponding to different values of Q and find the values of θ but we solve this equation numerically for $n=2,3,4$ as shown in Figs. 2 and 3. The values of constants C and K for $n=0$ are given in Table 3. We see that the values of K decrease gradually by increasing the value of charge.

Inserting the values of e^{ν} and $e^{-\lambda}$ in Eq. (61) and neglecting second as well as higher order terms in q, we obtain

$$\frac{(a\omega)^2}{q}\left\{\int_0^{\xi_1}\theta^n\xi^2\eta^2d\xi+\int_0^{\xi_1}H(\xi)\theta^{n-1}\xi^2\eta^2d\xi\right\}=\Gamma q(n+1)\int_0^{\xi_1}\frac{\theta^{n+1}}{\xi^2}$$
$$\times\left\{\left(\frac{GQ^2}{2M}-\xi\right)+3|\tilde{\theta}_1|\left(\frac{Q^2}{2M}-\xi_1\right)-3\theta\right\}\left[\frac{d}{d\xi}(\xi^2\eta)\right]^2d\xi+\Gamma\int_0^{\xi_1}H(\xi)$$

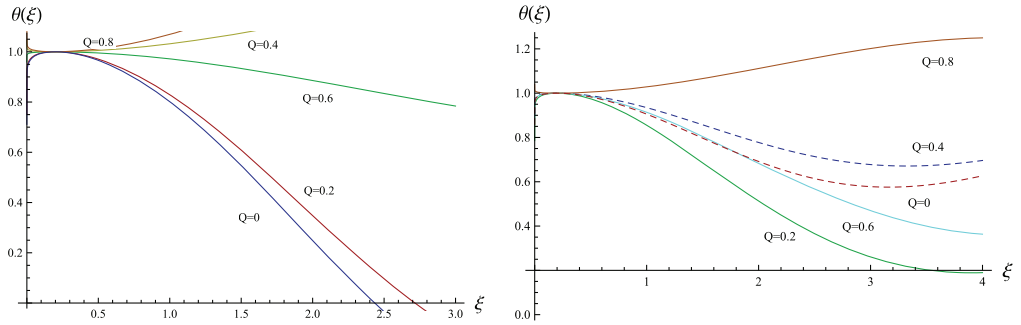

Fig. 2 Plots of classical Lane–Emden function for polytropes of index $n = 1, 2$ corresponding to different values of charge

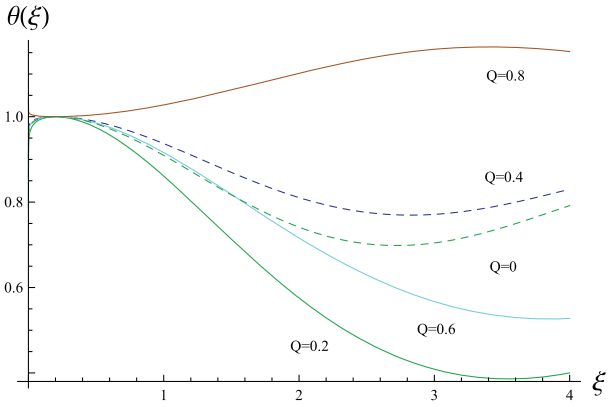

Fig. 3 Plots of classical Lane–Emden function for $n = 3$ corresponding to different values of charge

Table 3 Values of constants C and K with different values of charge for polytropes of index 0

C	K for $Q = 0.2$	K for $Q = 0.4$	K for $Q = 0.6$
0.243	0.6458	0.6372	0.576
0.826	2.1953	2.1662	1.9608
1.205	3.2034	3.161	2.8612
1.8095	4.809	4.745	4.296

$$\times\frac{\theta^{n+1}}{\xi^2}\left\{\frac{d}{d\xi}\left(\xi^2\eta\right)\right\}^2 d\xi + q(n+1)\int_0^{\xi_1} I(\xi)\theta^{n-1}\xi\eta^2 d\xi + q(n+1)\int_0^{\xi_1}\frac{d\theta}{d\xi}$$
$$\times\left[\left(\frac{GQ^2}{2M}-\xi\right)+|\tilde{\theta}_1|\left(\frac{Q^2}{2M}-\xi_1\right)-\theta\right]Y(\xi)d\xi + q(n+1)\int_0^{\xi_1}\theta^{n+1}\xi^2\eta^2$$
$$\times Z(\xi)d\xi + \frac{1}{(2\pi)^2}\int_0^{\xi_1}\frac{\eta^2Q^2}{(a^3\xi^2)^3}\left[\frac{\xi}{2a}-Q^2\right]d\xi - \frac{1}{8\pi}\int_0^{\xi_1}\frac{\eta}{a^3\xi^2}\frac{d^2}{d\xi^2}(Q^2)d\xi$$
$$-\frac{1}{2\pi}\int_0^{\xi_1}\frac{GQ^2}{a^3\xi^4}d\xi + \int_0^{\xi_1}\xi^2\eta\frac{d}{d\xi}\left(\frac{\beta Q_0\widetilde{Q}}{a\xi^3}\right)d\xi, \tag{68}$$

where

$$H(\xi)=2\theta^2(n+2)+3(n+1)\left(\frac{GQ^2}{2M}-\xi\right)\frac{d\theta}{d\xi}+\left(2\xi_1-\frac{Q^2}{2M}\right)\times(n+1)|\tilde{\theta}_1|, \tag{69}$$

$$I(\xi)=-4\theta(n+1)\frac{d\theta}{d\xi}\left[-\xi\frac{d\theta}{d\xi}-\theta-\xi|\tilde{\theta}_1|+\frac{Q^2}{2M}\left(G\frac{d\theta}{d\xi}+|\tilde{\theta}_1|\right)\right], \tag{70}$$

$$Y(\xi)=\frac{\eta^2Q^2}{2\pi^2(a^3\xi^2)^2}\left(\frac{\xi}{2a}-Q^2\right)-\frac{\eta^2}{2\pi a^3\xi^3}+\frac{GQ_0^2}{2\pi a^3\xi^4}-\frac{\eta}{4\pi a^3\xi^2}\times\frac{d^2}{d\xi^2}(Q^2)+\xi^2\eta\frac{d}{d\xi}\left\{\frac{\beta Q_0\widetilde{Q}}{a\xi^3}+\eta\xi^2\frac{d}{d\xi}\left(\frac{Q_0\delta Q}{\xi^4}\right)\right\}, \tag{71}$$

$$Z(\xi)=3\theta\left(\frac{Q^2}{2M}-\xi\right)\frac{d\theta}{d\xi}+\theta|\tilde{\theta}_1|\left(\frac{Q^2}{2M}-2\xi_1\right)-2\theta^2. \tag{72}$$

In pN approximation, we are interested to find the condition for marginal stability of polytropic configuration by taking $\eta=\xi$ and $\omega^2=0$ so that Eq. (68) takes the form

$$9\left(\Gamma-\frac{4}{3}-\frac{8Q^2}{21}\right)\int_0^{\xi_1}\theta^{n+1}\xi^2d\xi+q(n+1)\left[3\int_0^{\xi_1}\theta^nY(\xi)\widetilde{Y}(\xi)d\xi+\int_0^{\xi_1}\theta^{n-1}I(\xi)\xi^3d\xi+\int_0^{\xi_1}\theta^{n+1}\xi^4Z(\xi)d\xi\right]+\frac{1}{8\pi}\int_0^{\xi_1}\frac{\widetilde{Z}(\xi)}{a^3\xi^3}d\xi+\int_0^{\xi_1}\xi^3\frac{d}{d\xi}\left(\frac{\beta Q\widetilde{Q}}{a\xi^3}\right)d\xi=0, \tag{73}$$

with

$$\widetilde{Y}(\xi)=\left(3\Gamma\xi^2\theta+\theta^{-n}\right)\left\{\frac{d\theta}{d\xi}\left(\frac{GQ^2}{2M}-\xi\right)+3|\tilde{\theta}_1|\left(\frac{Q^2}{2M}-\xi_1\right)-3\theta\right\}, \tag{74}$$

$$\widetilde{Z}(\xi)=4Q^2\left(G+\frac{\xi}{2M}-Q^2\right)-\xi^3\left(1+\frac{d^2}{d\xi^2}(Q^2)\right). \tag{75}$$

In pN limit, the dynamical stability will require that $\Gamma>\Gamma_c=\frac{4}{3}+\frac{8Q^2}{21}+\epsilon$, where ϵ is a small quantity depending on q. To check the conditions for marginal stability as well as dynamical instability, we calculate values of K and plot different radii corresponding to polytropic indices $n=1,2,3$ as shown in Fig. 4, 5 and 6. It is found that K attains negative values for $n=1,2,3$, so we take both positive and negative values of Γ to obtain physically viable values of radii. Figures 4 and 5 show viable radii for $\Gamma>\frac{4}{3}+\frac{8Q^2}{21}$ corresponding to $n=1,2$. For $n=1$, we find that radii of stability along with non-physical region appear for $Q=0.6$ and positive values of Γ while negative values of Γ show the emergence of instability. The region of instability gets larger by increasing Q for both positive and negative values

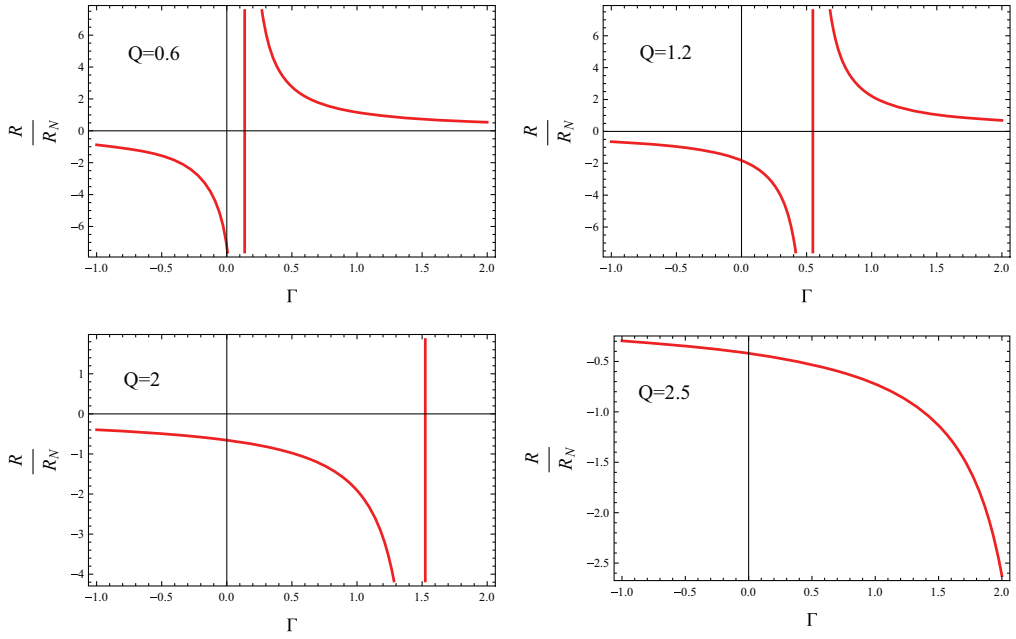

Fig. 4 Plots for radii of stability/instability corresponding to $n = 1$ and different values of charge

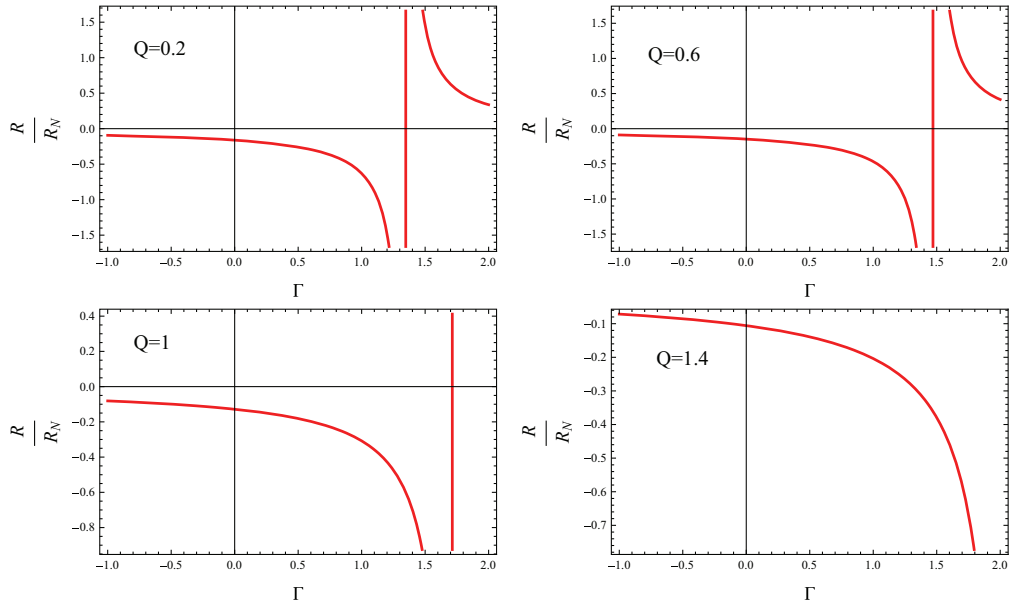

Fig. 5 Plots for radii of stability/instability corresponding to $n = 2$ and different values of charge

of Γ and the radii of marginal stability vanishes for $Q = 2$. We observe that the the corresponding polytropic model becomes unstable for $Q > 2.4$ (Fig. 4).

For $n = 2$, we analyze stable radii for $1.5 < \Gamma < 2$ and unstable radii for small values of Γ (both positive and negative) corresponding to $Q < 1$. The stability radius tends to decrease which leads to unstable region for $Q = 1$. We find that the non-physical region disappears and the polytropic model will remain unstable forever with $Q \geq 1.4$ (Fig. 5). For $n = 3$, we have viable ranges for radii with $0 < \Gamma < 2$, i.e., Γ

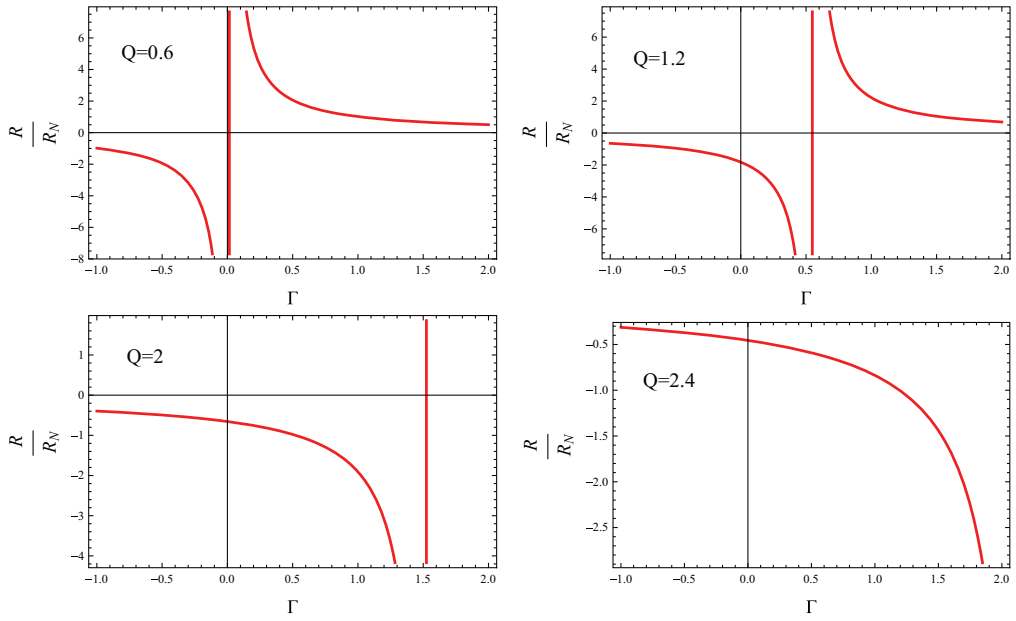

Fig. 6 Plots for radii of stability/instability corresponding to $n = 3$ and different values of charge

can be less than $\frac{4}{3} + \frac{8Q^2}{21}$ for stable stellar structures (Fig. 6). We find both stable and unstable radii for polytropic model with $0.1 < Q < 2$ which changes to unstable radii for $Q \geq 2$. The dynamical instability occurs when gaseous mass contracts to R_N.

6 Conclusions

This paper is devoted to investigate the role of electric charge on dynamical stability of spherical gaseous masses under radial oscillations. We have perturbed the system using Eulerian and Lagrangian radial perturbations to obtain linearized dynamical equations as well as perturbed pressure. This perturbed pressure in terms of adiabatic index is found using conservation of baryon number. The variational principle has been applied to the perturbed dynamical equations to formulate conditions of dynamical instability. We have also discussed conditions for dynamical instability of homogeneous sphere and relativistic polytropes in Newtonian as well as pN regimes.

We have found the values of adiabatic index Γ as well as radii for marginal stability of homogeneous sphere (Table 1). It turns out that Γ takes finite positive values less or greater than $\frac{4}{3} + \frac{8Q^2}{21}$ corresponding to different values of charge at Newtonian limit. The radius $\frac{R}{R_N}$ approaches to infinity for $\Gamma < 0$ which leads to expansion rather than collapse. In pN limit, the dynamical instability occurs if Γ exceeds $\frac{4}{3} + \frac{8Q^2}{21}$ by a small quantity and the gaseous mass is contracted to RN radius. We have found that $0.1 < Q < 0.4$ and $\Gamma > 1.5$ provide valid radii ranges for stability of sphere. It turns out that only unstable radii exist corresponding to $Q > 1.2$.

We have also discussed the stability/instability conditions for relativistic polytropic models of indices $0, 1, 2$ and 3. For $n = 3$, we have evaluated different values of Γ

for dynamical instability of polytropes and found that $\Gamma > \frac{4}{3} + \frac{8Q^2}{21}$ (Table 2). In order to discuss realistic models, we have evaluated radius of instability for different polytropic structures. We have also calculated the values of C and K for $n = 0$ (Table 3), which show that K decreases gradually by increasing the values of charge. For $n = 1, 2$, we have viable radii corresponding to $\Gamma > \frac{4}{3} + \frac{8Q^2}{21}$. For $n = 1$, we have found that radii of stability along with non-physical region exist for $Q = 0.6$ and $\Gamma > 0$ while negative values of Γ show the emergence of instability. The region of instability increases by increasing Q for both positive and negative values of Γ and we find only unstable radii for $Q > 2.4$. For $n = 2$, we have found both stable and unstable radii for $1.5 < \Gamma < 2$. The stability radius tends to decrease gradually which leads to unstable region for $Q = 1.4$. It is seen that Γ can be less than $\frac{4}{3} + \frac{8Q^2}{21}$ for $n = 3$. We have analyzed both stable and unstable radii for polytropic model with $0.1 < Q < 2$ which changes to unstable radii for $Q \geq 2$.

It is found that the dynamical instability occurs when the mass of polytropic configuration approaches to the RN radius limit. We observe that inclusion of charge in the gaseous sphere has significant effects as compared to the analysis [3]. For charged homogeneous sphere, the system becomes stable for both negative as well a as positive values of adiabatic index, while it remains stable for $\Gamma > \frac{4}{3}$ without charge system [3]. For the charged polytropes with $n = 1, 2, 3$, Γ can take both positive as well as negative values while K becomes negative. We also see that the radius of instability of polytropes ($n = 3$) for RN case is greater than that of the Schwarzschild limit showing that RN polytropes for $n = 3$ are more stable. Finally, we conclude that the presence of charge has substantial role in the emergence of instability of gaseous sphere.

References

1. Ayal, S., et al.: Astrophys. J. **550**, 846 (2001)
2. Marek, A., et al.: Astron. Astrophys. **445**, 273 (2006)
3. Chandrasekhar, S.: Astrophys. J. **140**, 417 (1964)
4. Chandrasekhar, S.: Astrophys. J. **142**, 1519 (1965)
5. Herrera, L., Le Denmat, G., Santos, N.O.: Mon. Not. R. Astron. Soc. **237**, 257 (1989)
6. Chan, R., Herrera, L., Santos, N.O.: Mon. Not. R. Astron. Soc. **267**, 637 (1994)
7. Nunez, L.A., Hernandez, H., Abreu, H.: Class. Quantum Gravit. **24**, 4631 (2007)
8. Sharif, M., Azam, M.: Gen. Relativ. Gravit. **44**, 1181 (2012)
9. Rosseland, S.: Mon. Not. R. Astron. Soc. **84**, 720 (1924)
10. Eddington, A.: Internal Constitution of the Stars. Cambridge University Press, Cambridge (1926)
11. Stettner, R.: Ann. Phys. **80**, 212 (1973)
12. Glazer, I.: Ann. Phys. **101**, 594 (1976)
13. Ghezzi, C.R.: Phys. Rev. D **72**, 104017 (2005)
14. Sharif, M., Azam, M.: J. Cosmol. Astropart. Phys. **02**, 043 (2012)
15. Sharif, M., Bhatti, M.Z.: J. Cosmol. Astropart. Phys. **10**, 056 (2013)
16. Chandrasekhar, S.: An Introduction to the Study of Stellar Structure. University of Chicago, Chicago (1939)
17. Tooper, R.F.: Astrophys. J. **140**, 434 (1966)
18. Ray, S., et al.: Braz. J. Phys. **34**, 310 (2004)
19. Fronsdal, C.: Lett. Math. Phys. **82**, 255 (2007)
20. Herrera, L., Barreto, W.: Phys. Rev. D **88**, 084022 (2013)
21. Breysse, P.C., Kamionkowski, M., Benson, A.: Mon. Not. R. Astron. Soc. **437**, 2675 (2014)
22. Horedt, G.P.: Polytropes: Applications in Astrophysics and Related Fields. Kluwer, Berlin (2004)

Monthly Notices
of the
ROYAL ASTRONOMICAL SOCIETY

MNRAS **471,** 1215–1221 (2017)
Advance Access publication 2017 July 8

doi:10.1093/mnras/stx1695

Dynamical instability of a charged gaseous cylinder

M. Sharif★ and Saadia Mumtaz★

Department of Mathematics, University of the Punjab, Quaid-e-Azam Campus, Lahore 54590, Pakistan

Accepted 2017 July 3. Received 2017 June 15; in original form 2017 April 28

ABSTRACT

In this paper, we discuss dynamical instability of a charged dissipative cylinder under radial oscillations. For this purpose, we follow the Eulerian and Lagrangian approaches to evaluate linearized perturbed equation of motion. We formulate perturbed pressure in terms of adiabatic index by applying the conservation of baryon numbers. A variational principle is established to determine characteristic frequencies of oscillation which define stability criteria for a gaseous cylinder. We compute the ranges of radii as well as adiabatic index for both charged and uncharged cases in Newtonian and post-Newtonian limits. We conclude that dynamical instability occurs in the presence of charge if the gaseous cylinder contracts to the radius R_*.

Key words: instabilities – stars: oscillations.

1 INTRODUCTION

A comprehensive study of collapsing systems and structure formation of self-gravitating objects reveal interesting physical perspectives. Charged self-gravitating objects may undergo various evolutionary phases during gravitational collapse that results in charged black holes or naked singularities. The stability of these solutions under fluctuations has remarkable significance in general relativity (GR). Initially, any stable system remains in a state of hydrostatic equilibrium unless its own gravity overcomes the pressure that causes the matter to collapse. The collapsing system contracts to a point under the influence of its own gravity leading to compact objects.

The dynamical instability of massive stars can be studied in Newtonian as well as post-Newtonian (pN) regimes (Ayal et al. 2001; Marek et al. 2006). This provides a platform to evaluate ranges of deviation and level of consistency between GR and Newton gravity. The analysis becomes ambiguous in strong-field regimes due to non-linear terms, hence the weak-field approximation schemes are used as an effective tool. Chandrasekhar (1964) was the pioneer who discussed the concept of dynamical instability of gaseous sphere by taking Newtonian perfect fluid in terms of adiabatic index. He followed Eulerian approach for linearized perturbed hydrodynamic equations and established a variational principle to find characteristic frequencies in Newtonian and pN limits. He also studied dynamical stability of sphere under radial and non-radial oscillations at the pN limit (Chandrasekhar 1965).

Herrera, Le Denmat & Santos (1989) investigated dynamical instability of the spherical system under perturbations by taking non-adiabatic fluid and found that the instability range increases in the Newtonian limit but decreases in the pN limit. Later, many researchers explored the influence of various physical parameters on the dynamical instability of self-gravitating systems under radial/non-radial perturbations (Chan, Herrera & Santos 1994; Nunez, Hernandez & Abreu 2007; Sharif & Azam 2012b). Also, there has been an extensive literature on the study of cylindrical gravitational collapse with and without the electromagnetic field (Sharif & Ahmad 2007; Di Prisco et al. 2009; Sharif & Abbas 2011). Sharif & Azam (2013) studied dynamical instability of an anisotropic collapsing cylinder in the context of an expansion-free model.

It is well known that various physical aspects of matter distribution play a substantial role in the dynamical evolution of self-gravitating systems. A star requires more electromagnetic charge for its stability in a strong gravitational field. The dynamical instability of collapsing systems in the presence of electromagnetic field has a primordial history starting with Rosseland (Rosseland 1924). Stettner (1973) discussed the role of surface charge in increasing the stability of a system with uniform density. Glazer (1976) studied dynamical stability of sphere under radial pulsations in the presence of electric charge. Ghezzi (2005) found that neutron stars having charge greater than the extreme value would explode. Sharif & Azam (2012a), Sharif & Bhatti (2013) and Sharif & Mumtaz (2016) studied the influence of electric charge on dynamical instability of collapsing systems at Newtonian and pN regimes.

In this paper, we study the impact of an electromagnetic field on dynamical instability of the cylindrically symmetric collapsing system by following Chandrasekhar approach (Chandrasekhar 1964). The format of the paper is as follows. In Section 2, we provide some basic equations and matter distribution for cylindrical geometry. Section 3 deals with equations of motion under radial oscillations following the Eulerian approach. We also formulate perturbed pressure and adiabatic index in terms of Lagrangian displacement by using conservation of baryon number. Section 4 is devoted to find

★ E-mail: msharif.math@pu.edu.pk (MS); sadiamumtaz17@gmail.com (SM)

conditions for dynamical instability of a homogeneous cylinder. Finally, we conclude our results in the last section.

2 FIELD EQUATIONS AND MATTER CONFIGURATION

We consider a cylindrically symmetric system in the interior region given by

$$\mathrm{d}s^2 = -A^2(t,r)\,\mathrm{d}t^2 + B^2(t,r)\,\mathrm{d}r^2 + C^2(t,r)\,\mathrm{d}\theta^2 + \mathrm{d}z^2, \tag{1}$$

where the following restrictions on coordinates are taken to preserve symmetry

$$-\infty < t < \infty, \quad 0 \le r < \infty, \quad 0 \le \theta \le 2\pi, \quad -\infty < z < \infty.$$

The corresponding *Einstein* field equations are given by

$$\frac{8\pi G}{c^4}T_0^0 = \frac{1}{B^2}\left\{\frac{C''}{C} - \frac{B'C'}{BC}\right\} - \frac{\dot{B}\dot{C}}{A^2BC}, \tag{2}$$

$$\frac{8\pi G}{c^4}T_1^1 = \frac{1}{A^2}\left\{\frac{\dot{A}\dot{C}}{AC} - \frac{\ddot{C}}{C}\right\} + \frac{A'C'}{AB^2C}, \tag{3}$$

$$\frac{8\pi G}{c^4}T_2^2 = \frac{1}{AB}\left\{\frac{A''}{B} - \frac{\ddot{B}}{A} + \frac{\dot{A}\dot{B}}{A^2} - \frac{A'B'}{B^2}\right\}, \tag{4}$$

$$\begin{aligned}\frac{8\pi G}{c^4}T_3^3 = {}& \frac{A''}{AB^2} - \frac{\ddot{B}}{A^2B} + \frac{\dot{A}\dot{B}}{A^3B} - \frac{A'B'}{AB^3} + \frac{\dot{A}\dot{C}}{A^3C} - \frac{\ddot{C}}{A^2C} \\ & - \frac{B'C'}{B^3C} + \frac{C''}{B^2C} + \frac{A'C'}{AB^2C} - \frac{\dot{B}\dot{C}}{A^2BC},\end{aligned} \tag{5}$$

$$\frac{8\pi G}{c^4}T_0^1 = \frac{1}{B^2}\left\{\frac{A'\dot{C}}{AC} + \frac{\dot{B}C'}{BC} - \frac{\dot{C}'}{C}\right\}, \tag{6}$$

where dot and prime denote derivatives with respect to t and r, respectively. The matter source is assumed to be locally charged dissipative perfect fluid defined by

$$\begin{aligned}T_\nu^\mu = {}& (\sigma + p)u^\mu u_\nu \\ & + p\delta_\nu^\mu + q^\mu u_\nu + q_\nu u^\mu \\ & + \frac{1}{4\pi}\left[F_{\nu\rho}F^{\mu\rho} - \frac{1}{4}\delta_\nu^\mu F_{\rho\lambda}F^{\rho\lambda}\right],\end{aligned} \tag{7}$$

where p is the isotropic pressure, σ is the energy density, $F_{\mu\rho}$ is the Maxwell field tensor, $u^\mu = \frac{\mathrm{d}x^\mu}{\mathrm{d}s}$ and q^μ represent four velocity and radial heat flux, respectively, satisfying $q_\mu u^\mu = 0$. Also, we have

$$u^\mu = A^{-1}\delta_0^\mu, \quad q^\mu = q\delta_1^\mu, \quad u^\mu u_\mu = -1.$$

We can define the electromagnetic field tensor in terms of four potential as $F_{\mu\nu} = \Phi_{\nu;\,\mu} - \Phi_{\mu;\,\nu}$, which satisfies the Maxwell field equations

$$F^{\mu\nu}_{\ ;\nu} = 4\pi J^\mu, \quad F_{[\mu\nu,\rho]} = 0,$$

where $J^\mu = \tilde{\rho}u^\mu$ is the four current. The conservation equation, $J^\mu_{\ ;\mu} = 0$, yields

$$Q(r) = 4\pi\int_0^r \zeta BC\,\mathrm{d}r,$$

which is the total amount of charge within the cylinder. We define the electric field intensity as

$$E(t,r) = \frac{Q(r)}{2\pi C}. \tag{8}$$

The conservation of energy-momentum tensor leads to the following relations:

$$\frac{\partial T_0^0}{\partial t} + \frac{\partial T_1^0}{\partial r} + \frac{\dot{B}}{B}\left(T_0^0 - T_1^1\right) + T_0^1\left(\frac{B'}{B} + \frac{A'}{A}\right) = 0, \tag{9}$$

$$\frac{\partial T_1^0}{\partial t} + \frac{\partial T_1^1}{\partial r} + \frac{A'}{A}\left(T_1^1 - T_0^0\right) + \left(\frac{\dot{A}}{A} + \frac{\dot{B}}{B}\right)T_1^0 = 0, \tag{10}$$

where $T_0^1 = -\frac{A^2}{B^2}T_1^0$. The components of energy-momentum tensor are

$$T_0^0 = -\sigma + \frac{\pi}{2}E^2, \quad T_1^1 = p + \frac{\pi}{2}E^2, \quad T_2^2 = T_3^3 = p - \frac{\pi}{2}E^2.$$

In hydrostatic equilibrium, all the quantities governing motion remain time-independent. In this context, equations (2), (3) and (10) become

$$\frac{\mathrm{d}}{\mathrm{d}r}\left(\frac{C_0'}{B_0}\right) = \frac{8\pi G}{c^4}B_0C_0\left(-\sigma_0 + \frac{\pi E^2}{2}\right), \tag{11}$$

$$\frac{\mathrm{d}A_0}{\mathrm{d}r}\frac{\mathrm{d}C_0}{\mathrm{d}r} = \frac{8\pi G}{c^4}A_0B_0^2C_0\left(p_0 + \frac{\pi E^2}{2}\right), \tag{12}$$

$$(\sigma_0 + p_0)\frac{\mathrm{d}A_0}{\mathrm{d}r} = -A_0\frac{\mathrm{d}}{\mathrm{d}r}\left(p_0 + \frac{\pi E^2}{2}\right), \tag{13}$$

where zero suffix describes equilibrium state of the surface stresses. We also have a useful relation through equations (2) and (3) given by

$$\begin{aligned}\frac{8\pi G}{c^4}(p_0 + \sigma_0) = {}& \frac{1}{A_0C_0}\left\{\frac{1}{B_0^2}\frac{\mathrm{d}A_0}{\mathrm{d}r}\frac{\mathrm{d}C_0}{\mathrm{d}r}\right\} \\ & - \frac{1}{B_0C_0}\left\{\frac{\mathrm{d}}{\mathrm{d}r}\left(\frac{C_0'}{B_0}\right)\right\}.\end{aligned} \tag{14}$$

We take the exterior region for cylindrically symmetric space–time in retarded time coordinate ν defined as

$$\begin{aligned}\mathrm{d}s^2 = {}& -\left(-\frac{2GM}{Rc^2} + \frac{GQ^2}{R^2c^4}\right)\mathrm{d}\nu^2 - 2\,\mathrm{d}\nu\,\mathrm{d}R \\ & + R^2(\mathrm{d}\theta^2 + \alpha^2\,\mathrm{d}z^2),\end{aligned} \tag{15}$$

where α is an arbitrary constant and M is the total mass. We choose the Schwarzschild coordinate as $C = r$ (Azam et al. 2016). Thorne (1935) defined C-energy for cylindrically symmetric space–time in the form of mass function given by

$$m(r) = \frac{1}{8}\left[1 - \frac{1}{B_0^2}\right] + 2\pi^2 rE^2. \tag{16}$$

Differentiating this equation and using equation (3), we have

$$\frac{\mathrm{d}m}{\mathrm{d}r} = \frac{2\pi rG}{c^4}\sigma_0 - \frac{r\pi^2GE^2}{c^4} + \frac{\mathrm{d}}{\mathrm{d}r}(2\pi^2rE^2), \tag{17}$$

whose integration leads to

$$m(r) = \frac{2\pi G}{c^4}\int_0^r r\sigma_0\,\mathrm{d}r - \frac{G}{4c^4}\int_0^r\frac{Q^2}{r}\mathrm{d}r + \frac{Q^2}{2r}. \tag{18}$$

The equation for hydrostatic equilibrium can be obtained as

$$\frac{\mathrm{d}p_0}{\mathrm{d}r} + \frac{G(8\pi r^2p_0 + Q^2)}{rc^4(1 - 8m + 4Q^2)} - \frac{rQQ' - Q^2}{4\pi r^3} = 0. \tag{19}$$

3 EQUATIONS GOVERNING RADIAL OSCILLATIONS

In this section, we study dynamical characteristics of gaseous mass undergoing radial oscillations. The non-vanishing components of four velocity can be written as

$$u^0 = \frac{1}{A_0}, \quad u_0 = -A_0, \quad u^1 = \frac{v}{A_0}, \quad u_1 = \frac{B_0^2}{A_0}v, \tag{20}$$

where $v = \frac{\mathrm{d}r}{\mathrm{d}t}$ corresponds to the radial velocity component. We can evaluate these components with respect to space–time coordinates by taking $u^i = \frac{\mathrm{d}x^i}{\mathrm{d}s}$. We perturb an equilibrium configuration in such a way that its cylindrical symmetry does not change. The perturbed state with linear terms yields

$$A = A_0 + \delta A, \quad B = B_0 + \delta B, \quad p = p_0 + \delta p, \quad \sigma = \sigma_0 + \delta\sigma,$$
$$Q = Q_0 + \delta Q, \quad q = q_0 + \delta q. \tag{21}$$

We apply the Eulerian approach (Chandrasekhar 1965) for perturbations through which the corresponding linearized forms (governing the radial perturbations) of equations (11) and (12) turn out to be

$$\frac{1}{r}\frac{\partial}{\partial r}\left(\frac{\delta B}{B_0^3}\right) = \frac{8\pi G}{c^4}\left(\delta\sigma - \frac{Q_0\delta Q}{4\pi r^2}\right), \tag{22}$$

$$\frac{8\pi G}{c^4}\left(\delta p + \frac{Q_0\delta Q}{4\pi r^2}\right) = \frac{1}{rA_0B_0^2}\frac{\partial}{\partial r}\left(\frac{\partial}{\partial r}\delta A - \frac{2\delta B}{B_0}\frac{\mathrm{d}A_0}{\mathrm{d}r}\right), \tag{23}$$

where δA, δB, $\delta\sigma$, δp and δQ define the Eulerian changes. The linearized form of equations (6) and (10) can be appropriately written as

$$\frac{1}{rB_0^3}\frac{\partial}{\partial t}\delta B = -\frac{8\pi G}{c^4}\left[(p_0+\sigma_0)v + \delta q\right], \tag{24}$$

$$(p_0+\sigma_0)\left(\frac{B_0}{A_0}\right)^2\frac{\partial v}{\partial t} + \frac{\partial}{\partial r}\delta p + \frac{1}{A_0}(p_0+\sigma_0)\frac{\partial}{\partial r}\delta A + \frac{1}{A_0}(\delta p + \delta\sigma)\frac{\mathrm{d}A_0}{\mathrm{d}r} + \frac{1}{4\pi r^2}\frac{\partial}{\partial r}(Q_0\delta Q) - \frac{1}{2\pi r^3}Q_0\delta Q + [(p_0+\sigma_0)v - q_0]\left(\frac{B_0}{A_0}\right)^2\left[\frac{1}{A_0}\frac{\partial}{\partial t}\delta A + \frac{1}{B_0}\frac{\partial}{\partial t}\delta B\right] = 0. \tag{25}$$

Let us introduce a Lagrangian displacement 'η' such that $v = \frac{\partial\eta}{\partial t}$. Integration of equation (24) gives

$$\frac{1}{B_0^3 r}\delta B = -\frac{8\pi G}{c^4}(p_0+\sigma_0)\eta + \int \delta q\,\mathrm{d}t, \tag{26}$$

which leads to

$$-\frac{1}{B_0}\delta B = \frac{1}{A_0}\frac{\mathrm{d}A_0}{\mathrm{d}r} + \frac{1}{B_0}\frac{\mathrm{d}B_0}{\mathrm{d}r}. \tag{27}$$

Solving equations (22) and (26), we have

$$\delta\sigma = -\eta\frac{\mathrm{d}\sigma_0}{\mathrm{d}r} - \eta\frac{\mathrm{d}p_0}{\mathrm{d}r} - \frac{1}{r}(p_0+\sigma_0)\frac{\partial}{\partial r}(r\eta) + \frac{Q_0}{4\pi r^2}\delta Q, \tag{28}$$

which, in accordance with equation (13), yields

$$\delta\sigma = -\eta\frac{\mathrm{d}\sigma_0}{\mathrm{d}r} - \frac{A_0}{r}(p_0+\sigma_0)\frac{\partial}{\partial r}\left[\frac{r\eta}{A_0}\right] - \frac{\eta}{8\pi}\frac{\mathrm{d}}{\mathrm{d}r}\left[\frac{Q^2}{r^4}\right] + \frac{Q_0}{4\pi r^2}\delta Q. \tag{29}$$

Substituting δB from equation (26) into equation (23), we have

$$\frac{1}{rA_0B_0^2}\frac{\partial}{\partial r}\delta A = \frac{8\pi G}{c^4}\left[\delta p - \frac{2(p_0+\sigma_0)\eta}{A_0}\frac{\mathrm{d}A_0}{\mathrm{d}r}\right] + \frac{2GQ_0}{r^2c^4}\delta Q - \frac{16\pi G}{c^4A_0}\frac{\mathrm{d}A_0}{\mathrm{d}r}\int \delta q\,\mathrm{d}t, \tag{30}$$

which, through equation (14), becomes

$$(p_0+\sigma_0)\frac{\partial}{\partial r}\delta A = \frac{\mathrm{d}A_0}{\mathrm{d}r} + \frac{A_0}{B_0}\frac{\mathrm{d}B_0}{\mathrm{d}r}\left[\delta p - \frac{2}{A_0}\frac{\mathrm{d}A_0}{\mathrm{d}r}\left\{(p_0+\sigma_0)\eta + \int \delta q\,\mathrm{d}t\right\} + \frac{Q_0}{4\pi r^2}\delta Q\right]. \tag{31}$$

Now we consider time-dependent perturbations $\eta\mathrm{e}^{\mathrm{i}\omega t}$, where ω and η represent characteristic frequency and Lagrangian displacement, respectively, which associate fluid elements in equilibrium with the perturbed configuration. These equations are time-dependent due to their natural modes of oscillations. We can rewrite equation (25) by taking $\delta A, \delta B, \delta p, \delta\sigma, \delta q$ and δQ as time-dependent amplitudes of the respective quantities as

$$\omega^2\eta(p_0+\sigma_0)\left(\frac{B_0}{A_0}\right)^2 = \frac{\mathrm{d}}{\mathrm{d}r}\delta p + \delta p\left[\frac{2}{A_0}\frac{\mathrm{d}A_0}{\mathrm{d}r} + \frac{1}{B_0}\frac{\mathrm{d}B_0}{\mathrm{d}r}\right] + \frac{1}{A_0}\delta\sigma\frac{\mathrm{d}A_0}{\mathrm{d}r} - \frac{2}{A_0}\left[(p_0+\sigma_0)\eta + \int q\,\mathrm{d}t\right]\left[\frac{1}{A_0}\frac{\mathrm{d}A_0}{\mathrm{d}r} + \frac{1}{B_0}\frac{\mathrm{d}B_0}{\mathrm{d}r}\right] + \frac{Q_0\delta Q}{4\pi r^2}\left[\frac{1}{A_0}\frac{\mathrm{d}A_0}{\mathrm{d}r} + \frac{1}{B_0}\frac{\mathrm{d}B_0}{\mathrm{d}r} - \frac{2}{r}\right] + [(\sigma_0+p_0)v - q_0] \times\left(\frac{B_0}{A_0}\right)^2\left[\frac{1}{A_0}\frac{\partial}{\partial t}\delta A + \frac{1}{B_0}\frac{\partial}{\partial t}\delta B\right]. \tag{32}$$

3.1 The conservation of baryon number

The study of perturbed pressure in terms of Lagrangian displacement requires an additional assumption through which one can discuss physical aspects of gaseous mass undergoing adiabatic radial oscillations. In this context, the required assumption can be justified by the conservation of baryon numbers as $(Nu^j)_{;j} = 0$ or

$$\frac{\partial}{\partial x^j}(Nu^j) + Nu^j\frac{\partial}{\partial x^j}\ln\sqrt{-g} = 0, \tag{33}$$

where N is the baryon number per unit volume. It plays a substantial role in the evolution of various cosmic models. According to this law, the total number of particles will remain conserved during the fluid flow. The change in particle numbers occurs due to the loss or gain of net fluxes. We consider a fluid that satisfies this identity. Equation (33) through equation (20) gives

$$\frac{\partial}{\partial t}\left(\frac{N}{A_0}\right) + \frac{\partial}{\partial r}\left(\frac{Nv}{A_0}\right) + \frac{Nv}{A_0}\left[\frac{1}{A_0}\frac{\partial A}{\partial t} + \frac{1}{B_0}\frac{\partial B}{\partial t}\right] + \frac{Nv}{A_0}\left[\frac{1}{A_0}\frac{\partial A}{\partial r} + \frac{1}{B_0}\frac{\partial B}{\partial r} + \frac{1}{r}\right] = 0. \tag{34}$$

We take a perturbation of the form

$$N = N_0(r) + \delta N(r,t), \tag{35}$$

such that equation (34) with linear terms in v yields

$$\frac{1}{r^2}\frac{\mathrm{d}}{\mathrm{d}r}\left(\frac{N_0r^2v}{A_0/2}\right) + \frac{1}{A_0}\frac{\partial}{\partial t}\delta N + \frac{N_0}{A_0B_0}\frac{\partial}{\partial t}\delta B + \frac{N_0v}{A_0B_0}\frac{\mathrm{d}B_0}{\mathrm{d}r} = 0, \tag{36}$$

whose integration leads to

$$\frac{1}{A_0}\delta N+\frac{1}{r^2}\frac{\mathrm{d}}{\mathrm{d}r}\left(\frac{N_0r^2\eta}{A_0}\right)+\frac{N_0}{A_0B_0}\left[\delta B+\eta\frac{\mathrm{d}B_0}{\mathrm{d}r}\right]=0. \tag{37}$$

Using equation (27), it follows that

$$\delta N=N_0\left[\frac{\eta}{A_0}\frac{\mathrm{d}A_0}{\mathrm{d}r}-rB_0^2\int\delta q\,\mathrm{d}t\right]-\eta\frac{\mathrm{d}N_0}{\mathrm{d}r}-\frac{N_0A_0}{r^2}\frac{\partial}{\partial r}\left(\frac{r^2\eta}{A_0}\right)=0. \tag{38}$$

We assume an equation of state of the form

$$N=N(\sigma,p). \tag{39}$$

Using equations (29) and (38), we have

$$\delta p=-\eta\frac{\mathrm{d}p_0}{\mathrm{d}r}-p_0\Gamma\frac{A_0}{r}\frac{\partial}{\partial r}\left(\frac{r\eta}{A_0}\right)+\beta, \tag{40}$$

where

$$\beta=\frac{1}{\partial N/\partial p}\left[\frac{1}{4\pi}\frac{\partial N}{\partial\sigma}\left\{\frac{\eta}{2}\frac{\mathrm{d}}{\mathrm{d}r}\left(\frac{Q^2}{r^4}-\frac{Q_0\delta Q}{r^2}\right)\right\}+N_0\left\{\frac{\eta}{A_0}\frac{\mathrm{d}A_0}{\mathrm{d}r}-rB_0^2\int\delta q\,\mathrm{d}t\right\}\right],$$

and Γ represents the adiabatic index defined by

$$\Gamma=\frac{1}{p(\partial N/\partial p)}\left\{N-(\sigma+p)\frac{\partial N}{\partial\sigma}\right\}, \tag{41}$$

which estimates the fluid stiffness and describes the pressure and density fluctuations.

4 PULSATION EQUATION AND VARIATIONAL PRINCIPLE

The linear pulsation is related to different modes of perturbations applied to equilibrium cylindrical configuration and their oscillation frequencies. Inserting $\delta\sigma$ and δp in equation (32), we have

$$\begin{aligned}\omega^2B_0^2(p_0+\sigma_0)\eta=&-\frac{\mathrm{d}}{\mathrm{d}r}\left(\eta\frac{\mathrm{d}p_0}{\mathrm{d}r}\right)-\eta\frac{\mathrm{d}p_0}{\mathrm{d}r}\left[\frac{2}{A_0}\frac{\mathrm{d}A_0}{\mathrm{d}r}+\frac{1}{B_0}\frac{\mathrm{d}B_0}{\mathrm{d}r}\right]\\&-\frac{1}{A_0}\frac{\mathrm{d}A_0}{\mathrm{d}r}\left[2(p_0+\sigma_0)\eta\left\{\frac{1}{A_0}\frac{\mathrm{d}A_0}{\mathrm{d}r}+\frac{1}{B_0}\frac{\mathrm{d}B_0}{\mathrm{d}r}\right\}\right.\\&\left.+\frac{1}{r}\frac{\partial}{\partial r}\{r(p_0+\sigma_0)\eta\}\right]\\&-\frac{\mathrm{d}}{\mathrm{d}r}\left(p_0\Gamma\frac{A_0}{r}\frac{\partial}{\partial r}\left(\frac{\eta r}{A_0}\right)+\beta\right)-\left[\frac{2}{A_0}\frac{\mathrm{d}A_0}{\mathrm{d}r}+\frac{1}{B_0}\frac{\mathrm{d}B_0}{\mathrm{d}r}\right]\\&\times\left[p_0\Gamma\frac{A_0}{r}\frac{\partial}{\partial r}\left(\frac{\eta r}{A_0}\right)+\beta\right]-\frac{2}{A_0}\frac{\mathrm{d}A_0}{\mathrm{d}r}\left[\frac{1}{A_0}\frac{\mathrm{d}A_0}{\mathrm{d}r}+\frac{1}{B_0}\frac{\mathrm{d}B_0}{\mathrm{d}r}\right]\\&\times\int\delta q\,\mathrm{d}t+\frac{Q_0\delta Q}{4\pi r^2}\left[\frac{1}{A_0}\frac{\mathrm{d}A_0}{\mathrm{d}r}+\frac{1}{B_0}\frac{\mathrm{d}B_0}{\mathrm{d}r}-\frac{2}{r}\right].\end{aligned} \tag{42}$$

Substituting $\frac{\mathrm{d}p_0}{\mathrm{d}r}$ from equation (13), this leads to

$$\begin{aligned}\omega^2B_0^2=&\frac{1}{A_0}\left[\frac{\mathrm{d}^2A_0}{\mathrm{d}r^2}-\frac{1}{B_0}\frac{\mathrm{d}B_0}{\mathrm{d}r}+\frac{1}{r}\frac{\mathrm{d}A_0}{\mathrm{d}r}\right]\\&-\frac{\eta}{8\pi}\frac{\mathrm{d}^2}{\mathrm{d}r^2}\left(\frac{Q^2}{r^2}\right)\left[\frac{2}{A_0}\frac{\mathrm{d}A_0}{\mathrm{d}r}+\frac{1}{B_0}\frac{\mathrm{d}B_0}{\mathrm{d}r}\right]+\frac{\eta}{8\pi}\frac{\mathrm{d}}{\mathrm{d}r}\left(\frac{Q^2}{r^2}\right)\\&-\frac{\mathrm{d}}{\mathrm{d}r}\left[p_0\Gamma\frac{A_0}{r}\frac{\partial}{\partial r}\left(\frac{\eta r}{A_0}+\beta\right)\right]-\left[p_0\Gamma\frac{A_0}{r}\frac{\partial}{\partial r}\left(\frac{\eta r}{A_0}+\beta\right)\right]\\&\times\left[\frac{2}{A_0}\frac{\mathrm{d}A_0}{\mathrm{d}r}+\frac{1}{B_0}\frac{\mathrm{d}B_0}{\mathrm{d}r}\right]-\frac{2}{A_0}\frac{\mathrm{d}A_0}{\mathrm{d}r}\tilde{q}\left[\frac{2}{A_0}\frac{\mathrm{d}A_0}{\mathrm{d}r}+\frac{1}{B_0}\frac{\mathrm{d}B_0}{\mathrm{d}r}\right]\\&-\frac{Q_0\delta Q}{4\pi r^2}\left[\frac{1}{A_0}\frac{\mathrm{d}A_0}{\mathrm{d}r}+\frac{1}{B_0}\frac{\mathrm{d}B_0}{\mathrm{d}r}-\frac{2}{r}\right],\end{aligned} \tag{43}$$

where $\int\delta q\,\mathrm{d}t=\tilde{q}$. Using equations (6) and (13), we have

$$\begin{aligned}\omega^2B_0^2(p_0+\sigma_0)\eta=&\frac{8\pi G}{c^4}p_0B_0^2(p_0+\sigma_0)\\&+\frac{\eta}{r}\left[\frac{\mathrm{d}p_0}{\mathrm{d}r}+\frac{1}{8\pi}\frac{\mathrm{d}}{\mathrm{d}r}\left(\frac{Q^2}{r^2}\right)\right]-\frac{\eta}{8\pi}\frac{\mathrm{d}^2}{\mathrm{d}r^2}\left(\frac{Q^2}{r^2}\right)\\&+\frac{\eta}{8\pi}\frac{\mathrm{d}}{\mathrm{d}r}\left(\frac{Q^2}{r^2}\right)\left[\frac{2}{A_0}\frac{\mathrm{d}A_0}{\mathrm{d}r}+\frac{1}{B_0}\frac{\mathrm{d}B_0}{\mathrm{d}r}\right]\\&-\frac{\mathrm{d}}{\mathrm{d}r}\left[p_0\Gamma\frac{A_0}{r}\frac{\partial}{\partial r}(\eta rA_0)+\beta\right]-\frac{2}{A_0}\frac{\mathrm{d}A_0}{\mathrm{d}r}\tilde{q}\\&\times\left[\frac{1}{A_0}\frac{\mathrm{d}A_0}{\mathrm{d}r}+\frac{1}{B_0}\frac{\mathrm{d}B_0}{\mathrm{d}r}\right]\\&+\frac{Q_0\delta Q}{4\pi r^2}\left[\frac{1}{A_0}\frac{\mathrm{d}A_0}{\mathrm{d}r}+\frac{1}{B_0}\frac{\mathrm{d}B_0}{\mathrm{d}r}-\frac{2}{r}\right],\end{aligned} \tag{44}$$

which is the required pulsation equation satisfying the boundary conditions

$$\eta=0,\quad r=0,\quad \delta p=0,\quad r=R.$$

Taking the product of pulsation equation with $\eta r^2A_0B_0$ and integrating over values of r, it yields a characteristic value problem for ω^2 as

$$\begin{aligned}\omega^2\int_0^R r^2\eta^2AB^3(p+\sigma)\mathrm{d}r=&\frac{8\pi G}{c^4}\int_0^R p(p+\sigma)r^2\eta^2AB^3\mathrm{d}r\\&+\int_0^R r\eta^2AB\left[\frac{\mathrm{d}p}{\mathrm{d}r}+\frac{1}{8\pi}\frac{\mathrm{d}}{\mathrm{d}r}\left(\frac{Q^2}{r^2}\right)\right]\mathrm{d}r-\int_0^R r^2\eta^2\frac{\mathrm{d}p}{\mathrm{d}r}\\&\times AB\left(p\Gamma\frac{A}{r}\frac{\mathrm{d}}{\mathrm{d}r}\left(\frac{\eta r}{A}\right)+\beta\right)\mathrm{d}r-\int_0^R r^2\eta^2AB\left[p\Gamma\frac{A}{r}\right.\\&\left.\times\frac{\mathrm{d}}{\mathrm{d}r}\left(\frac{\eta r}{A}\right)+\beta\right]\left[\frac{1}{A}\frac{\mathrm{d}A}{\mathrm{d}r}+\frac{1}{B}\frac{\mathrm{d}B}{\mathrm{d}r}\right]\mathrm{d}r-2\int_0^R r^2B\eta\frac{\mathrm{d}A}{\mathrm{d}r}\\&\times\tilde{q}\left[\frac{1}{A}\frac{\mathrm{d}A}{\mathrm{d}r}+\frac{1}{B}\frac{\mathrm{d}B}{\mathrm{d}r}\right]\mathrm{d}r+\frac{1}{8\pi}\int_0^R Q_0AB\eta\delta Q\left[\frac{1}{A}\frac{\mathrm{d}A}{\mathrm{d}r}\right.\\&\left.+\frac{1}{B}\frac{\mathrm{d}B}{\mathrm{d}r}-\frac{2}{r}\right]\mathrm{d}r.\end{aligned} \tag{45}$$

We can define the orthogonality relation associated with this equation as

$$\int_0^R AB^3r^2(p+\sigma)\eta^{(i)}\eta^{(j)}=0,\quad (i\neq j), \tag{46}$$

where $\eta^{(i)}$ and $\eta^{(j)}$ provide proper solutions corresponding to different characteristic values of ω^2. The study of dynamical instability of a star requires that the right-hand side of equation (45) must vanish by choosing a trial function ξ that satisfies the given boundary conditions.

In the following, we evaluate conditions for dynamical instability by taking a homogeneous model.

4.1 The homogeneous model of the cylinder

We study the conditions for dynamical instability of a homogeneous cylinder with constant energy density. Equations (18) and (19) governing the hydrostatic equilibrium allow the integration such that

we can write (Chandrasekhar 1964)

$$y^2=-\frac{r}{a^2}+\frac{b^2}{r^2},\quad y_1^2=-\frac{R}{a^2}+\frac{b^2}{R^2},\tag{47}$$

where $a^2=\frac{c^4}{2\pi G\sigma}$ and $b^2=\frac{GQ^2(1-2c^2)}{2c^4}$. We can determine solutions of the relevant physical quantities in terms of y and y_1 as

$$p=\sigma\frac{y-y_1}{3y_1-y},\quad A^2=\frac{1}{4}[3y_1-y]^2,\quad B^2=\frac{1}{y^2}.\tag{48}$$

For positivity of pressure, we have $3y_1>1$ that yields

$$\frac{R}{a^2}-\frac{b^2}{R^2}<\frac{1}{9}.$$

Using the inertial mass, this leads to

$$R>9\left(\frac{2GM}{c^2}-\frac{GQ^2}{Rc^4}\right)=9R_*,\tag{49}$$

where R_* is the limiting radius for the charged cylinder. Inserting the above physical quantities in equation (45), it follows that

$$\begin{aligned}
&2a\omega^2y_1\int_0^{\xi_1}\frac{\xi^2\eta^2}{y^3}\mathrm{d}\xi=6y_1\int_0^{\xi_1}\frac{y-y_1}{y^3(3y_1-y)^2}\xi^2\eta^2\mathrm{d}\xi\\
&+\frac{3}{2a}\int_0^{\xi_1}\frac{3y_1-y}{y}\xi\eta^2\frac{\mathrm{d}}{\mathrm{d}\xi}\left[\frac{y-y_1}{3y_1-y}+\frac{G}{3ac^4}\frac{\mathrm{d}}{\mathrm{d}\xi}\left(\frac{Q^2}{\xi^2}\right)\right]\mathrm{d}\xi\\
&-\frac{1}{2}\int_0^{\xi_1}\eta\xi^2\frac{3y_1-y}{y}\frac{\mathrm{d}}{\mathrm{d}\xi}\left[\frac{y-3y_1}{a^3\xi}\Gamma\frac{\partial}{\partial\xi}\left(\frac{\eta\xi}{3y_1-y}\right)+\frac{3c^4\beta}{8\pi G}\right]\mathrm{d}\xi\\
&-\frac{a^2}{2}\int_0^{\xi_1}\xi^2\eta\frac{3y_1-y}{y}\left[\frac{y-y_1}{a\xi}\Gamma\frac{\partial}{\partial\xi}\left(\frac{\eta\xi}{3y_1-y}\right)+\frac{3c^4\beta}{8\pi G}\right]\\
&\times\left[\frac{2}{3y_1-y}\frac{\mathrm{d}}{\mathrm{d}\xi}(3y_1-y)+y\frac{\mathrm{d}}{\mathrm{d}\xi}\left(\frac{1}{y}\right)\right]\mathrm{d}\xi-\frac{3ac^4}{8\pi G}\int_0^{\xi_1}\frac{\eta\xi^2}{y}\tilde{q}\\
&\times\frac{\mathrm{d}}{\mathrm{d}\xi}(3y_1-y)\left[\frac{1}{3y_1-y}\frac{\mathrm{d}}{\mathrm{d}\xi}(3y_1-y)+y\frac{\mathrm{d}}{\mathrm{d}\xi}\frac{1}{y}\right]\mathrm{d}\xi\\
&+\frac{3c^4}{(8\pi)^2G}\int_0^{\xi_1}Q_0\xi\delta Q\frac{3y_1-y}{2y}\\
&\times\left[\frac{2}{3y_1-y}\frac{\mathrm{d}}{\mathrm{d}\xi}(3y_1-y)+y\frac{\mathrm{d}}{\mathrm{d}\xi}\frac{1}{y}\right]\mathrm{d}\xi,
\end{aligned}\tag{50}$$

where $\xi=\frac{r}{a}$, $\xi_1=\frac{R}{a}-\frac{b}{R}$ and Γ is taken to be constant.

We consider a trial function

$$\eta=\xi A=\frac{1}{2}\xi(y_1-y),\tag{51}$$

such that equation (50) becomes

$$\begin{aligned}
&\frac{a\omega^2y_1}{2}\int_0^{\xi_1}\frac{\xi^4(3y_1-y)^2}{y^3}\mathrm{d}\xi=\frac{3y_1}{2a}\\
&\times\int_0^{\xi_1}\frac{\xi^4(y-y_1)(3y_1-y)}{4y^3}\mathrm{d}\xi+\frac{3}{2a}\int_0^{\xi_1}\frac{\xi^3(3y_1-y)^3}{2y}\\
&\times\frac{\mathrm{d}}{\mathrm{d}\xi}\left[\frac{y-y_1}{3y_1-y}+\frac{G}{3ac^4}\frac{\mathrm{d}}{\mathrm{d}\xi}\left(\frac{Q^2}{\xi^2}\right)\right]\mathrm{d}\xi-\frac{1}{4}\int_0^{\xi_1}\frac{\xi^3(3y_1-y)^2}{y}\\
&\times\frac{\mathrm{d}}{\mathrm{d}\xi}\left[\frac{y-3y_1}{a^3\xi}\Gamma\frac{\partial}{\partial\xi}\left(\frac{\xi^2}{2}\right)+\frac{3c^4\beta}{8\pi G}\right]\mathrm{d}\xi-\frac{a^2}{4}\int_0^{\xi_1}\xi^3\\
&\times\frac{(3y_1-y)^2}{y}\left[\frac{y-y_1}{a\xi}\Gamma\frac{\partial}{\partial\xi}\left(\frac{\xi^2}{2}\right)+\frac{3c^4\beta}{8\pi G}\right]\\
&\times\left[\frac{2}{3y_1-y}\frac{\mathrm{d}}{\mathrm{d}\xi}(3y_1-y)+y\frac{\mathrm{d}}{\mathrm{d}\xi}\left(\frac{1}{y}\right)\right]\mathrm{d}\xi\\
&-\frac{3ac^4}{16\pi G}\int_0^{\xi_1}\frac{\xi^3(3y_1-y)}{y}\tilde{q}\frac{\mathrm{d}}{\mathrm{d}\xi}(3y_1-y)\\
&\times\left[\frac{1}{3y_1-y}\frac{\mathrm{d}}{\mathrm{d}\xi}(3y_1-y)+y\frac{\mathrm{d}}{\mathrm{d}\xi}\frac{1}{y}\right]\mathrm{d}\xi\\
&+\frac{3c^4}{(16\pi)^2G}\int_0^{\xi_1}Q_0\xi\delta Q\frac{(3y_1-y)^2}{y}\\
&\times\left[\frac{2}{3y_1-y}\frac{\mathrm{d}}{\mathrm{d}\xi}(3y_1-y)+y\frac{\mathrm{d}}{\mathrm{d}\xi}\frac{1}{y}\right]\mathrm{d}\xi.
\end{aligned}\tag{52}$$

Table 1. Adiabatic index and radii for a homogeneous cylinder.

θ_1	R/R_*	Γ_c for $Q=0.4$
0^o	10.364	−4.365
10^o	33.163	2.894×10^7
20^o	8.549	3×10^7
30^o	4.000	23 647.19
40^o	2.4203	131 557
50^o	1.704	87 550
60^o	1.333	118 265.5

Inserting $y=\cos\theta$ and $\xi=\sin\theta$ in the above equation, we have

$$\begin{aligned}
&\frac{(a\omega)^2\cos\theta_1}{2}\int_0^{\theta_1}\frac{\sin^4\theta}{\cos^2\theta}(3\cos^2\theta_1-\cos\theta)^2\mathrm{d}\theta=\frac{3\cos\theta_1}{2}\\
&\times\int_0^{\theta_1}\frac{\sin^4\theta}{\cos^2\theta}[4\cos\theta\cos\theta_1-3\cos^2\theta_1\cos^2\theta]\,\mathrm{d}\theta\\
&+\frac{3}{4}\int_0^{\theta_1}(3\cos\theta_1-\cos\theta)^3\frac{\sin^3\theta}{\cos\theta}\frac{\mathrm{d}}{\mathrm{d}\theta}\left[\frac{\cos\theta-\cos\theta_1}{3\cos\theta_1-\cos\theta}\right.\\
&\left.-\frac{2GQ^2}{3ac}\frac{1}{\sin^3\theta}\right]\mathrm{d}\theta-\frac{a}{4}\int_0^{\theta_1}(3\cos\theta_1-\cos\theta)^2\frac{\sin^3\theta}{\cos\theta}\\
&\times\frac{\mathrm{d}}{\mathrm{d}\theta}\left[\frac{\cos\theta_1-\cos\theta}{a^3\sin^4\theta}\Gamma+\frac{3c^4\beta}{8\pi G}\right]\mathrm{d}\theta\\
&-\frac{a^3}{4}\int_0^{\theta_1}(3\cos\theta_1-\cos\theta)^2\sin^3\theta\left[\frac{\cos\theta-\cos\theta_1}{a}\Gamma+\frac{3c^4\beta}{8\pi G}\right]\\
&\times\left[\frac{2\sin\theta}{\cos\theta(3\cos\theta_1-\cos\theta)}+\tan\theta\sec\theta\right]\mathrm{d}\theta\\
&-\frac{3ac^4}{16\pi G}\int_0^{\theta_1}\frac{\sin^3\theta}{\cos\theta}(3\cos\theta_1-\cos\theta)\tilde{q}\frac{\mathrm{d}}{\mathrm{d}\theta}(3\cos\theta_1-\cos\theta)\\
&\times\left[\frac{\sin\theta}{\cos\theta(3\cos\theta_1-\cos\theta)}+\tan\theta\sec\theta\right]\mathrm{d}\theta+\frac{3c^4\beta}{(16\pi)^2G}\\
&\times\int_0^{\theta_1}Q_0\delta Q\sin\theta(3\cos\theta_1-\cos\theta)^2\\
&\times\left[\frac{2\sin\theta}{\cos\theta(3\cos\theta_1-\cos\theta)}+\tan\theta\sec\theta\right]\mathrm{d}\theta,
\end{aligned}\tag{53}$$

where $\theta_1=\sin^{-1}\left(\frac{R}{a}-\frac{b}{R}\right)$. By taking $\omega^2=0$ and solving the integrals, we find exact condition for marginal stability. We evaluate the values of Γ_c for θ such that $\Gamma\leq\Gamma_c$ for the existence of dynamical instability. We also consider the Newtonian limit that implies that the resulting criteria for marginal stability is $\Gamma>-\frac{9}{8}-\frac{81Q^2}{4}$. We compute Γ and radii of marginal stability for a homogeneous gaseous cylinder corresponding to $Q=0.4$ and $q=0.5$ which exhibit finite values of Γ in Newtonian and pN limits. We note that $\frac{R}{R_*}$ remains positive for $\Gamma>0$ showing marginal stability of the gaseous cylindrical model in the pN limit. The respective results are given in Table 1.

The perturbation diverges exponentially for $\omega^2<0$ which yields either expansion or contraction showing dynamical instability of the stellar model. In the Newtonian limit, we explore the ranges

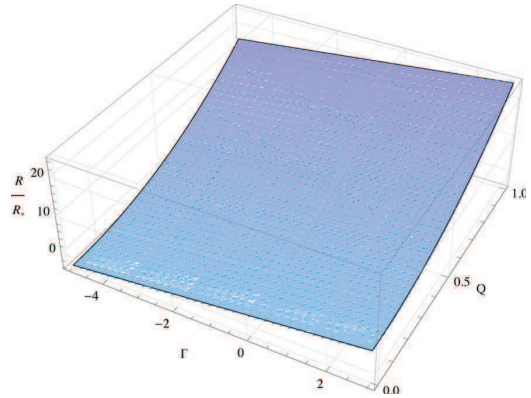

Figure 1. Plot of $\frac{R}{R_*}$ for dynamical stability/instability of a charged cylinder in the Newtonian limit.

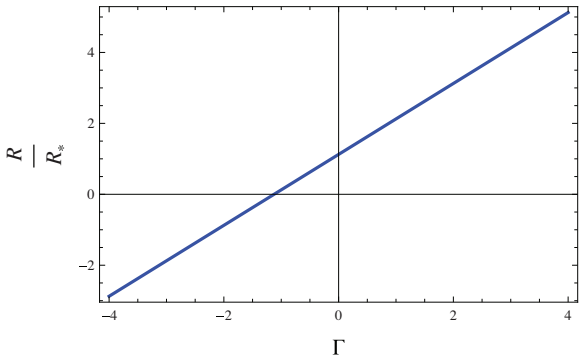

Figure 2. Plot of $\frac{R}{R_*}$ for dynamical stability/instability of an uncharged cylinder in the Newtonian limit.

of instability for both charged (Fig. 1) and uncharged cylinders (Fig. 2). Since the radius of stability is a factor of R_*, so physically interesting results can be obtained if $\frac{R}{R_*} \geq 0$. For a charged cylinder, we find unstable radii corresponding to smaller values of charge. The system becomes stable as charge increases. In case of an uncharged cylinder, dynamical instability occurs for $\Gamma < -1.125$. It is obvious from the graph that for $\Gamma > -\frac{9}{8}$, the resulting radius of stability is greater than R_*.

We obtain the following condition for dynamical instability of relativistic gaseous masses including charge as $\theta_1 \to 0$

$$\Gamma + \frac{3}{4}\left(\frac{3}{2} + 27Q^2\right) < \frac{57}{42}\theta_1^2 = \frac{57}{42}\left[\frac{R}{a^2} - \frac{b^2}{R^2}\right]. \tag{54}$$

We can write

$$R < \frac{57}{42\left[\Gamma + \frac{3}{4}\left(\frac{3}{2} + 27Q^2\right)\right]}\left[\frac{2GM}{c^2} - \frac{GQ^2}{Rc^4}\right], \tag{55}$$

which leads to

$$\frac{R}{R_*} < \frac{K}{\left[\Gamma + \frac{3}{4}\left(\frac{3}{2} + 27Q^2\right)\right]}, \tag{56}$$

where $K = \frac{57}{42}$ for the homogeneous cylinder. This means that if Γ exceeds $-\frac{3}{4}(\frac{3}{2} + 27Q^2)$ by a small amount, the dynamical instability can be prevented till the mass contracts to radius R_*. The gaseous cylinder remains stable if its radius is larger than R_*. The ranges of instability for a charged homogeneous cylindrical system are shown

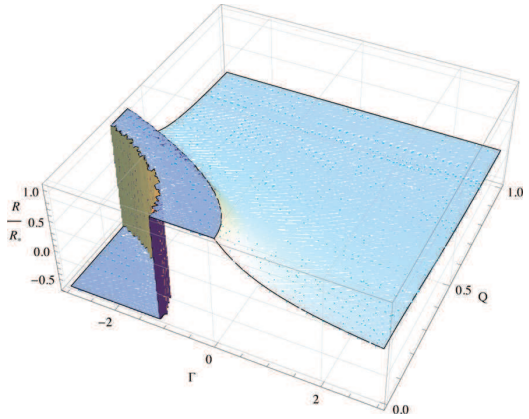

Figure 3. Plot of $\frac{R}{R_*}$ for dynamical stability/instability of a homogeneous charged cylinder.

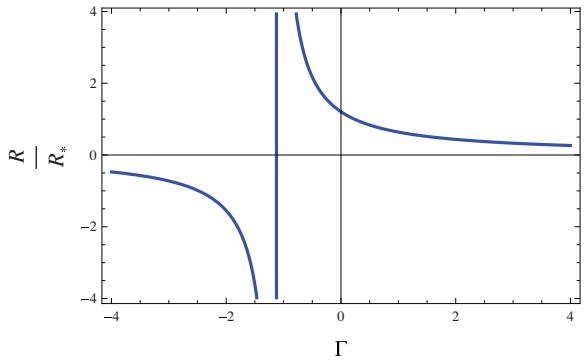

Figure 4. Plot of $\frac{R}{R_*}$ for dynamical stability/instability of a homogeneous uncharged cylinder.

in Fig. 3. It can be seen that the radius of stability is greater than R_* for $\Gamma > -1$ in the pN limit. We also discuss the criteria and ranges of instability for an uncharged cylinder (Fig. 4). It is found that $\frac{R}{R_*} \geq 0$ when Γ exceeds $-\frac{9}{8}$ by a small amount showing stable cylindrical configuration. It is observed that $\Gamma < -1.125$ leads to unphysical results as $\frac{R}{R_*} < 0$.

5 OUTLOOK

This paper is devoted to study the influence of electric charge on dynamical instability of a collapsing cylinder. We have followed Eulerian and Lagrangian approaches to find linearized dynamical equations as well as perturbed pressure. This perturbed pressure has been obtained in terms of adiabatic index by taking conservation of baryon numbers. A variational principle has been developed to formulate characteristic frequencies of oscillation which refers to the criteria of dynamical instability for a gaseous cylinder. We have also discussed conditions for dynamical instability by considering a homogeneous model of the cylinder.

We have computed particular values of radii as well as adiabatic index Γ to investigate the marginal stability of a homogeneous cylinder (Table 1). It is found that Γ takes finite values greater than or equal to $-\frac{3}{4}\left(\frac{3}{2} + 27Q^2\right)$ for $Q = 0.4$ and $q = 0.5$ in the Newtonian limit. In the pN limit, $\frac{R}{R_*}$ remains positive for $\Gamma > 0$ showing marginal stability of the gaseous cylindrical model. We

have also discussed the criteria for onset of dynamical instability of gaseous masses.

In the Newtonian limit, we have explored the ranges of instability for both charged (Fig. 1) and uncharged cylinders (Fig. 2). There is an extensive literature available for dynamical instability of cylindrical gaseous systems using different techniques in the Newtonian limit. Nakamura, Hanawa & Nakano (1993) studied dynamical instability of self-gravitating cylindrical gaseous cloud by means of normal mode analysis and found unstable solutions against various types of perturbations. Hanawa et al. (1993) discussed fragmentation of cylindrical molecular cloud with axial magnetic field on the basis of a magnetohydrodynamical stability analysis and found that the presence of a magnetic field or rotation shortens the wavelength of most unstable modes. Matsumoto, Nakamura & Hanawa (1994) studied dynamical instability of a self-gravitating magnetized cylindrical cloud by taking rotation around its axis which suffers from various instabilities. Fiege & Pudrit (2000) explored dynamical instability of molecular cylindrical clouds threaded by helical magnetic fields and found that all filamentary molecular clouds initially in an equilibrium state cannot be made to undergo radial collapse by increasing the external pressure. Toci & Galli (2015) discussed dynamical instability of cylindrical polytropic filaments and found that the cylindrical polytropes converge at large radii.

In our analysis, the gaseous cylinder remains stable as long as its radius is larger than R_* but becomes unstable as its radius contracts to the radius R_*. For a charged cylinder, dynamical instability occurs for smaller values of charge whereas the system becomes stable by increasing charge. The resulting radius of stability is greater than R_* for $\Gamma > -\frac{9}{8}$ in case of an uncharged cylinder while the dynamical instability occurs for $\Gamma < -1.125$. It is mentioned here that electric charge plays a substantial role to increase stability of the cylindrical system as the gaseous mass is more stable in the Newtonian limit for larger values of charge.

In the pN limit, the gaseous cylinder undergoes dynamical instability if Γ exceeds $-\frac{3}{4}(\frac{3}{2}+27Q^2)$ by a small amount. It is found that $\Gamma > -1$ and $Q > 0.3$ provide valid ranges of radii for the stability of cylinder whereas only unstable radii exist corresponding to $\Gamma < -1$ and $Q < 0.3$ (Fig. 3). There is no effect of dissipation on stability of the collapsing system in this case. It is worth mentioning here that the gaseous cylinder becomes unstable forever for smaller values of charge. For the uncharged cylinder, we have found that Γ exceeds $-\frac{9}{8}$ by a small amount showing stable cylindrical configuration (Fig. 4). It is observed that $\frac{R}{R_*} < 0$ for $\Gamma < -1.125$ leading to unphysical results. It is mentioned here that the cylindrical system is more stable in the Newtonian limit (Fig. 1) for larger values of charge as compared to the pN limit (Fig. 3). We conclude that the presence of electromagnetic field plays a remarkable role in the emergence of stability of the gaseous cylinder.

REFERENCES

Ayal S., Piran T., Oechslin R., Davies M. B., Rosswog S., 2001, ApJ, 550, 846

Azam M., Mardan S. A., Noureen I., Rehman M. A., 2016, Eur. Phys. J. C, 76, 510

Chan R., Herrera L., Santos N. O., 1994, MNRAS, 267, 637

Chandrasekhar S., 1964, ApJ, 140, 417

Chandrasekhar S., 1965, ApJ, 142, 1519

Di Prisco A. et al., 2009, Phys. Rev. D, 80, 064031

Fiege J. D., Pudrit R. E., 2000, MNRAS, 311, 85

Ghezzi C. R., 2005, Phys. Rev. D, 72, 104017

Glazer I., 1976, Ann. Phys., 101, 594

Hanawa T. et al., 1993, ApJ, 404, L83

Herrera L., Le Denmat G., Santos N. O., 1989, MNRAS, 237, 257

Marek A., Dimmelmeier H., Janka H.-Th., Müller E., Buras R., 2006, A&A, 445, 273

Matsumoto T., Nakamura F., Hanawa T., 1994, PASJ, 46, 243

Nakamura F., Hanawa T., Nakano T., 1993, PASJ, 45, 551

Nunez L. A., Hernandez H., Abreu H., 2007, Class. Quantum Grav., 24, 4631

Rosseland S., 1924, MNRAS, 84, 720

Sharif M., Abbas G., 2011, J. Phys. Soc. Japan, 80, 104002

Sharif M., Ahmad Z., 2007, Gen. Relativ. Gravit., 39, 1331

Sharif M., Azam M., 2012a, J. Cosmol. Astropart. Phys., 02, 043

Sharif M., Azam M., 2012b, Gen. Relativ. Gravit., 44, 1181

Sharif M., Azam M., 2013, MNRAS, 430, 3048

Sharif M., Bhatti M. Z., 2013, J. Cosmol. Astropart. Phys., 10, 056

Sharif M., Mumtaz S., 2016, Gen. Relativ. Gravit., 48, 92

Stettner R., 1973, Ann. Phys., 80, 212

Thorne K. S., 1935, Phys. Rev., 138, B251

Toci C., Galli D., 2015, MNRAS, 446, 2110

This paper has been typeset from a TEX/LATEX file prepared by the author.

Astrophys Space Sci (2016) 361:218
DOI 10.1007/s10509-016-2817-x

ORIGINAL ARTICLE

Influence of nonlinear electrodynamics on stability of thin-shell wormholes

M. Sharif[1] · Saadia Mumtaz[1]

Received: 12 May 2016 / Accepted: 3 June 2016 / Published online: 10 June 2016

Abstract The aim of this paper is to discuss stability of regular thin-shell wormholes coupled with non-linear electrodynamics and cosmological constant. The surface stresses are formulated by using Lanczos equations. We examine attractive and repulsive behavior of these constructed wormholes corresponding to outward and inward-directed acceleration components, respectively. We also investigate stability conditions for the existence of traversable thin-shell wormholes with arbitrarily small amount of different fluids as exotic matter. We consider linear, logarithmic and Chaplygin gas models and find that a modified generalized Chaplygin gas model provides maximum viable regions for stability of the respective thin-shell wormholes. It is found that formation of stable regions for ABGB thin-shell wormholes highly depends on the physically acceptable range of charge and other parameters.

Keywords Thin-shell wormholes · Israel formalism · Stability

1 Introduction

The stability of celestial objects has remained a challenging problem for researchers in gravitational physics. This study is closely related to the evolution of thin-shell wormholes which supports the fact that any relativistic object will be physically interesting if it is stable under perturbations. A "wormhole" is referred as a shortcut with two ends connecting different regions of the universe through a tunnel. It can be categorized into traversable and non-traversable wormhole which plays a significant role for its viability. In case of traversable wormholes, there is no event horizon and the wormhole throat is threaded by exotic matter which causes repulsion against the tidal gravitational force (Morris and Thorne 1988). The physical evidence of wormholes has always been a debatable issue due to the existence of exotic matter at the throat. Visser (1989) minimized its amount through cut and paste procedure and restricted it at the edges of throat to obtain a more viable thin-shell wormhole. The stress-energy tensor components are computed by applying Israel thin-shell formalism which characterizes exotic matter at the shell (Israel 1966).

The construction of thin-shell wormholes from the family of regular black holes (BH) is an interesting task. Regular BHs can be chosen for wormhole construction because they have regular centers which restrict the singularities to stay out from their horizons and provide viable wormhole solutions. Such type of BHs are more feasible in high energy collisions and require finite energy for their evolution. The first singularity-free regular BH solution was proposed by Bardeen in the presence of electromagnetic field (Bardeen 1968). Ayon-Beato and Garcia (1998) explored another regular static spherically symmetric BH described by its mass and electric charge known as ABG BH. Later, Bronnikov (2001) proposed similar type of massive regular BH solutions coupled with nonlinear electrodynamics named as ABGB spacetimes. Hayward (2006) found a similar class of regular BH which reduces to de Sitter for $r \to 0$ and Schwarzschild BH for $r \to \infty$. Recently, stability of thin-shell wormholes from regular Hayward BH was investigated by taking different models of exotic matter (Halilsoy et al. 2014).

The problem of stability of thin-shell wormholes can be resolved either through perturbations or by assuming equa-

✉ M. Sharif
msharif.math@pu.edu.pk

[1] Department of Mathematics, University of the Punjab, Quaid-e-Azam Campus, Lahore 54590, Pakistan

tion of state (EoS) for exotic matter. It has been a debatable subject to find some appropriate dark energy models for exotic matter. Eiroa (2009) discussed the dynamics of spherical thin-shell wormholes by taking generalized Chaplygin gas (GCG). Sharif and collaborators (Sharif and Azam 2013a; Sharif and Mumtaz 2014b, 2015, 2016a) investigated both stable and unstable thin-shell wormholes in the vicinity of Chaplygin gas (CG) models and Van der Waals quintessence. Mazharimousavi and Halilsoy (2014) studied the effects of angular momentum on the stability of counter-rotating thin-shell wormholes by assuming linear gas EoS and found stable wormhole solutions.

The stability analysis has been carried out by incorporating charge and the cosmological constant (Λ). Kim and Lee (2001) studied stability of charged thin-shell wormholes and found that charge affects stability without affecting the spacetime itself. Eiroa and Romero (2004) explored stability of Reissner-Nordström thin-shell wormholes and found stable solutions with increasing value of charge. Lobo and Crawford (2004) examined stability of spherically symmetric thin-shell wormholes with Λ and found that positive Λ increases the stability regions but these regions decrease with negative Λ. The role of electric charge and Λ on the stability of spherical thin-shell wormholes have been studied by taking different CG models (Sharif and Azam 2013b; Sharif and Mumtaz 2014a, 2016b).

This paper is devoted to analyze stability of thin-shell wormholes from regular BH coupled with nonlinear electrodynamics. The paper is organized as follows. In Sect. 2, we provide an overview of ABGB BH with nonlinear electrodynamics and construct ABGB thin-shell wormholes by employing standard cut and paste technique. Section 3 deals with standard approach for stability analysis of respective thin-shell wormholes. In Sect. 4, we choose linear, logarithmic and CG models and study stability formalism for the existence of traversable ABGB thin-shell wormholes. Section 5 is devoted to discuss the role of small velocity dependent perturbations for wormhole stability. Finally, we conclude our results in the last section.

2 Basic formalism

This section provides an overview to the construction of thin-shell wormholes from regular charged BH coupled with Λ. The study of regularity of BHs has attained remarkable importance to understand the final state of the initially regular configurations. It is well-known that electrovacuum asymptotically flat spacetimes are not sufficient for the existence of regular BH solutions. To derive the nonlinear electromagnetic field for regular BH, one needs to enlarge the class of electrodynamics to nonlinear ones (Ayon-Beato and Garcia 1998). These regular BHs behave as ordinary Reissner-Nordström BH solutions and the existence of these solutions does not contradict with the singularity theorems (Hawking and Ellis 1975). This motivates us to discuss stability of viable thin-shell wormholes in the framework of nonlinear electrodynamics.

The system of gravity coupled with nonlinear electrodynamics in the presence of Λ is described by the action

$$S=\frac{1}{16\pi}\int\sqrt{-g}\big[(R-2\Lambda)-\mathcal{L}(F)\big]d^4x, \tag{1}$$

where R is the scalar curvature, Λ is the cosmological constant and $\mathcal{L}(F)$ is the Lagrangian for nonlinear electrodynamics given by

$$\mathcal{L}(F)=F\left[1-\tanh^2\left(\frac{Q}{2M}\left(\frac{FQ^2}{2}\right)^{\frac{1}{4}}\right)\right], \tag{2}$$

which depends on a single invariant $F=F^{ij}F_{ij}$ with the electromagnetic tensor $F_{ij}=\Phi_{j;i}-\Phi_{i;j}$. The static spherically symmetric nonsingular ABGB BH is given by (Matyjasek et al. 2008)

$$ds^2=-N(r)dt^2+N^{-1}(r)dr^2+r^2\big(d\theta^2+\sin^2\theta d\phi^2\big), \tag{3}$$

where

$$N(r)=1-\frac{2M}{r}\left[1-\tanh\left(\frac{Q^2}{2Mr}\right)\right]-\frac{\Lambda r^2}{3}, \tag{4}$$

M and Q correspond to the mass and charge, respectively. It is noted that the presence of cosmological constant does not destroy the regularity of the solution describing a regular ABGB-de Sitter BH with $\Lambda>0$ which reduces to ABGB BH for $\Lambda=0$ (Bronnikov 2001). This metric is regular at the center $r=0$ while the metric function for small Q and $r\to\infty$ can be expanded as

$$N(r)=1-\frac{2M}{r}+\frac{Q^2}{r^2}-\frac{\Lambda r^2}{3}-\frac{Q^6}{12M^2r^4}+\cdots,$$

which behaves as Reissner-Nordström-de Sitter BH. Its event and cosmological horizons can be determined by the real roots of the metric function $N(r)=0$.

To construct thin-shell wormholes, we employ standard procedure by cutting the interior region of regular ABGB BH with $r<a$. The resulting 4D geometries are joined at the hypersurface $\Sigma^{\pm}=\Sigma=\{r=a\}$. A 3D induced spacetime is considered at the shell as

$$ds^2=-d\tau^2+a^2(\tau)\big(d\theta^2+\sin^2\theta d\phi^2\big), \tag{5}$$

where τ is the proper time on the shell. For dynamical evolution of thin-shell, we follow Israel formalism which enables the joining of two regions of spacetime partitioned by Σ.

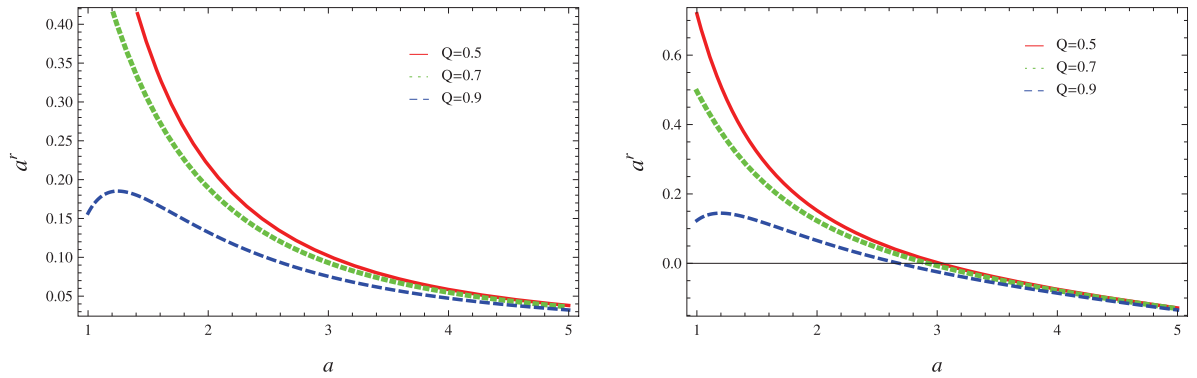

Fig. 1 Plots of a^r without Λ (*left hand side*) and with $\Lambda = 0.1$ (*right hand side*) corresponding to $\frac{Q}{M} = 0.5, 0.77, 0.99$

The surface stresses at the shell are determined by Lanczos equations defined as

$$S^i_j = \frac{1}{8\pi}\{[K]\delta^i_j - [K^i_j]\}, \tag{6}$$

where $[K^i_j]$ is the extrinsic curvature tensor and $K = \text{tr}[K^i_j]$. The surface energy density and surface pressure at the shell yield

$$\sigma = -\frac{1}{2\pi a}\sqrt{N(a)+\dot{a}^2}, \tag{7}$$

$$p = \frac{1}{4\pi}\left[\frac{\sqrt{N(a)+\dot{a}^2}}{a} + \frac{2\ddot{a}+N'(a)}{2\sqrt{N(a)+\dot{a}^2}}\right]. \tag{8}$$

It would be interesting to explore attractive and repulsive characteristics of the regular ABGB thin-shell wormholes for which observer's four-acceleration is defined as

$$a^\mu = u^\mu_{;\nu}u^\nu,$$

where $u^\mu = \frac{dx^\mu}{d\tau} = (\frac{1}{\sqrt{N(r)}}, 0, 0, 0)$ is the observer's four-velocity. The non-zero four-acceleration component is computed as

$$\begin{aligned} a^r &= \Gamma^r_{tt}\left(\frac{dt}{d\tau}\right)^2 \\ &= \frac{M}{r^2}\left\{1 - \tanh\left(\frac{Q^2}{2Mr}\right)\right\} \\ &\quad - \frac{1}{2}\frac{Q^2}{r^3}\cosh^{-2}\left(\frac{Q^2}{2Mr}\right) - \frac{\Lambda r}{3}. \end{aligned} \tag{9}$$

An important condition for traveling through wormhole implies that an observer should not be pushed away by enormous tidal forces which requires the observer's acceleration less than that of Earth's acceleration. It is observed that a wormhole exhibits attractive behavior if its radial acceleration is positive, i.e., $a^r > 0$ while it will have repulsive characteristics for $a^r < 0$. Figure 1 shows the respective plots for attractive and repulsive characteristics of regular ABGB thin-shell wormholes with and without Λ. We observe that regular ABGB thin-shell wormhole will remain attractive for different values of Q which supports the fact that an observer must maintain an outward-directed radial acceleration to avoid gravitational pull by the wormhole. In de Sitter case, we find that the wormhole is attractive for small throat radii while it shows repulsive behavior for larger throat radii. An observer must have an inward directed radial acceleration to keep away from being pushed by the wormhole.

3 Stability analysis

Here, we discuss a particular approach for stability of ABGB thin-shell wormholes through linear perturbations. The surface energy density and surface pressure for static wormhole configuration ($a = a_0$) yield

$$\sigma_0 = -\frac{\sqrt{N(a_0)}}{2\pi a_0}, \qquad p_0 = \frac{1}{4\pi}\left[\frac{\sqrt{N(a_0)}}{a_0} + \frac{N'(a_0)}{2\sqrt{N(a_0)}}\right]. \tag{10}$$

The surface stresses satisfy the conservation equation $S^{ij}_{;j} = 0$ which leads to

$$\frac{d}{d\tau}(\sigma\Delta) + p\frac{d\Delta}{d\tau} = 0, \tag{11}$$

where $\Delta = 4\pi a^2$ corresponds to wormhole throat area. We can formulate thin-shell equation of motion by rearranging Eq. (7) as $\dot{a}^2 + \Phi(a) = 0$, which provides wormhole dynamics while the potential function $\Phi(a)$ is given by

$$\Phi(a) = N(a) - [2\pi a\sigma]^2, \tag{12}$$

here σ represents the perturbed energy density. To discuss wormhole stability, we assume a linear perturbation in the

form of barotropic EoS

$$p = \Psi(\sigma), \tag{13}$$

such that $\Psi(\sigma)$ is taken arbitrarily for the shell which governs the polytropic EoS $p \approx \sigma^{1+\frac{1}{n}}$ as $0 \leq n < \infty$.

The basic condition for stability of wormhole static solution yields $\Phi'(a_0) = 0 = \Phi(a_0)$ and $\Phi''(a_0) > 0$. For this purpose, we use Eq. (13) and $\sigma' = \frac{\dot{\sigma}}{\dot{a}}$ in conservation equation as

$$\sigma' = -\frac{2}{a}(\sigma + \Psi), \tag{14}$$

which takes the form

$$\sigma'' = \frac{2}{a^2}(\sigma + \Psi)\big(3 - a\Psi'\big). \tag{15}$$

The first derivative of Eq. (12) through (14) turns out to be

$$\Phi'(a_0) = N'(a_0) + 8\pi^2 a_0 \sigma_0 \big[\sigma_0 + 2p(\sigma_0)\big], \tag{16}$$

leading to the second derivative of potential function as

$$\Phi''(a_0) = N''(a_0) - 8\pi^2 \big\{[\sigma_0 + 2p_0]^2 + 2\sigma_0[\sigma_0 + p_0]\big[1 + 2\Psi'(\sigma_0)\big]\big\}, \tag{17}$$

where $\Psi_0 = p_0$.

4 Some models for exotic matter

This section deals with stability of thin-shell wormholes from regular charged BH in the vicinity of different models for exotic matter. Here we consider linear, logarithmic and CG fluids to explore the stable behavior of regular ABGB and ABGB-de Sitter thin-shell wormholes. This would help us to investigate the role of charge and cosmological constant on the stability of wormhole configurations. In the following, we study the stability formalism by taking these candidates for exotic matter at the shell.

4.1 Linear gas

We choose a linear gas fluid (Richarte and Simeone 2009) to support the exotic matter at the shell. The EoS for linear gas is defined as

$$\Psi = p_0 + \mu(\sigma - \sigma_0), \tag{18}$$

where μ is a constant parameter. Differentiating this equation with respect to σ, we obtain $\Psi'(\sigma_0) = \mu$. We find that $\Phi(a)$ and $\Phi'(a)$ disappear by inserting the values of $\sigma(a_0)$ and $p(a_0)$. We are interested to explore the possibility of stable wormhole solutions and check the role of increasing charge in stability regions. We choose parameter $\frac{Q}{M} = 0, 0.707, 0.999, 1.1$ and explore stable zones for ABGB thin-shell wormholes in de Sitter background. Figure 2 displays stable regions (red curves) for regular ABGB thin-shell wormholes corresponding to linear gas EoS with $\frac{Q}{M} = 0, 0.5, 0.77, 0.99$. Here $\frac{Q}{M} = 0$ corresponds to the Schwarzschild case. The metric function $N(r)$ is also plotted to estimate the location of event horizon and wormhole throat. We assume $a_0 > r_h$ for the viability of thin-shell wormholes without event horizons. For $a_0 \leq r_h$, no static solution exists leading to non-physical region. We examine stability regions corresponding to positive and negative values of parameter μ. It is found that increasing value of $\frac{Q}{M}$ decreases stability areas for regular ABGB thin-shell wormholes.

We also plot stability regions for regular ABGB thin-shell wormholes coupled with $\Lambda = 0.1$ in de Sitter background. The wormhole throat must have the range $r_h < a_0 < r_c$ for the existence of viable static wormhole solutions, where r_c is the cosmological horizon. The respective results show that stability region for wormhole configurations decreases by increasing charge $\frac{Q}{M}$ (Fig. 3). It is found that more stable wormhole solutions are possible for de Sitter case as compared to the case without Λ.

4.2 Chaplygin gas

Here we consider CG model for which EoS is given by

$$\Psi(\sigma) = p_0 + \mu\left(\frac{1}{\sigma} - \frac{1}{\sigma_0}\right), \tag{19}$$

where $\Psi'(\sigma_0) = -\frac{\mu}{\sigma_0^2}$. Figures 4 and 5 show the results corresponding to regular ABGB and ABGB-de Sitter thin-shell wormholes along with CG model and different values of charge. In both cases, only one stability region is obtained with $\frac{Q}{M} = 0, 0.5$. We examine two stability regions for positive and negative values of parameter μ with $\frac{Q}{M} = 0.77$ while one stable region along with negative values of μ and $\frac{Q}{M} = 0.99$. It is observed that CG provides least stable regions for regular ABGB thin-shell wormholes which supports the fact that CG does not appear significant for stability regions.

4.3 Generalized Chaplygin gas

Now we consider GCG fluid for exotic matter governed by an EoS

$$\Psi(\sigma) = p_0 + \mu\left(\frac{1}{\sigma^\gamma} - \frac{1}{\sigma_0^\gamma}\right), \tag{20}$$

where γ denotes EoS parameter. We explore its role in increasing the stability regions of regular ABGB and ABGB-de Sitter thin-shell wormholes. In this context, we set $\mu =$

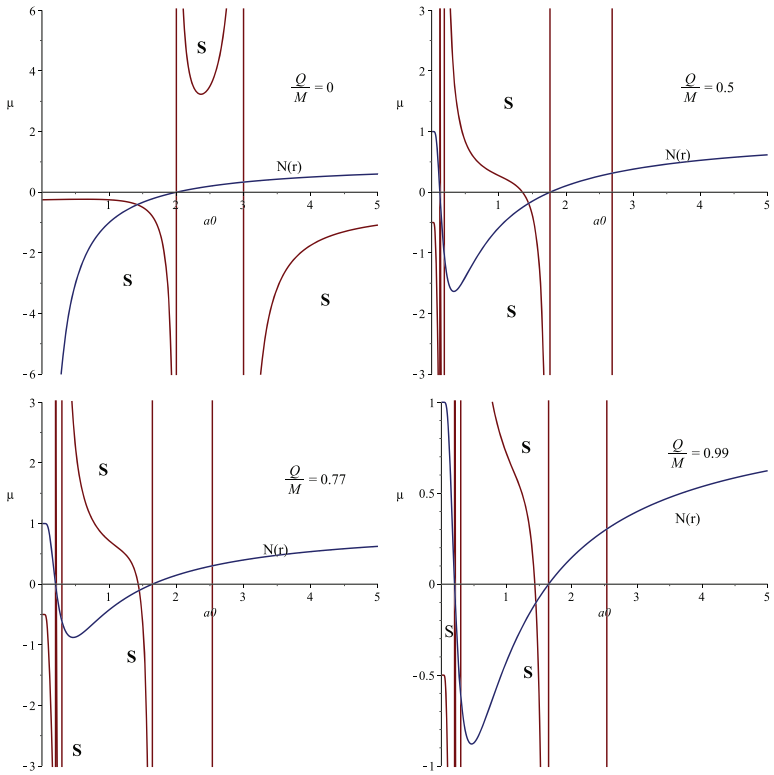

Fig. 2 Plots for regular ABGB thin-shell wormholes corresponding to linear gas EoS with $\frac{Q}{M} = 0, 0.5, 0.77, 0.99$. The stable regions and the metric function are represented by *red* and *blue curves*, respectively

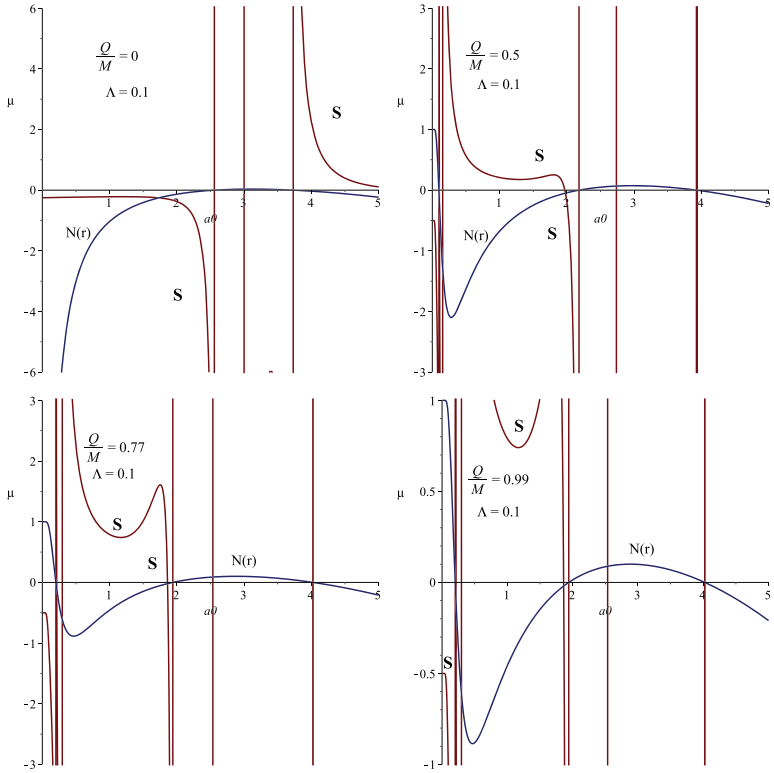

Fig. 3 Plots for regular ABGB thin-shell wormholes corresponding to linear gas EoS in de Sitter background

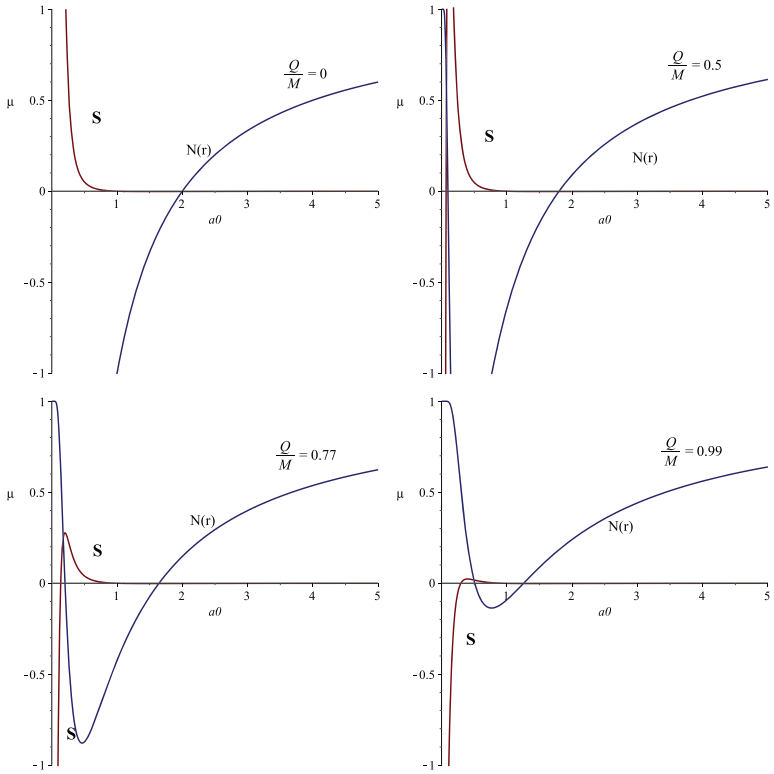

Fig. 4 Plots for regular ABGB thin-shell wormholes by taking CG EoS and $\frac{Q}{M}=0, 0.5, 0.77, 0.99$

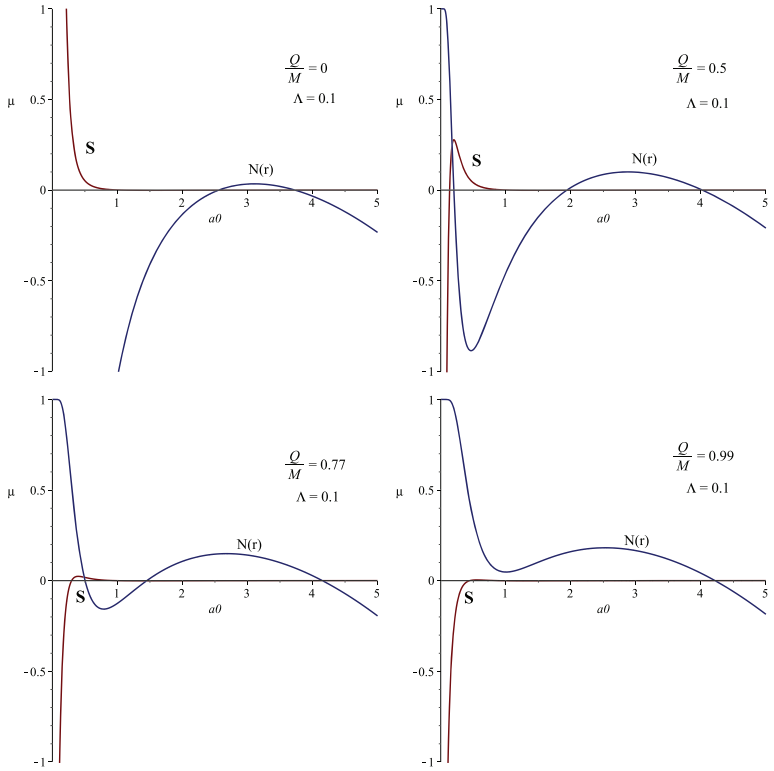

Fig. 5 Plots for regular ABGB thin-shell wormholes for CG EoS in de-Sitter background

$p_0\sigma^\gamma$ such that the above EoS becomes

$$\Psi(\sigma) = p_0\left(\frac{\sigma_0}{\sigma}\right)^\gamma, \tag{21}$$

which yields $\Psi'(\sigma_0) = -\frac{p_0}{\sigma_0}\gamma$. We plot the respective stability regions numerically as shown in Figs. 6 and 7. Here, we find three stability regions for regular ABGB thin-shell wormholes with $\frac{Q}{M} = 0, 0.5, 0.77$. It is noted that these regions decrease gradually by increasing $\frac{Q}{M}$ and reduce to only two stable regions for $\frac{Q}{M} = 0.99$. For regular ABGB-de Sitter configurations ($\Lambda = 0.1$), the stability regions are enlarged but have similar behavior as in the above case. We find that non-physical regions appear with small throat radii.

4.4 Modified generalized Chaplygin gas

The commonly known extension of GCG is called modified generalized Chaplygin gas (MGCG) defined as

$$\Psi(\sigma) = p_0 + \xi_0(\sigma - \sigma_0) - w\left(\frac{1}{\sigma^\gamma} - \frac{1}{\sigma_0^\gamma}\right), \tag{22}$$

where ξ_0 and w are free parameters. Its differentiation yields

$$\Psi'(\sigma_0) = \xi_0 + \frac{w\gamma}{\sigma_0^{\gamma+1}}.$$

Figure 8 shows the corresponding graphs for $\xi_0 = \gamma = 1$ and different values of charge. For MGCG, we find that the possibility of stability regions increases by increasing value of $\frac{Q}{M}$. For $\Lambda = 0.1$, it is observed that the increasing value of $\frac{Q}{M}$ provides more stable wormhole solutions corresponding to both positive and negative values of the parameter w (Fig. 9). It is worth mentioning here that MGCG provides maximum stable regions for wormhole configurations. We investigate that the effect of MGCG is to increase the stability regions for regular ABGB thin-shell wormholes by increasing $\frac{Q}{M}$ as depicted in our numerical plots.

4.5 Logarithmic gas

Finally, we take logarithmic gas defined by the EoS

$$\Psi(\sigma) = p_0 + w\ln\left|\frac{\sigma}{\sigma_0}\right|, \tag{23}$$

where $\Psi'(\sigma_0) = \frac{w}{\sigma_0}$. We plot the corresponding stable ABGB thin-shell wormholes for different values of charge without Λ as shown in Fig. 10. It is found that two stability regions exist for $\frac{Q}{M} = 0, 0.5, 0.77$ and $\xi_0 = \gamma = 1$, $\Lambda = 0.1, -0.5$ which reduce to only one stability region for maximum value of charge, i.e., $\frac{Q}{M} = 1.1$. In case of ABGB-de Sitter configurations, the number of stability region increases by increasing $\frac{Q}{M}$ and reduces to only one region for $\frac{Q}{M} = 1.1$ (Fig. 11). We analyze maximum number of stable regions for $\frac{Q}{M} = 0.5$ in de Sitter background.

5 Stability analysis against velocity perturbations

Here we are interested to investigate the effect of velocity perturbations on stability of regular ABGB thin-shell wormholes. We confine ourselves to small velocity perturbations about static configuration $a = a_0$ such that after any perturbation, an approximately static fluid can be taken for exotic matter. This fact supports the assumption that one can choose a dynamical EoS for wormhole instead of static EoS. For this purpose, we compute the following EoS through Eq. (10) as

$$p = -\frac{1}{2}\left(1 + \frac{aN'(a)}{2N(a)}\right)\sigma. \tag{24}$$

Substituting σ and p from Eqs. (7) and (8), it takes the form

$$\ddot{a} - \frac{N'(a)}{2N(a)}\dot{a} = 0, \tag{25}$$

which represents one-dimensional motion of the wormhole throat. Integration of this equation leads to

$$\dot{a} = \dot{a}_0\frac{\sqrt{N(a)}}{\sqrt{N(a_0)}}, \tag{26}$$

whose second integration gives

$$\frac{\dot{a}_0}{\sqrt{N(a_0)}}(\tau - \tau_0) = \int_{a_0}^{a}\frac{da}{\sqrt{N(a)}}. \tag{27}$$

Here $\dot{a}_0$ is considered to be non-zero initial small velocity of throat after perturbation. For regular ABGB spacetime, Eq. (27) upto the second order of small values of Q yields

$$\begin{aligned}&\frac{\dot{a}_0}{\sqrt{N(a_0)}}(\tau - \tau_0)\\ &= \frac{a(a-2M)+Q^2}{a\sqrt{N(a)}} - \frac{a_0(a_0-2M)+Q^2}{a_0\sqrt{N(a_0)}}\\ &\quad + M\ln\left(\frac{a - M + a\sqrt{N(a)}}{a_0 - M + a_0\sqrt{N(a_0)}}\right),\end{aligned} \tag{28}$$

which indicates that this motion is clearly not oscillatory. Consequently, the ABGB wormhole throat remains unstable against velocity perturbations. Equation (25) also shows that acceleration of the wormhole throat $\ddot{a} = \frac{N'(a)}{2N(a)}\dot{a}$ is positive leading to unstable ABGB thin-shell wormholes.

6 Conclusions

In this paper, we have constructed regular ABGB thin-shell wormholes with and without Λ by incorporating the effects of nonlinear electrodynamics. The surface stresses

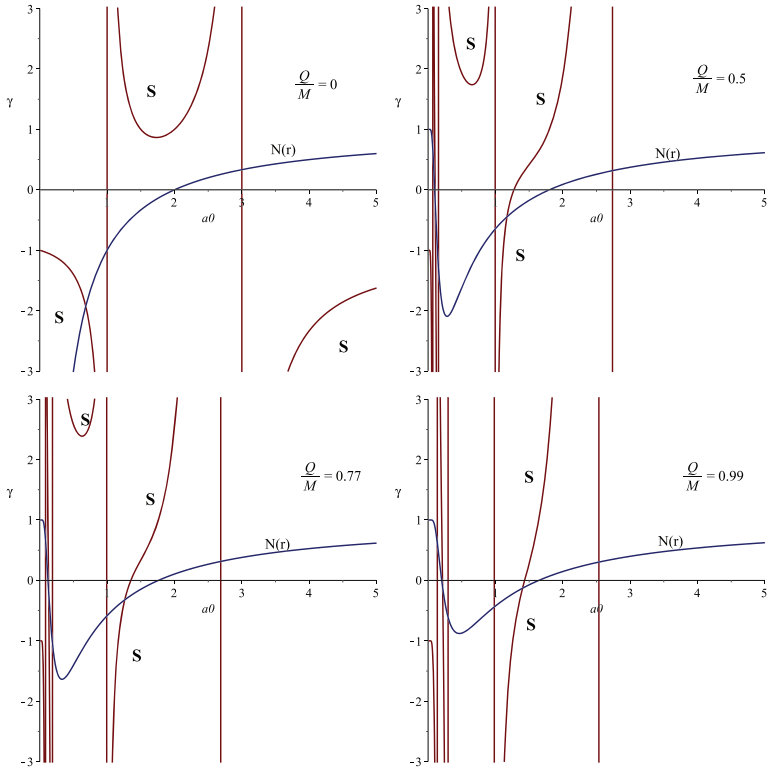

Fig. 6 Plots for stability of regular ABGB thin-shell wormholes in terms of γ by taking GCG and $\frac{Q}{M} = 0, 0.5, 0.77, 0.99$

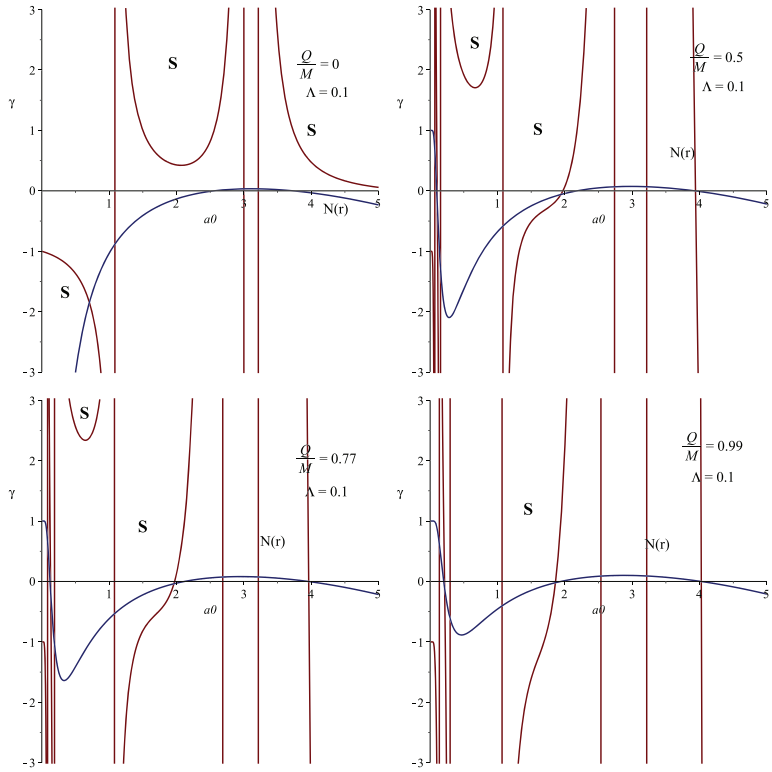

Fig. 7 Plots for the stability of regular ABGB thin-shell wormholes in terms of γ by taking GCG gas and $\Lambda = 0.1$

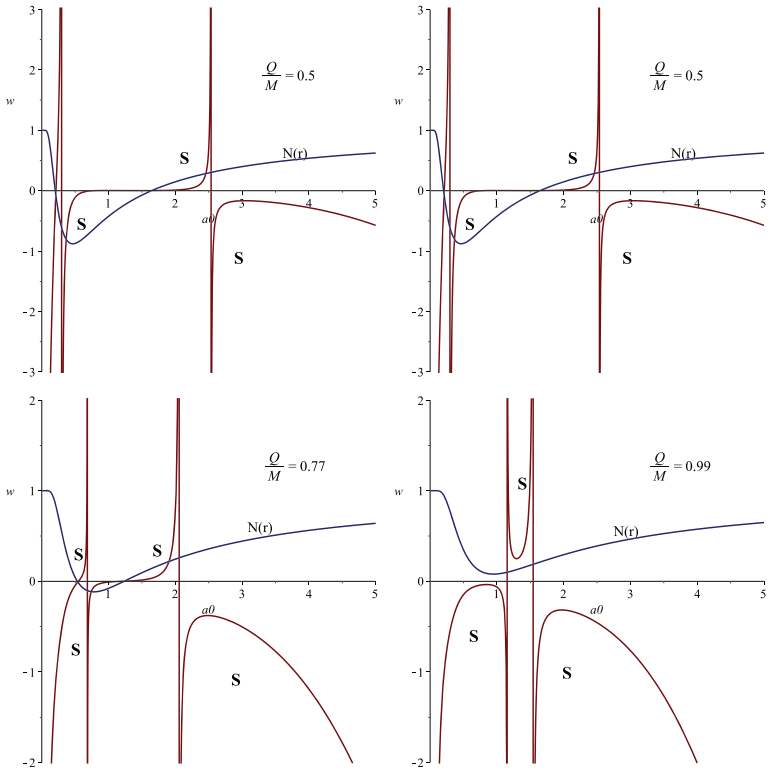

Fig. 8 Plots for stable regular ABGB thin-shell wormholes in the context of MGCG gas with $\xi_0 = \gamma = 1$ and different values of charge

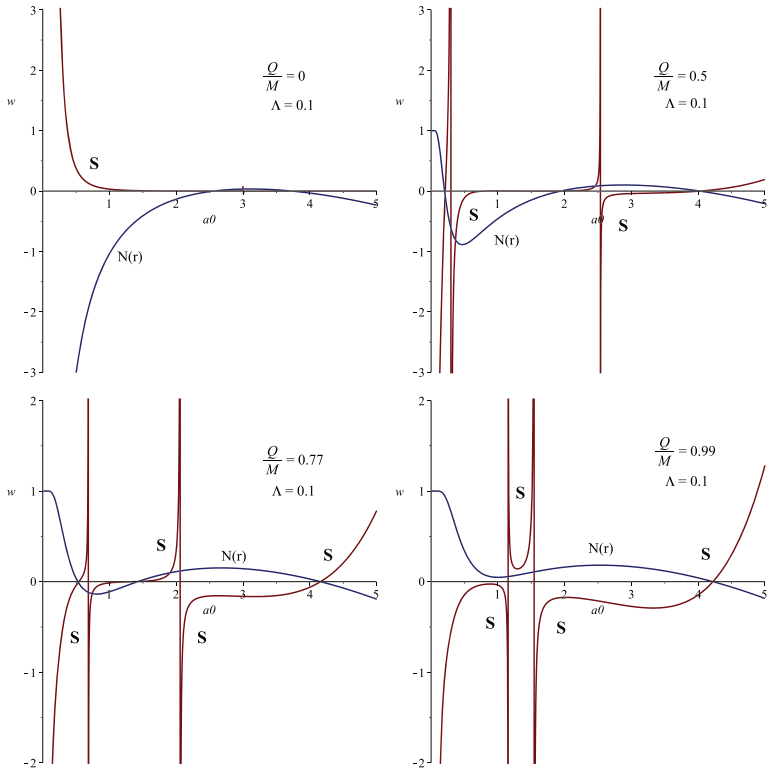

Fig. 9 Plots for stability regions of regular ABGB thin-shell wormholes by taking MGCG gas with $\xi_0 = \gamma = 1$ and different values of charge in de Sitter background

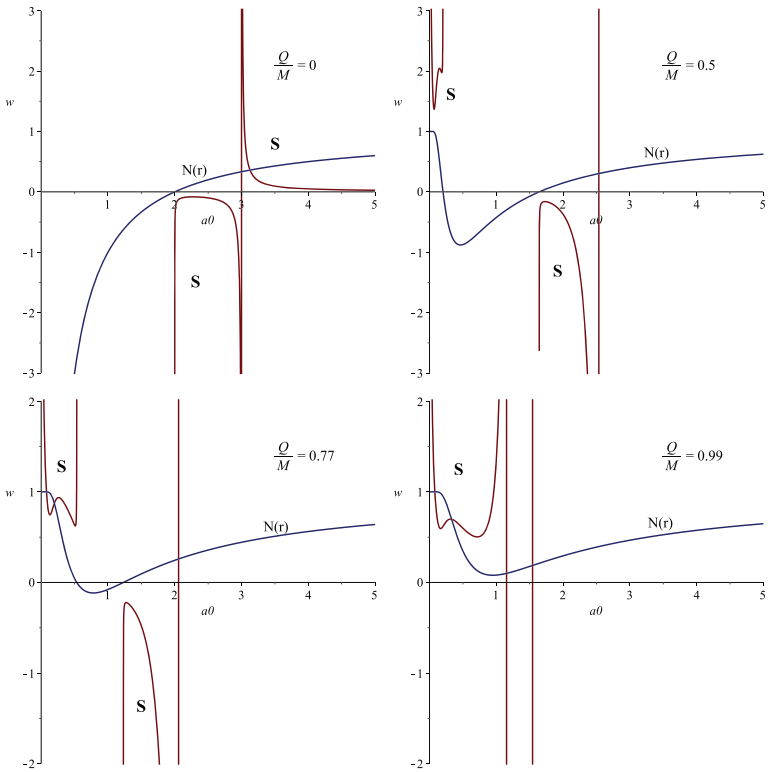

Fig. 10 Plots for regular ABGB thin-shell wormholes by taking logarithmic gas EoS for $\frac{Q}{M} = 0, 0.5, 0.77, 0.99$

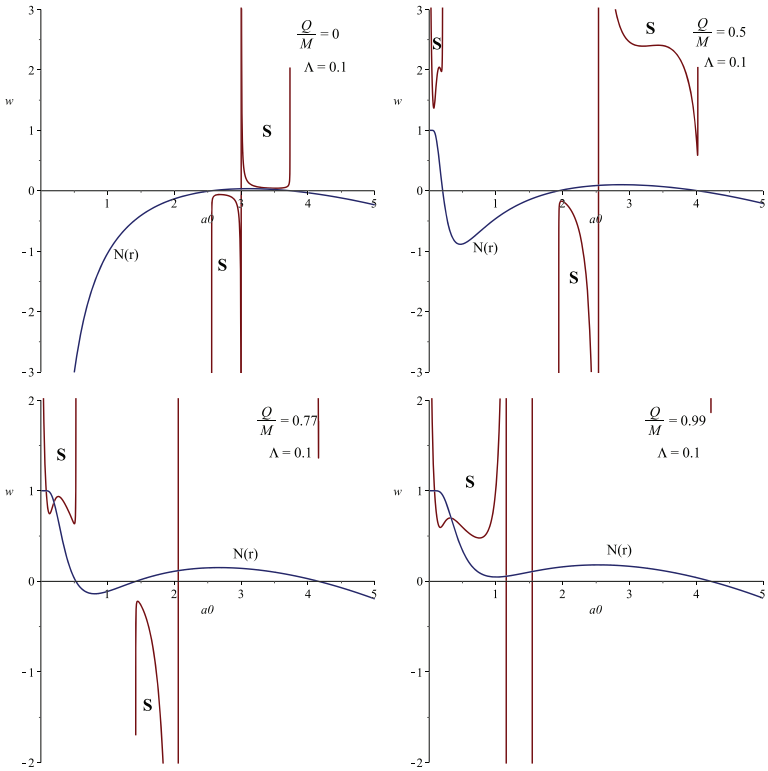

Fig. 11 Plots for regular ABGB thin-shell wormholes by taking logarithmic gas EoS with $\frac{Q}{M} = 0, 0.5, 0.77, 0.99$ and $\Lambda = 0.1$

have been computed by using Lanczos equation which indicate the violation of null energy condition leading to the existence of exotic matter. We have analyzed the attractive and repulsive behavior of thin-shell wormholes corresponding to $a^r > 0$ and $a^r < 0$, respectively. It is found that thin-shell wormhole remains attractive for $\Lambda = 0$ while it shows both attractive and repulsive characteristics for different throat radii in de Sitter background. We have chosen $r_h < a_0 < r_c$ to avoid the existence of event horizons for viability of wormhole configurations. We have taken a general EoS $p = \Psi(\sigma)$ as a linear perturbation and discussed stability conditions graphically for $\Phi'' > 0$.

In order to explore any realistic candidate of dark energy for viable wormhole solutions, we have considered linear gas, logarithmic gas and three different CG gas models for exotic matter. It is observed that one may construct a traversable wormhole theoretically with arbitrarily small amount of the fluid describing cosmic expansion. We have found that stable regions exist within a physically acceptable range of charge and other parameters for all models (Figs. 2–11). We have also plotted the metric function $N(r)$ to estimate the location of event horizon and wormhole throat. It is found that increasing value of $\frac{Q}{M}$ decreases stable zones for regular ABGB thin-shell wormholes by taking linear gas EoS. For CG, we have analyzed only one stability region for smaller values of $\frac{Q}{M}$ which seems to provide least stable solutions than the other models and does not appear significant for stability regions.

There exist three stability regions for regular ABGB thin-shell wormholes with GCG gas which decrease gradually by increasing $\frac{Q}{M}$ and reduce to only two stable regions for $\frac{Q}{M} = 0.99$. We have investigated non-physical regions for small throat radii and stability regions become enlarged for de Sitter configurations but have similar behavior as in the above case. For MGCG, the possibility of stability regions increases by increasing the value of $\frac{Q}{M}$ in both cases with and without Λ. It is worth mentioning here that MGCG has remarkable significance as it provides maximum stable regions for wormhole configurations which are more viable as compared to that of GCG. We have found that the effect of logarithmic gas is to increase the stability regions for regular ABGB-de Sitter thin-shell wormholes by increasing $\frac{Q}{M}$. We observe that there exist more stability regions for de Sitter case as compared to the general case without Λ. We have also studied small velocity dependent perturbations and found that ABGB wormhole configurations remain no more stable under these perturbations. We conclude that stable regions may expand or shrink accordingly depending on the tuning of charge and other parameters.

References

Ayon-Beato, E., Garcia, A.: Phys. Rev. Lett. **80**, 5056 (1998)
Bardeen, J.M.: Non-singular general relativistic gravitational collapse. In: Proc. International Conference GR5, Tbilisi, USSR (1968)
Bronnikov, K.A.: Phys. Rev. D **63**, 044005 (2001)
Eiroa, E.F.: Phys. Rev. D **80**, 044033 (2009)
Eiroa, E.F., Romero, G.E.: Gen. Relativ. Gravit. **36**, 651 (2004)
Halilsoy, M., Ovgun, A., Mazharimousavi, S.H.: Eur. Phys. J. C **74**, 2796 (2014)
Hawking, S.W., Ellis, G.F.R.: The Large Scale Structure of Spacetime. Cambridge University Press, Cambridge (1975)
Hayward, S.A.: Phys. Rev. Lett. **96**, 031103 (2006)
Israel, W.: Nuovo Cimento B **44S10**, 1 (1966)
Kim, S.W., Lee, H.: Phys. Rev. D **63**, 064014 (2001)
Lobo, F.S.N., Crawford, P.: Class. Quantum Gravity **21**, 391 (2004)
Matyjasek, J., Tryniecki, D., Klimek, M.: Mod. Phys. Lett. A **23**, 3377 (2008)
Mazharimousavi, S.H., Halilsoy, M.: Eur. Phys. J. C **74**, 3073 (2014)
Morris, M., Thorne, K.: Am. J. Phys. **56**, 395 (1988)
Richarte, M.G., Simeone, C.: Phys. Rev. D **80**, 104033 (2009)
Sharif, M., Azam, M.: Eur. Phys. J. C **73**, 2554 (2013a)
Sharif, M., Azam, M.: J. Cosmol. Astropart. Phys. **05**, 025 (2013b)
Sharif, M., Mumtaz, S.: Adv. High Energy Phys. **2014**, 13 (2014a)
Sharif, M., Mumtaz, S.: Astrophys. Space Sci. **352**, 729 (2014b)
Sharif, M., Mumtaz, S.: Can. J. Phys. **93**, 12 (2015)
Sharif, M., Mumtaz, S.: arXiv:1602.01434 (2016a)
Sharif, M., Mumtaz, S.: arXiv:1604.01012 (2016b)
Visser, M.: Phys. Rev. D **39**, 3182 (1989)

International Journal of Modern Physics D
Vol. 26, No. 5 (2017) 1741007 (14 pages)

DOI: 10.1142/S0218271817410073

World Scientific
www.worldscientific.com

Dynamics of thin-shell wormholes with different cosmological models

Muhammad Sharif* and Saadia Mumtaz†

Department of Mathematics, University of the Punjab, Quaid-e-Azam Campus, Lahore-54590, Pakistan
**msharif.math@pu.edu.pk*
†*sadiamumtaz17@gmail.com*

Received 29 September 2016
Accepted 20 October 2016
Published 22 March 2017

This work is devoted to investigate the stability of thin-shell wormholes in Einstein–Hoffmann–Born–Infeld electrodynamics. We also study the attractive and repulsive characteristics of these configurations. A general equation-of-state is considered in the form of linear perturbation which explores the stability of the respective wormhole solutions. We assume Chaplygin, linear and logarithmic gas models to study exotic matter at thin-shell and evaluate stability regions for different values of the involved parameters. It is concluded that the Hoffmann–Born–Infeld parameter and electric charge enhance the stability regions.

Keywords: Thin-shell wormholes; stability; nonlinear electrodynamics.

PACS Number(s): 04.20.−q, 04.70.Bw

1. Introduction

In the last few decades, physicists have paid much attention to the wormhole dynamics due to its interesting features. Traversable wormholes are the hypothetical objects which are characterized by a throat associating different remote areas of the universe through a shortcut.[1] Besides the lack of physical significance, wormholes were assumed to be interconvertible with black holes family leading to nontraversable wormholes.[2] The Einstein–Rosen bridge is the best fitted example of nontraversable wormhole whose throat shrinks and hence collapses due to the presence of event horizon.[3]

The wormhole throat must fulfill the flare-out condition where its geometry opens up. In the case of traversable wormholes, the throat is threaded by a fluid that violates the null energy condition known as exotic matter. This matter makes the wormhole traversable such that an observer requires much less time as compared to that of normal traveling without any hindrance. It is suggested that a small amount

of this matter is required for the physical viability of wormhole configurations. Visser[4] illustrated an efficient technique to minimize the unavoidable amount of exotic matter such that a traveler does not observe any tidal force during its trip through wormhole. This matter is restricted at the edges of wormhole throat. Israel thin-shell formalism is the most useful way to compute pressure and energy density identifying exotic matter at the shell.[5]

The stability of thin-shell wormholes (TSWs) can be performed either by implementing linear perturbations or via equation-of-state (EoS) for exotic matter. In this context, Kim and Lee[6] studied stability of spherically symmetric wormhole configurations in the presence of increasing charge. Eiroa and Romero[7] investigated stable Reissner–Nordström TSWs whose stability increases by increasing the electric charge. Many authors have discussed the stability of TSWs by taking different candidates of dark energy for exotic matter. Eiroa and Simeone[8] analyzed stable spherically symmetric wormhole solutions with and without charge by taking Chaplygin gas (CG). Sharif and his collaborators[9] studied the role of van der Waals quintessence and different CG EoS on the stability of both spherical and cylindrical TSWs.

Nonlinear electrodynamics (NED) is the generalization of Maxwell theory which is considered as the most viable theory to remove singularity of classical charged particles. Born and Infeld[10] introduced NED to avoid divergence of the field in Maxwell theory. Hoffmann[11] described gravitational field of a charged spherically symmetric solution by coupling general relativity (GR) with Born–Infeld electrodynamics which defines a black hole. NED has attained great interest in the wormhole construction. Eiroa and Aguirre[12] analyzed the stability of spherical TSWs in Born–Infeld theory for generalized CG. Sharif and Azam[13] found stable TSWs for large values of Born–Infeld parameter by taking modified CG. We have explored the effects of NED on stability of regular TSWs and found stable solutions.[14]

In this paper, we study the stability of TSWs by considering different dark energy models. The paper has the following format. In Sec. 2, we discuss the construction of TSWs coupled with Einstein–Hoffmann–Born–Infeld (HBI) theory and study various physical aspects. Section 3 provides stability of the respective wormhole configurations in the context of CG, linear and logarithmic gas models. Finally, we conclude our results in the last section.

2. Einstein–Hoffman–Born–Infeld Electrodynamics and TSWs

It is well-known that singularity of any charged particle leads to infinite self-electromagnetic energy which should be removed from classical charged particles. NED with various compositions has restorative effects on the divergent results that appear naturally in linear Maxwell theory. In this context, Born and Infeld[10] proposed the most prominent constituent of viable NED theories to resolve this problem upto some extent. However, this theory has some drawbacks that are not completely eliminated.

To overcome this specific issue, Hoffman and Infeld[15] proposed a Lagrangian having a logarithmic term with significant consequences which removed the singularity arising in the Cartesian components of the electric field E. Mazharimousavi *et al.*[16] rediscovered the global logarithmic term of Lagrangian in Einstein NED theory. They used HBI Lagrangian in both GR as well as Gauss–Bonnet gravity to construct black holes and TSWs.[16,17] Motivated by this proposal, we examine the role of HBI electrodynamics on the stability of $4D$ TSWs in the framework of GR. We consider Einstein HBI Lagrangian

$$\mathcal{L}(F) = \begin{cases} \mathcal{L}_+ = -\dfrac{2}{b^2}(k + \beta\xi_+ - \ln \xi_+), & r \geq \sqrt{qb}, \\ \mathcal{L}_- = -\dfrac{2}{b^2}(k + \beta\xi_- - \ln |\xi_-|), & r \leq \sqrt{qb}, \end{cases} \tag{1}$$

in which $\beta = 1$, $k = \ln 2 - 2$ and $\xi_\pm = 1 \pm \sqrt{1 + 2b^2 F}$, where b is the constant HBI parameter, F is the trace of electromagnetic field tensor and q is the constant charge. This Lagrangian imposes $\mathcal{L}_+ = \mathcal{L}_-$ at $r^4 = q^2 b^2$. The coupling of GR with HBI electrodynamics leads to intriguing features that make it worth while to apply on strong electromagnetic and gravitational fields. The coupling of Einstein gravity with $4D$ HBI electrodynamics is defined by the action

$$S = \frac{1}{2}\int \sqrt{-g}[R + \mathcal{L}(F)]d^4x. \tag{2}$$

The static electrically charged spherically symmetric black hole in HBI theory is given by

$$ds^2 = -F(r)dt^2 + F^{-1}(r)dr^2 + r^2(d\theta^2 + \sin^2\theta d\phi^2), \tag{3}$$

where

$$F(r) = 1 - \frac{2m}{r} + \frac{r^2q^2}{3q^2b^2}\ln\left(\frac{r^4}{r^4 + q^2b^2}\right) - \frac{q^2\sqrt{2}}{3r\sqrt{qb}}\left[\tan^{-1}\left(\frac{r\sqrt{2}}{\sqrt{qb}} + 1\right) + \tan^{-1}\left(\frac{r\sqrt{2}}{\sqrt{qb}} - 1\right)\right] - \frac{q^2\sqrt{2}}{6r\sqrt{qb}}\ln\left(\frac{r^2 + qb - r\sqrt{2qb}}{r^2 + qb + r\sqrt{2qb}}\right) + \frac{q^2\pi\sqrt{2}}{3r\sqrt{qb}}, \tag{4}$$

m is the mass of HBI solution. The horizons of the spacetime can be found numerically by taking $F(r) = 0$. Here, one can easily find that the given line element reduces to Reissner–Nordström and Schwarzschild spacetimes in the limit $b \to 0$ and $b \to \infty$, respectively.

The mathematical construction of TSWs follows the usual steps of cut and paste technique. For this purpose, we take two copies of HBI spacetimes such that we cut the interior region with $r \leq a$ from each geometry given by $\mathcal{M}^{1,2} = \{x^\mu_{1,2} : r_{1,2} \leq a \,|\, a > \sqrt{qb}\}$, where we assume $a > r_h$ to avoid the presence of singularities. These $4D$ copies are pasted at the hypersurface such that we obtain a new geodesically complete manifold $\mathcal{M} = \mathcal{M}^1 \cup \mathcal{M}^2$. The flare-out condition must be satisfied by

the wormhole throat because the surface area $4\pi r^2$ becomes minimal when $r = a$ representing a wormhole with two regions connected by throat a. We adopt a time like induced metric with coordinates $\xi^i = (\tau, \theta, \phi)$ at thin-shell defined by

$$ds^2 = -d\tau^2 + a^2(\tau)(d\theta^2 + \sin^2\theta d\phi^2), \tag{5}$$

where τ is the proper time. The unit four-vector normals to $\mathcal{M}^{1,2}$ are computed as

$$n_\alpha^{1,2} = \pm\left|g^{\mu\nu}\frac{\partial\eta}{\partial x^\mu}\frac{\partial\eta}{\partial x^\nu}\right|^{-\frac{1}{2}}\frac{\partial\eta}{\partial x^\alpha} = \left(-\dot{a}, \frac{\sqrt{F(r)+\dot{a}^2}}{F(r)}, 0, 0\right), \tag{6}$$

which satisfy the relation $n^\alpha n_\alpha = \epsilon = 1$. In order to study the dynamical evolution, we apply Israel formalism which yields matching of two spacetime regions. The surface stresses are computed by employing Lanczos equation defined as

$$S_j^i = \frac{1}{8\pi}\{[K]\delta_j^i - [K_j^i]\}, \tag{7}$$

where $[K_j^i]$ is the extrinsic curvature whose nontrivial components are given by

$$K_{\tau\tau}^{1,2} = \mp\frac{F'(a) + 2\ddot{a}}{2\sqrt{F(a)+\dot{a}^2}}, \quad K_{\theta\theta}^{1,2} = \pm a\sqrt{F(a)+\dot{a}^2}, \quad K_{\phi\phi}^{1,2} = \alpha^2 K_{\theta\theta}^{1,2}, \tag{8}$$

dot and prime show differentiation w.r.t. $\frac{d}{d\tau}$ and $\frac{d}{dr}$, respectively. The surface stresses at shell are obtained by using Eq. (8) in Lanczos equation which yields

$$\sigma = -\frac{1}{2\pi a}\sqrt{F(a)+\dot{a}^2}, \quad p = \frac{1}{4\pi}\left[\frac{\sqrt{F(a)+\dot{a}^2}}{a} + \frac{2\ddot{a} + F'(a)}{2\sqrt{F(a)+\dot{a}^2}}\right]. \tag{9}$$

These equations give rise to the violation of null and weak energy conditions at the shell and hence indicate the presence of exotic matter which should be reduced for viable TSWs.

It would be interesting to investigate whether the respective wormhole configurations show attractive or repulsive behavior. For this purpose, we need to compute observer's four-acceleration given by

$$a^\mu = u^\mu_{;\nu}u^\nu,$$

where $u^\mu = \frac{dx^\mu}{d\tau} = (\frac{1}{\sqrt{F(r)}}, 0, 0, 0)$ is the observer's four-velocity. We determine the nonzero radial four-acceleration's component as

$$a^r = \frac{m}{r^2} + \frac{r}{3b^2}\ln\left(\frac{r^4}{r^4+q^2b^2}\right) + \frac{2(r^4+q^2b^2)}{3r^2b^2}\left(\frac{r^3}{r^4} - \frac{r^7}{(r^4+q^2b^2)^2}\right)$$
$$+ \frac{q^2}{3r^2\sqrt{2qb}}\left[\tan^{-1}\left(\frac{r\sqrt{2}}{\sqrt{qb}}+1\right) + \tan^{-1}\left(\frac{r\sqrt{2}}{\sqrt{qb}}-1\right)\right]$$

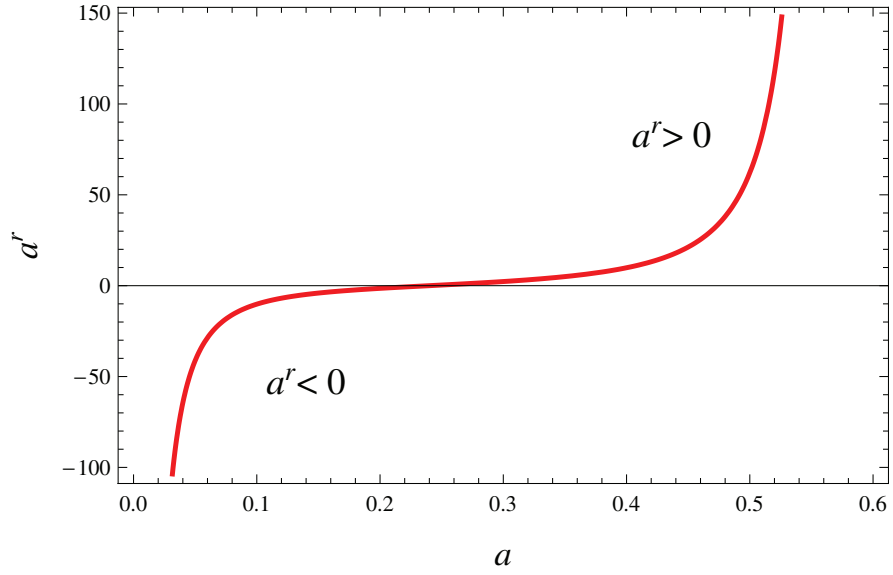

Fig. 1. Plot of a^r for $\frac{q}{m} = 1.1$ and $b = 0.6$.

$$+\frac{q^2}{3rqb}\left[\frac{1+\tan\left(\frac{r\sqrt{2}}{\sqrt{qb}}+1\right)^2}{\tan\left(\frac{r\sqrt{2}}{\sqrt{qb}}+1\right)^2}+\frac{1+\tan\left(\frac{r\sqrt{2}}{\sqrt{qb}}-1\right)^2}{\tan\left(\frac{r\sqrt{2}}{\sqrt{qb}}-1\right)^2}\right]$$
$$+\frac{q^2}{6r^2\sqrt{2qb}}\ln\left(\frac{r^2+qb-r\sqrt{2qb}}{r^2+qb+r\sqrt{2qb}}\right)-\frac{q^2(r^2+qb+r\sqrt{2qb})}{6r\sqrt{2qb}(r^2+qb-r\sqrt{2qb})}$$
$$\times\left(\frac{2r-\sqrt{2qb}}{r^2+qb+r\sqrt{2qb}}-\frac{(2r+\sqrt{2qb})(r^2+qb-r\sqrt{2qb})}{(r^2+qb+r\sqrt{2qb})^2}\right)-\frac{q^2\pi}{3r^2\sqrt{2qb}}. \quad (10)$$

The respective results for TSWs coupled with HBI electrodynamics are shown in Fig. 1. It is noted that a wormhole has attractive or repulsive features if $a^r > 0$ or $a^r < 0$, respectively. We find that the constructed wormhole configurations have repulsive behavior for smaller throat radius which will become attractive on increasing throat radius.

3. General Approach for Stability

Here we discuss standard conditions to study stability of the constructed TSWs under linear perturbations. The energy density and pressure of wormhole solutions under static background ($a = a_0$) yield

$$\sigma_0 = -\frac{\sqrt{F(a_0)}}{2\pi a_0}, \quad p_0 = \frac{1}{4\pi}\left[\frac{\sqrt{F(a_0)}+}{a_0}+\frac{F'(a_0)}{2\sqrt{F(a_0)}}\right]. \quad (11)$$

We are interested to explore wormhole stability by taking barotropic EoS as a linear perturbation in the form

$$p = \Theta(\sigma), \tag{12}$$

which takes the form of polytropic EoS $p \approx \sigma^{1+\frac{1}{n}}$ with $0 \leq n < \infty$, where $\Theta(\sigma)$ is chosen arbitrarily. The surface stresses must obey the conservation identity $S^{ij}_{;j} = 0$ which, for the induced metric (5), turns out to be

$$\frac{d}{d\tau}(\sigma\Phi) + p\frac{d\Phi}{d\tau} = 0, \tag{13}$$

where $\Phi = 4\pi a^2$ shows throat's area. The thin-shell equation of motion describing wormhole dynamics can be determined from Eq. (9) as $\dot{a}^2 + G(a) = 0$, where $G(a)$ is the potential function defined by

$$G(a) = F(a) - [2\pi a\sigma]^2. \tag{14}$$

The wormhole will be stable if the potential function satisfies the conditions $G'(a_0) = 0 = G(a_0)$ and $G''(a_0) > 0$. The conservation equation through Eq. (12) and $\sigma' = \frac{\dot{\sigma}}{\dot{a}}$ leads to

$$\sigma' = -\frac{2}{a}(\sigma + \Theta), \tag{15}$$

whose second derivative takes the form

$$\sigma'' = \frac{2}{a^2}(\sigma + \Theta)(3 - a\Theta'). \tag{16}$$

Differentiation of Eq. (14) through (15) yields

$$G'(a_0) = G'(a_0) + 8\pi^2 a_0\sigma_0[\sigma_0 + 2p(\sigma_0)], \tag{17}$$

which further becomes

$$G''(a_0) = G''(a_0) - 8\pi^2\{[\sigma_0 + 2p_0]^2 + 2\sigma_0[\sigma_0 + p_0][1 + 2\Theta'(\sigma_0)]\}, \tag{18}$$

where $\Theta_0 = p_0$.

It is well-known that the choice of any cosmological model for exotic matter has significant relevance in dynamical investigation of wormhole configurations. Here we study stability of TSWs in the vicinity of different dark energy candidates. In a recent work, the stability of regular TSWs has been analyzed for linear, logarithmic and three CG models at the wormhole throat.[18] In the following, we consider three of the above-mentioned models to explore stability of HBI TSWs.

3.1. *Chaplygin gas*

First we consider CG model governed by the following EoS

$$\Theta(\sigma) = p_0 + \gamma\left(\frac{1}{\sigma} - \frac{1}{\sigma_0}\right), \tag{19}$$

where γ is a constant parameter. The first derivative of this equation w.r.t. σ gives $\Theta'(\sigma_0) = -\frac{\gamma}{\sigma_0^2}$. It is observed that $G(a)$ and $G'(a)$ vanish by substituting $\sigma(a_0)$ and

$p(a_0)$. We explore the role of increasing values of charge as well as HBI parameter in the wormhole stability. We also plot the metric function $F(r)$ to find the position of event horizon and the wormhole throat. The corresponding results for the wormhole stability are shown in Figs. 2 and 3.

For $\frac{q}{m} = 0.5, 0.7$ and $b = 0.6$, we find one stable region (red curve) for both positive as well as negative values of parameter γ while the metric function $F(r)$ cuts the radial axis once showing an event horizon. It is mentioned here that $\frac{q}{m} = 1.1$ provides only one stable region for negative values of parameter γ in the absence of event horizon (Fig. 2). For $b = 1$, we analyze enlargement in the stability areas (two regions) for both positive and negative values of γ corresponding to $\frac{q}{m} = 0.5, 0.7, 0.9$. In this case, we observe that the event horizon does not vanish for

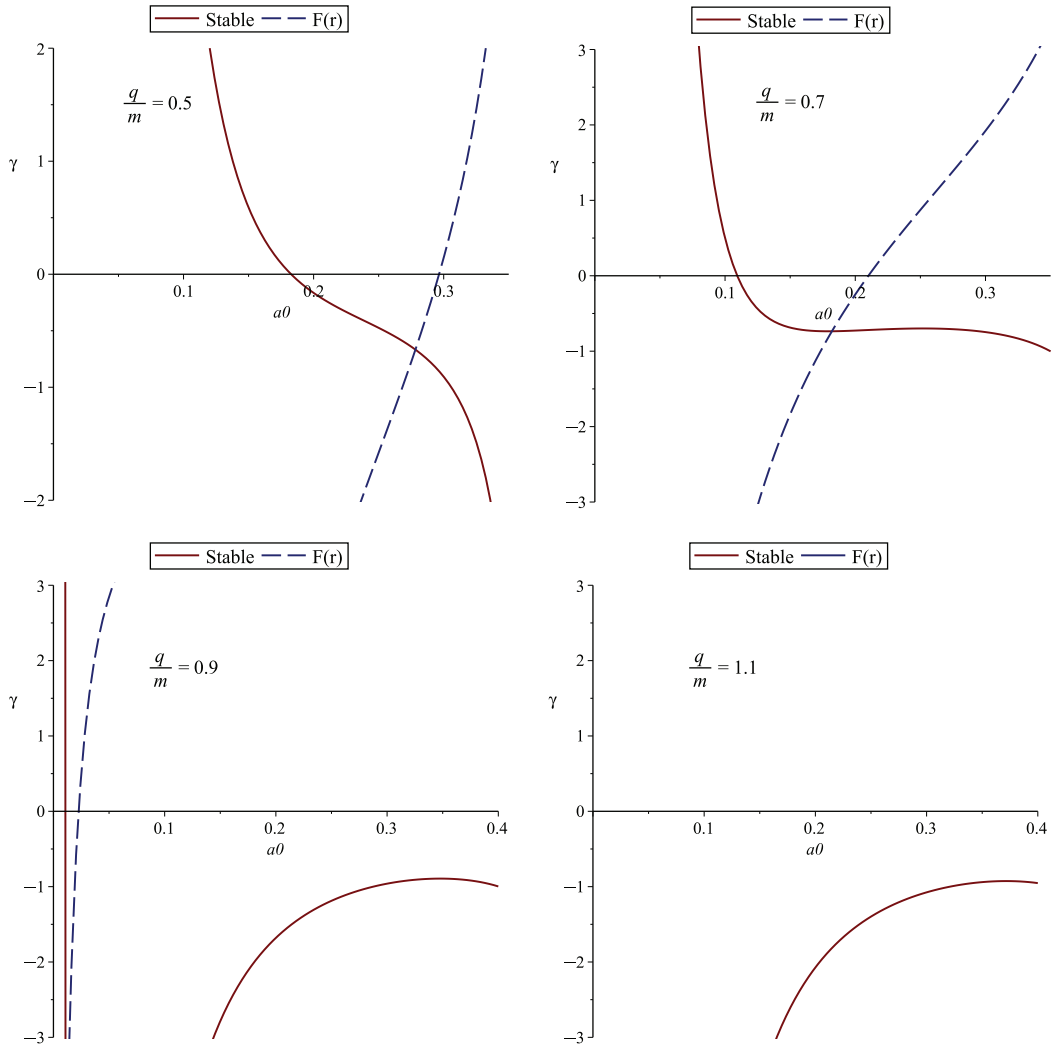

Fig. 2. (Color online) Plots for stable regions of TSWs taking CG EoS and HBI parameter $b = 0.6$ with different values of charge. We choose throat radius a_0 and parameter γ along abscissa and ordinate, respectively.

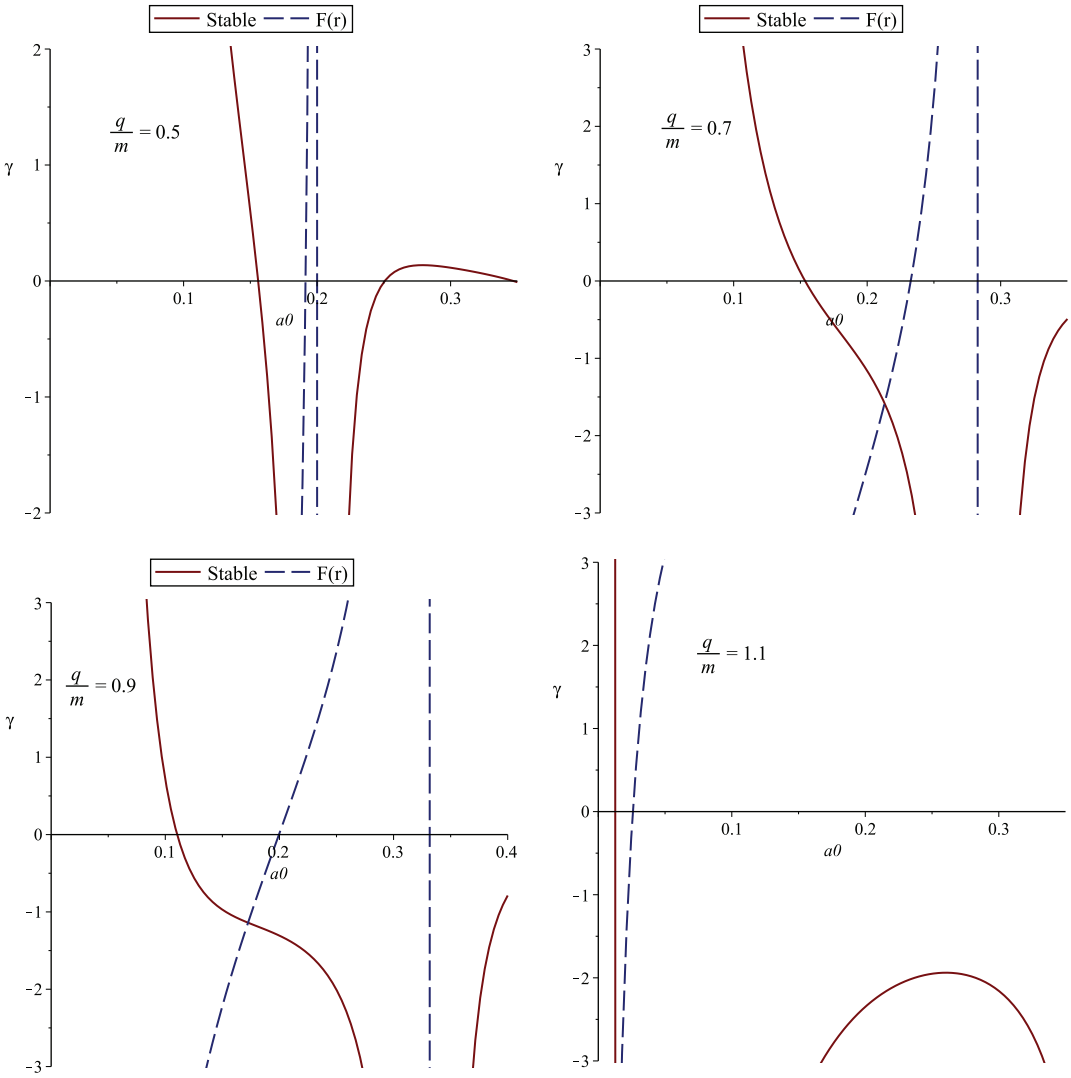

Fig. 3. Plots for stable wormholes with CG EoS, $b = 1$ and different values of charge.

$\frac{q}{m} = 1.1$ but reduces to one (Fig. 3). The HBI parameter is effective to increase the wormhole stability for CG model while the increasing values of the charge $\frac{q}{m}$ tend to diminish the presence of event horizon.

3.2. *Linear gas*

Here we take linear gas model given by the following EoS

$$\Theta = p_0 + \gamma(\sigma - \sigma_0), \tag{20}$$

where $\Theta'(\sigma_0) = \gamma$. We plot stable solutions for linear gas corresponding to $b = 0.6$ as shown in Fig. 4. The event horizon gets smaller by enlarging the values of charge and finally vanishes for the maximum value of $\frac{q}{m}$. The possibility of stability regions

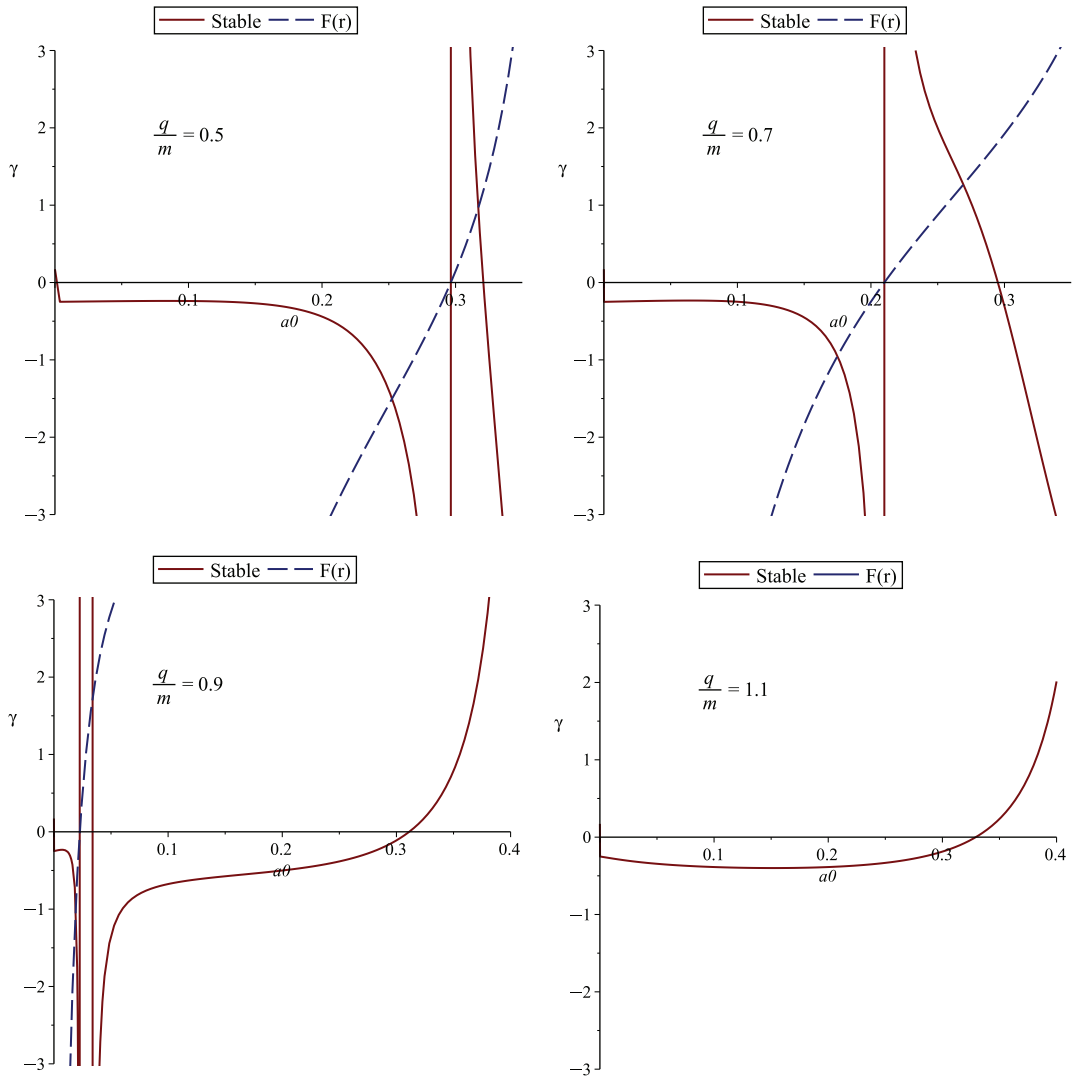

Fig. 4. Plots for stability of TSWs with linear gas and HBI parameter $b = 0.6$.

increases by increasing HBI parameter such that we find maximum stability regions for $b = 1$. We investigate stable regions for both positive as well as negative values of γ with $\frac{q}{m} = 0.5,\ 0.7$ while stable regions exist only for negative values of γ corresponding to large values of charge. The event horizon does not vanish for maximum value of charge (Fig. 5).

3.3. *Logarithmic gas*

The logarithmic gas is defined by

$$\Theta(\sigma) = p_0 + \mu \ln \left| \frac{\sigma}{\sigma_0} \right|, \tag{21}$$

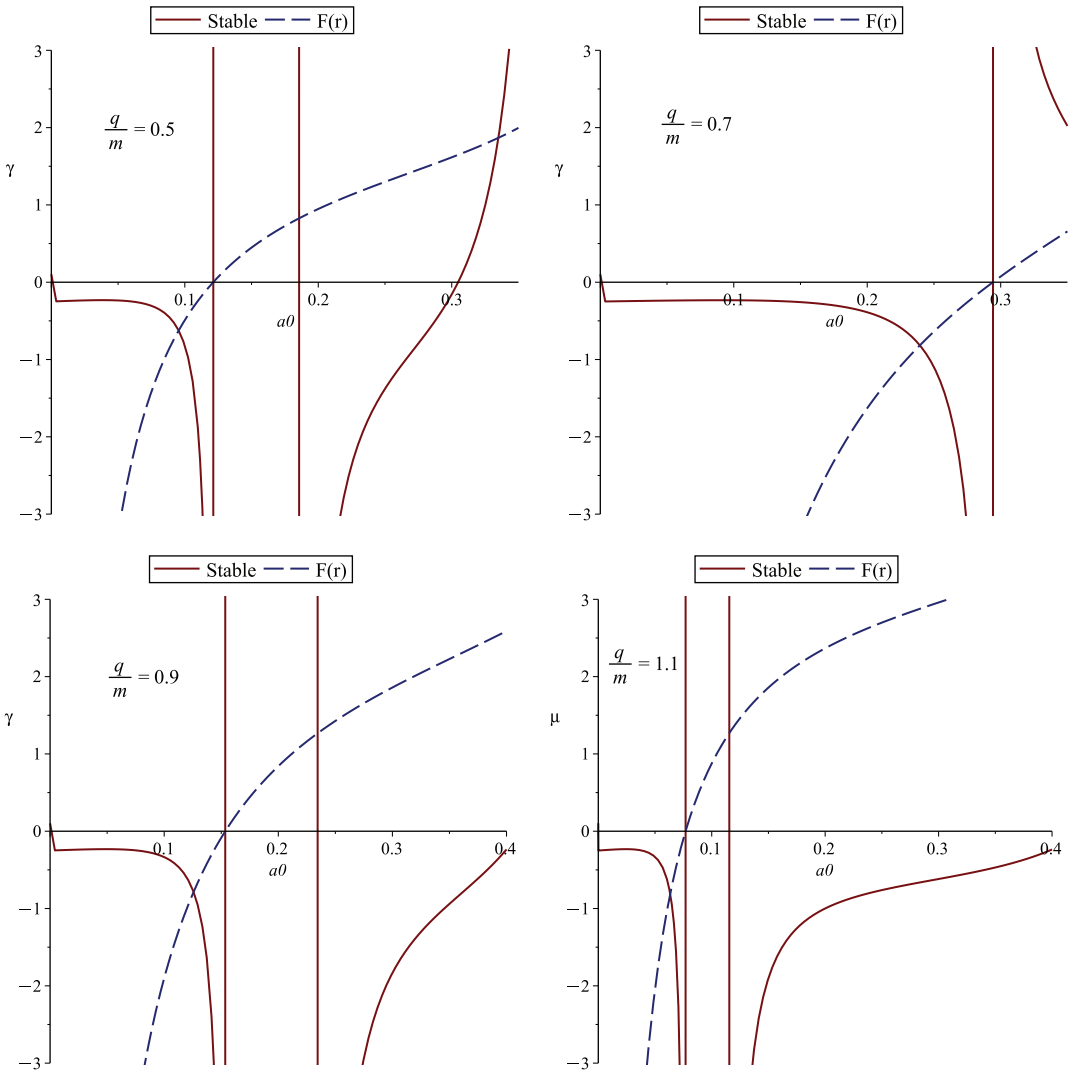

Fig. 5. Plots for stability regions of wormhole configuration with linear gas corresponding to $b = 1$.

where μ is EoS parameter and $\Theta'(\sigma_0) = \frac{\gamma}{\sigma_0}$. The respective stable HBI TSWs for $\frac{q}{m} = 0.5,\ 0.7,\ 0.9,\ 1.1$ and $b = 0.6$ are shown in Fig. 6. Here, we find least stable solutions for smaller values of charge as compared to the previous case which tend to increase on increasing charge. We also analyze more stable solutions by increasing b for larger values of $\frac{q}{m}$ while the event horizon does not disappear in this case (Fig. 7).

3.4. *Velocity perturbations*

Now we discuss stability of the constructed TSWs under velocity perturbations. We assume small velocity perturbations around static configuration $a = a_0$ which gives an approximately static fluid after any perturbation. This assumption supports the

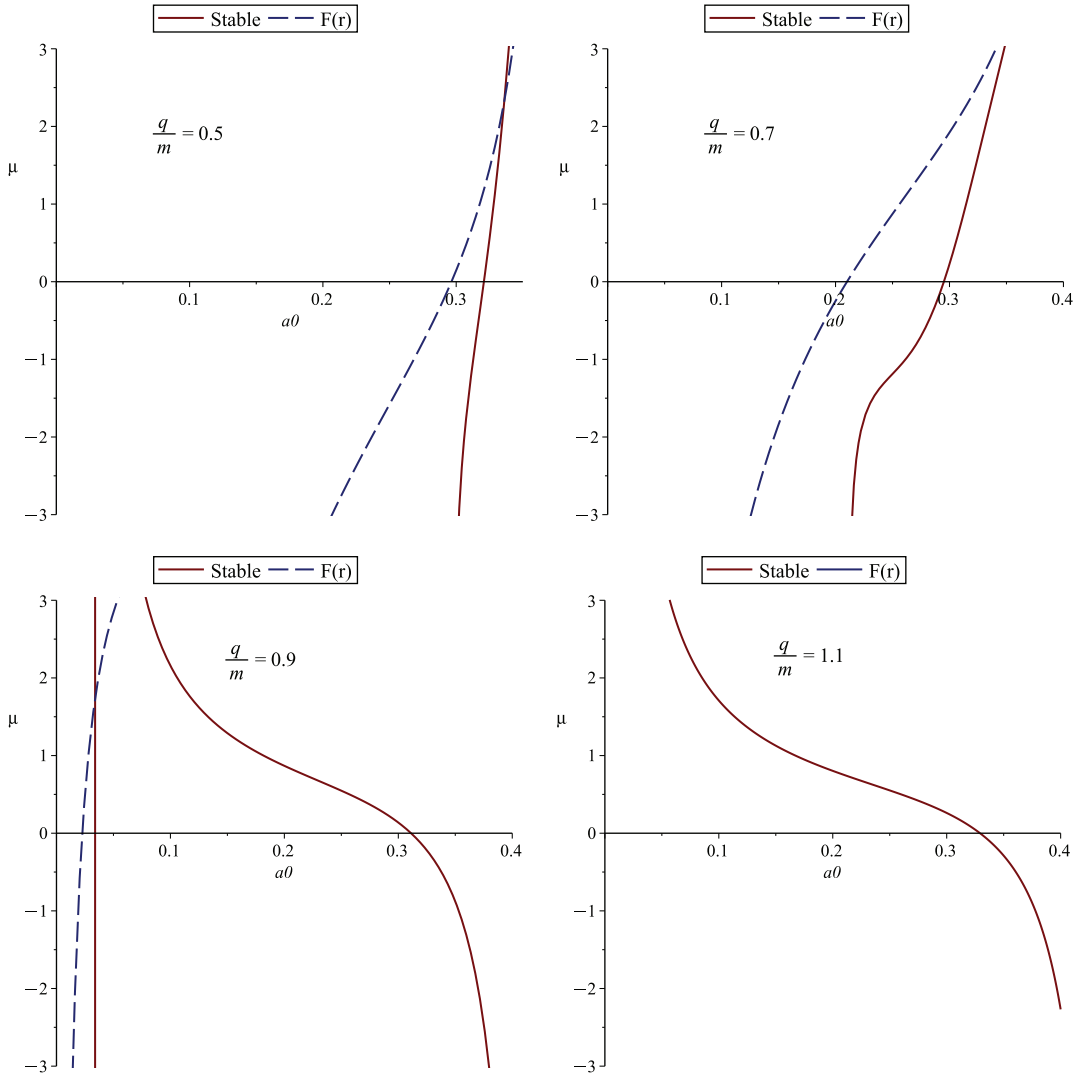

Fig. 6. Plots for logarithmic gas and HBI parameter $b = 0.6$ with different values of charge.

fact that the dynamic EoS for wormhole is same as the static EoS. Equation (11) leads to

$$p = -\frac{1}{2}\left(1 + \frac{aF'(a)}{2F(a)}\right)\sigma. \tag{22}$$

Substituting Eq. (9), we have

$$\ddot{a} - \frac{F'(a)}{2F(a)}\dot{a} = 0, \tag{23}$$

which shows wormhole's throat motion. Integrating this equation, it follows that

$$\dot{a} = \dot{a}_0 \frac{\sqrt{F(a)}}{\sqrt{F(a_0)}}, \tag{24}$$

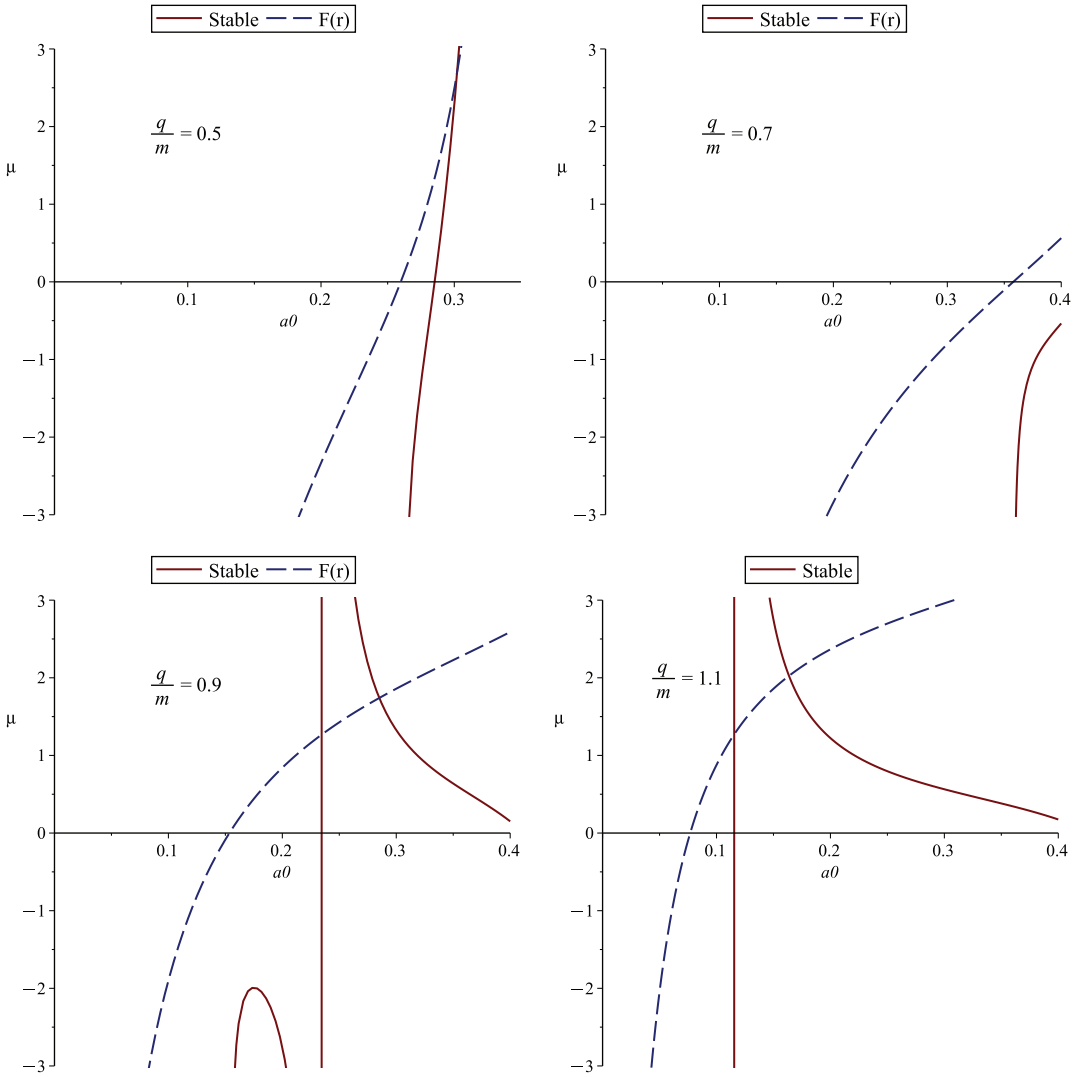

Fig. 7. Plots for logarithmic gas with $b = 1$ and different values of charge.

which further yields

$$\frac{\dot{a}_0}{\sqrt{F(a_0)}}(\tau - \tau_0) = \int_{a_0}^{a} \frac{da}{\sqrt{F(a)}}. \tag{25}$$

This corresponds to the nonoscillatory motion of the constructed wormhole solution, where $\dot{a}_0$ is the nonzero component of initial small velocity of throat. Equation (23) gives positive acceleration of the wormhole throat leading to unstable TSWs.

4. Outlook

In this paper, we have studied the effects of HBI parameter as well as electric charge on the stability of wormhole configurations. We have formulated surface stresses by applying Lanczos equation which gives rise to the presence of exotic

matter by violating null and weak energy conditions. It is found that wormholes have repulsive or attractive characteristics corresponding to smaller or larger values of throat radius, respectively. We have chosen $a > r_h$ to neglect the presence of singularities for the sake of viable wormhole solutions.

We have taken a linear perturbation of the form $p = \Theta(\sigma)$ and explored wormhole stability graphically for $G''(a_0) > 0$. We have chosen CG, linear and logarithmic gas models as exotic matter for its dynamical investigation. We have explored stable regions for the respective wormholes within a physically acceptable range of different parameters (Figs. 2–7). We have also plotted the metric function to find the position of wormhole throat and black hole's event horizon. It is found that there exists only one stable region as well as event horizon for CG with smaller value of HBI parameter such that the event horizon diminishes for $\frac{q}{m} = 1.1$. We have analyzed enlargement in stable regions by increasing the HBI parameter but the event horizon does not disappear for $b = 1$.

In case of linear gas, it provides more stable regions as compared to that of CG. It is found that the HBI parameter has remarkable significance to increase stable regions. The event horizon decreases by increasing the values of electric charge and finally vanishes. We have investigated that logarithmic gas provides least stable solutions as compared to other cases for smaller values of charge. These regions expand by enlarging the values of HBI parameter and charge. It is found that the role of HBI parameter and electric charge is to enhance stable regions for TSWs, whereas maximum value of the charge provides horizon-free solutions. Also, the linear gas is more significant in wormhole configuration which provides maximum stable regions as compared to other models while CG gives the least stable regions. We have also performed stability analysis under velocity perturbations and examined unstable configurations. We conclude that wormhole stability highly depends on the choice of model for exotic matter and values of the other involved parameters.

Acknowledgment

One of us (MS) would like to thank the organizers for the local hospitality during the V Italian–Pakistani Workshop on Relativistic Astrophysics in Lecce.

References

1. M. Morris and K. Thorne, *Am. J. Phys.* **56** (1988) 395.
2. S. A. Hayward, arXiv:gr-qc/0203051v1.
3. A. Einstein and N. Rosen, *Phys. Rev. D* **48** (1935) 73.
4. M. Visser, *Phys. Rev. D* **39** (1989) 3182.
5. W. Israel, *Nuovo Cimento B* **44S10** (1966) 1; *Erratum* **B48** (1967) 463.
6. S. W. Kim and H. Lee, *Phys. Rev. D* **63** (2001) 064014.
7. E. F. Eiroa and G. E. Romero, *Gen. Relativ. Gravit.* **36** (2004) 651.
8. E. F. Eiroa and C. Simeone, *Phys. Rev. D* **76** (2007) 024021.
9. M. Sharif and M. Azam, *Eur. Phys. J. C* **73** (2013) 2554; M. Sharif and S. Mumtaz, *Astrophys. Space Sci.* **352** (2014) 729; *Adv. High Energy Phys.* **2014** (2014) 639759; *Can. J. Phys.* **93** (2015) 12.

10. M. Born and L. Infeld, *Proc. R. Soc. A* **144** (1934) 425.
11. B. Hoffmann, *Phys. Rev.* **47** (1935) 877.
12. E. F. Eiroa and F. G. Aguirre, *Eur. Phys. J. C* **72** (2012) 2240.
13. M. Sharif and M. Azam, *Phys. Lett. A* **378** (2014) 2737.
14. M. Sharif and S. Mumtaz, *Astrophys. Space Sci.* **361** (2016) 218; *Eur. Phys. J.* **132** (2017) 26.
15. B. Hoffmann and L. Infeld, *Phys. Rev.* **51** (1937) 765.
16. S. H. Mazharimousavi, M. Halilsoy and Z. Amirabi, arXiv:0908.3967.
17. S. H. Mazharimousavi, M. Halilsoy and Z. Amirabi, *Phys. Lett. A* **375** (2011) 3649.
18. M. Halilsoy, A. Ovgun and S. H. Mazharimousavi, *Eur. Phys. J. C* **74** (2014) 2796; M. Sharif and S. Mumtaz, *Adv. High Energy Phys.* **2016** (2016) 2868750.

Eur. Phys. J. C (2017) 77:136
DOI 10.1140/epjc/s10052-017-4704-1

THE EUROPEAN PHYSICAL JOURNAL C

Regular Article - Theoretical Physics

Stability of the accelerated expansion in nonlinear electrodynamics

M. Sharif[a], **Saadia Mumtaz**[b]

Department of Mathematics, University of the Punjab, Quaid-e-Azam Campus, Lahore 54590, Pakistan

Received: 27 October 2016 / Accepted: 14 February 2017 / Published online: 27 February 2017

Abstract This paper is devoted to the phase space analysis of an isotropic and homogeneous model of the universe by taking a noninteracting mixture of the electromagnetic and viscous radiating fluids whose viscous pressure satisfies a nonlinear version of the Israel–Stewart transport equation. We establish an autonomous system of equations by introducing normalized dimensionless variables. In order to analyze the stability of the system, we find corresponding critical points for different values of the parameters. We also evaluate the power-law scale factor whose behavior indicates different phases of the universe in this model. It is concluded that the bulk viscosity as well as electromagnetic field enhances the stability of the accelerated expansion of the isotropic and homogeneous model of the universe.

1 Introduction

Many astronomical observations (type Ia supernova, large scale structure, and cosmic microwave background radiation) predict that our universe is expanding at an accelerating rate in its present stage [1–3]. These observations suggest two cosmic phases, i.e., the cosmic state before radiation (the primordial inflationary era) and ultimately the present cosmos phase after the matter dominated era. In the last couple of decades, it has been speculated that the source for this observed cosmic acceleration with an unusual antigravitational force may be an unknown energy component, dubbed dark energy (DE). The existence of this energy with large negative pressure can be recognized by its distinctive nature from ordinary matter which may lead to cosmic expansion. The study of the dominant contents of matter distribution in the universe has remained one of the most challenging issues. Recent observations show that the visible part of our universe is made up of baryonic matter contributing only 5% of the total budget, while the remaining ingredients yield the total energy density composed of non-baryonic fluids (68% DE and 27% dark matter) [4,5].

Several cosmological proposals have been introduced in the literature to explore the ambiguous nature of DE. The cosmological constant (Λ) governed by a negative equation of state (EoS) parameter ($\gamma = -1$) is taken to be the simplest characterization of DE. However, this identification has two well-known problems, i.e., fine-tuning and cosmic coincidence. In addition, there are several cosmological models which can be considered as an alternative to a Λ like scalar field model [6,7], a phantom model [8], a tachyon field [9] and k-essence [10], which also suggest expanding behavior of the universe. Another approach involves the generalization of simple barotropic EoS to more exotic forms such as the Chaplygin gas [11] and its modification [12]. It has also been demonstrated that a fluid with the bulk viscosity may cause accelerated expansion of the model of the universe without cosmological constant or scalar field [13,14]. Our main concern is to find another approach which can minimize exotic forms of matter by introducing dissipation through viscous effects of fluids.

During the last few years, cosmological models including nonlinear electromagnetic fields have attained remarkable interest. The application of this electrodynamics to different models of the universe may lead to many significant results. Nonlinear electrodynamics (NLED) is the generalization of Maxwell theory which is considered as the most viable theory to remove the initial singularities. Vollick [15] considered the FRW model of the universe with NLED and found that the model entailed will show a period of late-time acceleration for $E^2 < 3B^2$. Kruglov [16] found that the universe tends to accelerate in a magnetic background at the early era due to NLED model. Ovgun [17] formulated an analytical nonsingular extension of isotropic and homogeneous solutions by presenting a new mathematical model in nonlinear magnetic monopole fields.

[a] e-mail: msharif.math@pu.edu.pk
[b] e-mail: sadiamumtaz17@gmail.com

The study of possible stable late-time attractors has attained remarkable significance for different models of the universe. A phase space analysis manifests dynamical behavior of a cosmological model through a global view by reducing the complexity of the equations (converting the system of equations to an autonomous system) which may help to understand the different stages of the evolution. Copeland et al. [18] studied a phase plane analysis of standard inflationary models and found that these models cannot solve the density problem. Guo et al. [19] explored a phase space analysis of the FRW model of the universe filled with barotropic fluid and phantom scalar field in which a phantom dominated solution is found to be a stable late-time attractor.

Garcia-Salcedo [20] examined the dynamics of the FRW universe with NLED and found that the critical points have no effects. Yang and Gao [21] discussed a phase space analysis of k-essence cosmology in which critical points play an important role for the final state of the universe. Xiao and Zhu [22] analyzed the stability of the FRW model of the universe in loop quantum gravity via phase space portraits by taking barotropic fluid as well as positive field potential. Acquaviva and Beesham [23] made a phase space analysis of the FRW spacetime filled with a noninteracting mixture of fluids (dust and viscous radiation) and found that the nonlinear viscous model shows the possibility of current cosmic expansion.

This paper is devoted to the phase space analysis of the FRW model of the universe with nonlinear viscous fluid. The plan of the paper is as follows. In Sect. 2, we provide a basic formalism for NLED and general equations as well as a nonlinear model for the bulk viscosity. An autonomous system of equations is established to analyze the stability of the system by introducing normalized dimensionless variables in Sect. 3. Section 4 provides the formulation of power-law scale factor. Finally, we conclude our results in the last section.

2 Nonlinear electrodynamics and general equations

The standard cosmological model is successful in resolving many issues but still there are some issues which remain to be solved. One of them is the initial singularity which leads to a troubling state of affairs, because at this point all known physical theories break down. If the early universe is governed by Maxwell's equations, then there will be a spacelike initial singularity in the past. However, if Maxwell's equations become modified in the early universe, when the electromagnetic field is large, it might help avoiding the occurrence of cosmic singularities [24]. For the situations where a strong electromagnetic field occurs, it makes sense to couple gravitation with NLED. The coupling of Einstein gravity with NLED is defined by the action

$$S=\frac{1}{16\pi}\int\sqrt{-g}[R-\mathcal{L}(F,F^{*})]\mathrm{d}^{4}x. \tag{1}$$

We consider a nonlinear extension of the Maxwell Lagrangian density up to second order terms in the field invariants $F=F_{\mu\nu}F^{\mu\nu}$ and $F^{*}=F^{*}_{\mu\nu}F^{\mu\nu}$ given by [15]

$$\mathcal{L}=\mathcal{L}(F,F^{*})=-\frac{1}{4\mu_{0}}F+\alpha F^{2}+\beta F^{*2}, \tag{2}$$

where μ_0 denotes the magnetic permeability, $\alpha,\beta>0$ are arbitrary constants which yield a linear density for $\alpha,\beta\to 0$, and $F^{*}_{\mu\nu}$ is the dual of the electromagnetic field tensor. We do not consider the term FF^{*} involving F^{*} in order to preserve the parity [25,26]. The linear term of this Lagrangian dominates during a radiation dominated era, while the quadratic terms dominate in the early universe, which corresponds to the bouncing behavior of the universe to avoid initial singularity [27]. The mechanisms behind the bounce have been demonstrated in [28,29]. The energy-momentum tensor associated with this Lagrangian has the following form:

$$T_{\mu\nu(EM)}=-4\partial_{F}\mathcal{L}F^{\eta}_{\mu}F_{\eta\nu}+(\partial_{F^{*}}\mathcal{L}F^{*}-\mathcal{L})g_{\mu\nu}. \tag{3}$$

In order to fulfill the requirement of isotropic and homogeneous universe, i.e., the electromagnetic field to act as its source, the energy density and the pressure corresponding to the electromagnetic field can be computed by averaging over volume [26,28]. It is assumed that the electric and magnetic fields have coherent lengths that are much shorter than the cosmological horizon scales. After posing several conditions, the energy momentum tensor of the electromagnetic field associated with $\mathcal{L}(F,F^{*})$ can be written as that of a perfect fluid,

$$T_{\mu\nu}=(\rho+p)u_{\mu}u_{\nu}+pg_{\mu\nu}, \tag{4}$$

such that

$$\rho_{EM}=-\mathcal{L}-4E^{2}\partial_{F}\mathcal{L}, \tag{5}$$

$$p_{EM}=\mathcal{L}-\frac{4}{3}(2B^{2}-E^{2})\partial_{F}\mathcal{L}, \tag{6}$$

where ∂_F represents a partial derivative with respect to $F=F_{\mu\nu}F^{\mu\nu}=2(B^{2}-E^{2})$, and E and B denote the averaged electric and magnetic fields, respectively.

We consider an isotropic and homogeneous model of the universe given by

$$\mathrm{d}s^{2}=-\mathrm{d}t^{2}+a(t)(\mathrm{d}r^{2}+r^{2}\mathrm{d}\theta^{2}+r^{2}\sin^{2}\theta\mathrm{d}\phi^{2}), \tag{7}$$

where $a(t)$ is the scale factor. We assume the model of the universe to be filled with two cosmic fluids, i.e., a noninteracting electromagnetic fluid with energy density ρ_{EM} as well as pressure p_{EM} and a viscous fluid having energy density ρ_v as well as pressure $p=p_v(\rho_v)+\Psi$. Here p_v represents the equilibrium part of viscous pressure whereas Ψ is the non-equilibrium part, i.e., the bulk viscous pressure satisfying an evolution equation. The bulk viscosity plays an important role in stabilizing the density evolution and overcomes rapid changes in cosmos. It also promotes a negative energy

field in the fluid and hence can play the role of dark energy to describe the dynamics of cosmos. It has been suggested that a fluid with bulk viscosity may cause an accelerated expansion of the model of the universe without cosmological constant or scalar field [14]. The main contribution of the bulk viscosity to the effective pressure is its dissipative effect. We obtain the Raychaudhuri and constraint equations from the field equations given by

$$\dot{\Theta} = -\frac{1}{3}\Theta^2 - \frac{1}{2}\left[\rho_{EM} + \rho_v + 3(p_{EM} + p_v + \Psi)\right], \tag{8}$$

$$0 = \rho_{EM} + \rho_v - \frac{1}{3}\Theta^2, \tag{9}$$

where a dot means the derivative with respect to time. The conservation of the energy-momentum tensor yields the following evolution equations for the viscous and electromagnetic field components:

$$\dot{\rho}_v = -[\rho_v + p_v + \Psi]\Theta, \tag{10}$$

$$\dot{\rho}_{EM} = -[\rho_{EM} + p_{EM}]\Theta. \tag{11}$$

We consider a barotropic EoS for a viscous fluid defined by

$$p_v = (\gamma - 1)\rho_v, \tag{12}$$

where $1 \leq \gamma \leq 2$. Using Eqs. (8) and (9), the Raychaudhuri and conservation equations for viscous fluid turn out to be

$$\dot{\Theta} = -\frac{1}{2}\Theta^2 - \frac{3}{2}[p_{EM} + (\gamma - 1)\rho_v + \Psi], \tag{13}$$

$$\dot{\rho}_v = -[\gamma\rho_v + \Psi]\Theta. \tag{14}$$

We characterize the viscous pressure variable by the following evolution equation [30]:

$$\tau\dot{\Psi} = -\zeta\Theta - \Psi\left(1 + \frac{\tau_*}{\zeta}\Psi\right)^{-1} - \frac{1}{2}\tau\Psi\left[\Theta + \frac{\dot{\tau}}{\tau} - \frac{\dot{\zeta}}{\zeta} - \frac{\dot{T}}{T}\right], \tag{15}$$

where ζ, T, τ, and τ_* denote the bulk viscosity, local equilibrium temperature, linear relaxation time, and the characteristic time in the nonlinear background, respectively. This equation is derived by using a nonlinear model describing a relationship between thermodynamic flux Ψ and the thermodynamic force χ in the form

$$\Psi = -\frac{\zeta\chi}{1 + \tau_*\chi}. \tag{16}$$

This is a nonlinear extension of the Israel–Stewart equation, which reduces to its linear form as $\tau_* \to 0$. The nonlinear term in Eq. (15) must be positive for thermodynamic consistency and positivity of entropy production rate. The parameters involved in Eq. (15) can be defined by the relations $\zeta = \zeta_0\Theta$ ($\zeta > 0$), $\tau = \frac{\zeta}{\gamma\nu^2\rho_v}$, $\tau_* = k^2\tau$, and $T = T_0\rho^{(\gamma-1)/\gamma}$. Here k is a constant such that $k = 0$ gives the linear (Israel–Stewart) case, while T_0 represents a constant temperature. Also, ν corresponds to the dissipative effect of the speed of sound V such that $V^2 = c_s^2 + \nu^2$, where c_s^2 is its adiabatic contribution. By causality, $V \leq 1$ and $c_s^2 = \gamma - 1$, which yields

$$\nu^2 \leq 2 - \gamma, \quad 1 \leq \gamma \leq 2. \tag{17}$$

The explicit form of the evolution equation by using the above relations yields

$$\dot{\Psi} = -\gamma\nu^2\rho_v\Theta - \frac{\gamma\nu^2\Psi\rho_v}{\zeta_0\Theta}\left(1 + \frac{k^2\Psi}{\gamma\nu^2\rho_v}\right)^{-1} - \frac{1}{2}\Psi\left[\Theta - \left(\frac{2\gamma - 1}{\gamma}\right)\frac{\dot{\rho}_v}{\rho_v}\right]. \tag{18}$$

3 Phase space analysis

In this section, we discuss the phase space analysis of the isotropic and homogeneous model of the universe for the radiation case. Due to there being many arbitrary parameters, it seems difficult to find an analytical solution of the evolution equation. In this context, we define normalized dimensionless variables $\Omega = \frac{3\rho_v}{\Theta^2}$ and $\tilde{\Psi} = \frac{3\Psi}{\Theta^2}$ such that the corresponding dynamical system can be reduced to autonomous one. We also define a new variable $\tilde{\tau}$ for the time for which the corresponding derivative is represented by a prime such that $\frac{dt}{d\tilde{\tau}} = \frac{3}{\Theta}$. Here each term is associated with some physical explicit background, since the chosen dimensionless variables Ω and $\tilde{\Psi}$ occur due to the physical impact of the viscous energy density and pressure, respectively. The system of Eqs. (13) and (14) in terms of these normalized variables takes the form

$$\frac{\Theta'}{\Theta} = -\frac{3}{2}[1 + p_{EM} + (\gamma - 1)\Omega + \tilde{\Psi}], \tag{19}$$

$$\frac{3\rho_v'}{\Theta^2} = -3[\gamma\Omega + \tilde{\Psi}]. \tag{20}$$

Differentiation of the dimensionless variable for the energy density gives

$$\Omega' = \frac{3\rho_v'}{\Theta^2} - 2\Omega\frac{\Theta'}{\Theta}. \tag{21}$$

Using Eqs. (19) and (20), this equation turns out to be

$$\Omega' = 3(\Omega - 1)[\Omega(\gamma - 1) + \tilde{\Psi} + 3p_{EM}]. \tag{22}$$

Now we introduce the concept of a new evolution equation for $\tilde{\Psi}$. The first derivative of $\tilde{\Psi}$ with respect to $\tilde{\tau}$ through Eq. (19) leads to an evolution equation of the form

$$\tilde{\Psi}' = -3\gamma\nu^2\Omega\left[1+\frac{\tilde{\Psi}}{3\zeta_0}\left(1+\frac{k^2\tilde{\Psi}}{\gamma\nu^2\Omega}\right)^{-1}\right] + 3\tilde{\Psi}\left[1+3p_{EM}\left(1-\frac{3}{\Omega}\frac{2\gamma-1}{2\gamma}\right)\right] - 3(\gamma-1)\tilde{\Psi}(1-\Omega). \quad (23)$$

It is mentioned here that Eqs. (22) and (23) play a remarkable role in describing the dynamical system entailed for the phase space analysis.

In order to find the critical points $\{\Omega_c, \tilde{\Psi}_c\}$, we need to solve the dynamical system by imposing the condition $\Omega' = \tilde{\Psi}' = 0$. The stability of the FRW model of the universe can be analyzed according to the nature of the critical points. Here we restrict the phase space region by a condition which is necessary for the positivity of the entropy production rate given by [23,30]

$$\tilde{\Psi} > -\frac{\gamma\nu^2\Omega}{k^2}. \quad (24)$$

This condition makes the possible negative values of $\tilde{\Psi}$ tend toward zero for $k^2 \gg \nu^2$. Contrarily, the bulk pressure will be less restrictive if $k^2 \ll \nu^2$. It is noted that finite values of k allow only positive values of the bulk pressure in the limit $\nu \to 0$. It would be more convenient to consider $k^2 \leq \nu^2$ along with $\nu^2 \leq 2-\gamma$ and $\tau_* = k^2\tau$, which leads to the fact that the characteristic time for nonlinear effects τ_* does not exceed the characteristic time in linear background τ. We characterize the critical points by the deceleration parameter $q = -1 - \frac{\Theta'}{\Theta}$ and the effective EoS parameter $\gamma_{\text{eff}} = -\frac{2\Theta'}{3\Theta}$, which yield

$$q = \frac{1}{2}[1+9p_{EM}+3(\gamma-1)\Omega+3\tilde{\Psi}], \quad (25)$$

$$\gamma_{\text{eff}} = 1+3p_{EM}+(\gamma-1)\Omega+\tilde{\Psi}. \quad (26)$$

To examine a region of phase space undergoing accelerated expansion, we impose $q < 0$ in Eq. (25) which gives

$$\tilde{\Psi} < -\frac{1}{3}-3p_{EM}-(\gamma-1)\Omega. \quad (27)$$

The possibility of the accelerated expansion in the physical phase space is determined by comparing Eqs. (24) and (25) through $q < 0$ given by

$$\frac{\nu^2}{k^2} > \frac{1+9p_{EM}+3(\gamma-1)\Omega}{3\gamma\Omega}. \quad (28)$$

Substituting $\Omega' = 0$ in Eq. (22), we find the following conditions:

$$\Omega_c = 1, \quad (29)$$

$$(\gamma-1)\Omega_c + \tilde{\Psi}_c + 3p_{EM} = 0. \quad (30)$$

We insert these conditions in $\tilde{\Psi}'$ to find the location of critical points. This analysis is carried out by characterizing the viscous fluid through the choice of its EoS parameter γ (radiation). We consider $0 < k^2 = \nu^2 \leq 2-\gamma$ for which the case of stiff matter ($\gamma = 2$) is excluded from the analysis as it yields $\nu^2 = 0$.

3.1 Radiation case ($\gamma = \frac{4}{3}$)

We consider the radiation case for the phase space analysis by taking $\gamma = \frac{4}{3}$. Imposing the condition (29) and $\tilde{\Psi}' = 0$ in Eq. (23), we have

$$\frac{3\nu^2}{4\zeta_0}\tilde{\Psi}^3 - \frac{\nu^2}{\zeta_0}\tilde{\Psi}^2 - 3\tilde{\Psi}\left(1-\frac{4\nu^2}{9\zeta_0}-\frac{21p_{EM}}{8}\right)+4\nu^2 = 0. \quad (31)$$

This cubic equation yields three roots among which we retain only those roots that lie in the physical phase space. The general form of the dynamical system is given by

$$\Omega' = X(\Omega, \tilde{\Psi}), \quad \tilde{\Psi}' = Y(\Omega, \tilde{\Psi}). \quad (32)$$

The eigenvalues of the system can be determined by the Jacobian matrix

$$Z = \begin{pmatrix} \frac{\partial X}{\partial\Omega} & \frac{\partial X}{\partial\tilde{\Psi}} \\ \frac{\partial Y}{\partial\Omega} & \frac{\partial Y}{\partial\tilde{\Psi}} \end{pmatrix}_{|P_i^{\pm}}. \quad (33)$$

The eigenvalues for the above stability matrix corresponding to the points $P_r^{\pm}$ are given by

$$\lambda_1 = 1+3\tilde{\Psi}+9p_{EM}, \quad (34)$$

$$\lambda_2 = -\frac{16\nu^2}{3\zeta_0}\left[\frac{1}{4+\tilde{\Psi}}-\frac{\tilde{\Psi}}{(4+\tilde{\Psi})^2}\right]-\frac{63p_{EM}}{8}+6\tilde{\Psi}+3. \quad (35)$$

The fixed point is called a source (respectively, a sink) if both eigenvalues consist of positive (respectively, negative) real parts. In the case of a viscous radiating fluid, we can explore source and sink according to the sign of eigenvalues as well as direction of the trajectories. We investigate two critical points $P_r^+ = \{1, \tilde{\Psi}_c^+\}$ and $P_r^- = \{1, \tilde{\Psi}_c^-\}$ corresponding to positive ($\tilde{\Psi}_c^+$) and negative ($\tilde{\Psi}_c^-$) roots, respectively. By taking $\Omega_c = 0$ and the second condition (30) with $\tilde{\Psi}_c = -\frac{\Omega_c}{3} - 3p_{EM}$, we obtain $P_r^0 = \{0, -3p_{EM}\}$.

3.1.1 Case I

We are interested in analyzing the impact of the electromagnetic field on the stability of the critical points in the presence of the nonlinear bulk viscosity. The energy density (5) and pressure (6) are given by

$$\rho_{EM} = \frac{1}{2\mu_0}(B^2+E^2)-4\alpha(B^2-E^2)(B^2+3E^2), \quad (36)$$

$$p_{EM} = \frac{1}{6\mu_0}(B^2+E^2)-\frac{4\alpha}{3}(B^2-E^2)(5B^2-E^2). \quad (37)$$

The dynamical behavior of critical points for different values of electric and magnetic fields as well as other parameters is shown in Figs. 1 and 2. The green trajectory depicts a flow from the point P_d^+ toward P_d^-. The white region corresponds to the negative entropy production rate that diverges on its boundary whereas the green region shows accelerated expansion of the universe ($q < 0$). Here the point P_d^0 shows varying behavior, i.e., either it is a saddle point or a sink, depending on the values of the different parameters.

In these plots, we have taken $\zeta_0 = 0.2, 1$ by varying ν, k, B and E. For $\nu = k = \sqrt{1/5}$ and $\zeta_0 = 0.2$, it is found that the global attractor P_d^- lies in the green region showing accelerated expansion for the same values of B and E. This region tends to decrease by increasing E such that the point P_d^- lies in the deceleration region. By increasing ζ_0, we find accelerated expansion with different values of B, E and larger values of the parameters ν and k. For $\nu = k = 1$ and $\zeta_0 = 1$, we find accelerated expansion of the model of

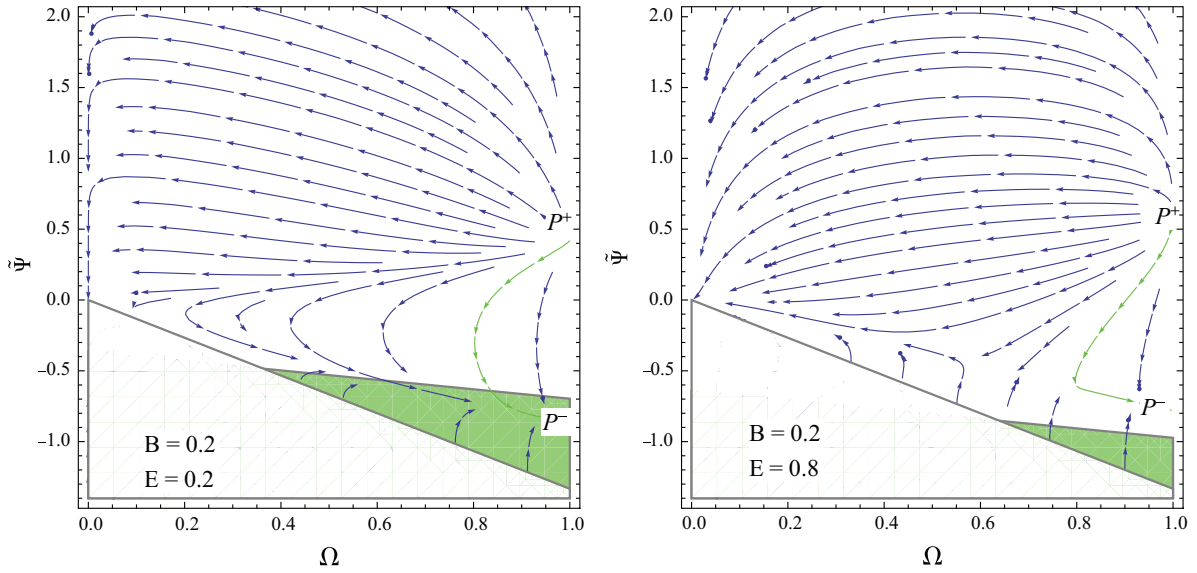

Fig. 1 Plots for the phase plane evolution of viscous radiating fluid with $\gamma = 4/3$, $\nu = k = \sqrt{1/5}$, $\zeta_0 = 0.2$, $\alpha = 0.01$, and different values of B and E

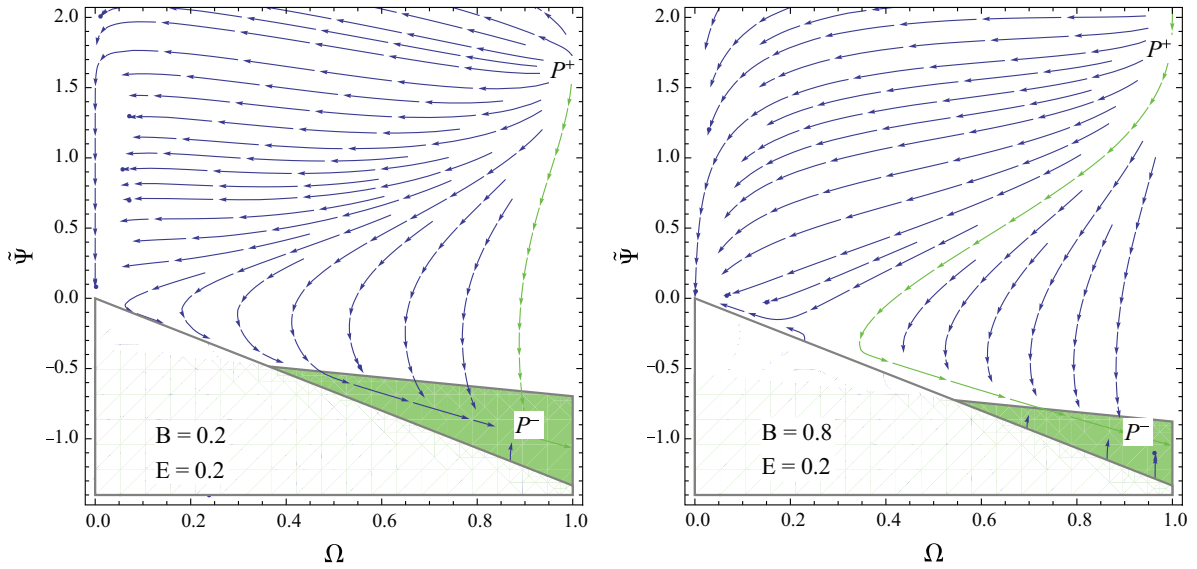

Fig. 2 Plots for the phase plane evolution of viscous radiating fluid with $\gamma = 4/3$, $\nu = k = 1$, $\zeta_0 = 1$, $\alpha = 0.01$, and different values of B and E

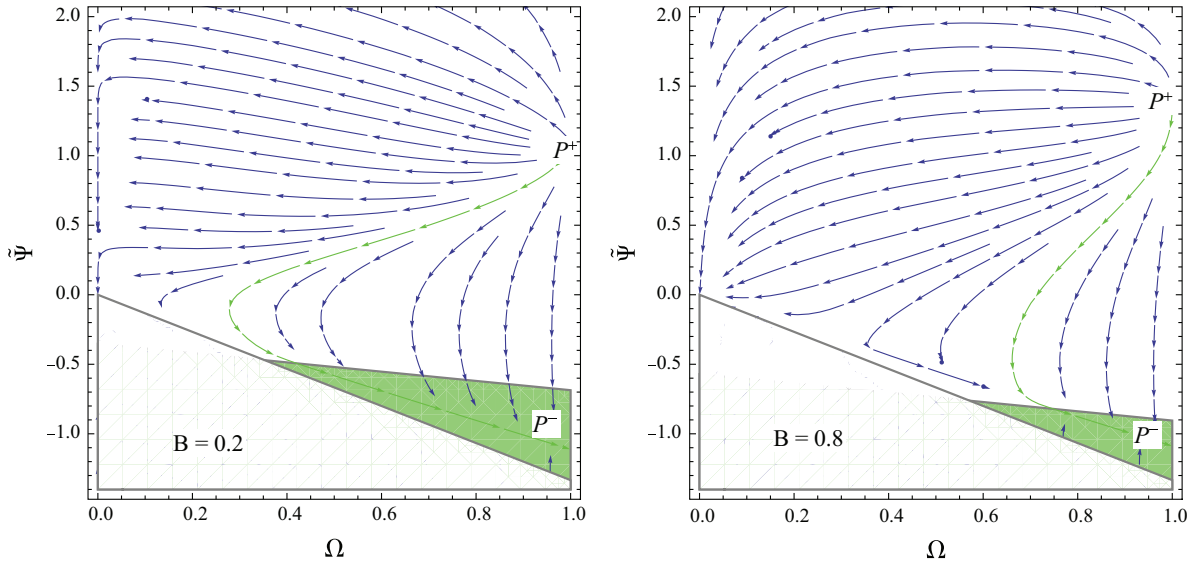

Fig. 3 Plots for the phase plane evolution of viscous radiating fluid with $\gamma = 4/3$, $\nu = k = \sqrt{2/3}$, $\zeta_0 = 1$, $\alpha = 0.01$, and $B = 0.2, 0.8$

the universe for all choices of electric and magnetic fields. The point P_d^0 behaves as a sink for $\zeta_0 = 0.2$ which becomes a saddle point for larger values of ζ_0. We observe that the increasing value of the bulk viscosity increases the region for accelerated expansion in the presence of NLED. In the following, we discuss two different cases for the electric as well as the magnetic universe.

3.1.2 Case II ($E = 0$)

It is well known that NLED helps to diminish the initial singularity in the early universe where only the primordial plasma identifies matter [31]. Some recent results indicate that a magnetic universe is appropriate to avoid the initial singularity and ultimately shows late-time accelerated expansion [25,28,32]. Here we assume the squared electric field $\langle E^2 \rangle$ to be zero such that the magnetic field ($F = 2B^2$) rules over the universe; this is known as a magnetized universe. Thus the energy density (5) and pressure (6) take the form

$$\rho_B = \frac{B^2}{2\mu_0}(1 - 8\mu_0\alpha B^2), \tag{38}$$

$$p_B = \frac{B^2}{6\mu_0}(1 - 40\mu_0\alpha B^2). \tag{39}$$

The respective evolution plots are given in Fig. 3. For $\nu = k = \sqrt{2/3}$ and $\zeta_0 = 1$, we find that the sink lies in the green region showing the stability of the accelerated expansion for the magnetized universe. This region tends to decrease by increasing the value of magnetic field B. The point P_d^0 behaves as a saddle for small values of magnetic field. It is mentioned here that increasing values of the bulk viscosity and the parameters ν as well as k with different values of B give rise to the stability of the accelerated expansion of the universe for different choices of B. We also find that a smaller value of the bulk viscosity shows decelerated expansion with increasing values of B.

3.1.3 Case III ($B = 0$)

Here, we deal with the electric universe by setting $\langle B^2 \rangle = 0$. The corresponding energy density and pressure are given by

$$\rho_E = \frac{E^2}{2\mu_0}(1 + 24\mu_0\alpha E^2), \tag{40}$$

$$p_E = \frac{E^2}{6\mu_0}(1 - 8\mu_0\alpha E^2). \tag{41}$$

The plots corresponding to different choices of electric field E are shown in Fig. 4. For $\nu = k = \sqrt{2/3}$ and $\zeta_0 = 1$, we analyze the sink P_d^- in the green region showing accelerated expansion of the universe for different values of E. The point P_d^0 behaves as a saddle for small values of the magnetic field. We find that the region for accelerated expansion tends to decrease by increasing electric field E. It is observed that an accelerated expanding region exists for increasing values of the bulk viscosity and parameters ν as well as k with all choices of E. It supports the fact that the role of the bulk viscosity and electric field is to increase the stability of the accelerated expansion of the model of the universe. The summary of our results filled with viscous radiating fluid is given in Table 1.

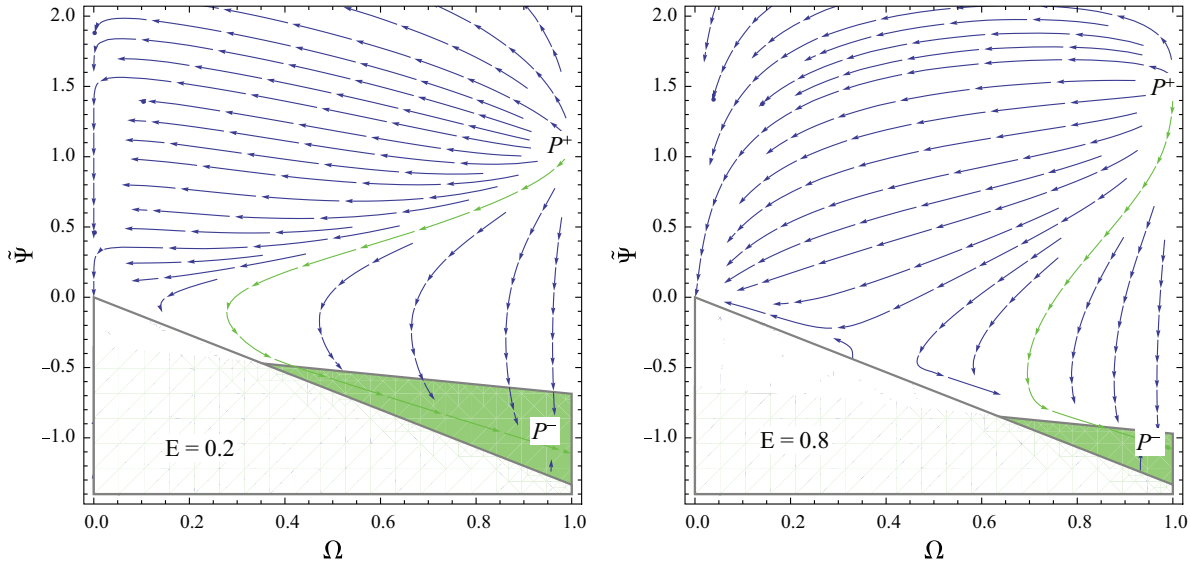

Fig. 4 Plots for the phase plane evolution of viscous radiating fluid with $\gamma = 4/3$, $v = k = \sqrt{2/3}$, $\zeta_0 = 1$, $\alpha = 0.01$ and $E = 0.2, 0.8$

Table 1 Stability analysis of critical points for radiation dominated fluid

Critical point	Behavior	Stability
P_r^+	Source	Unstable
P_r^-	Sink	Stable
P_r^0	Saddle/sink	Unstable/stable

4 Power-law scale factor

In this section, we discuss the power-law behavior of the scale factor corresponding to the critical points. For this purpose, we integrate Eq. (19), which leads to

$$\dot{\Theta} = -\frac{1}{2}[1 + 3p_{EM} + (\gamma - 1)\Omega + \tilde{\Psi}]\Theta^2. \tag{42}$$

For $\Theta \neq 0$, we formulate a power-law scale factor whenever $1 + 3p_{EM} + (\gamma - 1)\Omega + \tilde{\Psi} \neq 0$. Solving $\Theta = \frac{3\dot{a}}{a}$ for $a(t)$, we obtain the generic critical point as

$$a = a_0(t - t_0)^{\frac{2}{3[1+3p_{EM}+(\gamma-1)\Omega_c+\tilde{\Psi}_c]}}. \tag{43}$$

The following condition must hold for exponentially expanding models (identified by the condition $1 + 3p_{EM} + (\gamma - 1)\Omega + \tilde{\Psi} = 0$) to be present in the physical phase space region (bounded by Eq. (24)):

$$(1 - \gamma)\Omega_c - 3p_{EM} - 1 > -\frac{\gamma v^2}{k^2}\Omega. \tag{44}$$

This condition is not satisfied in the physical phase space for $v^2 = k^2$. If $v^2 > k^2$, the above inequality must be satisfied in the following physical phase space region:

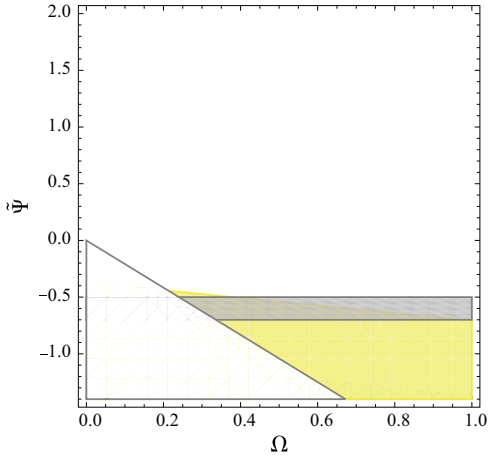

Fig. 5 Plot of qualitative phase space analysis for power-law scale factor with $v^2 > k^2$. *Yellow* and *dark gray regions* indicate the accelerated and exponential expansion of the model of the universe, respectively

$$(1 + 3p_{EM})\left[1 - \gamma\left(1 - \frac{v^2}{k^2}\right)\right]^{-1} < \Omega \leq 1. \tag{45}$$

It is mentioned here that the sign of the term $1+3p_{EM}+(\gamma-1)\Omega+\tilde{\Psi}$ is quite important in evaluating different cosmological stages. If $1+3p_{EM}+(\gamma-1)\Omega+\tilde{\Psi} = 0$, it corresponds to the exponential expansion of the model of the universe. Also, $1+3p_{EM}+(\gamma-1)\Omega+\tilde{\Psi} \gtrless 0$ yields accelerated expansion or contraction of the cosmological model, respectively. If $v^2 < k^2$, the possibility of having accelerated expansion will narrow down. Figure 5 shows the physical phase space region (excluding the white region with negative entropy production rate) whereas yellow and dark gray regions correspond

Table 2 Power-law scale factors for different critical points

Critical point	Scale factor for $\gamma = 4/3$
P_r^0	$a_0(t-t_0)^{-\frac{2}{9p_{EM}}}$
P_r^+	$a_0(t-t_0)^{\frac{2}{3(3p_{EM}+\tilde{\Psi}_c^+ +\frac{4}{3})}}$
P_r^-	$a_0(t-t_0)^{\frac{2}{3(3p_{EM}+\tilde{\Psi}_c^- +\frac{4}{3})}}$

to accelerated and exponential expansion of the model of the universe for $v^2 > k^2$, respectively. Table 2 provides the polynomial behavior of power-law scale factor for different critical points with $1 + 3p_{EM} + (\gamma - 1)\Omega + \tilde{\Psi} \neq 0$.

5 Outlook

In this paper, we have discussed the impact of NLED on the phase space analysis of isotropic and homogeneous model of the universe by taking noninteracting mixture of the electromagnetic and viscous radiating fluids. This analysis has been proved to be a remarkable technique for the stability of dynamical system. An autonomous system of equations has been developed by defining normalized dimensionless variables. We have evaluated the corresponding critical points for different values of the parameters to discuss stability of the system. We have also calculated eigenvalues which characterize these critical points. We summarize our results as follows.

Firstly, we have discussed stability of critical points through their eigenvalues corresponding to different values of E and B for viscous radiation dominated model of the universe. It is found that the critical points P_d^+ and P_d^- correspond to source (unstable) and sink (stable), respectively (Figs. 1 and 2). It is mentioned here that the green region corresponds to an accelerated expansion of the universe. The point P_d^- is a global attractor in the physical phase space region which leads to an expanding model dominated by viscous matter for various choices of the cosmological parameters. In the presence of both electric and magnetic fields, we find that the bulk viscosity increases the region for accelerated expansion, while the increasing values of E show a deceleration region for smaller values of the bulk viscosity. It is mentioned here that large values of the bulk viscosity as well as other parameters correspond to accelerated expansion of the ensuing model of the universe for all choices of electric and magnetic fields.

We have also studied the electric and magnetic cases for the universe separately. It is found that a sink lies in the green region showing accelerated expansion of the magnetized universe for smaller values of the bulk viscosity and the other parameters, while an increasing value of magnetic field decreases this region. For $B = 0$, we have analyzed accelerated expansion of the model of the universe corresponding to large values of the parameters, which tends to decrease by increasing E. It is worth mentioning here that the role of the bulk viscosity is to increase the green region for accelerated expansion with different choices of E and B for both electric as well as magnetic universe. Moreover, we have also studied the behavior of a power-law scale factor corresponding to the critical points. It is found that the power-law scale factor indicates various phases of the evolution (accelerated or exponential expansion) of the model of the universe entailed.

Funded by SCOAP[3].

References

1. A.G. Riess et al., Astron. J. **116**, 1009 (1998)
2. S.J. Perlmutter et al., Astrophys. J. **517**, 565 (1999)
3. C.L. Bennett et al., Astrophys. J. Suppl. **148**, 1 (2003)
4. V. Sahni, A.A. Starobinsky, Int. J. Mod. Phys. A **9**, 373 (2000)
5. M. Tegmark et al., Phys. Rev. D **69**, 03501 (2004)
6. R.R. Caldwell, R. Dave, P.J. Steinhardt, Phys. Rev. Lett. **80**, 1582 (1998)
7. T. Chiba, T. Okabe, M. Yamaguchi, Phys. Rev. D **62**, 023511 (2000)
8. S.M. Carroll, M. Hoffman, M. Trodden, Phys. Rev. D **68**, 023509 (2003)
9. V. Gorini et al., Phys. Rev. D **69**, 123512 (2004)
10. L.P. Chimento, Phys. Rev. D **69**, 123517 (2004)
11. A. Kamenshchik, U. Moschella, V. Pasquier, Phys. Lett. B **511**, 265 (2001)
12. M.C. Bento, O. Bertolami, A.A. Sen, Phys. Rev. D **66**, 043507 (2002)
13. M. Heller, Z. Klimek, L. Suszycki, Astrophys. Space Sci. **20**, 205 (1973)
14. W. Zimdahl, Phys. Rev. D **53**, 5483 (1996)
15. D.N. Vollick, Phys. Rev. D **78**, 063524 (2008)
16. S.I. Kruglov, Int. J. Mod. Phys. D **25**, 1640002 (2016)
17. A. Ovgun, Eur. Phys. J. C **77**, 105 (2017)
18. E.J. Copeland, A.R. Liddle, D. Wands, Phys. Rev. D **57**, 4686 (1998)
19. Z.K. Guo et al., Phys. Lett. B **608**, 177 (2005)
20. R. Garcia-Salcedo et al., arXiv:0905.1103
21. R.J. Yang, X.T. Gao, Class. Quantum Gravity **28**, 065012 (2011)
22. K. Xiao, J. Zhu, Phys. Rev. D **83**, 083501 (2011)
23. G. Acquaviva, A. Beesham, Phys. Rev. D **90**, 023503 (2014)
24. R. Garcia-Salcedo, N. Bretonn, Class. Quantum Gravity **22**, 4783 (2005)
25. V.A. De Lorenci et al., Phys. Rev. D **65**, 063501 (2002)
26. T. Bandyopadhyay, U. Debnath, Phys. Lett. B **704**, 95 (2011)
27. M. Sharif, S. Waheed, Astrophys. Space Sci. **346**, 583 (2013)
28. M. Novello et al., Class. Quantum Gravity **24**, 3021 (2007)
29. M. Novello, S.E.P. Bergliaffa, Phys. Rep. **463**, 127 (2008)
30. R. Maartens, V. Méndez, Phys. Rev. D **55**, 1937 (1997)
31. M. Giovannini, M. Shaposhnikov, Phys. Rev. D **57**, 2186 (1998)
32. M. Novello, S.E.P. Bergliaffa, J. Salim, Phys. Rev. D **69**, 127301 (2004)

Stability of Universe Model Coupled with Phantom and Tachyon Fields

M. Sharif *and Saadia Mumtaz †
Department of Mathematics, University of the Punjab,
Quaid-e-Azam Campus, Lahore-54590, Pakistan.

Abstract

In this paper, we study phase space analysis of locally rotationally symmetric Bianchi type I universe model by taking different linear combinations for the interactions between scalar field models and dark matter. An autonomous system of equations is established by defining normalized dimensionless variables. In order to investigate stability of the system, we find corresponding critical points for different values of the parameters. We also evaluate power-law scale factor whose behavior shows different cosmological phases. The dynamical analysis indicates a matter dominated epoch ultimately followed by a late accelerated expansion phase. It is found that all the critical points indicate accelerated expansion of the universe for tachyon coupled field. We conclude that negative values of m provide more stable future attractors as compared to its positive values.

Keywords: Cosmology of theories beyond the SM; Phase space analysis; LRS Bianchi I model.
PACS: 04.20.-q; 95.36.+x; 98.80.-k.

1 Introduction

Recent observations (type Ia supernova, large scale structure and cosmic microwave background radiation (CMBR)) suggest that our universe is ex-

*msharif.math@pu.edu.pk
†sadiamumtaz17@gmail.com

panding at an accelerating rate [1]. These observational probes indicate two cosmic phases, i.e., the cosmos phase before radiation and ultimately the current cosmic era. Many substantial attempts have been taken to explore the facts behind the current cosmic acceleration. Some mysterious source of unusual anti-gravitational force, known as dark energy (DE), was proposed by physicists while trying to examine the formation of galaxies in cosmic scenario. It is an exotic energy constituent having large negative pressure which dominates over the matter content of cosmos. This energy is supposed to be responsible for the current cosmic expansion.

There have been several proposals of DE to study its ambiguous nature. The cosmological constant (Λ) is considered as the simplest candidate but its characterization has two well-known problems, i.e., fine-tuning and cosmic coincidence. There are various alternative dynamical models which can be taken as a substitute of Λ like quintessence [2], phantom model [3], tachyon field [4] and k-essence [5] that also predict cosmic expansion. The generalization of simple barotropic equation of state (EoS) to more exotic forms like Chaplygin gas [6] and its modification [7] also correspond to DE candidates.

The concept of introducing scalar field, with an EoS parameter other than -1, has played a remarkable role to interpret the universe evolution due to its progressive implementation in various cosmological problems like cosmic acceleration and cosmic coincidence problem. The scalar field models can also predict the early inflationary cosmic era. We can choose scalar field models (in particular, phantom and tachyon) as a dynamical DE candidate interacting with DM by interchanging energy between them which may solve the coincidence problem. Researchers have paid an extensive attention to the tachyon cosmology where the tachyon is basically attributed by string theory [8, 9]. Gibbons discussed cosmological influence of the tachyon rolling down to its ground phase [10]. The universe model undergoes accelerated expansion as the tachyon field rolls down [9]. A tachyonic matter may yield inflation at early era and ultimately some new form of DM at late times [11]. A phantom field was also presented as an alternative of DE which constitutes large negative pressure with EoS parameter $w < -1$ and plays an important role for accelerated expansion of the universe [12]. One of the significant features of the phantom model is that the universe will end with a big-rip (future singularity). The interaction of DE (phantom or tachyon) and DM describes energy flow between the components such that no component remains conserved separately [13]. It is also demonstrated that an interaction between the components may alleviate the coincidence problem [14].

A phase space describes all possible states (position and momentum) associated with each point of the system. The analysis of viable stable late-time attractors has remarkable significance for different cosmological models. This provides dynamical behavior of a cosmological model by minimizing complexity of the equations. It is useful to study different patterns of evolution by transforming the system of equations to an autonomous one. This investigates the influence of initial data on stability of any system by checking whether the system remains stable for a long time [15]. The stability of different universe models via phase space helps to explore their qualitative features.

Copeland et al. [16] discussed phase space analysis of inflationary models which was unable to solve density problem. Guo et al. [17] studied stability of FRW universe model filled with barotropic fluid as well as phantom scalar field and found that phantom dominated solution is a stable late-time attractor. Guo et al. [18] analyzed phase space analysis of interacting phantom energy with DM. Yang and Gao [19] explored phase space analysis for k-essence cosmology and found that stability of critical points play a substantial role for the cosmic evolution. Xiao and Zhu [20] investigated stability of FRW universe model in loop quantum gravity by using phase space analysis along with barotropic fluid and positive field potential. Acquaviva and Beesham [21] discussed this analysis for FRW model and found that nonlinear viscous model describes possibility of current cosmic expansion. Recently, we have studied the impact of nonlinear electrodynamics on stability of accelerated expansion of FRW universe model [22]. Shahalam et al. [23] presented dynamical analysis of coupled phantom and tachyon fields by taking linear combinations of the coupling for FRW universe model.

Bianchi universe models have widely been discussed in literature to study expected primordial anisotropy and some large angle anomalies detected by CMBR which yield violation of statistical isotropy of cosmos [24]. Belinkskii and Khalatnikov [25] studied phase plane technique for Bianchi type I (BI) model under the influence of shear and bulk viscosity. Coley and Dunn [26] used phase plane approach to study dynamical behavior of Bianchi type V model containing a viscous fluid. Burd and Coley [27] investigated the effects of shear as well as bulk viscosity on the stability of Bianchi universe models. Goliath and Ellis [28] discussed dynamical evolution of Bianchi universe model via phase space by including Λ. Sharif and Waheed [29] explored phase space analysis of locally rotationally symmetric (LRS) BI universe for chameleon scalar field in Brans-Dicke gravity. Chaubey and

Raushan [30] studied phase space analysis of LRS BI model in the presence of scalar field.

This paper investigates stability of LRS BI universe by taking linear interactions of phantom and tachyon fields coupled with DM via phase space analysis. The plan of the paper is as follows. In section **2**, we provide some basic formalism for evolution equations. An autonomous system of equations is developed by introducing normalized dimensionless variables. Section **3** deals with dynamical analysis of interacting phantom energy and DM by taking three different forms of interactions. We discuss phase space analysis of tachyon field coupled with DM in section **4**. Section **5** deals with the formulation of power-law scale factor. Finally, we conclude our results in the last section.

2 General Equations

Bianchi universe models are the simplest extensions of FRW universe by adding anisotropic effects. It has been observed that some large angle anomalies in CMBR tend to violate the statistical isotropy of present cosmic models [24]. In this context, homogeneous anisotropic universe models under plane symmetric background has substantial role to understand these anomalies. The LRS BI model with anisotropic effects is defined by the line element

$$ds^2 = -dt^2 + a(t)dx^2 + b(t)(dy^2 + dz^2), \tag{1}$$

where $a(t)$ and $b(t)$ represent the cosmic expansion radii. We can define the mean Hubble parameter as

$$H = \frac{1}{3}[H_1 + H_2] = \frac{1}{3}\left[\frac{\dot{a}}{a} + \frac{2\dot{b}}{b}\right] = \frac{1}{3}\left(\frac{\dot{v}}{v}\right), \tag{2}$$

where $H_1 = \frac{\dot{a}}{a}$, $H_2 = \frac{\dot{b}}{b}$ are directional Hubble parameters. For a spatially homogeneous spacetime, the normal congruence to homogeneous expansion leads to a constant ratio, i.e., the expansion and shear scalars are proportional to each other. We assume a power-law relation $a = b^m$, $m \neq 0, 1$, where m is a constant anisotropic parameter which differentiates the expansion along x and y directions and represents the deviation of anisotropic universe model from isotropic. We define the average Hubble expansion by a relationship

between mean and directional Hubble parameters as

$$H_1 = mH_2 = \left(\frac{3m}{m+2}\right) H. \tag{3}$$

This assumption can be justified by velocity redshift relation for extragalactic sources which indicates that Hubble cosmic expansion may attain isotropy when shear to expansion scalar ratio is constant [31]. Collins [32] studied its physical consequences by taking perfect fluid and barotropic EoS in a more general way. Many other authors have also used this condition in literature [33].

The cosmic fluid is considered by coupling phantom field and matter. We consider that these two components interact through the interaction term Q such that the conservation of energy yield

$$\begin{aligned} \dot{\sigma}_m + 3(\sigma_m + p_m)H &= Q, & (4)\\ \dot{\sigma}_\phi + 3(\sigma_\phi + p_\phi)H &= -Q, & (5)\\ \dot{\sigma} + 3(\sigma + p)H &= 0, & (6) \end{aligned}$$

where dot represents derivative with respect to time, $\sigma = \sigma_m + \sigma_\phi$, $p = p_m + p_\phi$, σ_m, σ_ϕ, p_m and p_ϕ correspond to energy densities and pressures of matter and phantom energy, respectively. It is noted that the sign of interaction term denotes the transfer of energy between two components. For $Q > 0$, the energy flows from phantom to matter while $Q < 0$ corresponds to vice versa. The interaction term gives an additional degree of freedom which can be restricted by the constant energy density ratio at late times. It has always been interesting to study cosmological consequences of these interactions by considering their several forms [34]. It is clear from the above conservation equations that $Q = Q(H, \sigma_m, \sigma_\phi)$. The constraint and Raychaudhuri equations obtained from the field equations are given by

$$\begin{aligned} H^2 &= \frac{(m+2)^2}{9(2m+1)}(\sigma_m + \sigma_\phi), & (7)\\ 0 &= \left(\frac{6}{m+2}\right)\dot{H} + \frac{27}{(m+2)^2}H^2 + p_\phi, & (8) \end{aligned}$$

where $\sigma_\phi = -\frac{1}{2}\dot{\phi}^2 + V(\phi)$, $p_\phi = -\frac{1}{2}\dot{\phi}^2 - V(\phi)$. Due to many arbitrary parameters, it seems difficult to find analytical solution of the evolution equation.

For this purpose, we define the following normalized dimensionless quantities

$$\mu=\frac{(m+2)\dot{\phi}}{\sqrt{6}(2m+1)H},\quad \nu=\frac{(m+2)\sqrt{V}}{\sqrt{3}(2m+1)H},\quad \lambda=-\frac{V'}{V}, \tag{9}$$

that direct the evolution equations into an autonomous system. Differentiating μ and ν with respect to $N=\frac{m+2}{3m}\ln a$, we have

$$\mu' = \frac{(m+2)}{3m}\mu\left[\frac{\ddot{\phi}}{H\dot{\phi}}-\frac{\dot{H}}{H^2}\right], \tag{10}$$

$$\nu' = -\frac{(m+2)}{3m}\nu\left[\sqrt{6}\mu\lambda+\frac{\dot{H}}{H^2}\right]. \tag{11}$$

For an exponential potential, Raychaudhuri and conservation equations in terms of these dimensionless quantities become

$$\frac{\dot{H}}{H^2} = -\frac{1}{2(m+2)}\left[9+(2m+1)^2\{\mu^2-\nu^2\}\right], \tag{12}$$

$$\frac{\ddot{\phi}}{H\dot{\phi}} = 3-\sqrt{\frac{3}{2}}\frac{2m+1}{m+2}\frac{\lambda\nu^2}{\mu}+\frac{Q}{H\dot{\phi}^2}, \tag{13}$$

where λ is taken as a constant. We can write from the constraint equation

$$\Omega_\phi=\frac{(m+2)^2}{9(2m+1)}\frac{\sigma_\phi}{H^2}=\frac{2m+1}{3}[-\mu^2+\nu^2]. \tag{14}$$

The effective EoS for the cosmic fluid and phantom field are given by

$$w_{eff}=-1-\frac{2\dot{H}}{3H^2},\quad w_\phi=\frac{w_eff}{\Omega_\phi}. \tag{15}$$

3 Dynamics of Interacting Phantom Energy

This section deals with stability of LRS BI model through phase space analysis by taking interaction between phantom energy and matter. In order to find critical points $\{\mu,\nu\}$, we need to solve the dynamical system of Eqs.(10) and (11) by imposing the condition $\mu'=\nu'=0$. The stability of LRS BI universe model will be discussed according to the nature of critical points and the corresponding eigenvalues. In the following, we consider three different forms of interactions between phantom field and matter.

3.1 Coupling $Q = \alpha\dot{\sigma}_m$

Firstly, we take a model of interaction $Q = \alpha\dot{\sigma}_m$ for cosmos where both phantom field as well as DM are present. Equation (13), in terms of this coupling, turns out to be

$$\frac{\ddot{\phi}}{H\dot{\phi}} = 3 - \sqrt{\frac{3}{2}}\frac{2m+1}{m+2}\frac{\lambda\nu^2}{\mu} - \frac{3\alpha\Omega_m}{2(1-\alpha)\mu}, \tag{16}$$

where $\Omega_m = 1 - \Omega_\phi$. The corresponding autonomous system of equations reduces to

$$\begin{aligned}
\mu' &= \frac{(m+2)}{3m}\mu\left[3 - \sqrt{\frac{3}{2}}\frac{2m+1}{m+2}\frac{\lambda\nu^2}{\mu} - \frac{3\alpha\Omega_m}{2(1-\alpha)\mu^2} + \frac{1}{2(m+2)}\right. \\
&\times \left.\{9 + (2m+1)^2(\mu^2-\nu^2)\}\right], \qquad (17) \\
\nu' &= -\frac{(m+2)}{3m}\nu\left[\sqrt{6}\mu\lambda - \frac{1}{2(m+2)}\{9 + (2m+1)^2(\mu^2-\nu^2)\}\right]. \qquad (18)
\end{aligned}$$

The eigenvalues can be determined by the Jacobian matrix

$$A = \begin{pmatrix} \frac{\partial f}{\partial \mu} & \frac{\partial f}{\partial \nu} \\ \frac{\partial g}{\partial \mu} & \frac{\partial g}{\partial \nu} \end{pmatrix}_0, \tag{19}$$

where suffix 0 gives the values at critical points (μ_c, ν_c). The critical point is called a source (respectively, a sink) if both eigenvalues consist of positive (respectively, negative) real parts. The real parts of the eigenvalues having opposite signs correspond to a saddle point of the system. We evaluate the following critical points in this case. For $P_1 = (\mu_c, \nu_c) = \left(-\frac{1}{\sqrt{6}\lambda}\left\{\frac{6-\alpha(2m+7)}{2(1-\alpha)}\right\}, 0\right)$, the eigenvalues of Jacobian matrix are given by

$$\begin{aligned}
\eta_1 &= \frac{(m+2)}{3m}\left[3 - \frac{3\alpha}{2(1-\alpha)}\left\{\frac{24(1-\alpha)^2\lambda^2}{[6-\alpha(2m+1)]^2} - \frac{2m+1}{3}\right\}\right. \\
&+ \left.\frac{1}{2(m+2)}\left\{9 + \frac{(2m+1)^2[6-\alpha(2m+7)]^2}{8(1-\alpha)^2\lambda^2}\right\}\right], \qquad (20) \\
\eta_2 &= -\frac{(m+2)}{3m}\left[\frac{\alpha(2m+7)-6}{2(1-\alpha)} - \frac{1}{2(m+2)}\{9\right. \\
&+ \left.\frac{(2m+1)^2[6-\alpha(2m+7)]^2}{24(1-\alpha)^2\lambda^2}\right\}\Bigg]. \qquad (21)
\end{aligned}$$

We are interested to study the impact of parameters m and α on the stability of critical points in the presence of scalar field model. We plot the dynamical behavior of critical points for $Q=\alpha\dot{\sigma}_m$ by taking different values of α and m as shown in Figure **1**. In these numerical plots, we observe that the eigenvalues are positive indicating the point P_1 as an unstable past attractor for $m>0$ in the physical phase space except for $\alpha=1, m=-2$ at which the system becomes undetermined. For $m<0$, this point becomes stable future attractor. The dynamical analysis shows a matter dominated era ultimately followed by a late accelerated expansion phase of the universe. For $P_2=\left(\frac{\sqrt{6}\lambda\pm\sqrt{6\lambda^2-\left(\frac{3(2m+1)}{m+2}\right)^2}}{\frac{(2m+1)^2}{m+2}},0\right)$, the corresponding eigenvalues are

$$\begin{aligned}\eta_1 &= \frac{(m+2)}{3m}\left[3-\frac{3\alpha}{2(1-\alpha)}\left\{\frac{(2m+1)^4}{(m+2)^2\left[\sqrt{6}\lambda\pm\sqrt{6\lambda^2-\left(\frac{3(2m+1)}{m+2}\right)^2}\right]^2}\right.\right.\\ &- \left.\left.\frac{2m+1}{3}\right\}+\frac{1}{2(m+2)}\left\{9+(2m+1)^2\left[\frac{(2m+1)^4}{(m+2)^2}\right.\right.\right.\\ &\times \left.\left.\left.\frac{1}{\left[\sqrt{6}\lambda\pm\sqrt{6\lambda^2-\left(\frac{3(2m+1)}{m+2}\right)^2}\right]}\right]\right\}\right], \qquad (22)\\ \eta_2 &= -\frac{(m+2)}{3m}\left[\sqrt{6}(m+2)\lambda\left\{\frac{\sqrt{6}\lambda\pm\sqrt{6\lambda^2-\left(\frac{3(2m+1)}{m+2}\right)^2}}{(2m+1)^2}\right\}-\frac{1}{2(m+2)}\right.\\ &\times \left.\left\{9+(2m+1)^2(m+2)^2\left[\frac{\sqrt{6}\lambda\pm\sqrt{6\lambda^2-\left(\frac{3(2m+1)}{m+2}\right)^2}}{2m+1}\right]^2\right\}\right]. \qquad (23)\end{aligned}$$

This point corresponds to unstable past attractor without accelerated expansion for $m>0$. By taking negative values of parameter m, this point

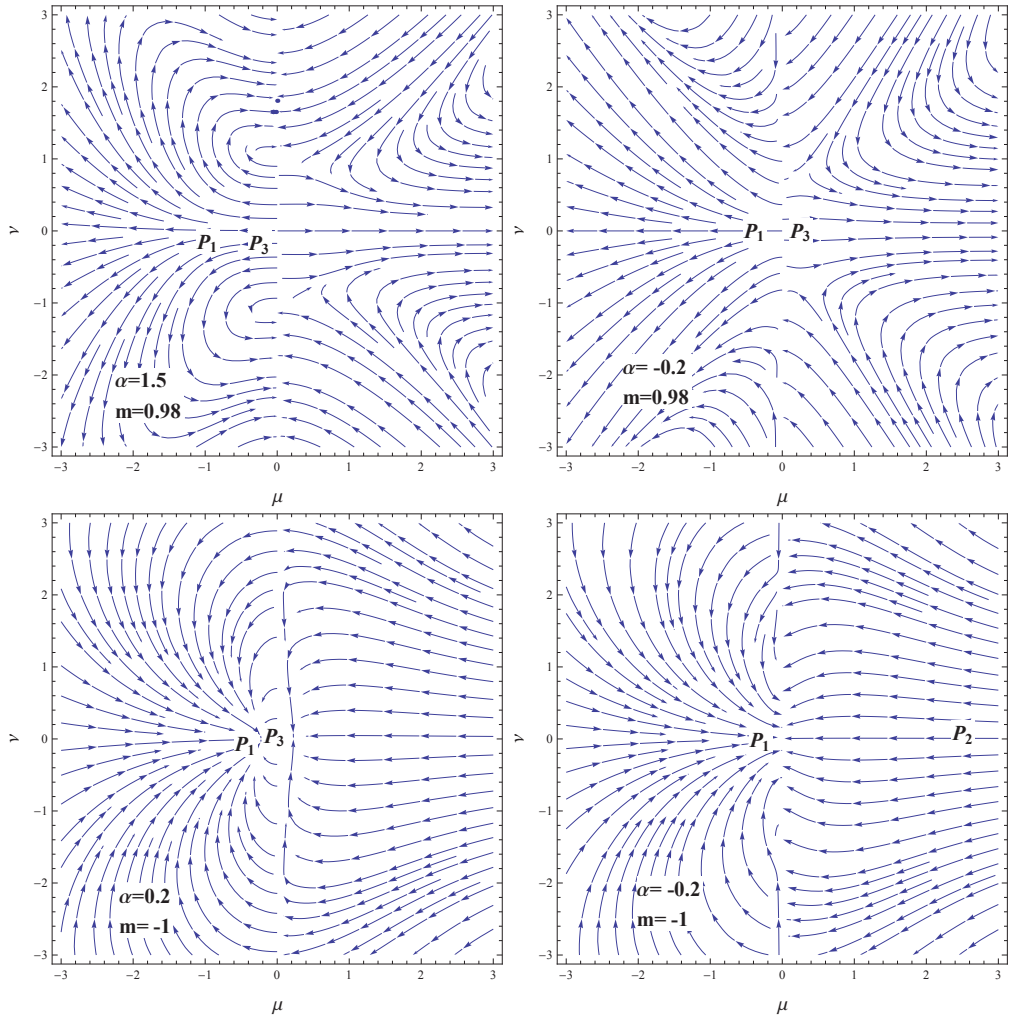

Figure 1: Plots for the phase plane evolution of phantom coupled universe model with $Q = \alpha\dot{\sigma}_m$ and $\lambda = 2$.

becomes stable future attractor or a saddle point depending on values of α. It is noted that the stable point undergoes accelerated expansion as $q<0$.

For $P_3=\left(\frac{\sqrt{3(2m+7)+\alpha(2m^2-m-19)+\sqrt{[3(2m+7)+\alpha(2m^2-m-19)]^2-\alpha(\alpha-1)(m+2)(2m+1)}}}{2(\alpha-1)(2m+1)},0\right)$, we have

$$\begin{aligned}\eta_1 &= \frac{(m+2)}{3m}\left[3-\frac{3\alpha}{2(1-\alpha)}\left\{\frac{2(\alpha-1)(2m+1)}{3(2m+7)+\alpha(2m^2-m-19)+\xi}\right.\right.\\ &- \left.\frac{2m+1}{3}\right\}+\frac{1}{2(m+2)}\left\{9+\frac{3(2m+1)^2}{2(\alpha-1)(2m+1)}\left[3(2m+7)\right.\right.\\ &+ \left.\left.\alpha(2m^2-m-19)+\xi\right]\right\}\Big], \qquad (24)\\ \eta_2 &= -\frac{(m+2)}{3m}\left[\frac{\sqrt{3}\lambda\sqrt{3(2m+7)+\alpha(2m^2-m-19)+\xi}}{(\alpha-1)(2m+1)}\right.\\ &- \frac{1}{2(m+2)}\left\{9+\frac{(2m+1)^2}{2(\alpha-1)(2m+1)}[3(2m+7)\alpha(2m^2-m-19)\right.\\ &+ \left.\left.\xi]\right\}\right], \qquad (25)\end{aligned}$$

where $\xi=\sqrt{[3(2m+7)+\alpha(2m^2-m-19)]^2-\alpha(\alpha-1)(m+2)(2m+1)}$. We find the same behavior of this point for positive values of m. This point is also a stable future attractor for $m<0$ showing accelerated expanding universe model. The effective potential for the cosmic fluid is given by

$$w_{eff}=-1+\frac{1}{m+2}[9+(2m+1)(\mu^2-\nu^2)]. \qquad (26)$$

The effective EoS parameter and deceleration parameter are given by

$$\begin{aligned}w_\phi &= \frac{1}{\mu^2+\nu^2}\left[-1+\frac{1}{m+2}\{9+(2m+1)(\mu^2-\nu^2)\}\right], \qquad (27)\\ q &= -1+\frac{1}{m+2}[9+(2m+1)(\mu^2-\nu^2)]. \qquad (28)\end{aligned}$$

It is mentioned here that points P_1 and P_2 undergo decelerated expansion while the point P_3 is a stable future attractor that lies in accelerated expanding phase of the universe as $q<0$ and $\omega_\phi<-1$. The summary of the results for evolution as well as stability of LRS BI model coupled with phantom energy and matter is given in Table **1**.

Table 1:
Stability Analysis for the Phantom Coupled System with $Q=\alpha\dot{\sigma}_m$.

Ranges of α and m for Critical Points	**Stability**	**Acceleration**
P_1		
$\alpha>0,\ m>0\ (\alpha\neq 1)$	Unstable	No
$\alpha<0,\ m>0$	Unstable	No
$\alpha<0,\ m<0\ (m\neq -2)$	Stable	No
$\alpha>0,\ m<0$	Stable	No
P_2		
$\alpha>0,\ m>0\ (\alpha\neq 1)$	Unstable	No
$\alpha<0,\ m>0$	Unstable/Saddle	No
$\alpha<0,\ m<0\ (m\neq -0.5,-2)$	Stable/Saddle	Yes
$\alpha>0,\ m<0$	Stable/Saddle	Yes
P_3		
$\alpha>0,\ m>0\ (\alpha\neq 1)$	Unstable/Saddle	No
$\alpha<0,\ m>0$	Saddle	No
$\alpha<0,\ m<0\ (m\neq -0.5,-2)$	Stable	Yes
$\alpha>0,\ m<0$	Stable	No

3.2 Coupling $Q=\beta\dot{\sigma}_\phi$

For this coupling, Eq.(13) takes the form

$$\frac{\ddot{\phi}}{H\dot{\phi}}=3-\sqrt{\frac{3}{2}}\frac{2m+1}{m+2}\frac{\lambda\nu^2}{\mu}-\frac{3\beta}{1+\beta}. \tag{29}$$

The autonomous system of equations becomes

$$\begin{aligned}\mu' &= \frac{(m+2)}{3m}\mu\left[3-\sqrt{\frac{3}{2}}\frac{2m+1}{m+2}\frac{\lambda\nu^2}{\mu}-\frac{3\beta}{1-\beta}+\frac{1}{2(m+2)}\right.\\ &\times \left.\{9+(2m+1)^2(\mu^2-\nu^2)\}\right], \qquad (30)\\ \nu' &= -\frac{(m+2)}{3m}\nu\left[\sqrt{6}\mu\lambda-\frac{1}{2(m+2)}\{9+(2m+1)^2(\mu^2-\nu^2)\}\right], \qquad (31)\end{aligned}$$

We follow the same procedure to find the critical points. For $P_1=(0,0)$, we have

$$\eta_1=\frac{3}{2m}+\frac{m+2}{m(1+\beta)},\quad \eta_2=\frac{3}{2m}. \tag{32}$$

This point shows a varying behavior for different values of parameters β and m. For $\alpha = 0.8, -0.2$, we find that point P_1 is unstable/saddle node by taking only positive values of m and $\lambda = 2$ (Figure **2**). For $\beta = -1$, the eigenvalues become undetermined, hence we neglect it. We observe that negative values of m show a stable future attractor. It is mentioned here that point P_1 undergoes decelerated cosmic expansion since $q < 0$ for all choices of parameters.

For $P_2 = \left(\frac{1}{2m+1}\sqrt{\frac{3[3\beta-(2m+1)]}{1+\beta}}, 0\right)$, the eigenvalues are given by

$$\eta_1 = \frac{m+2}{m(1+\beta)} + \frac{3[1+4\beta-2(m+1)]}{2m(1+\beta)}, \tag{33}$$

$$\eta_2 = -\frac{\sqrt{2}(m+2)\lambda}{m(2m+1)}\sqrt{\frac{3\beta-(2m+1)}{1+\beta}} + \frac{3+6\beta-2(m+1)}{2m(1+\beta)}. \tag{34}$$

This point shows opposite behavior as compared to the previous point. Here all choices of m and α give stable nodes except $m > 0$ and $\alpha > 0$ that correspond to unstable node. In this case, the universe is in decelerated expansion phase for all values of m. For $P_3 = \left(-\frac{1}{2m+1}\sqrt{\frac{3[3\beta-(2m+1)]}{1+\beta}}, 0\right)$, the corresponding eigenvalues yield

$$\eta_1 = \frac{m+2}{m(1+\beta)} + \frac{3[1+4\beta-2(m+1)]}{2m(1+\beta)}, \tag{35}$$

$$\eta_2 = \sqrt{\frac{2}{3}}\frac{(m+2)\lambda}{m(2m+1)}\sqrt{\frac{3[3\beta-(2m+1)]}{1+\beta}} + \frac{3+6\beta-2(m+1)}{2m(1+\beta)}. \tag{36}$$

We find that point P_3 is an unstable past attractor for all values of α and m except for $-0.9 < \beta < -0.1$ at which it behaves as a stable node. For $P_4 = \left(0, \pm\frac{3}{2m+1}\right)$, the eigenvalues are

$$\eta_1 = \frac{m+2}{m(1+\beta)}, \quad \eta_2 = \frac{m+2}{m(1+\beta)}. \tag{37}$$

This point is also an unstable past attractor for positive values of m. It is noted that for $Q = \beta\dot{\sigma}_\phi$, all points lie in a region of decelerated expansion. A general dynamical analysis is given in Table **2**.

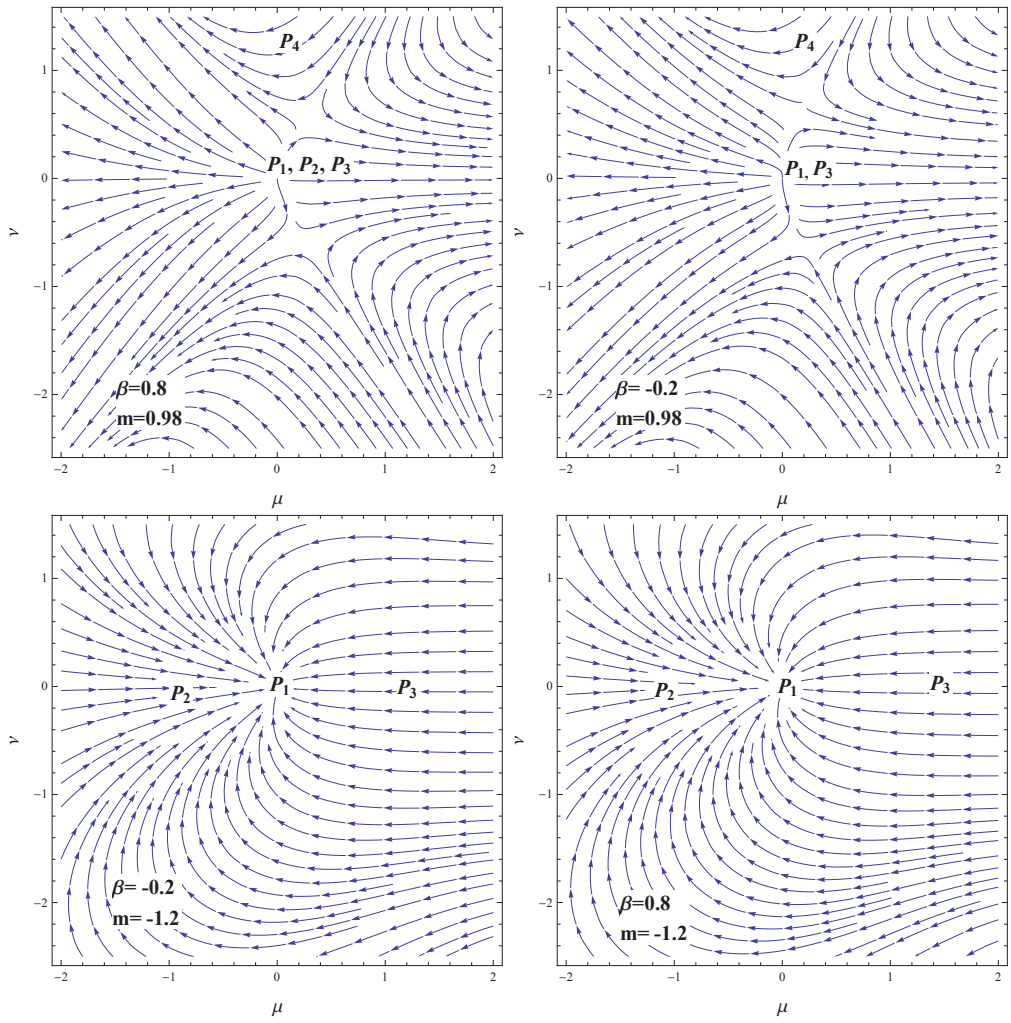

Figure 2: Plots for the phase plane evolution of phantom coupled universe model with $Q = \beta\dot{\sigma}_\phi$ and $\lambda = 2$.

Table 2: Stability Analysis for the Phantom Coupled System with $Q=\beta\dot{\sigma}_{\phi}$.

Ranges of β and m for Critical Points	**Stability**	**Acceleration**
P_1		
$\beta>0,\ m>0$	Unstable	No
$\beta<0,\ m>0,\ \beta\neq-1$	Unstable/Saddle	No
$\beta<0,\ m<0$	Stable	No
$\beta>0,\ m<0$	Stable	No
P_2		
$\beta>0,\ m>0$	Unstable	No
$\beta<0,\ m>0,\ \beta\neq-1$	Stable	No
$\beta<0,\ m<0,\ m\neq-0.5$	Stable	No
$\beta>0,\ m<0$	Stable	No
P_3		
$\beta>0,\ m>0$	Unstable	No
$\beta<0,\ m>0,\ \beta\neq-1$	Stable/Unstable	No
$\beta<0,\ m<0,\ m\neq-0.5$	Unstable	No
$\beta>0,\ m<0$	Stable for $-0.9<\beta<-0.1$	No
P_4		
$\beta>0,\ m>0$	Unstable	No
$\beta<0,\ m>0,\ \beta\neq-1$	Unstable	No
$\beta<0,\ m<0$	Stable	No
$\beta>0,\ m<0$	Stable	No

3.3 Coupling $Q=\gamma(\dot{\sigma}_m+\dot{\sigma}_{\phi})$

Here we consider the coupling as a linear combination of $\dot{\sigma}_m$ and $\dot{\sigma}_{\phi}$ for which Eq.(13) becomes

$$\frac{\ddot{\phi}}{H\dot{\phi}}=3-\sqrt{\frac{3}{2}}\frac{2m+1}{m+2}\frac{\lambda\nu^2}{\mu}-\frac{3\gamma\Omega_m}{2(1-\gamma)\mu^2}-\frac{3\gamma}{1+\gamma}. \tag{38}$$

The evolution and conservation equations yield

$$\begin{aligned}\mu' &= \frac{(m+2)}{3m}\mu\left[3-\sqrt{\frac{3}{2}}\frac{2m+1}{m+2}\frac{\lambda\nu^2}{\mu}-\frac{3\gamma\Omega_m}{2(1-\gamma)\mu^2}-\frac{3\gamma}{1+\gamma}+\frac{1}{2(m+2)}\right.\\ &\times \left.\{9+(2m+1)^2(\mu^2-\nu^2)\}\right], \end{aligned}\tag{39}$$

$$\nu' = -\frac{(m+2)}{3m}\nu\left[\sqrt{6}\mu\lambda - \frac{1}{2(m+2)}\{9+(2m+1)^2(\mu^2-\nu^2)\}\right]. \qquad (40)$$

For $P_1 = \left(\frac{\sqrt{6}\lambda+\sqrt{6\lambda^2-\left(\frac{3(2m+1)}{m+2}\right)^2}}{(2m+1)^2/2(m+2)}, 0\right)$, the corresponding eigenvalues are

$$\begin{aligned}\eta_1 &= \frac{(m+2)}{3m}\left[3-\left\{\frac{(2m+1)^4}{4(m+2)^2\left\{\sqrt{6}\lambda+\sqrt{6\lambda^2-\left(\frac{3(2m+1)}{m+2}\right)^2}\right\}}\right.\right. \\ &- \left.\left.\frac{2m+1}{3}\right\}\frac{3\gamma}{2(1-\gamma)} - \frac{3\gamma}{1+\gamma} + \frac{1}{2(m+2)}\left\{9+12(m+2)^2\right.\right. \\ &- \left.\left.\left[\frac{\sqrt{6}\lambda+\sqrt{6\lambda^2\left(\frac{3(2m+1)}{m+2}\right)^2}}{2m+1}\right]^2\right\}\right], \qquad (41)\end{aligned}$$

$$\begin{aligned}\eta_2 &= -\frac{(m+2)}{3m}\left[2\sqrt{6}(m+2)\lambda\left\{\frac{6\lambda+\sqrt{6\lambda^2-\left(\frac{3(2m+1)}{m+2}\right)^2}}{(2m+1)^2}\right\}\right. \\ &- \left.\frac{1}{2m+1}\left\{9+4(m+2)^2\left[\frac{6\lambda+\sqrt{6\lambda^2-\left(\frac{3(2m+1)}{m+2}\right)^2}}{(2m+1)}\right]^2\right\}\right]. \qquad (42)\end{aligned}$$

In this case, the nature of eigenvalues indicates unstable nodes for $m > 0$ with all choices of γ except for $\gamma = 1, -1$ (Figure **3**). We find both eigenvalues negative for $m = -0.2$ showing stable attractors. All the choices of parameters m and γ show decelerated expanding universe as $q > 0$. The summary of respective results is shown in Table **3**.

For $P_2 = \left(\frac{\sqrt{6}\lambda-\sqrt{6\lambda^2-\left(\frac{3(2m+1)}{m+2}\right)^2}}{(2m+1)^2/2(m+2)}, 0\right)$, the corresponding eigenvalues are

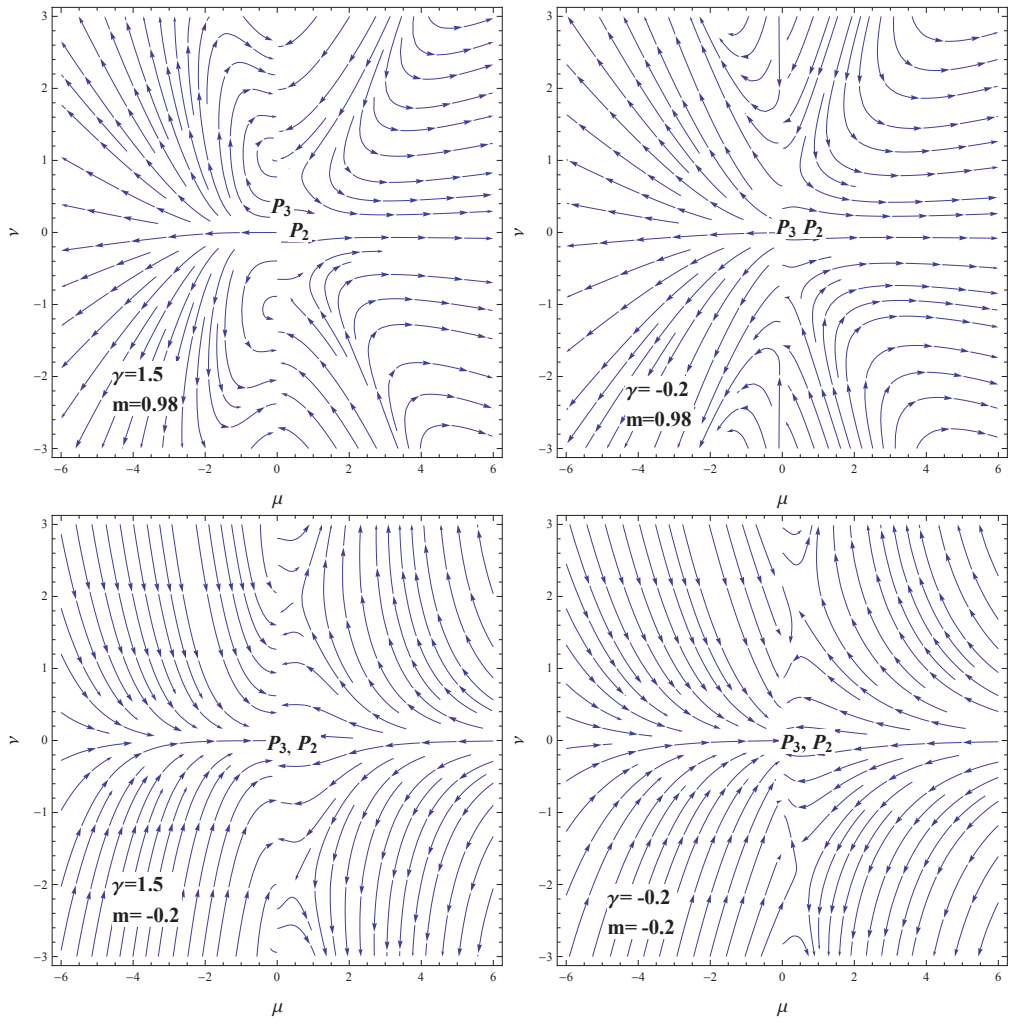

Figure 3: Plots for the phase plane evolution of phantom coupled universe model with $Q = \gamma(\dot{\sigma}_m + \dot{\sigma}_\phi)$ and $\lambda = 2$.

Table 3: Stability Analysis for the Phantom Coupled System with $Q=\gamma(\dot{\sigma}_m+\dot{\sigma}_\phi)$.

Ranges of γ and m for Critical Points	**Stability**	**Acceleration**
$\mathbf{P}_1$		
$\gamma>0,\ m>0,\ \gamma\neq 1$	Unstable	No
$\gamma<0,\ m>0,\ \gamma\neq -1$	Unstable	No
$\gamma<0,\ m<0,\ m\neq -0.5,-2$	Stable for $m=-0.2$	No
$\gamma>0,\ m<0$	Stable for $m=-0.2$	No
$\mathbf{P}_2$		
$\gamma>0,\ m>0,\ \gamma\neq 1$	Unstable	No
$\gamma<0,\ m>0,\ \gamma\neq -1$	Unstable/Saddle	No
$\gamma<0,\ m<0,\ m\neq -0.5,-2$	Saddle	No
$\gamma>0,\ m<0$	Saddle	No
$\mathbf{P}_3$		
$\gamma>0,\ m>0,\ \gamma\neq 1$	Unstable/Saddle	No
$\gamma<0,\ m>0,\ \gamma\neq -1$	Unstable/Saddle	No
$\gamma<0,\ m<0,\ m\neq -2$	Stable	Yes
$\gamma>0,\ m<0$	Stable	Yes

given as

$$\begin{aligned}
\eta_1 &= \frac{(m+2)}{3m}\left[3-\left\{\frac{(2m+1)^4}{4(m+2)^2\left\{\sqrt{6}\lambda-\sqrt{6\lambda^2-\left(\frac{3(2m+1)}{m+2}\right)^2}\right\}}\right.\right.\\
&- \left.\left.\frac{2m+1}{3}\right\}\frac{3\gamma}{2(1-\gamma)}-\frac{3\gamma}{1+\gamma}+\frac{1}{2(m+2)}\left\{9+12(m+2)^2\right.\right.\\
&- \left.\left.\left[\frac{\sqrt{6}\lambda-\sqrt{6\lambda^2-\left(\frac{3(2m+1)}{m+2}\right)^2}}{2m+1}\right]^2\right\}\right], \qquad (43)\\
\eta_2 &= -\frac{(m+2)}{3m}\left[2\sqrt{6}(m+2)\lambda\left\{\frac{6\lambda-\sqrt{6\lambda^2-\left(\frac{3(2m+1)}{m+2}\right)^2}}{(2m+1)^2}\right\}\right.
\end{aligned}$$

$$- \quad \frac{1}{2m+1}\left\{9+4(m+2)^2\left[\frac{6\lambda-\sqrt{6\lambda^2-\left(\frac{3(2m+1)}{m+2}\right)^2}}{(2m+1)}\right]^2\right\}\Bigg], \tag{44}$$

which corresponds to either unstable or saddle node that lies in matter dominated era for all choices of different parameters. For $P_3 = \left(\frac{\tilde{\xi_1}}{\sqrt{2}}, 0\right)$, the eigenvalues are

$$\begin{aligned}
\eta_1 &= \frac{(m+2)}{3m}\left[3-\frac{3\gamma}{2(1-\gamma)}\left\{\frac{2}{\tilde{\xi_1}^2}-\frac{2m+1}{3}\right\}-\frac{3\gamma}{1+\gamma}\right. \\
&+ \left.\frac{1}{2(m+2)}\left\{9+\frac{3(2m+1)^2\tilde{\xi_1}^2}{2}\right\}\right], \qquad (45)\\
\eta_2 &= -\frac{(m+2)}{3m}\left[\sqrt{3}\lambda\tilde{\xi_1}-\frac{1}{2(m+2)}\left(9+\frac{(2m+1)\tilde{\xi_1}^2}{2}\right)\right], \qquad (46)
\end{aligned}$$

where

$$\begin{aligned}
\tilde{\xi_1} &= \sqrt{\frac{3(2m+3)+\gamma(2m^2-m-10)+\gamma^2(2m^2-5m-25)}{(2m+1)^2(\gamma^2-1)}}+\tilde{\xi}_2,\\
\tilde{\xi_2} &= \sqrt{(-12\gamma(\gamma+1)(\gamma^2-1)(m+2)(2m+1)^2+39-5\gamma(5\gamma+2)+\tilde{\xi}_3)^2},\\
\tilde{\xi_3} &= 2m^2\gamma(\gamma+1)+m(5\gamma^2-\gamma+6)^2.
\end{aligned}$$

The nature of eigenvalues as well as trajectories show that point P_3 is unstable past attractor in deceleration region for $m > 0$ with $\gamma \neq 1, -1$. This point becomes a stable global attractor for negative values of m except for $m = -0.5, -2$ that give undetermined eigenvalues. In this case, $q < 0$ and $\omega_\phi < -1$ showing accelerated expansion of the universe.

4 Coupled Tachyon Dynamics

Now we discuss phase space analysis of the universe model by taking a tachyon coupled cosmic component. The conservation equations are

$$\dot{\sigma}_m + 3(\sigma_m + p_m)H = Q, \tag{47}$$

$$\dot{\sigma}_\phi + 3(\sigma_\phi + p_\phi)H = -Q, \tag{48}$$

where $\sigma_\phi = \frac{V(\phi)}{\sqrt{1-\dot{\phi}^2}}$ and $p_\phi = -V(\phi)\sqrt{1-\dot{\phi}^2}$. The evolution equations yield

$$H^2 = \frac{(m+2)^2}{9(2m+1)}\left[\frac{V(\phi)}{\sqrt{1-\dot{\phi}^2}} + \sigma_m\right], \tag{49}$$

$$\frac{\ddot{\phi}}{1-\dot{\phi}^2} = -\left[3H\dot{\phi} + \frac{V'(\phi)}{V(\phi)} + \frac{Q\sqrt{1-\dot{\phi}^2}}{V(\phi)\dot{\phi}}\right]. \tag{50}$$

We introduce the following dimensionless parameters

$$\mu = \frac{(m+2)\dot{\phi}}{2m+1}, \quad \nu = \frac{(m+2)\sqrt{V}}{\sqrt{3}(2m+1)H}, \quad \lambda = -\frac{V'}{V\sqrt{V}}, \tag{51}$$

such that the autonomous system of equations takes the form

$$\mu' = \frac{(m+2)^2}{3m(2m+1)}\frac{\ddot{\phi}\mu}{H\dot{\phi}}, \tag{52}$$

$$\nu' = -\frac{(2m+1)\lambda\mu\nu^2}{2\sqrt{3}m(m+2)} - \frac{(m+2)\nu}{3m}\frac{\dot{H}}{H^2}. \tag{53}$$

We take inverse square potential with constant parameter λ. In this case, we consider the only coupling $Q = \beta\dot{\sigma}_\phi$ for which Eqs.(49) and (50) give

$$\frac{\dot{H}}{H^2} = \frac{(2m+1)^2}{2(m+2)}\nu^2\sqrt{1-\left(\frac{2m+1}{m+2}\right)^2\mu^2} - \frac{9}{2(m+2)}, \tag{54}$$

$$\frac{\ddot{\phi}}{\dot{\phi}H} = \left[1-\left(\frac{2m+1}{m+2}\right)^2\mu^2\right]\left[\frac{\sqrt{3}\nu\lambda}{\mu} + \frac{3\beta}{1+\beta} - 3\right]. \tag{55}$$

The effective EoS and deceleration parameters are given by

$$w_{eff} = -1 - \frac{1}{3(m+2)}\left[(2m+1)^2\nu^2\sqrt{1-\left(\frac{2m+1}{m+2}\right)^2\mu^2} - 9\right], \tag{56}$$

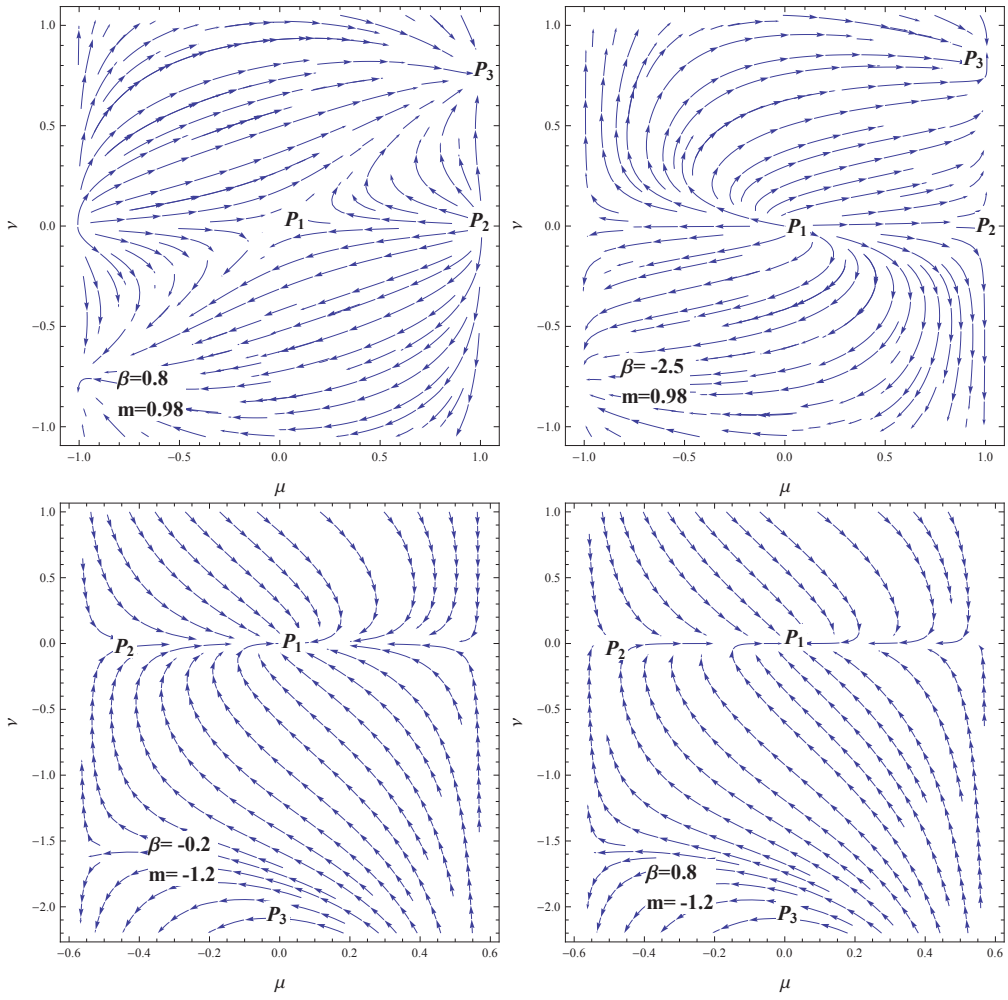

Figure 4: Plots for the phase plane evolution of tachyon coupled universe model with $Q = \beta\dot{\sigma}_\phi$ and $\lambda = 2$.

$$q = -1 - \frac{1}{2(m+2)}\left[(2m+1)^2\nu^2\sqrt{1-\left(\frac{2m+1}{m+2}\right)^2\mu^2} - 9\right]. \quad (57)$$

The critical points and their corresponding eigenvalues for tachyon coupled field are given as follows. For $P_1 = (0, 0)$, we have

$$\eta_1 = -\frac{(m+2)^2}{m(2m+1)(1+\beta)}, \quad \eta_2 = \frac{3}{2m}. \quad (58)$$

In case of tachyon coupled field, source and sink can be observed according to the sign of eigenvalues. We investigate stability of critical points corresponding to different values of m and other parameters. The cosmic portrait includes a matter dominated epoch ultimately followed by a late accelerated expansion phase. We find that point P_1 is saddle/unstable node for positive values of m (Figure **4**). This point becomes global stable node for $m < 0$ $(m \neq -0.5, \beta \neq -1)$ showing accelerated expansion of the universe model as $q < 0$. The summary of the obtained results is given in Table **4**.

Table 4: Stability Analysis for the Tachyon Coupled System with $Q = \beta\dot{\sigma}_\phi$.

Ranges of β and m for Critical Points	**Stability**	**Acceleration**
$\mathbf{P}_1$		
$\beta > 0,\ m > 0,\ \beta \neq -1$	Saddle	Yes
$\beta < 0,\ m > 0$	Unstable	Yes
$\beta < 0,\ m < 0,\ m \neq -0.5$	Stable	Yes
$\beta > 0,\ m < 0$	Stable	Yes
$\mathbf{P}_2$		
$\beta > 0,\ m > 0$	Unstable	Yes
$\beta < 0,\ m > 0,\ \beta \neq -1$	Unstable	Yes
$\beta < 0,\ m < 0,\ m \neq -0.5$	Saddle	Yes
$\beta > 0,\ m < 0$	Saddle	Yes
$\mathbf{P}_3$		
$\beta > 0,\ m > 0$	Stable	Yes
$\beta < 0,\ m > 0,\ \beta \neq -1$	Stable	Yes
$\beta < 0,\ m < 0,\ m \neq -0.5$	Saddle/Unstable	Yes
$\beta > 0,\ m < 0$	Saddle/Unstable	Yes

For $P_2 = \left(\pm\frac{m+2}{2m+1}, 0\right)$, the eigenvalues become

$$\eta_1 = \frac{2(m+2)^2}{m(2m+1)(1+\beta)}, \quad \eta_2 = \frac{3}{2m}, \tag{59}$$

which correspond to unstable nodes for positive values of parameter m lying in accelerated expanding phase of cosmos. For $m < 0$, we have stable global attractors undergoing accelerated expansion of the universe. When $P_3 = \left(0, \pm\frac{3}{2m+1}\right)$, the eigenvalues are given by

$$\eta_1 = -\frac{(m+2)^2}{m(2m+1)(1+\beta)}, \quad \eta_2 = -\frac{3}{m}. \tag{60}$$

In this case, the nature of eigenvalues indicate stable future attractor for $\beta > 0$ and $m > 0$ which undergoes accelerated expansion of the universe as $q < 0$. For $\beta < 0$ and $m > 0$, the point P_3 is stable except for $\beta = -1$. In this case, $q = -1$ and $w_{eff} = -1$ which indicate de Sitter phase of the universe. It is found that the respective point corresponds to saddle/unstable nodes for $\beta < 0,\ m < 0$ ($m \neq -0.5$) indicating accelerated expansion ($q < 0$). For $\beta > 0,\ m < 0$, it also shows saddle/unstable node which corresponds to de Sitter ($q = -1$, $w_{eff} = -1$) phase of cosmos.

5 Power-Law Scale Factor

In this section, we discuss the power-law behavior of the scale factor by applying some assumptions corresponding to both phantom as well as tachyon coupled fields. In this context, we integrate Eq.(12) which leads to

$$\dot{\Theta} = -\frac{1}{6(m+2)}[9 + (2m+1)^2(\mu^2 - \nu^2)]\Theta^2, \tag{61}$$

where $\Theta = 3H$ is the expansion scalar. For $\Theta \neq 0$, we determine power-law scale factor whenever $9 + (2m+1)^2(\mu^2 - \nu^2) \neq 0$. We find the corresponding generic critical point by solving $\Theta = \frac{\dot{a}}{a} + \frac{2\dot{b}}{b}$ for $a(t)$ and $b(t)$ as

$$b^{(m+2)} = b_0^{(m+2)}(t - t_0)^{\frac{6(m+2)}{9+(2m+1)^2(\mu^2-\nu^2)}}. \tag{62}$$

It is noticed that behavior of the term "$9 + (2m+1)^2(\mu^2 - \nu^2)$" is quite important to assess different cosmological phases. If $9 + (2m+1)^2(\mu^2 -$

$\nu^2) = 0$, it gives exponential expansion of the cosmological model. Also, $9+(2m+1)^2(\mu^2-\nu^2) \gtrless 0$ corresponds to accelerated expansion or contraction of the universe, respectively. Figure **5** shows different cosmological phases for power-law scale factor, where blue and gray regions correspond to contraction and accelerated expansion of the universe model, respectively. It is found that the region for decelerated expansion tends to increase by increasing m. For $m < 0$, there exists gray region only which shows that the universe model undergoes accelerated expansion.

In case of tachyon coupled fluid, Eq.(54) yields

$$\dot{\Theta} = -\frac{1}{6(m+2)}\left[(2m+1)^2\nu^2\sqrt{1-\left(\frac{2m+1}{m+2}\right)^2\mu^2} - \frac{9}{2(m+2)}\right]\Theta^2. \quad (63)$$

For $\Theta \neq 0$, we again evaluate power-law scale factor if $(2m+1)^2\nu^2\sqrt{1-\left(\frac{2m+1}{m+2}\right)^2\mu^2} - \frac{9}{2(m+2)} \neq 0$. The generic critical point is found by solving $\Theta = \frac{\dot{a}}{a} + \frac{2\dot{b}}{b}$ as

$$b^{(m+2)} = b_0^{(m+2)}(t-t_0)^{\frac{6(m+2)}{(2m+1)^2\nu^2\sqrt{1-\left(\frac{2m+1}{m+2}\right)^2\mu^2}-\frac{9}{2(m+2)}}}. \quad (64)$$

We explore different cosmological phases according to $(2m+1)^2\nu^2\sqrt{1-\left(\frac{2m+1}{m+2}\right)^2\mu^2} - \frac{9}{2(m+2)} \gtrless 0$. In contrast to the phantom coupled matter, we find different results for tachyon coupled field. We observe that the region for decelerated expansion decreases by increasing m while $m < 0$ shows contraction region only which means that the universe model undergoes decelerated expansion for negative values of m (Figure **6**).

6 Summary

This work is devoted to discuss phase space analysis of LRS BI universe model by taking a coupling between scalar field models and DM. An autonomous system of equations has been developed by defining normalized dimensionless variables which plays a remarkable role to study the stability of dynamical system. We have evaluated the corresponding critical points for different values of the parameters. We have also calculated eigenvalues characterizing these critical points and investigated the impact of m on their stability in

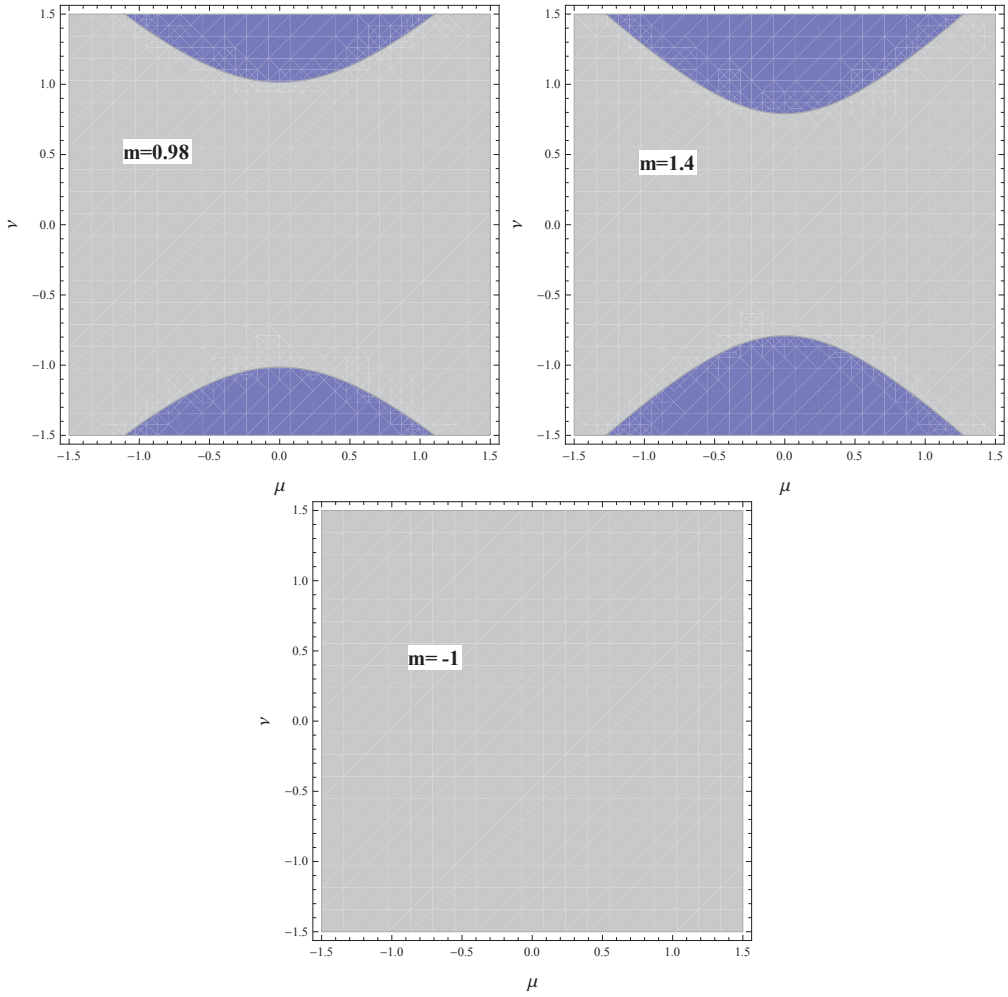

Figure 5: Plots of qualitative phase space analysis for power-law scale factor with phantom coupled matter. Blue and gray regions indicate contraction and accelerated expansion of the universe model, respectively.

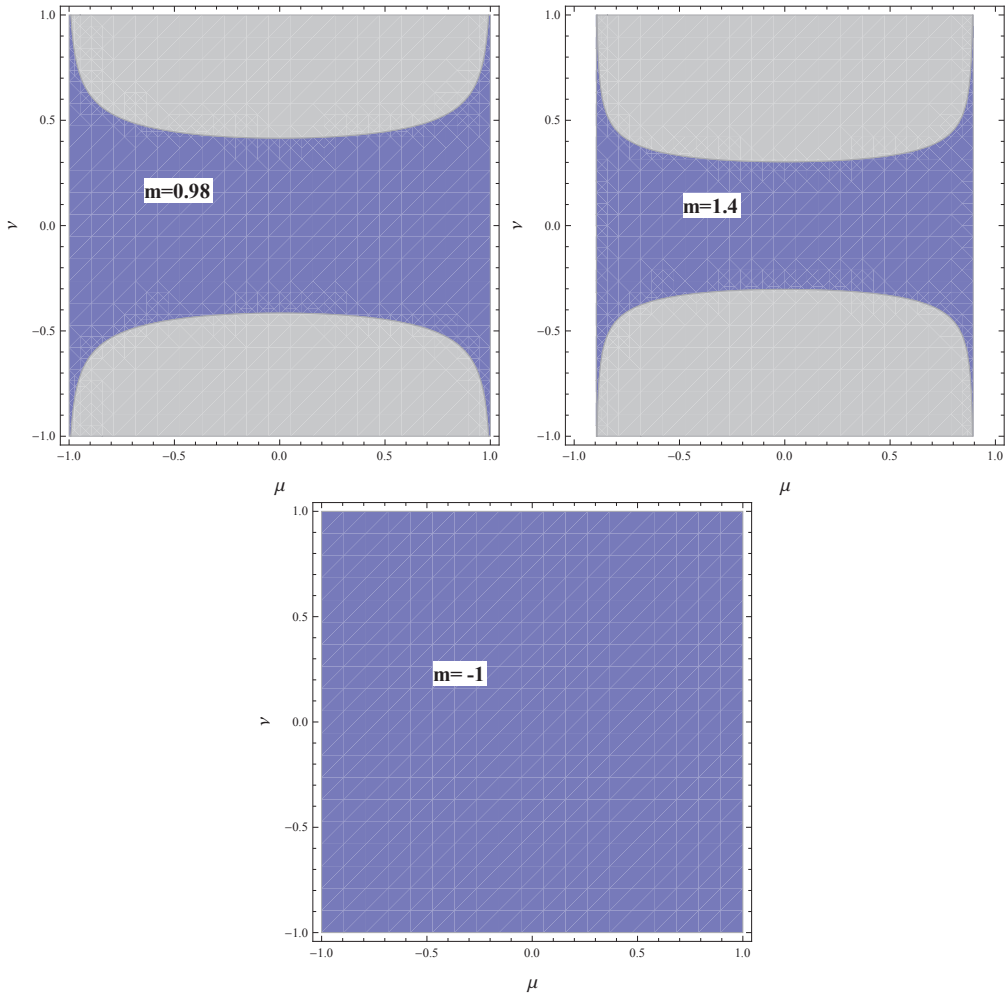

Figure 6: Plots of qualitative phase space analysis for power-law scale factor with tachyon coupled matter.

the presence of phantom and tachyon fields. We summarize our results as follows.

Firstly, we have discussed stability of the universe dominated by the coupling of phantom energy and DM through their eigenvalues corresponding to different values of m (Figures **1-3**). We have considered three different linear combinations for the coupling constant. For $Q = \alpha\dot{\sigma}_m$, we have found an unstable matter dominated state undergoing decelerated expansion for all points with $m > 0$ and various choices of α (Figures **1**). The dynamical analysis shows a matter dominated era ultimately followed by a late accelerated expansion phase of the universe. For $m < 0$, all the points become stable future attractor undergoing accelerated expansion as $q < 0$ except the point P_1 which lies in decelerated expanding region. In this case, the results for points P_2 and P_3 do not solve the coincidence problem which is well consistent with the results for FRW universe model [23, 35].

For $Q = \beta\dot{\sigma}_\phi$, all the eigenvalues and trajectories show unstable nodes for positive values of m which become stable for $m < 0$ corresponding to different choices of α (Figure **2**). These points lie in non-accelerating phase of the universe as $q > 0$ for all choices of parameters m and β which may alleviate coincidence problem as compared to [23]. For the coupling $Q = \gamma(\dot{\sigma}_m + \dot{\sigma}_\phi)$, we have found unstable past attractor for positive values of m. When $m < 0$, stable node is observed for point P_1 while point P_2 corresponds to saddle node undergoing decelerated expansion (Figure **3**). In this case, point P_3 shows stable future attractor in accelerating phase as compared to FRW universe model [23]. It is worth mentioning here that all the critical points for the couplings $Q = \beta\dot{\sigma}_\phi$ and $Q = \gamma(\dot{\sigma}_m + \dot{\sigma}_\phi)$ indicate decelerated expanding universe except point P_3.

Secondly, we have studied stability of the universe model by taking interaction between tachyon field and DM. In this case, we consider $Q = \beta\dot{\sigma}_\phi$ only. The cosmic portrait shows a matter dominated epoch ultimately followed by a late accelerated expansion phase (Figure **4**). For $m > 0$, we have found unstable/saddle node for points P_1 and P_2 while point P_3 gives stable future attractor which undergoes an accelerated expansion. For $m < 0$, the point P_1 corresponds to stable node showing accelerated expansion of the universe while the remaining points give saddle/unstable node that corresponds to de Sitter phase of the universe. We note that all the points show accelerated expansion of the universe for tachyon coupled field. We conclude that negative values of m enhance stability of the universe model as compared to its positive values.

Finally, we have studied the behavior of power-law scale factor corresponding to different values of m. The power-law scale factor indicates various phases of evolution (accelerated or exponential expansion) for the respective universe model as shown in Figures **5** and **6**. For phantom coupled matter, it is found that the region for decelerated expansion gets larger by increasing m while $m < 0$ corresponds to accelerated expansion of cosmos. In case of tachyon coupled field, the contraction region decreases by increasing m while the gray region becomes larger. Also, $m < 0$ shows only blue region which corresponds to the decelerated expanding universe model.

References

[1] Riess, A.G. et al.: Astron. J. **116**(1998)1009; Perlmutter, S.J. et al.: Astrophys. J. **517**(1999)565; Bennett, C.L. et al.: Astrophys. J. Suppl. **148**(2003)1.

[2] Caldwell, R.R., Dave, R. and Steinhardt, P.J.: Phys. Rev. Lett. **80**(1998)1582; Chiba, T., Okabe, T. and Yamaguchi, M.: Phys. Rev. D **62**(2000)023511.

[3] Carroll, S.M., Hoffman, M. and Trodden, M.: Phys. Rev. D **68**(2003)023509.

[4] Gorini, V. et al.: Phys. Rev. D **69**(2004)123512.

[5] Chimento, L.P.: Phys. Rev. D **69**(2004)123517.

[6] Kamenshchik, A., Moschella, U. and Pasquier, V.: Phys. Lett. B **511**(2001)265.

[7] Bento, M. C., Bertolami, O. and Sen, A.A.: Phys. Rev. D **66**(2002)043507.

[8] Feinstein, A.: Phys. Rev. D **66**(2002)063511.

[9] Sami, M.: Mod. Phys. Lett. A **18**(2003)691.

[10] Gibbons, G.W.: Phys. Lett. B **537**(2002)1.

[11] Sami, M., Chingangbam, P. and Qureshi, T.: Phys. Rev. D **66**(2002)043530.

[12] Parker, L. and Raval, A.: Phys. Rev. D **60**(1999)063512; Polarski, D. and Starobinsky, A.A.: Phys. Rev. Lett. **85**(2000)2236; Caldwell, R.R.: Phys. Lett. B **545**(2002)23; Coley, A.A., Hervik, S. and Latta, J.: Mod. Phys. Lett. A **21**(2006)1099.

[13] Billyard, A.P. and Coley, A.A.: Phys. Rev. D **61**(2000)083503.

[14] Chimento, L.P. et al.: Phys. Rev. D **67**(2003)083513; Chimento, L.P. and Pavon, D.: Phys. Rev. D **73**(2006)063511.

[15] Bogoyavlensky, O.I.: *Qualitative Theory of Dynamical System in Astrophysics and Gas Dynamics* (Springer, 1985)

[16] Copeland, E.J., Liddle, A.R. and Wands, D.: Phys. Rev. D **57**(1998)4686.

[17] Guo, Z.K. et al.: Phys. Lett. B **608**(2005)177.

[18] Guo, Z.K., Cai, R.G. and Zhang, Y.Z.: J. Cosmol. Astropart. Phys. **05**(2005)002.

[19] Yang, R.J. and Gao, X.T.: Class. Quantum Grav. **28**(2011)065012.

[20] Xiao, K. and Zhu, J.: Phys. Rev. D **83**(2011)083501.

[21] Acquaviva, G. and Beesham, A.: Phys. Rev. D **90**(2014)023503.

[22] Sharif, M. and Mumtaz, S.: Eur. Phys. J. C **77**(2017)136.

[23] Shahalam, M. et al.: arXiv:1702.04720v2.

[24] Eriksen, H.K. et al.: Astrophys. J. **605**(2004)14.

[25] Belinkskii, V.A. and Khalatnikov, I.M.: Sov. Phys. JETP **42**(1976)205.

[26] Coley, A.A. and Dunn, K.A.: J. Math. Phys. **33**(1992)1772.

[27] Burd, A. and Coley, A.: Class. Quantum Grav. **11**(1994)83.

[28] Goliath, M. and Ellis, G.F.R.: Phys. Rev. D **60**(1999)023502.

[29] Sharif, M. and Waheed, S.: Astrophys. Space Sci. **351**(2014)329.

[30] Chaubey, R. and Raushan, R.: Astrophys. Space Sci. **361**(2016)215.

[31] Kantowski, R., Sachs, R. K.: J. Math. Phys. **7**(1966)433.

[32] Collins, C.B.: Phys. Lett. A **60**(1977)397.

[33] Throne, K. S.: Astrophys. J. **148**(1967)51; Roy, S.R. and Banerjee, S.K. Class. Quantum Grav. **11**(1995)1943; Bali, R. and Kumawat, P.: Phys. Lett. B **665**(2008)332; Shamir, F.M.: Eur. Phys. J. C **75**(2015)354.

[34] Wang, B., Gong, Y.G. and Abdalla, E.: Phys. Lett. B **624**(2005)141; Gumjudpai, B. et al.: J. Cosmol. Astropart. Phys. **007**(2005)0506; Campo, S.D., Herrera, R. and Pavon, D.: Int. J. Mod. Phys. D **20**(2011)561; Wei, H. and Cai, R.G.: Phys. Rev. D **71**(2005)043504.

[35] Chen, X., Gong, Y. and Saridakis, E.N.: J. Cosmol. Astropart. Phys. **04**(2009)001.